A study on eclogite bodies in Dabie Shan (China):

petrology, geothermobarometry and timing of metamorphic events

Master thesis Earth sciences, specialisation Solid Earth (450199)

By Mirek Groen

Departments of Petrology and Isotope Geochemistry
Faculty of Earth and Life Sciences
VU University Amsterdam

Supervisors:
Dr. Jan R. Wijbrans
Dr. Fraukje M. Brouwer

1 April 2009

VU University Amsterdam

A study on eclogite bodies in Dabie Shan (China): petrology, geothermobarometry and timing of metamorphic events

Mirek Groen, 1337289

Frontpage: (top left) valley near the Bixiling eclogite body
(top middle) banded eclogite from Xiong Dian (07XD01)
(top right) view of the Mifengjian valley (07YS04)
(bottom left) quartz layers in greenschist, Mulan (Macheng)
(bottom middle) braided river, along the road from Taihu to the west
(bottom right) eclogite body with thick rim of amphibolite

Abstract

A narrow mountain belt of several thousand kilometres long, extending from Sulu in the east to Dabie, Qinling into Western China, contains ultrahigh-pressure rocks which are the key to understanding processes of deep subduction of continental crust into the mantle. Supracrustal rocks together with denser mafic and ultramafic bodies are subducted to minimal depths of 100 km and then brought to the surface. During Paleozoic and Triassic deformation two cratons and several smaller units collided and amalgamated to form the Dabie Shan Mountain Belt at the suture between the Yangtze craton and the Qinling microcontinent. After more than 20 years of research there is a reasonable understanding of the processes involved. However, there is still debate regarding the exact number of (U)HP metamorphic events and their ages. The results show controversy about the timing of events in West Dabie and East Dabie. It is suggested that the entire area experienced Paleozoic deformation and is later overprinted by Triassic deformation.

Lu-Hf dating on eclogites, using garnet and omphacite show only Triassic ages for both East and West Dabie. The regions show ages around 231 and 249 Ma. PT-modelling using the program Thermocalc indicates that UHP metamorphism occurred only in East Dabie. The eclogites from West Dabie were metamorphosed at lower pressure or show a stronger influence by retrograde metamorphism that may have obliterated evidence of UHPM. $^{40}Ar/^{39}Ar$ analyses of phengite, biotite and amphibole result in a range of ages. Two already known peaks are visible around 120 and 220 Ma. In addition, evidence is found suggesting that additional metamorphic events have occurred around 300, 400 and 500 Ma. Such events are entirely plausible in the light of the known histories of the Dabie and Qinling mountain ranges. However, in terms of interpretation of isotopic results it apparently indicates that ages obtained with the K-Ar system can survive quite high overprinting events.

Table of contents

Chapter 1 Introduction

Subduction systems are very complex geologic features, because processes of tectonics, metamorphism, magmatic processes and even sedimentology coincide. Whereas such systems have been extensively studied, the mechanics of subduction of continental crust to extreme depths is still not completely understood. In Central East China ultrahigh-pressure rocks surrounded by felsic country rocks are exposed and therefore of high value to get insight in deep mantle processes. The Dabie Mountains, part of an orogen extending from Sulu to Qinling and further into western China (Figure 2.1 and Figure 2.2), show evidence for at least two major deformation phases. While the western part represents Paleozoic deformation, Triassic deformation primarily dominates the eastern part.

In collaboration with the Guangzhou Institute of Geochemistry (CAS) a three year program is set up as part of a KNAW (Royal Netherlands Academy of Arts and Sciences) project to achieve a better insight of processes involved during UHP metamorphism. The project focuses on the evolution of the eclogite belt of central China. As part of a master thesis for the VU University of Amsterdam, field work was carried out in May 2007, in order to sample key outcrops in Dabie Shan and Sulu. During four weeks of sampling the main goal was to collect a representative set of eclogites from Dabie Shan, especially in the central part where eclogite outcrops are rare. The aim was to link the two different geological histories of east and west Dabie Shan.

Field work started near Wuhan, driving north. During the first 10 days samples were collected from outcrops near Macheng, Xinxian and Sujiahe (Appendix I and Appendix II). The most western location visited was Tongbai. Subsequently, eclogite spots near Luotian and Yingshan were sampled, representing the poorly exposed area of Dabie Shan. Bixiling, Taihu, Zhoujiachong and Qianshan are the most important locations for sample collection in East Dabie. The final part covered areas further north, near Dong Hai and Shan Dong, representing Sulu. All outcrops were found using information acquired by previous research, a geologic map (Appendix I) and GPS information.

Dabie Shan is part of a narrow mountain belt extending over several thousand kilometres. After the collision of two cratons, the Yangtze craton in the south subducted beneath the Sino-Korean craton in the north. According to *Ratschbacher et al.* (2006) several slabs of continental crust, oceanic crust, arc systems, flysch, etc. were subducted and exposed to ultrahigh-pressure conditions. A major question is which of the two deformation phases (Paleozoic or Triassic) was responsible for extremely deep subduction and therefore for the (U)HP environment. Has the Paleozoic metamorphic event been overprinted by younger Triassic metamorphism in West Dabie, or have different units experienced different events? How are the eastern and western parts linked to each other? The main purpose of this research is to find evidence of both age peaks in the same rock, using the Lu-Hf and the $^{40}Ar/^{39}Ar$ dating methods.

Furthermore, if different tectonic slices were evolved independently, it is interesting to model thermodynamically the (maximum) depth due to subduction. Have all units undergone UHP metamorphism? And how, if existing, can (lateral) anomalies be explained? Electron microprobe (EMP) analyses will be used to model PT-conditions of stable mineral assemblages, using the program Thermocalc. Combining the thermobarometry results with the ages, it may be possible to obtain some clues about the characteristics of metamorphic events. When did the peak metamorphic conditions occur, and when did retrogression play a major role?

Finally, it is suggested that more than two deformation phases are responsible for the evolution of Dabie Shan (e.g. *Wu et al.*, 2009). Its geologic history is even more complex than suggested previously. Therefore this study attempts to find evidence for other events, useful for completing the history of Dabie Shan.

In Chapter 2 a short overview of the evolution of the area will be given, followed by a detailed description of every major unit present in the orogen. The next Chapter will discuss the methods used to solve the problems of this study. Subsequently, the field observations are described. In Chapter 5 the results will be listed for every method separately. The following Chapter will discuss thermodynamic modelling and associated interpretation. In a final Chapter "discussion and conclusion" all the results will be taken together and answers to the questions and problems are presented.

Chapter 2 Geologic setting

In the Dabie and Sulu Mountain belt one of the most extensive ultrahigh-pressure metamorphic regions is exposed at the surface of the Earth. This is a result of a continent-continent collision event, where supra-crustal rocks were subducted to eclogite facies metamorphic conditions. This chapter discusses the geological history of the orogenesis of the Dabie Mountains, followed by a description of the different geological units.

2.1 Introduction

The Dabie Mountains are part of a ~2000 km long belt, extending from Qinling to Sulu (Figure 2.1 and Figure 2.2), which is the result of the collision between the Yangtze craton in the south and the Sino-Korean craton in the north. Different microcontinents were merged to each other and were subducted within several slabs to different depths, triggering the development of magmatic systems in the overlying plate (Figure 2.4). Although the Sulu area is offset by 500 km to the northeast along the Tanlu fault, it is clear that this area belongs to the Qinling-Dabie orogen (*Chavagnac and Jahn*, 1996; *Zheng*, 2008).

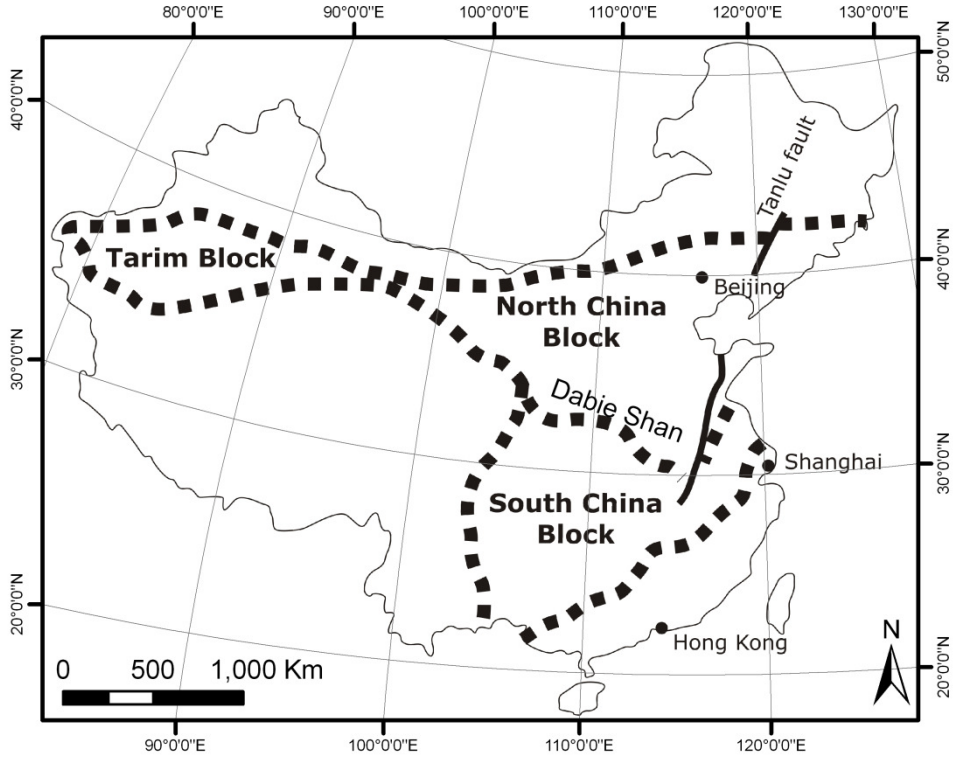

Figure 2.1 Map of China showing the different cratons; where the North China Block corresponds to the Sino-Korean craton and the South China Block to the Yangtze craton. Original map taken from *Xue et al.* (1995).

In the core of the belt, in the Dabie area, coesite and diamond inclusions were found in garnet (*Chavagnac and Jahn*, 1996; *R.Y. Zhang et al.*, 2002; *Schmidt et al.*, 2008), indicating that ultrahigh-pressure conditions were reached. During subduction, the crust must have reached depths of at least 80-120 km, and possibly as much as 200 km (*R.Y. Zhang et al.*, 1995b; *Liou and Zhang*, 1998; *Liu et al.*, 2002; *R.Y. Zhang et al.*, 2007). According to *Schmidt et al.* (2008) three different stages of metamorphism can be recognized which formed the Dabie-Sulu UHP terrain: (1) a first UHP event, with peak conditions within the coesite/diamond stability field at temperatures of 800-700°C and pressures >2.8 GPa; (2) a second HP event within the high-pressure quartz-eclogite stability field at temperatures of 750-600°C and pressures of 2.4-1.2 GPa; and (3) a retrograde amphibolite facies overprint at temperatures of 600-450°C and pressures of 1.0-0.6 GPa.

Hacker et al. (2006) dated these events at Triassic ages:

- Precursor UHP event 244-236 Ma
- HP Main event 230-220 Ma
- Amphibolite facies overprint 220-205 Ma

Although the temperature exceeded the closure temperature (T_C) during peak metamorphism and therefore the measured ages are all after the peak (*Scherer et al.*, 2000), it can be said with certainty that these numbers illustrate that metamorphism took place during the Triassic. On the other hand evidence for Devonian metamorphism is also found (*Sun et al.*, 2002; *Cheng et al.*, 2008) and therefore the development of the area needs further investigation.

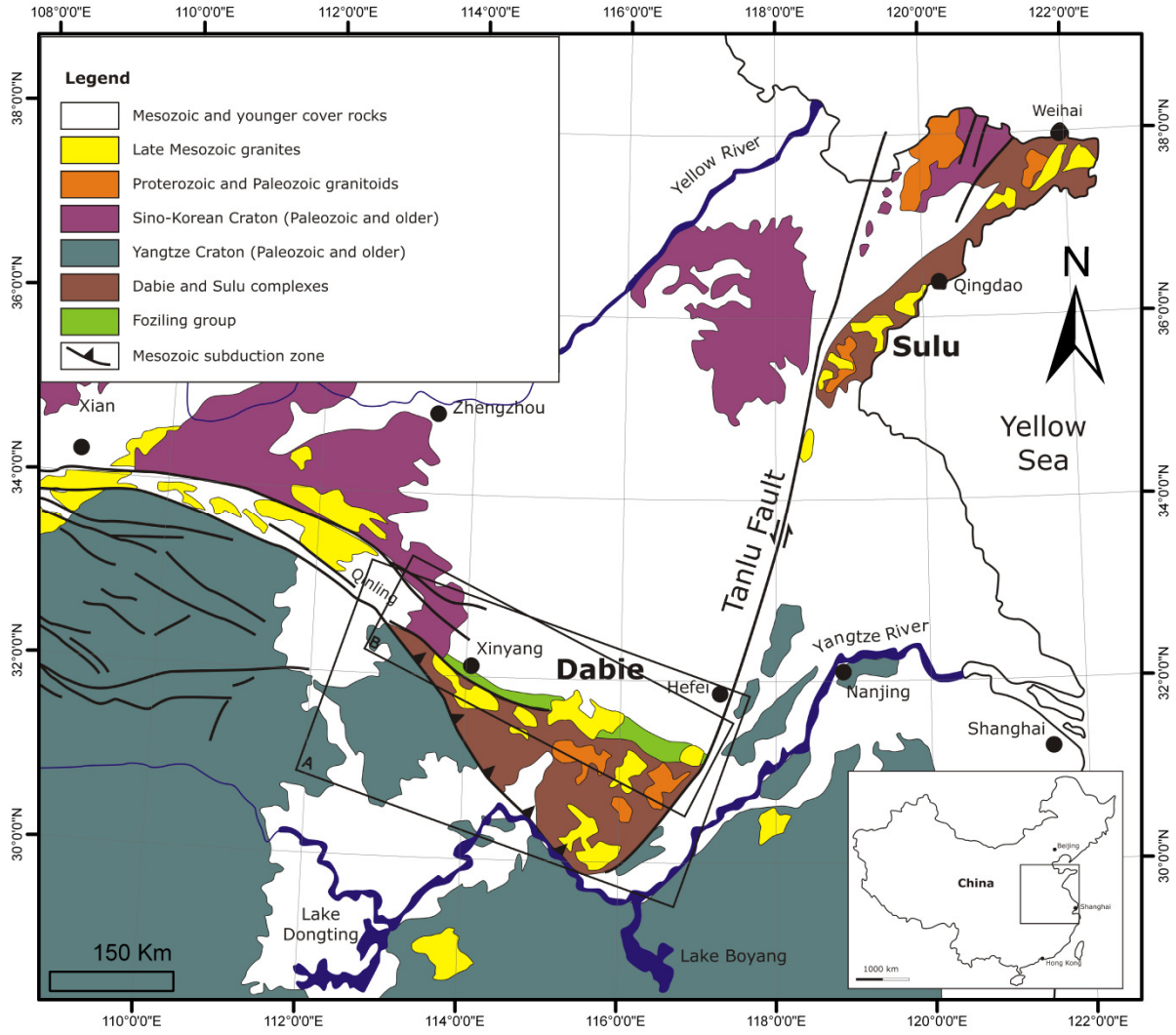

Figure 2.2 Geological map of the Dabie-Sulu orogen. The Yangtze craton in the south is separated from the Sino-Korean craton by the Qinling-Tongbai-Dabie orogenic belt. The Sulu terrain is offset by the Tanlu fault, but considered as the eastern extension of the orogen. Square A and B refer to Appendix II and Figure 2.3, respectively. Original picture taken from *Chavagnac et al.* (1996).

2.2 The formation of the orogen in a chronological view

From north to south three different sutures have been identified (*Ratschbacher et al.*, 2006): (1) The Sino-Korean craton-Erlangping intra-oceanic arc suture, (2) the Erlanping arc-Qinling unit suture and (3) the Qinling unit-Yangtze craton suture (Figure 2.3). It is believed that these sutures were not formed simultaneously (*Xue et al.*, 1996, *S.G. Li et al.*, 2000; *X.P. Li et al.*, 2004; *Liu et al.*, 2007). These sutures divide the Dabie Mountains into the following geological units (from north to south): the Sino-Korean craton, the Erlangping unit, the Qinling microcontinent, the Huwan mélange and the

Yangtze craton. Although the units are named differently by the different research teams, these are the most common ones and used hereafter.

Figure 2.4 shows a schematic view of the development of the Dabie Shan orogen. Starting from 0.7 Ga, when the Yangtze craton was moving away from the Qinling microcontinent (*Ratschbacher et al.*, 2003) and the Sino-Korean craton in the north moved northwards. Between the continents oceanic crust was present and between the Qinling continent and the Yangtze craton new oceanic crust was formed. This ocean was part of the large (paleo-)Tethys ocean that extended to the Middle East and Europe. Based on U/Pb dating methods on zircons, the protolith of the Sino-Korean craton formed at 771 ±86 and 752 ±70 Ma (*Wu et al.*, 2008a). The protolith of North Dabie, which is equivalent to the Qinling microcontinent or the Yangtze craton, formed around 700-800 Ma (U-Pb age) (*Wu et al.*, 2007).
The Erlangping microcontinent formed as an intra-oceanic arc (Figure 2.4b) at 490-470 Ma (*Zhang et al.*, 1989; *Xue et al.*, 1996). It is unclear which source is feeding this continent, but the Erlangping unit is generally interpreted as an intra-oceanic arc, because of the existence of basaltic, andesitic and dacitic volcanics (*Niu et al.*, 1993).
From 440 Ma on, the stress field changed dramatically. Compressional forces drove the continents towards each other. The first collision occurred between the Sino-Korean craton and the Erlangping microcontinent, when the arc is subducted beneath the craton. Directly after this event the Qinling microcontinent is subducted beneath the Erlangping unit. According to *Ratschbacher et al.* (2006) these two sutures are younger than Erlangping arc, but older than Silurian subduction magmatism on the Qinling unit (404 Ma). This means that the two sutures must have been formed between 490 and 404 Ma.
After ongoing subduction of the Qinling microcontinent, due to slab dehydration mantle started to melt and magmatism occurred (*Ratschbacher et al.*, 2003). A complicated complex containing several volcanic arc formed, which is better known as the Silurian-Early Devonian arc. Another consequence of the magmatic event is local low-grade contact metamorphism (*Ratschbacher et al.*, 2006).
Because of the subduction of oceanic crust and overlying sediments smaller units between the continents were accumulated in accretionary wedges or flysch. Even Foreland basins developed, were filled with sediments and later subducted or scraped off and collected in a wedge. The Nanwan complex, the northern part of the Qinling microcontinent, is formed as flysch. Between the Qinling microcontinent and the Yangtze craton an accretionary wedge was formed at 315 Ma and subsequently exhumed; now called Huwan mélange (*Sun et al.*, 2002). Oceanic crust subduction terminated with the transition to subduction of frontal margin of the Yangtze craton (*Hacker et al.*, 2000). Because of a very flat subduction angle and the length of the craton magmatism occurred beneath the Sino-Korean craton.
Due to Cretaceous and Cenozoic unroofing exhumation rocks from mid crustal depth are now exposed to the surface (*Ratschbacher et al.*, 2000). Eclogite bodies produced from the Yangtze craton were subducted and exhumed together with their country rock and subjected to coeval UHP metamorphism (*Wang and Liou*, 1991; *R.Y. Zhang et al.*, 1995a; *Ye et al.*, 2000; *J. Liu et al.*, 2001; *F. Liu et al.*, 2003, 2004, 2005). This is proved by the discovery of kyanite- and coesite inclusions in quartzite and eclogitic garnet, respectively (*R.Y. Zhang et al.*, 2002). Gravitational traction of high-density oceanic lithosphere pulled the relative buoyant continental crust to depths of at least 80-120 km (*Xue et al.*, 1996). However, it is not widely accepted that continental crust can be subducted to such extreme depths. It is now hypothesized that these units are subducted and exhumed back to the surface when the orogen is still under compression. It is suggested that different slabs rose to the surface along the same path they were subducted. Together with buoyancy forces, because of a relative light crust, and a current extensional environment the UHP- rocks are now exposed at the surface (*Wu et al.*, 2008a).
For a very large UHP-metamorphic complex located at the Yangtze craton called Bixiling eclogite complex, uplift rates were measured using different isotopic systems with different closure temperatures; U-Pb on zircon, Sm-Nd on garnet, Rb-Sr on phengite and biotite. According to *Chavagnac and Jahn* (1996) fast initial uplift of 10 mm/yr decreased

to 3 mm/yr. Compared to exhumation rates of eclogites observed in the Alps (20-30 mm/yr) Dabie exhumation was slow (*Rubatto and Hermann*, 2001). It is believed that these differences depend on the size of the bodies: the bigger the eclogite bodies are, the lower the exhumation rate is.
After the latest Triassic deformation stage rocks were only brought to the surface by doming. No new major events occurred except for reactivation of faults due to the collision of India and Asia during the Eocene (*Ratschbacher et al.*, 2006).

Nowadays different tectonic units or metamorphic zones are recognized. Observations are made from different localities, but give more or less the same results. From North to South the following zones can be found (*Zhong et al.*, 2003; *Wu et al.*, 2007; *Wu et al.*, 2008b):

- Beihuaiyang greenschist-facies zone
- North Dabie high-T granulite-facies zone
- Central Dabie medium-T/HP eclogite-facies zone
- South Dabie low-T/HP eclogite-facies zone
- Susong blueschist-facies zone

All contain early Cretaceous igneous intrusions. The temperature decreases where the pressure increases to the south. The metamorphic zones or more or less equivalent to the lithological units defined by *Ratschbacher et al.* (2006). Every unit is separated by a detachment zone. It is sometimes possible to find the high-pressure unit direct on top of the core complex, when the UHP-unit is missing due to crustal thinning (*Suo et al.*, 2000).

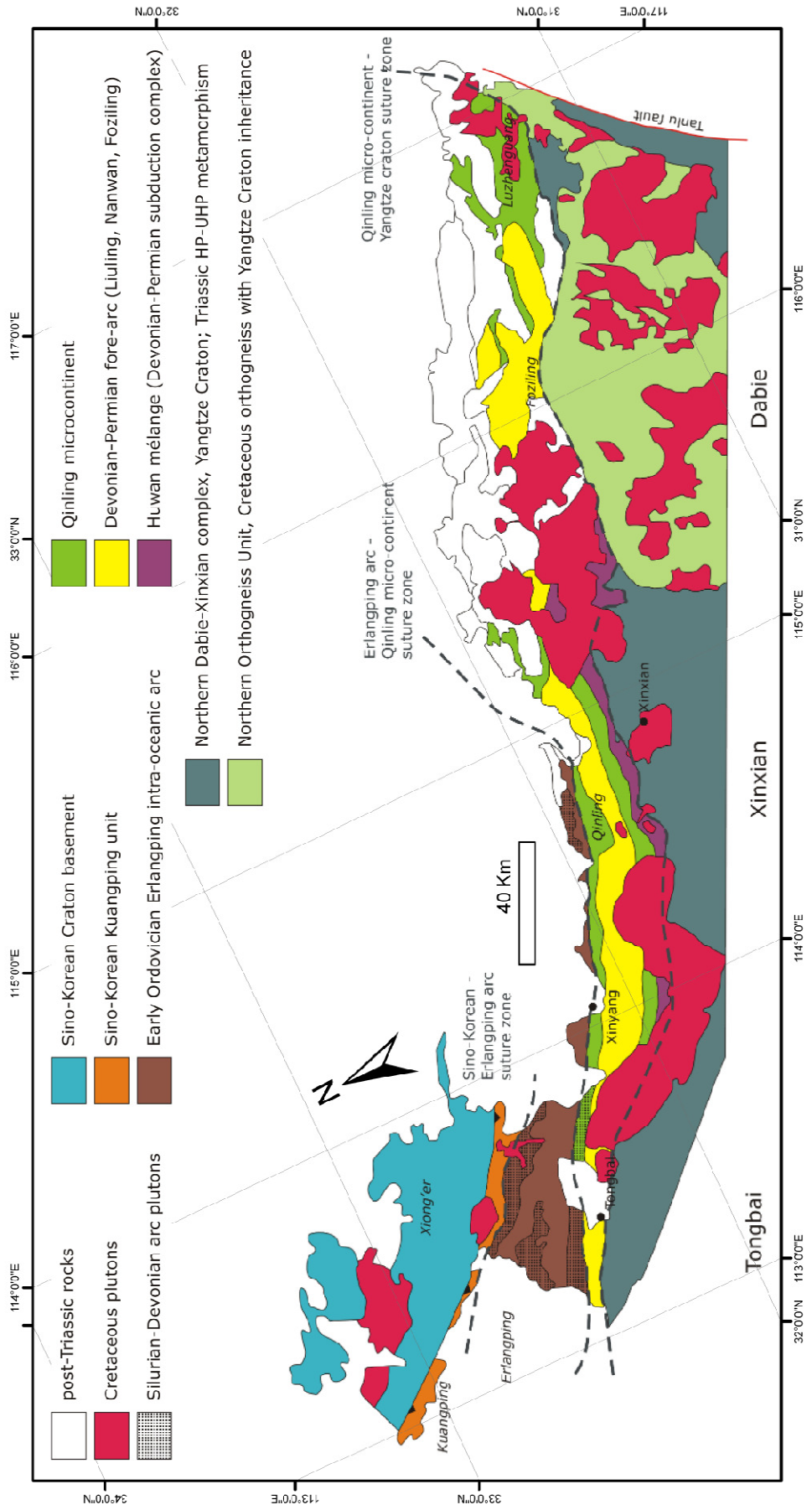

Figure 2.3 Geologic map of Dabie Shan. Picture taken from *Ratschbacher et al.* (2006).

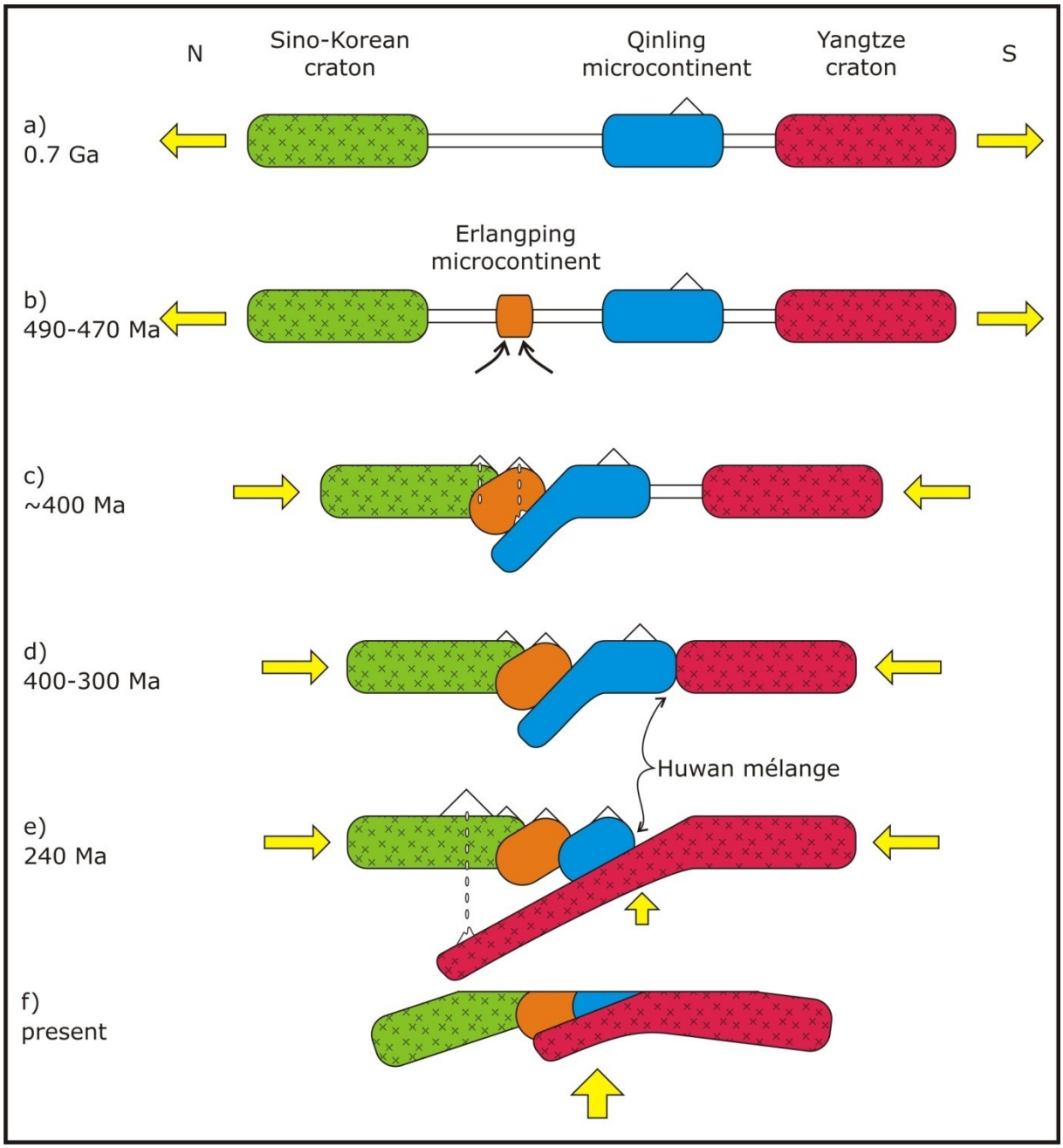

Figure 2.4 Schematic view of the development of the Dabie Shan orogen. Two colliding cratons with different intervening continents, ending up with a core complex with UHP-rocks exposed to the surface after doming (g).

2.3 Tectonic units

In west-central China, at the Qin Mountains, the different units of the Qinling-Tongbai-Dabie orogen can be clearly distinguished (*Ratschbacher et al.*, 2003). This is more complicated in the Tongbai-Dabie area relevant to the Qinling unit, the focus of this study. This section will give an overview of all units of the Dabie Shan orogen in a north to south order.

2.3.1 Sino-Korean craton

The Sino-Korean craton, also known as North China block, covers the entire northern part of China (Figure 2.1). Its basement consists mainly of high-grade tonalitic quartzofeldspathic gneisses and tectonically interbanded supracrustal rocks (*Kröner et al.*, 1988). A unit located direct on top is interpreted as overlying passive margin existing of sedimentary rocks or as an accretionary wedge (*Ratschbacher et al.*, 2003). This unit is exposed to greenschist- amphibolite-facies, where marble and two-mica quartz schist was formed. The craton act as rigid body.

2.3.2 Erlangping unit

The Erlangping unit is formed at 490-470 Ma by intra-oceanic volcanism (*Zhang et al.*, 1989; *Xue et al.*, 1996). It is composed of greenschist to amphibolites facies volcanic and plutonic rocks, fine grained clastic rocks and chert with Cambrian-Silurian fossils (*Nui et al.*, 1993).

2.3.3 Qinling microcontinent

The Qinling microcontinent is the most complicated unit found in this orogen. It is believed that it is a very narrow but "ribbon" continent extending through the Qinling/Dabie area and probably into Sulu (*Ratschbacher et al.*, 2006, and references therein). In the western part of the orogen, at the Qin Mountains, this unit exists of only two units. The lower unit contains biotite-plagioclase gneiss, amphibolite, calc-silicate rocks, garnet-sillimanite gneiss and marble (*Xue et al.*, 1996). The upper part consists of marble with minor lenses of amphibolite and garnet-sillimanite gneiss (*You et al.*, 1993). Figure 2.5 shows the names of the upper and lower part of the Qinling unit further to the east, in Xinxian and Northern Dabie.

Figure 2.5 Overview of Qinling unit in Qin, Xinxian and Northern Dabie. For locations see Figure 2.3.

Since the structure of the Qinling unit in the vicinity of Xinxian is suggested to be a synform stretching E-W, the Guishan and Dingyuan units form the same unit, with the Nanwan formation on top of them and therefore in the core of the synform (middle part of Figure 2.5). The Guishan and Dingyuan formations consist of gneiss, amphibolite, garnet-mica schist, chlorite-albite schist, marble and quartzite. The Nanwan formation exists of greenschist-grade turbiditic slate, phyllite, quartz-mica schist and quartzite. In the northern part of Dabie these formations can be compared with respectively the Luzhenguan complex and Foziling formation, but they do not form a synform structure. The Luzhenguan complex contains metavolcaniclastic rocks, granitoid and gneiss from amphibolilte facies in the lower part, and quartz-mica schist in the upper part. The Foziling formation is formed by greenschist- amphibolite-facies monotonous mostly fine-grained well-bedded siltstone and shale and minor volcanic rocks, with a local basal quartzite and marble (*Chen et al.*, 2003). Various interpretations exist for the last two units; they are thought to represent the Yangtze passive margin, the Sino-Korean craton forearc flysch, the Sino-Korean craton backarc flysch or an accretionary wedge (*Li et al.*,

2001). According to *Ratschbacher et al.* (2006) the most suitable interpretation for this unit is a forearc flysch.

2.3.4 Imprint of Andean-type magmatism

After the subduction of the Qinling unit an Andean-type continental margin arc was developed, due to the subduction of oceanic crust. From 440 to 390 Ma bodies of granite, granodiorite, tonalite, gabbro and quartz-monzodiorite intruded the Sino-Korean, Erlangping and Qinling amalgamated continent (*Ratschbacher et al.*, 2003, and references therein).

2.3.5 Huwan mélange

Between the Qinling microcontinent and the Yangtze craton a separate unit, called Huwan mélange, is recognized (*Ye et al.*, 1993, 1994). It consists of elongated blocks of eclogite, gabbro, amphibolite, marble and quartzite surrounded by a matrix of gneiss, quartzofeldspathic schist and graphitic schist (*Ratschbacher et al.*, 2006). The mélange is strongly deformed at the southern part of the Qinling microcontinent, in the Xinxian vicinity it forms the northern part of the HP- and UHP units. In the Chinese literature this unit is seen as the southern part of the Sujiahe group, which is part of the northern Dingyuan formation (Paragraph 2.3.3), but the protolith of the blocks exists of oceanic basalt and can therefore be distinguished from eclogites of adjacent continental units. The matrix of the mélange constitutes a tectonic and possibly sedimentary mixture of rocks from the Qinling microcontinent, the Silurian-Devonian arc, the Paleotethyan ocean floor and the Yangtze craton. The oceanic crust formed an accretionary complex during Carboniferous-Permian subduction. Age determinations give results around 309 Ma (average number) and 320 Ma (Xiongdian location, stop 10 in Appendix II.b, 07XD01/04 in Appendix II.d) for the HP-deformation (Qtz-ecl. Stability field) (*Sun et al.*, 2002). Therefore, eclogite facies metamorphism in the Huwan shear zone is significantly older than HP/UHP metamorphism (220-230 Ma) in Dabie (*Li et al.*, 2000).

2.3.6 Yangtze craton

The northern margin of the Yangtze craton, also known as the southern China Block (Figure 2.1), forms the northern-Dabie, Xinian complex. Its basement contains mainly granitic and granodioritic gneiss and supracrustal rocks, that were exposed to HP- and UHP metamorphic conditions. The northern HP part exists of eclogite boudins with quartz inclusions within garnet and clinopyroxene, whereas in the southern UHP part eclogitic garnet and clinopyroxene contains coesite inclusions. Average PT-conditions are determined at 470-500°C and 1.4-1.7 GPa and 620-670°C and 2.6-2.9 Gpa, for the northern and southern part, respectively (*X. Liu et al.*, 2004b). According to *Sun et al.* (2002) the age of the protolith of eclogite is determined at 752 ±17 Ma, and peak HP metamorphism in the quartz-eclogites occurred at 232 ±10 Ma. Based on Rb/Sr isotopic dating the peak of metamorphism for the coesite-eclogites is defined at 212 ±7 Ma (phengite) and 213 ±5 Ma (13 zircon ages from the same rock), but these ages illustrate post UHP-recrystallization (*X. Liu et al.*, 2004a). Argon dating of phengites from the basement units demonstrates that the deformation here was exclusively Triassic-Jurrasic (*Xu et al.*, 2000; *Ratschbacher et al.*, 2006).

2.3.7 Cretaceous magmatism

Cooling ages in orthogneiss plutons cluster around 130-115 Ma, due to magma injection (*Niu et al.*, 1994; *Ratschbacher et al.*, 2000). Because of regional Cretaceous heating contact metamorphism occurred and therefore isotope decay systems can be reset. It is believed that the magmatic process can be triggered by one of two mechanisms, both controlled by the Pacific plate: either by normal subduction of the plate (*Wu et al.*, 2005), or by a change of subduction direction of the already subducting plate (*Zhao et al.*, 2007). The latter theory is based on the observation of the Pacific super plume. The plume is the cause for the change in direction, which can then be a source for a thermal anomaly due to rapid mantle convection. It is believed that the increase of the temperature is large enough to melt parts of the core complex (*X. Zhang et al.*, 2002).

However, the first episode of partial melting is older than post-collision igneous rocks, so there was no large-scale magmatism which rules out the plume model (*Wu et al.*, 2007).

2.4 The formation of eclogites in a tectonic setting

Eclogite bodies are of great importance to unravel the history of Dabie Shan. They can give some insight in the processes which brought mafic bodies to extreme depths. In Northern Dabie the junction between the western (Qinling-Tongbai) and eastern (Dabie-Sulu) is exposed (*Sun et al.*, 2002), where key outcrops can possibly give the link between the two different areas, using different systems like Rb-Sr, Ar/Ar, Sm-Nd, Lu-Hf. However, these chronometers are possibly disturbed because of retrograde metamorphism, multiple growth and recrystallization events and isotope disequilibrium (*Wu et al.*, 2008a).

Peak UHP-metamorphic conditions are determined at 222-224 Ma by Sm-Nd and Lu-Hf analyses on eclogites from Zhoujiachong and Shima in Southeast Dabie (*Cheng et al.*, 2008). Pressure temperature calculations of a Bixiling eclogite (East Dabie, stop 34-37, Appendix II.b) result in 700-800°C and ≥2.7 GPa (*Chavagnac and Jahn*, 1996). The closure temperature of the Lu-Hf system in garnet seems to be higher than that of the Sm-Nd system, 540-700°C relative to 485-500°C, respectively (*Scherer et al.*, 2000; *Schmidt et al.*, 2008) and can therefore register an age closer to the peak of metamorphism. However, age calculations on Dabie eclogites, from Bixiling and Shima using both methods resulted in ages which all range between 220 and 224 Ma (*Schmidt et al.*, 2008). The error lies around 3 m.y. what makes the results of the two methods indistinguishable.

As illustrated in Figure 2.7 Triassic UHP metamorphism occurred due to the subduction of the Yangtze craton. Here the Qinling microcontinent (yellow) and the Erlangping arc (green) are stacked at the subsurface between the Yangtze and Sino-Korean cratons. UHP metamorphism occurred around 220 Ma. Mafic bodies, such as basaltic oceanic crust within the lighter buoyant continental crust, were metamorphosed within the eclogite facies (*Wu et al.*, 2009). The mafic bodies from West Dabie in this study originate from the Huwan mélange, which was located between the Yangtze craton and Qinling microcontinent.

In western Dabie metamorphic ages of around 400 Ma are observed (*Ratschbacher et al.*, 2006). Argon measurements on phengite show a possible influence of excess argon (*Li et al.*, 1994; *Hacker and Wang*, 1995), which increases the age. In contrast according to *Qiu & Wijbrans* (2006, 2008) Argon dating on fluid inclusions of garnet acquired with stepwise crushing show the evidence for an early Paleozoic UHP metamorphic event; excess argon is already excluded from the results.

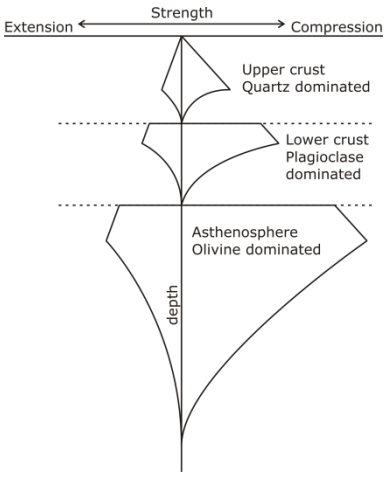

Figure 2.6 Example of a strength envelope for the crust and mantle. Strength of layers depend on brittle-ductile transition and the dominating mineral phase.

Whether UHP metamorphism occurred in West or East Dabie or both regions, during Paleozoic or Triassic events it is not giving information about the process bringing the units back to the surface. Figure 2.7 shows a Triassic subduction event subsequently followed by extension. Due to slab break-off and crustal thinning the UHP core is finally exposed. However, when UHP metamorphism already occurred during Paleozoic times, the orogenic belt was still under compression (*Xue et al.*, 1996; *Ratschbacher et al.*, 2003; *Ratschbacher et al.*, 2006). Other processes must have been responsible for the exhumation of Paleozoic eclogitic bodies. *Brueckner and Roermund* (2004) introduced a model for the Scandinavian Caledonides, showing that slabs can educt back to the surface along the path they were brought down, even during a compressional stage, but only when low angle subduction occurred. Figure 2.6 shows a theoretical strength envelope for the upper and lower crust and the asthenosphere. Along the weaker zones delamination can occur. When the down going slab is still subducting the overriding plate brings the UHP terrane to the surface.

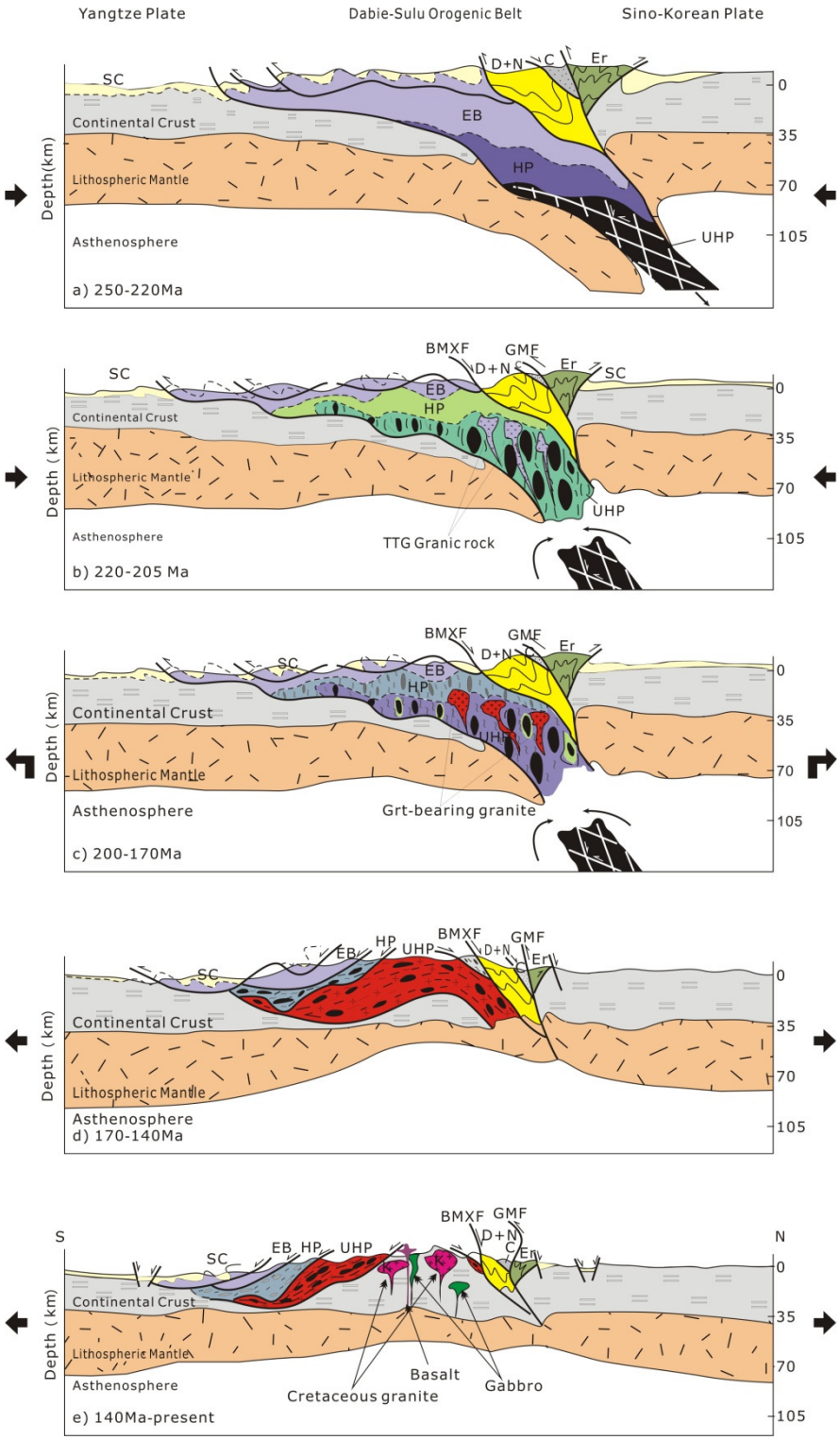

Figure 2.7 Cartoon showing the development of Dabie Shan within five timeframes starting from 250 Ma till present. In a compressional regime the Yangtze craton subducted (a) and UHP metamorphism occurred. Microcontinents between the this craton and the Sino-Korean craton stacked. Due to slab break-off (b) and the change of the stress field (from compression to extension) the UHP unit exhumed to mid-crustal depth (b+c). The UHP unit is exposed to amphibolite facies retrograde metamorphism. Partial melting occurred due to decompression (c). During the post-collision episode crust thinned and different metamorphic units are were exposed at surface (d). Further extension and doming resulted in the current situation where even the metamorphic core is exposed. Cretaceous magmatism in the basement developed different plutons.
SC: Cover Sequence; EB: Ep-Blueschist facies; HP: High-Pressure Units; UHP: Ultrahigh-Pressure Units; Er: Erlangping Group; D+N: Dingyuan-Nanwan Period; C:Carboniferous System; GMF: Guimei Fault; BMXF; Balifang-Mozitang-Xiaotian Fault; The faults (GMF and BMXF) are equivalent to the second and third suture between the Erlangping unit, Qinling microcontinent and Yangtze craton, respectively. Figure taken from *Q. Yang* (unpublished).

Chapter 3 Methods

This chapter describes all the methods used in this study. To answer the research questions it was necessary to do field work, collect samples, study thin sections and carry out chemical analyses. 16 of the 119 samples were selected for $^{40}Ar/^{39}Ar$ dating. 4 samples were used for Lu and Hf isotope analysis and for microprobe analysis. Of the same last 4 samples XRF analysis is done as well, but finally not used in this study.

3.1 Field work

Field work was carried out for four weeks in May 2007 in the area of Dabie Shan and Sulu, Central East China. The area extends from Tongbai in the west, to the Tanlu fault in the east, and further to the north connected by this fault to the Sulu area, represented by two areas called Donghai and Shan Dong. Small eclogite lenses, or boudins, were sampled, trying to get some information about the age and pressure-temperature conditions of the (U)HP-metamorphic event(s). Previous GPS-data together with the geological map (Appendix I) were used to find the locations of the eclogite outcrops. An overview of all the visited localities can be found in Appendix II.a, b & c. Strategic (or key) outcrops were sampled to find the link between the western and eastern part of Dabie Shan. Granitic or Dacitic dykes, marble and jadeitite lenses in the vicinity of the eclogite lenses were sometimes sampled as well.

3.2 Sample selection

Of all the collected samples thin sections were made, but kept at a thickness of 60 µm, instead of the normal 30 µm. Therefore it is still possible to prepare a covered or polished thin section after the selection is done. For the Lu and Hf isotope analysis the most fresh eclogites were selected, where the following criteria were applied:

- the eclogite must contain inclusion-free garnet and clinopyroxene;
- no amphibole as a retrograde mineral, as rims around garnet and clinopyroxene or as single grains;
- phengite may be present as a mineral formed on the prograde path;
- coesite may be present as an inclusion in garnet, indicating that the rock experienced ultrahigh-pressure conditions.

Together with the (Lu-Hf) age calculations, information on the PT-conditions can possibly unravel the history of the orogen, therefore the same samples were used for microprobe analysis. Two samples were chosen from the western part (07HA11 and 07XD01), one from the central part (07YS04) and one from the eastern part (07WH07), to get a good sample coverage of the area.

For the $^{40}Ar/39Ar$ dating method potassium-rich minerals are required. Phengite, biotite, actinolite, hornblende and k-feldspar are minerals with a high potassium content, and present within the rocks collected. The only other criteria are that the grains must be large enough and inclusion-free. The following samples were chosen for mineral separation:

- 07XX20, 07XX24, 07XX29, 07HA01, 07HA02, 07XD04 (Phg)
- 07LT01, 07TH03 (Bt)
- 07XX20, 07XX06, 07HA11, 07XD01, 07LT04 (Act)
- 07XX23, 07LT01 (Hbl)
- 07LT01 (Kfs)

3.3 Thermobarometry

Four samples are selected for microprobe analysis. This section describes the methods used for analysis and thermodynamic modelling.

3.3.1 Electron microprobe (EMP)

For quantitative major element analysis of the minerals the Jeol JXA-8800M electron microprobe (EMP) is used. Before the measurements were done the polished thin

sections were coated with a conductive carbon layer. With an acceleration voltage of 15 kV, a beam current of 25 nA and a focused spot elements are detected by an electronic beam. A counting interval of 25 seconds is used for the peak signal, where an interval of 12.5 seconds is used to detect the background signal. For minor elements these numbers are increased to 36 and 18 seconds, respectively. To prevent damage, a defocused spot with a diameter of ~10 µm is used for phengite analysis.

The error can be reduced below a level of 0.5% by offline corrections, but to keep further calculations reliable an error of 2% will be used. The weight percentages are all rounded to 2 decimal places. Negative values are set to 0.00, because these values are caused by overlap corrections, meaning that the element is not present.

3.3.2 Technical aspects of Thermocalc

EMP results are used to set up input files (example in Appendix V) for the application Thermocalc (v. 3.25 & 3.31), which is used to model PT-conditions at which a specific mineral assemblage equilibrated (mode 2). The mineral chemistry data is used to calculate different ratios (Equation 3.1-3.10). This is done for two mineral assemblages: Grt-Omp-Phg-Coe/Qtz-H_20 and Grt-Omp-Phg-Ky-Coe/Qtz-H2O. It is assumed supported by textural evidence that this assemblage was once in equilibrium during (U)HP-metamorphic circumstances.
For all phases Thermocalc calculates all possible reaction between available endmembers from the database file (ds55). Subsequently, it is possible to calculate a reaction line for each reaction possible between the endmembers available in the adjacent stability fields. The more different mineral phases used, the more accurate the estimation of the pressure and temperature is; because of the higher number of possible independent reactions. At the point where two reaction lines intersect, at an invariant point, all involved endmembers are stable. In an ideal situation the exact pressure and temperature values are indicated by the invariant point when 3 or more lines intersect. In a more common situation the reaction lines intersect each other at different values, creating triangles. The smaller the triangle, the better the PT-estimation. This is indicated by sigfit.

EMP data of the first three minerals is used to calculated the following parameters:

$$x = Fe^{2+}/(Fe^{2+} + Mg) \quad \text{(3.1, Grt \& Omp)}$$
$$z = Ca/(Ca + Fe^{2+} + Mg) \quad \text{(3.2, Grt)}$$
$$j = Na/2 \quad \text{(3.3, Omp)}$$
$$f = \left(x_{Fe^{3+}}^{M1a} + x_{Fe^{3+}}^{M1m}\right)/\left(x_{Al}^{M1a} + x_{Al}^{M1m} + x_{Fe^{3+}}^{M1a} + x_{Fe^{3+}}^{M1m}\right) \quad \text{(3.4, Omp)}$$
$$Q = (x_{Na}^{M2n} - x_{Na}^{M2c})/2 \quad \text{(3.5, Omp)}$$
$$Q_{af} = \left(x_{Fe^{3+}}^{M1a} - x_{Fe^{3+}}^{M1m}\right)/2 \quad \text{(3.6, Omp)}$$
$$Q_{fm} = -x + x_{Fe^{3+}}^{M1a}/\left(x_{Fe^{3+}}^{M1a} + x_{Mg}^{M1a}\right) \quad \text{(3.7, Omp)}$$
$$fe = Fe^{2+}/(Fe^{2+} + Mg) \quad \text{(3.8, Phg)}$$
$$y = 4 - Si\ (Al\ op\ A - site) \quad \text{(3.9, Phg)}$$
$$na = Na \quad \text{(3.10, Phg)}$$

Appendix V shows an example of an input file used for sample 07HA11. All the files are generated based on this example, where the only changing parameters are those for garnet, omphacite and phengite. Note that [fe] for phengite (equation 3.10) has the same definition as [x] for garnet and omphacite (equation 3.1). The values for [Q] are based on the state of order in the crystal lattice of omphacite. It is assumed that disorder is dominant, therefore there is no preference for Fe^{3+}, Mg, Al and Na to enter M1a, M1m, M2n, or M2c sites. The elements are equally divided. Based on the presence of coesite in 07WH07, an average pressure and temperature of 30 kbar and 700°C is taken, respectively.

3.3.3 Ferric iron

For equations 3.1, .2, .4, .6, .7 and .8 ferrous and ferric iron values should be used, but with the EMP it is not possible to distinguish between Fe^{2+} and Fe^{3+}. However, four options are available to tackle this problem; 1) assume all iron is Fe^{2+}, 2) calculate Fe^{3+} by charge balance, 3) calculate Fe^{3+} by stoichiometric calculation or 4) use Mössbauer spectrometry. In Table 3.1 all results for iron of one Dabie Shan eclogite sample (*Proyer et al.*, 2004) are listed, but instead of a stoichiometric calculation a "best fit analysis" was done. When it is assumed that the Mössbauer spectrometer gives the exact number of cations, all the other analyses still result in lower amounts of ferric iron. Therefore, if such a spectrometer is not available, the best results are acquired with the "best fit analysis".

Method	Fe^{3+}	Fe^{2+}
All Fe as Fe^{2+}	0	0.11303
Charge balance	0.00079	0.11222
Best fit analysis	0.03518	0.07853
Mössbauer	0.06117	0.05211

Table 3.1 analysed and recalculated values for ferric en ferrous iron of garnet-clinopyroxene sample. Analysis done by *Proyer et al.*, 2004.

As an example, for sample (07XD01) the number of ferric iron cations is calculated using the first three methods as described above. Figure 3.1 shows the differences between the three results. Although the results do not vary much between the different methods, the error for stoichiometric calculations is a factor 3 lower than when assuming all Fe as Fe^{2+}.

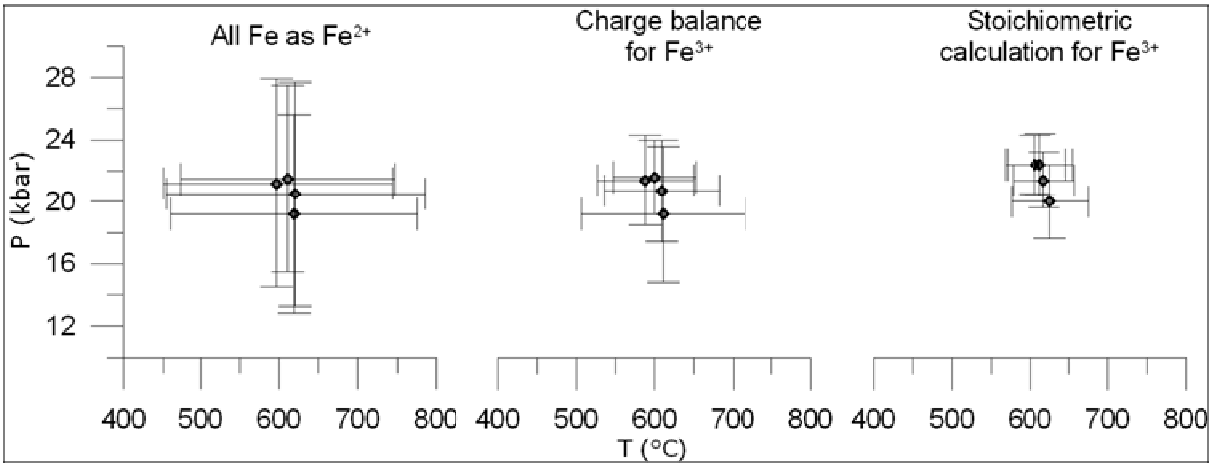

Figure 3.1 PT-conditions for 07XD01 using three different methods to calculate ferric iron.

For the charge balance ferric iron is calculated by the number of cations at the different sites in its crystal lattice. The total charge of cations in the M1 and in M2 sites should be equal, but when there is a difference this can be compensated by taken Fe^{3+} into account. This is a naive way of calculating ferric iron, but it comes closer to reality. A better way is introduced by *Droop* (1987), which makes it possible to calculate Fe^{3+} using the following equation:

$$F = 2X(1 - T/S) \qquad (3.11)$$

where T is the ideal number of cations per formula unit, and S is the observed cation total per X number of oxygen atoms. The equation has been derived using stoichiometric criteria assuming that iron is the only element present with variable valence and that oxygen is the only anion.

3.3.4 Standard deviation

Thermocalc (v. 3.25) has the built-in possibility to calculate the standard deviation for given input, without using the error level of 2% obtained by the microprobe. However, when this possibility is not used and the standard deviation for the input is based on the 2% error, the results seems to be more precise according to smaller sdT and sdP. Thus,

the latter method is preferable, but for an unknown reason it is not possible to calculate PT-conditions for 07WH07 and 07YS04. The pressure and temperature seems to be too high and therefore only the first option is available, resulting in higher errors and slightly lower values for temperature and pressure.

3.3.5 Mineral phases

The set of independent reactions exists of all mineral phases present in a system formed by the mineral assemblage Grt-Omp-Phg-(Ky)-Coe-H_2O. It is possible to select or rule out certain phases based on their fit. When the fit is lower than 1.73, the level of confidence is higher than 95%. Grossular, almandine and pyrope are the included endmembers of garnet, diopside and hedenbergite are the pyroxene endmembers and muscovite and celadonite are used as mica endmembers. Furthermore, quartz, coesite and H_2O are the other available phases. The problem of ruling out one of the endmembers is that the number of possible independent reactions will lower. Because of a solid-solution between relatively few endmembers, it is preferred to use all the possible endmembers, even when the fit is higher than 1.73.

Using mode 2 of Thermocalc it is possible to calculate pressure and temperature conditions in three different ways; 1) average P over a temperature range, 2) average T over a pressure range or 3) average PT conditions. First, option 1 is used to specify a limited temperature range where the sigfit gives the lowest results, which is an indication for the best suitable conditions when the rock was in equilibrium. Subsequently, option 3 is used which gives the final pressure and temperature values as listed in Section 5.2.

3.4 Mineral separation

The selected samples are all crushed successively with a rock splitter and jaw crusher, before they are sieved in 5 different grain size ranges; >500 µm, 365-500 µm, 200-365 µm, 150-200 µm and <150 µm. The largest and smallest grain size ranges are not used. For the final step (hand picking) using the second largest grain size range (365-500 µm) gives the most convenient way of picking. When the minerals are too small and intergrown with each other, smaller grains are used.

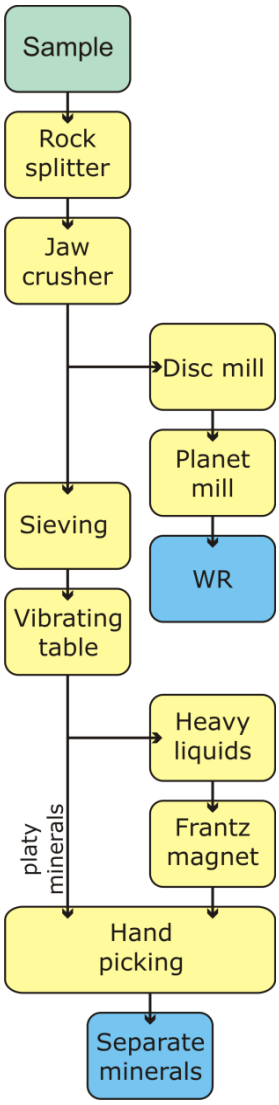

Figure 3.2 Steps taken for sample preparation.

3.4.1 Preparation method for XRF-analyses

For the four samples used for Lu-Hf dating and microprobe analysis beads were made for XRF-analysis, using whole-rock (WR) powder. Therefore, an aliquot of each sample is set apart before sieving. The WR-aliquots were crushed to a grain size of <2 µm, using the agate mill and the planet mill. The resulting powders are dried at 100°C for approximately 12 hours. The powders also need to be free of carbon for the fusion process of bead preparation, and are therefore heated to 1000°C for 30 minutes. The powders are then mixed with a flux of lithium-tetraborate at a ratio of 4:1 in order to lower the melting point of the silicates. After melting the mix at temperatures of 1150°C, the material is poured onto a platinum tray and cooled. The bead is then ready for XRF measurements.

3.4.2 Preparation for separation

Before the actual mineral separation could start, dust and other unwanted particles had to be removed from the surfaces of the minerals. This was done by exposing the minerals to ultrasound waves. In the device, implosions of air bubbles are created by electric currents running through a liquid; the implosions remove unwanted particles from the mineral grains.

3.4.3 Vibrating table

Mineral separation started by using a vibrating table, separating minerals based on their shape. Platy minerals, like biotite and phengite, can be separated, leading to an almost pure concentrate of these minerals. Further purification is applied by hand picking only (Figure 3.2).

3.4.4 Heavy liquids

The rest of the minerals is separated using heavy liquids; this technique separates minerals according to a difference in density, which is given in Table 3.2. A centrifuge (LOC50) is used to create a gravitational force of approximately 700 times stronger than earth's gravity, by rotating the sample at a speed of 5000 rpm. Material more buoyant than the selected fluid medium will end up in the float, denser material in the sink.

Mineral	**Density**
Grt, Cpx	>3.30 g/cm^3
Act, Hbl	3.00 – 3.30 g/cm^3
Kfs	2.52 – 2.62 g/cm^3

Table 3.2 density range of separated minerals

3.4.5 Frantz magnet

Depending on the mineral and on the sample itself, different magnetic fluxes are used to separate minerals based on their magnetic susceptibility. Due to a high susceptibility garnet is separated early, whereas clinopyroxene is separated later. These are followed by actinolite and k-feldspar. The latter has the lowest susceptibility; the electric current is set at maximum value (2.7 A) to create the largest possible magnetic field and separate the mineral.

3.4.6 Hand picking

For this technique the good minerals (positive picking) or the bad ones (negative picking) are selected. The minerals are picked with a needle by making use of a vacuum. The selected grains are collected in a glassy vial.

3.5 Preparation methods for isotope analysis

Four samples of eclogite are used for Lu-Hf isotope analyses to determine the age of the (U)HP metamorphic peak. In previous research radiogenic systems like Rb/Sr, Sm-Nd and Lu-Hf are used. But the latter is expected to record the highest metamorphic conditions as it has the highest closure temperature (*Scherer et al.*, 2000).

3.5.1 Preparation of the samples

To dissolve the sample 15 ml savillex vials are used. The vials were cleaned by heating them in HNO_3 and HCl for two hours, filled with double-distilled HF, put on a hotplate for one night and finally rinsed with milli-Q water. Then the samples were weighed and spiked with a Lu-Hf and a Sm-Nd solution with a known isotopic ratio. In order to check the cleanliness of the procedures, two blanks were used; one for the Grt/Cpx procedure, one for the WR procedure. Garnet is diluted with spikes B and 2, for clinopyroxene and WR spikes A and 1 are used. The amounts of sample and spike are listed in the table below.

Sample	Weight (mg)	Spike Lu-Hf (B)	Spike Sm-Nd (2)
07YS04/01 Grt	54.97	107.97	115.87
07YS04/02 Grt	55.66	132.78	124.77
07YS04/03 Grt	59.43	125.04	121.16
07XD01/01 Grt	56.45	125.43	119.03
07XD01/02 Grt	54.80	127.39	103.07
07XD01/03 Grt	51.69	118.29	122.75
07HA11/01 Grt	45.76	108.02	98.76
07HA11/02 Grt	48.11	162.19	110.00
07HA11/03 Grt	45.05	127.06	108.45
07WH07/01 Grt	41.42	107.42	106.68
07WH07/02 Grt	52.30	112.15	107.05
07WH07/03 Grt	56.46	110.58	106.68

Sample	Weight (mg)	Spike Lu-Hf (A)	Spike Sm-Nd (1)
07YS04/04 cpx	105.95	111.76	110.97
07XD01/04 cpx	119.70	116.25	101.19
07HA11/04 cpx	101.32	102.29	106.71
07WH07/04 cpx	109.07	104.91	112.82
07YS04/05 WR	111.68	106.13	114.53
07XD01/05 WR	107.38	118.56	116.76
07HA11/05 WR	108.04	119.47	111.32
07WH07/05 WR	119.12	117.30	124.76
BLK1	-	27.10	31.04
BLK2	-	26.85	33.94

Table 3.3 Weight and spike values (in mg) of the various samples. Note that the spike in the left and right table is not the same. BLK stands for blank. Mixed spikes are used for $Sm/Nd^{(1)}$ with a ratio 0.31 and for $Sm/Nd^{(2)}$ with a ratio 0.87, both enriched in ^{149}Sm (97.6%), for $Lu/Hf^{(A)}$ with a ratio 0.1222 enriched in ^{176}Lu (64.3%) and ^{178}Hf (94.4%) and for $Lu/Hf^{(B)}$ with a ratio 0.9496 enriched in ^{176}Lu (64.3%) and ^{178}Hf (94.8%). The atomic numbers of the Sm/Nd spike may change slightly when exact numbers are calculated.

For each sample three batches of garnet of approximately 50 mg, one of clinopyroxene (100 mg) and one of whole rock (100 mg) are needed. This gives 5-point isochron plot, which will lower the error, compared to a 2-point plot. The amount of spike added to the sample is based on literature describing the same procedure, using the same rock type, or using rocks from the same area (*Münker et al.*, 2001; *Morel et al.*, 2008; *Cheng et al.*, 2008).

Inclusions, in particular of zircon, in garnet and clinopyroxene are known to disturb the Lu and especially the Hf content (*Scherer et al.*, 2000). Therefore the minerals will be dissolved stepwise. At least 11 steps of adding and extracting 5 ml of weak acid (10 M HCl/0.2 M HF) were needed to dissolve the garnet and clinopyroxene, but to leave the inclusions behind. With every step, the samples were left on a hotplate for 24 hours. For the WR 50 drops of HF-HNO_3 (concentrated, 1:1) were used to dissolve the sample completely.

3.5.2 Extraction of Lu and Hf (and Nd and LREE)

After the first cleaning steps the sample solution (dissolved in 5 ml 3 M HCl) is loaded on a column of Eichrom© Ln-spec resin. Based on the chromatographic characteristics Lu and Hf can be separated from all other elements. Figure 3.3 shows that different elements will be separated using different concentrations of acid; during the first washout (3M HCl) the rock matrix together with LREE (including Sm and Nd) are collected in savillex beakers. These elements will be stored for further research. Lutetium and Yb are removed using 6M HCl and collected in PTFE beakers. The solution is dried

down after adding a drop of H_2O_2 to prevent formation of black tar. Titanium, Zr and Hf are separated in two steps. By using weak citric acid and weak HF, respectively Ti and Zr will wash off. Both elements are collected in different waste beakers to prevent the formation of aquaregia. Hafnium leaves the resin when a concentration of HF stronger than 0.5 M is added. Because a low concentration is expected, it is important to collect all the Hf and therefore a concentration of 2M is used. Hafnium is collected in the same beakers used for the sample dissolution, after cleaning them with 0.24 M HF/0.56 M HNO_3. The solution is dried down and nitrated with one drop concentrated HNO_3. Once the elements were isolated, they can be measured with a mass spectrometer (Neptune).
The total isotope dilution procedure is described by *Münker et al.* (2001) and listed in Table 3.4.

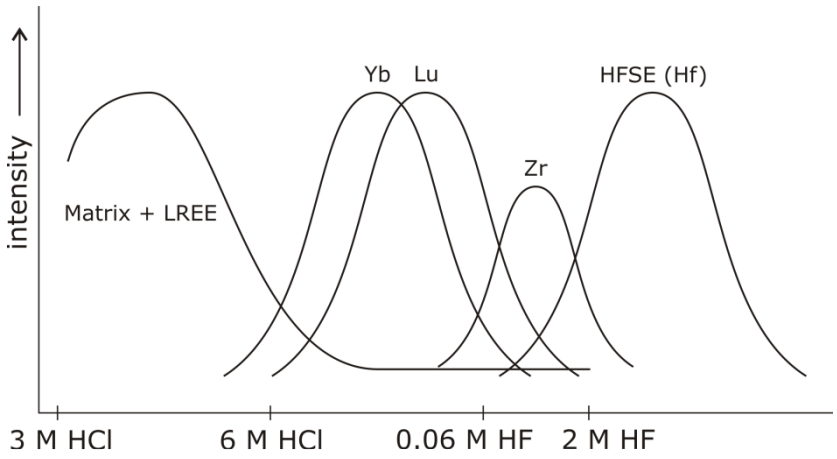

Figure 3.3 Diagram indicating how the elements can be separated from the bulk sample. Taken from *Münker et al.*, (2001).

Material	**Amount**	**Comment**
2M HF	1 rr.	precleaning
6M HCl	1 rr.	precleaning
3M HCl	2x ½ rr.	conditioning, HF must be removed
2-3 M HCl	1-10 ml	loading sample
3M HCl	Up to 10 ml	collect matrix and LREE (Sm, Nd)
6M HCl	10 ml	**collect Lu**
H_2O	2x 2 ml	wash #1
0.09M Hcit/0.4 M HNO_3/1% H_2O_2	10 ml	remove Ti
0.09M Hcit/0.4 M HNO_3/1% H_2O_2	10 ml	remove Ti
0.09M Hcit/0.4 M HNO_3/1% H_2O_2	10 ml	remove Ti
0.09M Hcit/0.4 M HNO_3/1% H_2O_2	10 ml	remove Ti
H_2O	2x 2 ml	wash #2
6M HCl/0.06M HF	10 ml	remove Zr
6M HCl/0.06M HF	10 ml	remove Zr
6M HCl/0.06M HF	10 ml	remove Zr
6M HCl/0.06M HF	10 ml	remove Zr
6M HCl/2M HF	10-12 ml	**collect Hf**
2M HF	1 rr.	rinse
6M HCl	1 rr.	rinse
2M HF	1 rr.	rinse
6M HCl	1 rr.	rinse

Table 3.4 Steps taken for element fractionation with the Lu-Hf one column procedure. rr stands for reservoir, one column volume is ±15 ml.

3.6 Neptune for Lu and Hf measurements

The amounts of isotopes of Hafnium and Lutetium are measured on the Thermo Finnigan NEPTUNE, also known as MC/ICPMS (Multi Collector Inductively Coupled Plasma Mass Spectrometer). The mass spectrometer is located at the VU University Amsterdam.

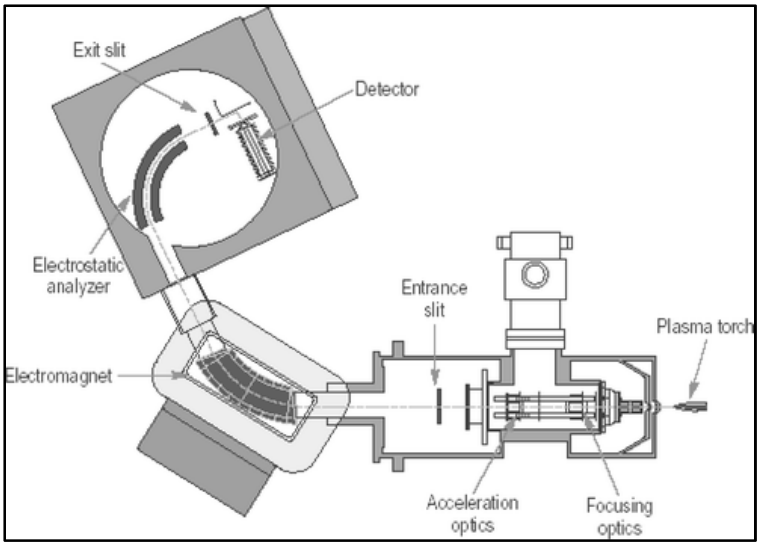

Figure 3.4 The layout of a Neptune mass spectrometer. The plasma beam starts at the bottom. Taken from www.rsc.org

Mass separation is accomplished by an electrostatic field and a magnet (Figure 3.4). During measurement, all isotopes are ionized to plasma. Depending on the mass of the isotope the angle at which it is bent differs. Seven cups can be used to detect seven different masses simultaneously. Before the plasma enters the machine, it moves through two conically shaped slits. Divergent forces between the negatively charged ions results in a separation between heavier and lighter isotopes: the heavier isotopes remain in the centre of the beam while the lighter ones are driven outwards. This leads to heavier isotopes being drawn into the mass spectrometer more than lighter material. This mass bias is removed by measuring the fixed ratio of $^{179}Hf/^{177}Hf$. The β- factor is calculated to correct for this problem.
By diluting the sample with a mixed spike, which is enriched in ^{178}Hf and ^{176}Lu, it is possible to calculate the measured isotopic ratios: $^{176}Hf/^{177}Hf$, $^{178}Hf/^{177}Hf$ and $^{179}Hf/^{177}Hf$, and $^{176}Lu/^{175}Lu$.

The NEPTUNE MC/ICPMS is very sensitive for all elements present in the solution and in the gasses that flow through. In order to be able to obtain good measurements, the solution containing the isotopes has to be as pure as possible. This is done by chemical chromatography, described in Section 3.5.2.

3.6.1 Isoplot

Age calculations are done with isoplot, an add-on application of Microsoft Excel®. It is assumed that when the minerals formed simultaneously, all points in an isochron plot at the same line. When during cooling the blocking temperature is passed, the daughter products of the decay systems are captured (Equation 3.11). If all minerals in the system initially plotted on a horizontal line, then the steepness of the new line is an indication for its age. By using equation 3.12 it is possible to calculate *t* for every measurement. This is an indication for the metamorphic age.

$$^{176}_{71}Lu = {}^{176}_{72}Hf + \beta + \bar{\nu} + Q \qquad (3.11)$$

$$\frac{^{176}Hf}{^{177}Hf} = \left(\frac{^{176}Hf}{^{177}Hf}\right)_i + \frac{^{176}Lu}{^{177}Hf} \times \left(e^{\lambda t} - 1\right) \qquad (3.12)$$

Isotopic ratios of each measurement are then plotted in a diagram. The regression line through this point is an isochron. The closer the points plot to the isochron, the lower the MSWD, which is a degree of the reliability. The steepness of the line is an indication for the age of the rock.

3.7 Laser line for Ar measurements

This section describes the Argon dating method. A detailed description of the technique can be found in Appendix VII, which contains a part of the Master report written by *Groen et al.* (2006).

3.7.1 Introduction

Argon age calculations are based on the decay of ^{40}K to ^{40}Ar and ^{40}Ca. By measuring the abundance of these isotopes it is possible to calculate an age according to the decay equation. However, it is not possible to measure potassium on the same mass-spectrometer as argon is measured on. To avoid a higher error due to double measurements all ^{39}K is altered to ^{39}Ar. This is done by exposing the samples to a nuclear reactor in Petten. ^{39}Ar can be used as a proxy for the amount of ^{40}K, because the $^{40}K/^{39}K$ is constant for this system. This increases the analytical precision. After several corrections the outcome of the measurements can be used to calculate a very precise age.

3.7.2 Preparation methods for $^{40}Ar/^{39}Ar$ isotopic dating

Before the dating can start, a batch of sample is needed, which is prepared the same way as the Lu-Hf samples, as described in Section 3.4. The cleanest grains of actinolite, hornblende, k-feldspar, biotite and phengite are selected. For the first three minerals approximately 30 mg is picked, for the mica's a few grains are sufficient. The samples wrapped in aluminium foil stacked together with standards in a glass tube. The tube is sent to the high flux reactor in Petten, where they are exposed to irradiation with fast neutrons. Due to the radioactivity of short-lived isotopes, the samples are stored for at least three months before measurements can start.

3.7.3 The laser line

The laser line is a setup, consisting of a CO_2-laser, a cleaning line and a mass-spectrometer, located at the VU University Amsterdam. The device can be used to heat very small amounts of material, within a short time and with high spatial resolution, to high temperatures. In order to extract gas from the samples, single fusion or stepwise heating can be applied. In this study all the samples are heated stepwise. After the sample tray is put into the holder, it is heated to 150°C for one night; to burn off any absorbed atmospheric argon. Using a turbo pump, unwanted 'dirty' material will be pumped away and the system will be in a permanent vacuum in the order of 10^{-9} bar. In order to improve the accuracy the laser beam is filtered only for the first steps to decrease the intensity with a factor between 6 and 8. The number of steps with a filter depends on the amount of gas released by the sample. Laser intensity is increased with every new measurement, starting with ~20% and ending with ~80%. Subsequently, the measurements are finished without a filter with a laser intensity ranging from ~8% to ~25%. These numbers are comparable to approximately 1-4 and 3-10 W, respectively. The exact intensity used depends on the amount of gas extracted from the sample. After extraction, the gas is purified, using getters, in order to lose interfering isotopes. It also removes reactive gasses and volatiles such as H_2, CH_4, N_2, O_2, CO_2 and H_2O. Finally, the gas is expanded into the mass spectrometer. Here, the intensities of the five different masses of Argon (^{36}Ar, ^{37}Ar, ^{38}Ar, ^{39}Ar and ^{40}Ar) are measured in 12 cycles. This complete cycle will be repeated for every sample as long as the sample is not melted.

3.7.4 Data reduction

The raw measurement data are processed using the program ArArCalc, a program designed by *A. Koppers* (2002) as add-in for Microsoft Excel®. First, the data of all samples, standards, blanks, airs and reference gasses are reduced, by deleting unreliable measurements. The standards together with their blanks are used to calculate the J-value, which is used to calculate the mass discrimination. Subsequently, the air and reference gas measurements are used to calculate the mass discrimination. Finally these results are applied on the sample data, which results in ages (see Appendix VII for detailed information).

Chapter 4 Field observations

In this chapter I will describe the studied field area and the various rock types and their structures. The field area is divided into four different areas, but the main focus is on the Dabie region. A detailed geological map and maps showing the sample locations can be found in Appendix I and Appendix II, respectively.

4.1 Field areas

As said in Chapter 1, one of the main purposes of this study is to find a relationship between the east- and west Dabie (U)HP metamorphic terranes. Herein Central Dabie plays an important role. During field work different eclogite localities were visited and useful (fresh) eclogite rocks were sampled, where most of the samples belong to the Yangtze craton, South of the 3rd suture (Section 2.2). The Dabie mountains form a moderate high mountain belt, with in the west an average elevation of 300-400 m, with peaks of maximum 900 m. The eastern part is slightly higher, averaging more than 1000 m. Peaks rise to around 1500 m. The entire mountain belt is heavily forested, with a coverage of about 65%. The Sulu area is located at the coast and differs significantly from Dabie. It is nearly flat with a lot of agriculture and therefore it has a very low exposure rate.

4.1.1 West Dabie

The most western city of Dabie Shan, Tongbai, marks the western border of the western Dabie area. A major NS-thrust zone east of Macheng represents the eastern border. In this area HP-metamorphic rocks are exposed. Outcrops of eclogite bodies are of a 1 to 5 km size and mostly well exposed. However, most of the known outcrops are road crops; there are probably more undiscovered bodies. The basement exists of (bt)-mica-plagio-gneiss, called the Yingshan gneiss (Appendix I). Five to 10 km sized bodies of this gneiss contain lenses of marble and jadeitite. In the northern part elongated (ultra)mafic bodies like gabbro are exposed parallel to the ductile thrust zone. Coesite is sporadically present as inclusions in garnet (*Chavagnac and Jahn*, 1996; *Ratschbacher et al.*, 2006; Schmidt *et al.*, 2008), but it was not found in the samples collected for this study. Large intrusions of lower Cretaceous monzonitic granite can be found around Xinxian and in the northeast. Because of the good accessibility, most samples were taken from outcrops along the roads or railway and only from eclogite and other directly surrounding rocks. All the spots are well distributed throughout West Dabie.

4.1.2 Central Dabie

The difficulty of this area is the very low degree of exposure. Most of the rocks are covered by Quartenary sediments. The basement exists mostly of tonalitic gneiss but also contain biotite-plagio-gneiss, marble and granofels with ultramafic and eclogite lenses. Locally the gneiss is more granodioritic. The rest of the area is characterized by the same monzonitic granite intrusions as occur in West Dabie. In the entire area ~50 km long NE-SW sinistral strike-slip faults may be found. In the northern and southern parts, along the upper and lower boundary of the Dabie orogen, granitic dykes are exposed parallel to the shear zones. Samples were collected only at two spots along the road, near the villages Luotian and Yingshan, at known locations of eclogite boudins.

4.1.3 East Dabie

At the core of the eastern part of Dabie a large eclogite complex is well exposed. This complex, Bixiling, forms the core of the UHP-metamorphic belt. During previous scientific research indications for ultrahigh-pressure conditions like coesite and microdiamond were found as inclusions in garnets. The entire area is bounded by a large strike-slip fault in the east (Tanlu fault) and thrust zone in the west (near Yingshan). The basement is formed by biotite-plagio-gneiss, tonalitic gneiss and granodioritic gneiss. Lenses of eclogite, marble and jadeitite occur as boudins (100-1000 m) throughout the area, but are concentrated in the core and along the Tanlu (strike-slip) fault. Intrusions of metagranitoid can be found here as well. This is where the rocks with the highest

metamorphic grade are exposed and therefore most samples were collected. Through the whole area small bodies of lower cretaceous granite intrusions are present, but a slightly older event intruded the basement with upper Jurassic monzonitic granite, which makes it different from the two areas described before.

4.1.4 Sulu

Another core with UHP-metamorphic rocks is exposed to the surface and offset by 500 km to the north, by the large Tanlu strike-slip fault. This is in the area called Sulu. Fresh eclogite boudins occur in a basement of strongly deformed gneiss. During Paleozoic times metagranitoids intruded, followed by Cretaceous granites. The outcrops are comparable to those of Bixiling in the eastern Dabie area. Samples were taken from two different areas, Dong Hai in the south and Shan Dong in the north at the coast. From the latter location the least retrogressed eclogites were collected.

4.2 Rock descriptions

Figure 4.1 a) garnet-bearing mylonitic gneiss with clasts, 07BX27, collected in Bixiling, stop 35 (Appendix II.b); b) Mafic boudins within matrix of gneiss, Tianpu, stop 19; c) pyrite clast with pressure shadow, 07XX12, Sujiahe vicinity, stop 12; d) fractured mafic lenses in gneiss, 07BX27, Bixiling, stop 35; e) upright spatial cleavage, recrystallization of mica in S2-direction, Ganghe, stop 38; f) folded leucosome, 07XX12, Sujiahe vicinity, stop 12; coin and lens cap for scale.

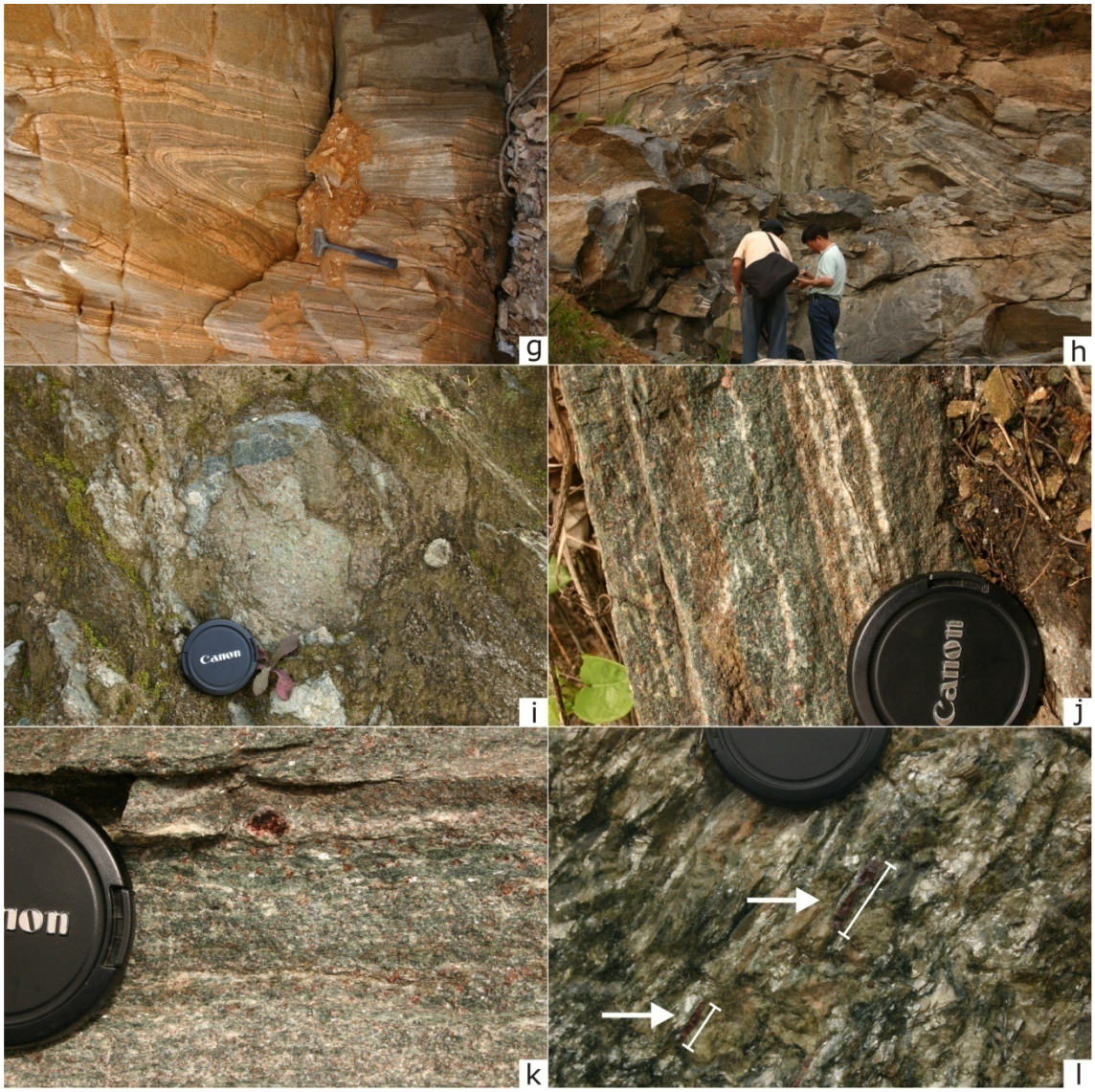

Figure 4.1 (continued) g) isoclinal fold, Zeku, at the coast in Sulu, stop 62 (Appendix II.c); h) eclogite boudin (2 m) in a basement of foliated gneiss, near the village Sidaohe, collected at stop 4 (Appendix II.b); i) eclogite boudin with rim (4 cm) of amphibolite, 07WH01, along the road between Changpu and Wuhe, stop 42; j,k) banded eclogite with cpx-rich and cpx-poor layers, and different sized garnet crystals, 07XD01, Xiong Dian, stop 10; l) large elongated rutile crystals (up to 4 cm) in quartz vein, Zhoujiachong, stop 52; hammer and lens cap for scale.

4.2.1 Country rock types

The major part of the basement exists of gneiss. Deformation was concentrated in the weaker, felsic rocks. Mafic bodies within the basement became eclogite, but remained rather undeformed. Different groups of gneiss can be recognized, where the Yingshan gneiss and Hong'an gneiss are most common in the west and a banded (unnamed) gneiss is abundant in eastern Dabie. The Yingshan gneiss is a mica-plagio-gneiss and contains marble, jadeitite and eclogite lenses. The Hong'an gneiss is a muscovite-albite-gneiss with mafic and ultramafic lenses. The banded gneiss consists of biotite-plagio-gneiss with lenses of marble and eclogite, tonalitic gneiss and granodioritic gneiss.

Banding of granite forming gneiss is characteristic for high temperature metamorphism of the lower crust. Locally the temperature may have been high enough for migmatization to occur. Jadeite present in the gneiss (Wuhe, stop 42, Appendix II.b) indicates that the buoyant rocks have been exposed to ultrahigh-pressure metamorphism.

Different structures can be recognized in the gneiss indicating the amount of deformation and the direction of the stress field. During field work these indicators are not measured, but most observed features will be named hereafter. Figure 4.1a & b show small clasts

and lenses of more competent mafic material, that are less-deformed than the surrounding basement. Locally these clasts are sigma or delta clasts, indicating the sense of shear (Figure 4.1c). Figure 4.1d shows lenses which are fractured. In a mica-rich gneiss (Figure 4.1e) cleavage (S_1) was formed due to compression. During a later deformation stage this cleavage is folded. At the fold bents mica is finally recrystallized. This results in spatial cleavage (S_2), which locally developed into gneiss banding. Ongoing strong deformation has folded the gneiss and formed isoclinal folds (Figure 4.1 f & g).

4.2.2 Eclogite

Eclogite is mostly present as boudins (Figure 4.1h). These boudins can range in size between cm-scale to a few hundred meters long. The freshest eclogite samples only contain garnet and omphacite as main minerals. Phengite can be present as another high-pressure stable mineral, together with kyanite and epidote. Glaucophane can be stable on the prograde path, when temperatures are low enough.
When the eclogite is retrogressed, omphacite reacts to amphibole and plagioclase. This will form a matrix of symplectite or subhedral crystals. When the retrograde reaction goes on, a rim of amphibole can also form around garnet minerals. Finally garnet can be completely replaced by amphibole. Figure 4.1i shows an eclogite boudin with its rim altered to darker amphibolite facies.
Due to variations in the degree of equilibrium during metamorphic processes, different types of eclogite may be recognized in the field: dark fresh eclogite, light fresh eclogite (only found in Bixiling and Sulu) and banded eclogite. Figure 4.1j & k shows banded eclogite, with cpx-rich and -poor layers, and Grt-rich and -poor layers. Garnet crystals vary in size as well, from several mm to cm-scale.
During younger stages, faults may be filled forming quartz veins. These veins contain minerals typically for HP facies. Rutile is found as elongated crystals, up to 4 cm in length (Figure 4.1l).

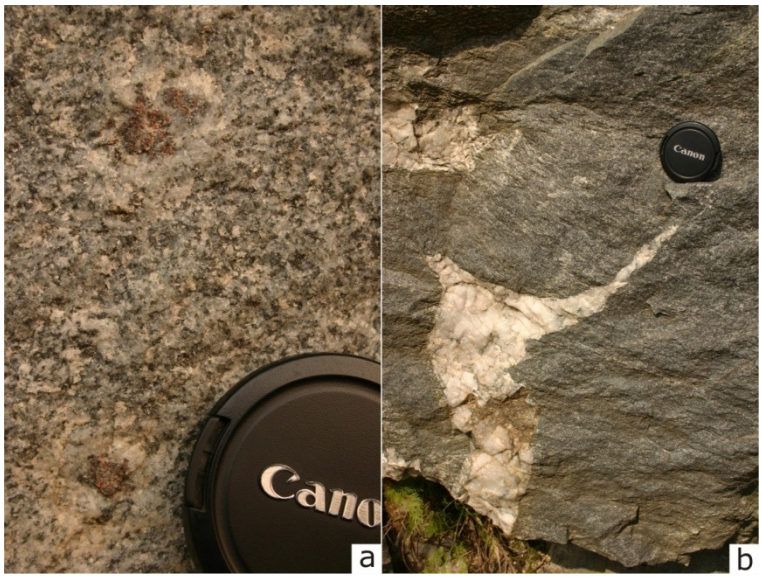

Figure 4.2 a) garnet bearing metagranite, garnet in clusters with a felsic (depleted) rim, 07MC06, Sidaohe, stop 4 (Appendix II.b); b) quartz vein through basement of gneiss, 07BX37, Bixiling, stop 35; lens cap for scale.

4.2.3 Granite intrusions

During the Early Cretaceous large bodies of granite intruded the basement. The size of the intrusions varies between several meters to kilometres. Only near the village Luotian samples are collected. This metagranite (sometimes called orthogneiss) with pegmatite veins (Figure 4.2b) contains k-feldspar, which can be used for Argon dating (e.g. 07LT01,

Section 5.4). The surrounding rocks are possibly affected by the intrusion due to contact metamorphism.

4.2.4 Dykes

Different generations of dykes are present, which vary in thickness from 20 cm to several meters. Basalt dykes are also present, but most dykes are fed by a more evolved source (diorite). Some of the dykes are dated by previous research and can be of key importance with dating the rocks.

Chapter 5 Results

This chapter presents petrographic descriptions, electron microprobe data and results of isotopic measurements.

5.1 Petrography

Thin sections were prepared of all 118 collected samples. A selection of 15 samples is left after the procedure given in Section 3.2. Five major rock types can be distinguished: eclogite, amphibolite, gneiss, (garnet-bearing) granite and post-Triassic granite. A short description of every rock type based on the thin sections is given in this paragraph.

5.1.1 Eclogite

Eight samples are eclogite, or were eclogite and are slightly altered passing through the amphibolite stability field. In the literature this rock type is described as an eclogite-jadeitite-quartzite-marble suite. Fresh eclogites consist of garnet, omphacite and phengite. Epidote, clinozoisite, rutile, kyanite and quartz are present in minor quantities. Figure 5.1 shows three different stages of eclogite, with the upper one (a) as the most fresh rock gradually changing to a retrogressed eclogite (c). Note that these pictures were not taken from the same sample.

Evidence for UHP metamorphism is found in sample 07WH07 (Figure 5.1a), showing coesite in omphacite. Figure 5.1b shows an eclogite with two different amphiboles, with a core of glaucophane and an actinolite rim. Glaucophane may be stable during prograde and (U)HP metamorphism. When the temperature is too high the crystallization of glaucophane is no longer possible. Actinolite formed as a rim around glaucophane due to retrogression. Figure 5.1c shows kyanite, which is found as needles in several samples.
Clinopyroxene will first react to lower grade metamorphic minerals, followed by garnet. Figure 5.2a shows low grade retrogression, where the rim of clinopyroxene crystals breaks down to form symplectite. Subsequently, during later processes symplectite can recrystallize to actinolite. Figure 5.2b shows a more pervasive stage, where only a few omphacite crystals are left, and symplectite of plagioclase and actinolite is formed. Here garnet is also surrounded by actinolite.

Phengite can either grow simultaneously with garnet and omphacite, or form during a later stage. This is shown in Figure 5.2c, where phengite contains inclusions of garnet and omphacite. This phengite postdates the crystallization of garnet and omphacite.

From previous research it is known that east Dabie experienced higher metamorphic conditions than west Dabie. From thin section observations it is clear that samples from the east contain less inclusions than from the west. Pressure conditions in East Dabie were probably higher than in West Dabie, resulting in fresher eclogites. In addition, retrograde metamorphism had a stronger effect in eastern Dabie. Sample 07WH07 (Figure 5.1a) shows fresh garnet, whereas sample 07XX20 (Figure 5.3a) contains inclusions of quartz, zircon, rutile, etc. This makes the selection for Lu-Hf dating more complicated for the western samples.

Clinozoisite is present in sample 07XX24 (Figure 5.3b). This mineral can be stable during (U)HP metamorphism. However, it is not present in samples selected for EMP analysis and therefore not used in the mineral assemblage for thermobarometry.

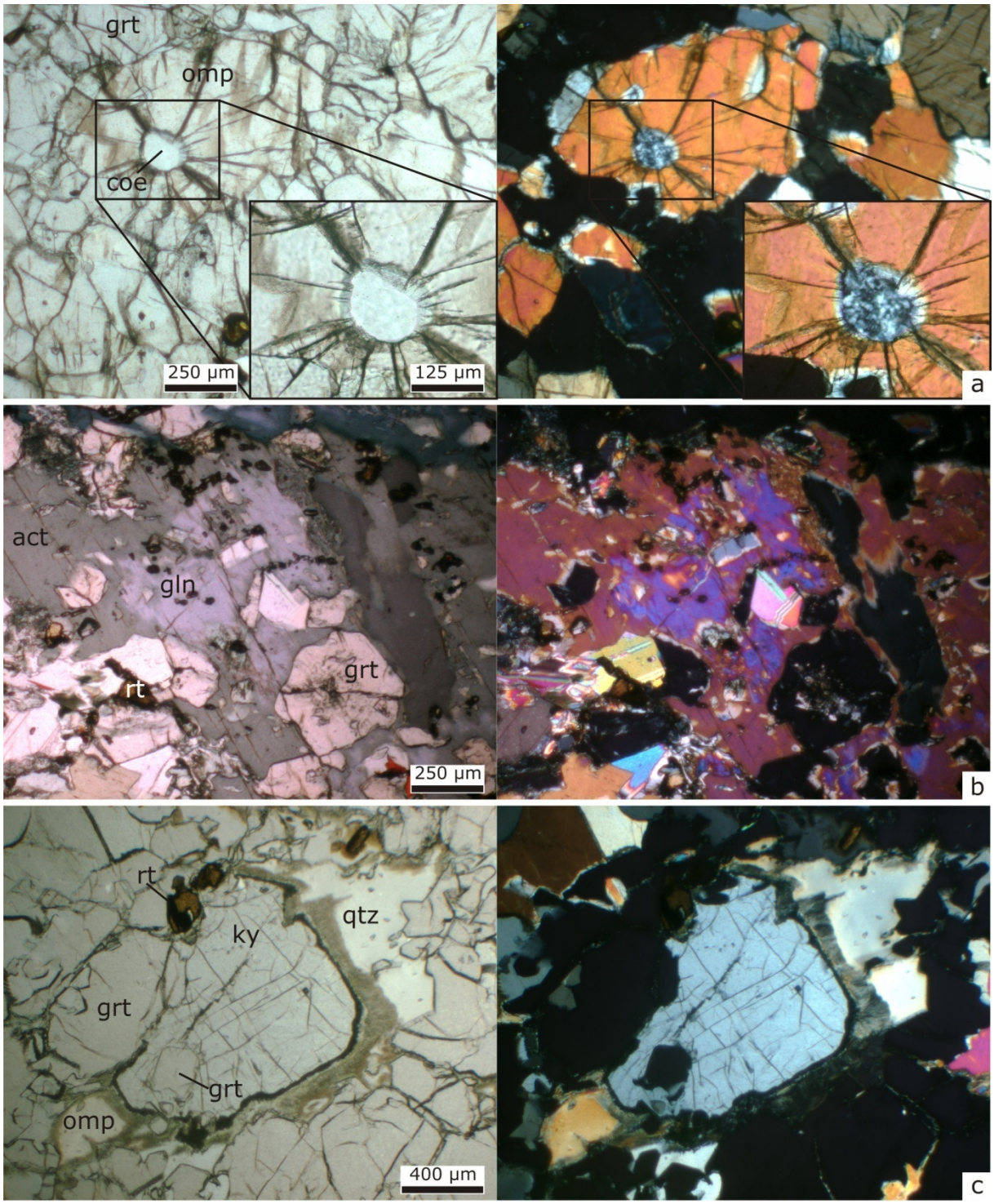

Figure 5.1 Plane polarized light on the left side and crossed nicols on the right side; a) 07WH07, coesite in omphacite, with characteristic radial cracking; b) 07HA11, eclogite with amphibole including a glaucophane core and actinolite rim. Actinolite is formed as retrograde product during a later stage, after garnet and omphacite were stable; c) 07XX24, eclogite with kyanite surrounded by symplectite.

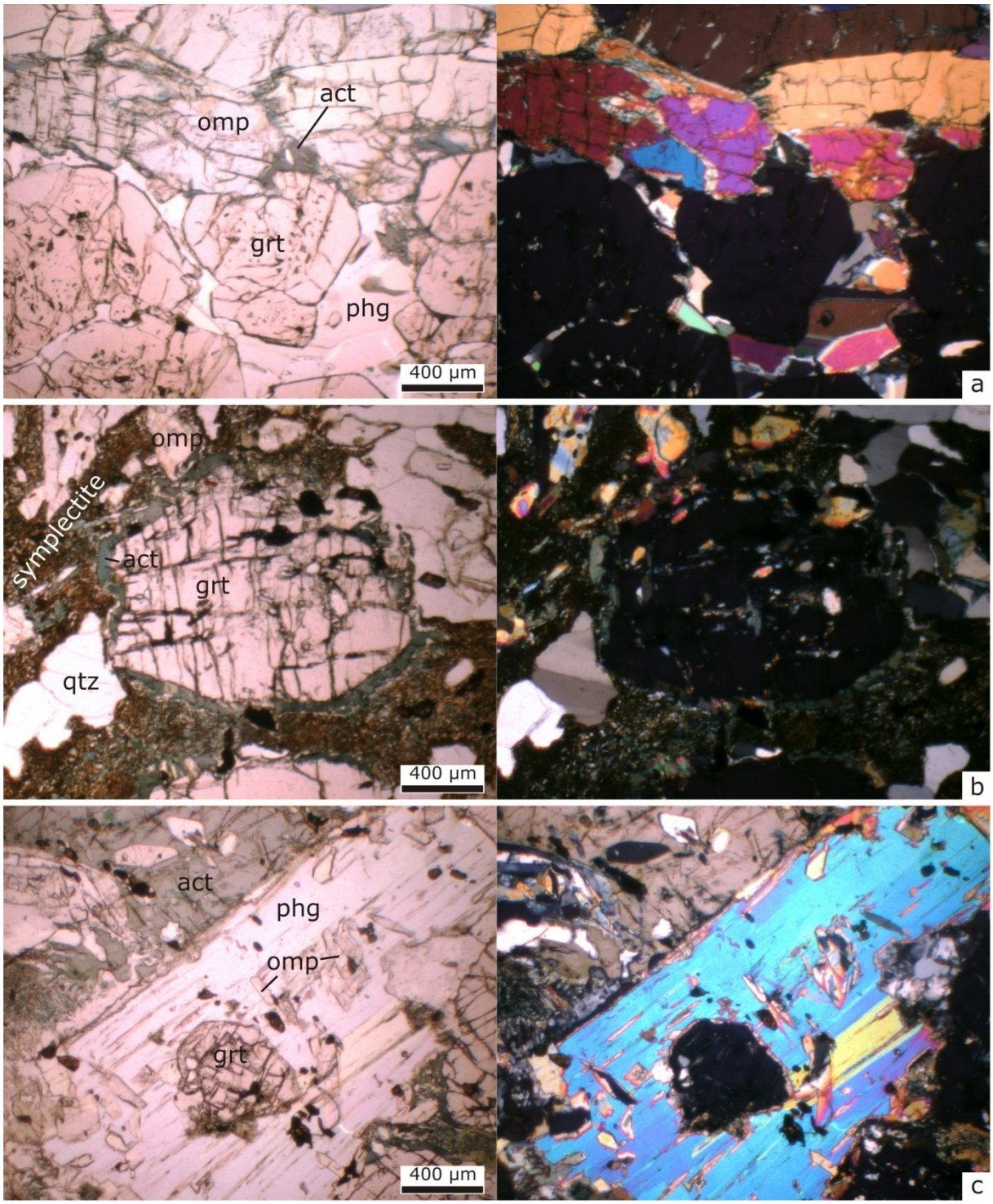

Figure 5.2 Plane polarized light on the left side and crossed nicols on the right side; a) 07XD01, banded eclogite with a layer of garnet and phengite beneath a layer of omphacite with retrograde actinolite rims; b) 07XX20, garnet with rims replaced by actinolite and mantled by symplectite; c) 07XX20, large phengite (~2.5 mm) with inclusions of garnet and omphacite.

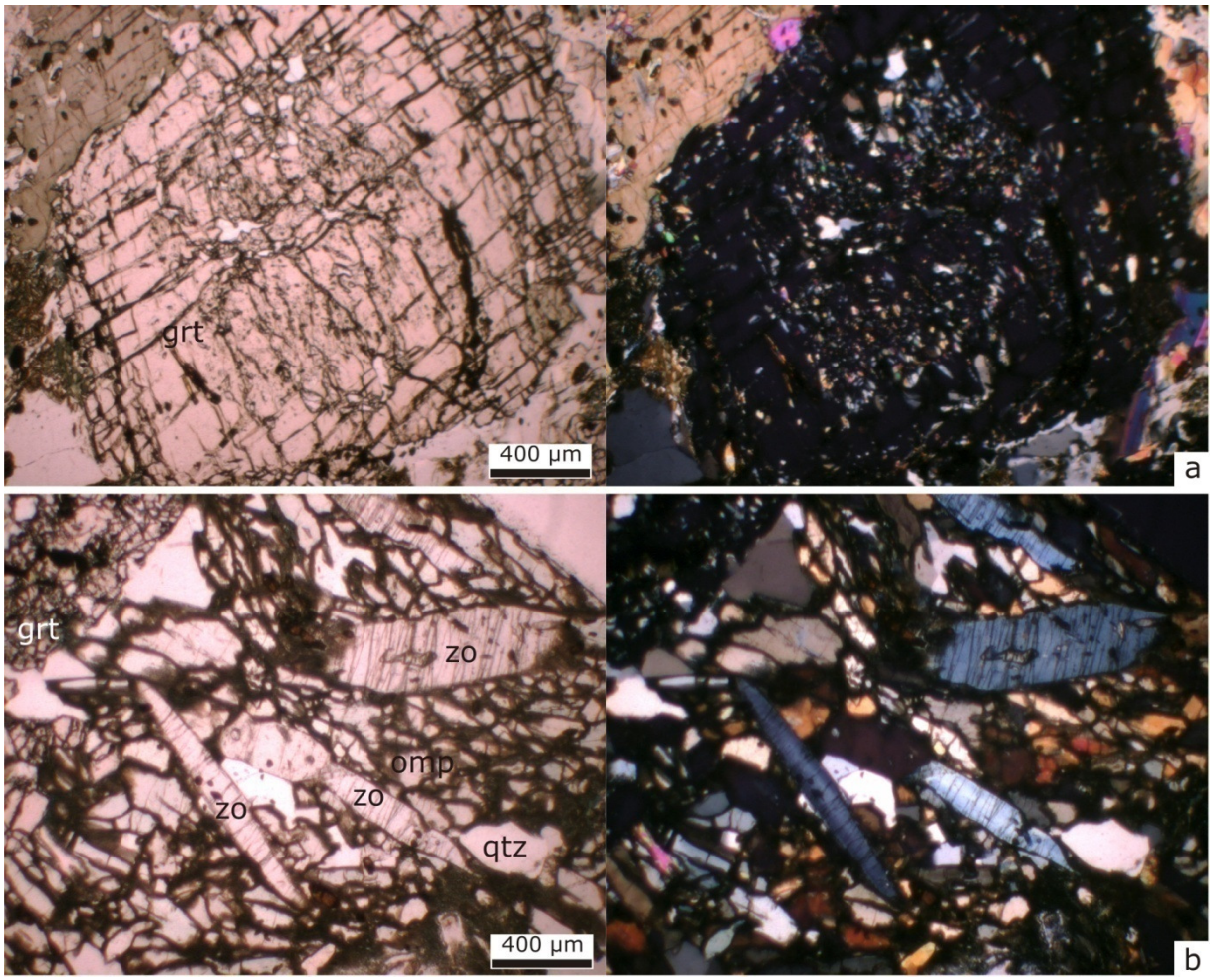

Figure 5.3 Plane polarized light on the left side and crossed nicols on the right side; a) 07XX20, very large (>2 mm) cracked garnet with inclusions of quartz, omphacite, rutile; b) 07XX24, eclogite with zoisite surrounded by omphacite.

5.1.2 Amphibolite

Five samples of the selection are categorized as amphibolite. The major minerals are amphibole (actinolite, hornblende), plagioclase and quartz. Rutile and opaque minerals are present as accessory minerals. Two samples, 07TH03 and 07XX06, contain garnet and are therefore called garnet-amphibolite. As shown in Figure 5.2b, garnet crystals have a rim of actinolite, due to the reaction of garnet with matrix. This is an early stage of retrogression, which can develop into complete replacement of garnet. Symplectite formed after the breakdown of pyroxene. Figure 5.4a shows a vein-like structure of actinolite + plagioclase symplectite. Phengite is most probably a secondary mineral, crystallized as the result of a later event, whereas zoisite and epidote show evidence of cogenetic formation with the original eclogite mineral assemblage. This can be proven by the fact that phengite contains garnet and omphacite inclusions. Garnet and omphacite together with zoisite and epidote are partially replaced by amphibole, plagioclase and phengite due to retrogression.

Several types of textural and mineralogical evidence for amphibolites which have been in high-pressure stability fields are described by *Brouwer et al.* (2005). Amphibolites in this study experienced high-pressure metamorphism proven by the following features:

- The presence of some relics of the HP-assemblage garnet-omphacite-rutile (Figure 5.4b).
- Symplectite of amphibole and plagioclase, which replaces HP omphacite and garnet
- Relic, resorbed garnet grains, mostly visible in crossed polarized light.

- Plagioclase occurs only in symplectite domains, and apparently results from the breakdown of a former high-grade assemblage.

Because actinolite is a secondary product, formed after the breakdown of high-pressure minerals, this mineral will be used for argon dating trying to date retrograde metamorphism.

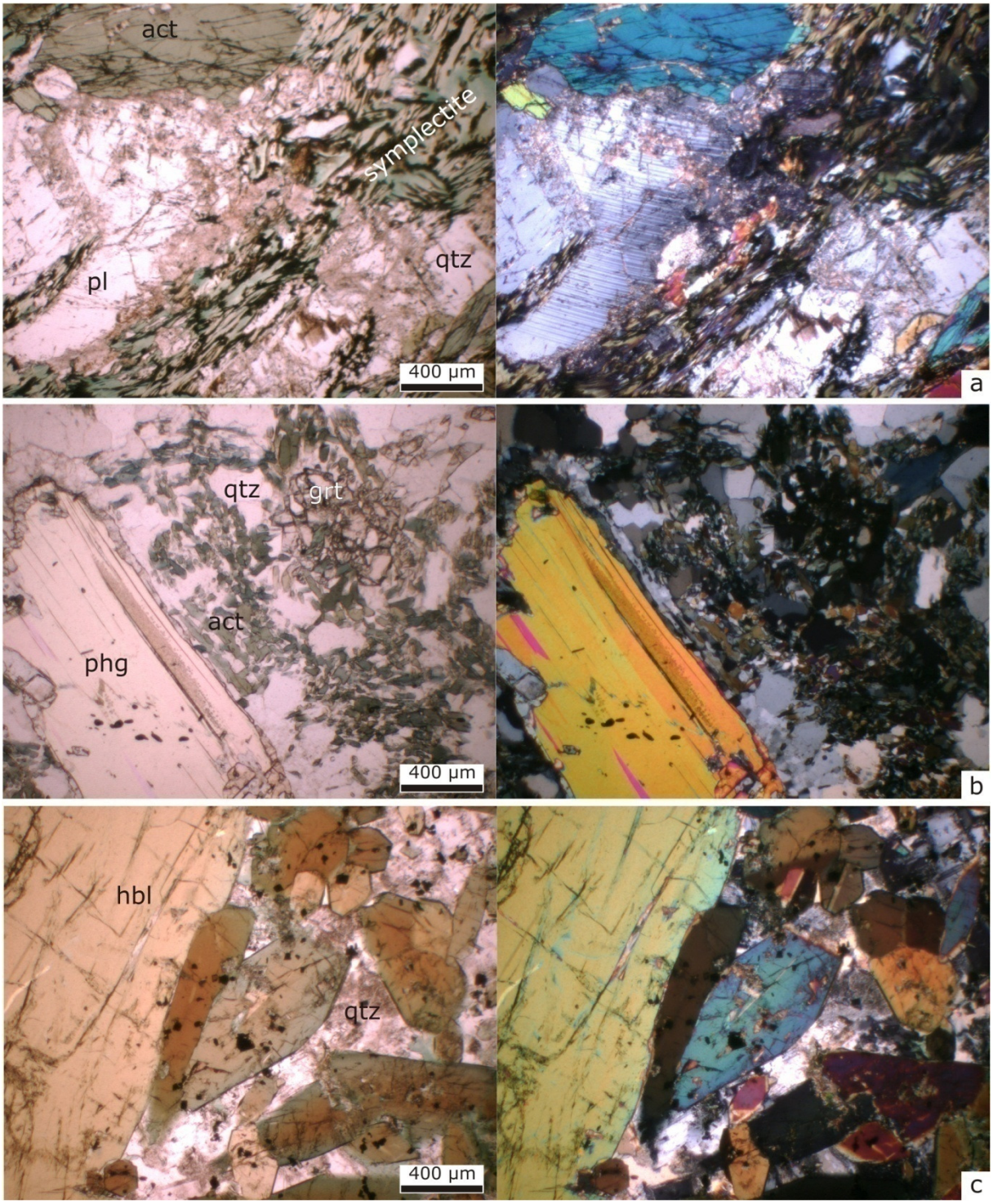

Figure 5.4 Plane polarized light on the left side and crossed nicols on the right side; a) 07LT04, veins of symplectite of plagioclase and actinolite in amphibolite; b) 07HA01, amphibolite with large phengite, garnet is almost replaced by actinolite and quartz; c) 07XX23, mafic dyke, which contains hornblende with many opaque inclusions.

5.1.3 Gneiss

Most outcrops in Dabie Shan are dominated by gneiss. This basement rock type can be found within different formations (Appendix I). In the selection only two gneiss samples are included; 07HA02 and 07LT01, both categorized as orthogneiss. Deformation of felsic intrusive bodies, like the abundant granite intrusions, has resulted in gneiss. The selected gneiss is composed of quartz, plagioclase, K-feldspar, biotite and hornblende. Plagioclase crystals are very large compared to the other minerals. Phengite, present in bands, is probably the product of HP-metamorphism. When the eclogite boudins were subducted, the relative light basement was subducted as well.

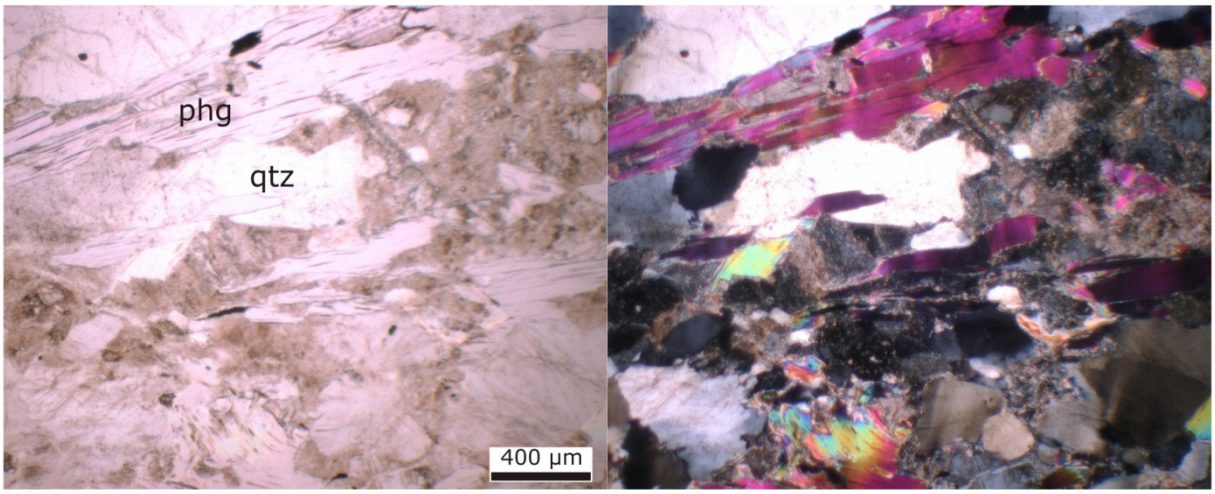

Figure 5.5 Plane polarized light on the left side and crossed nicols on the right side; 07HA02, gneiss. Very fresh phengite in a mottled matrix; suitable for Argon dating.

5.2 Microprobe data

The Electron Microprobe (EMP) is used in order to obtain the composition of different minerals present in the samples 07HA11, 07WH07, 07XD01 and 07YS04. A complete overview of the results is given in Appendix IV. Table 5.1 shows the detected oxides (including F and Cl) per mineral. Error values are not mentioned, because a standard value of 2% is taken for every measurement. The error for EMP analysis can be reduced using offline corrections to a level of about 0.5%, but to be sure of reliable modelling results a higher error is used.

The results are used for further PT-modelling, using the program Thermocalc. This will be described in Section 6.1, together with the output of the models.

	Grt	**Cpx**	**Phg**	**Amp**	**Fsp**
SiO_2	√	√	√	√	√
TiO_2	√	√	√	√	
Al_2O_3	√	√	√	√	√
Cr_2O_3	√	√	√	√	
FeO	√	√	√	√	√
MnO	√	√	√	√	
MgO	√	√	√	√	
CaO	√	√	√	√	√
Na_2O	√	√	√	√	√
K_2O			√	√	√
BaO			√		√
SrO					√
F			√	√	
Cl			√	√	

Table 5.1 Oxides measured on the EMP for the different minerals. Grt = garnet, Cpx = clinopyroxene, Phg = phengite, Amp = amphibole, Fsp = feldspar.

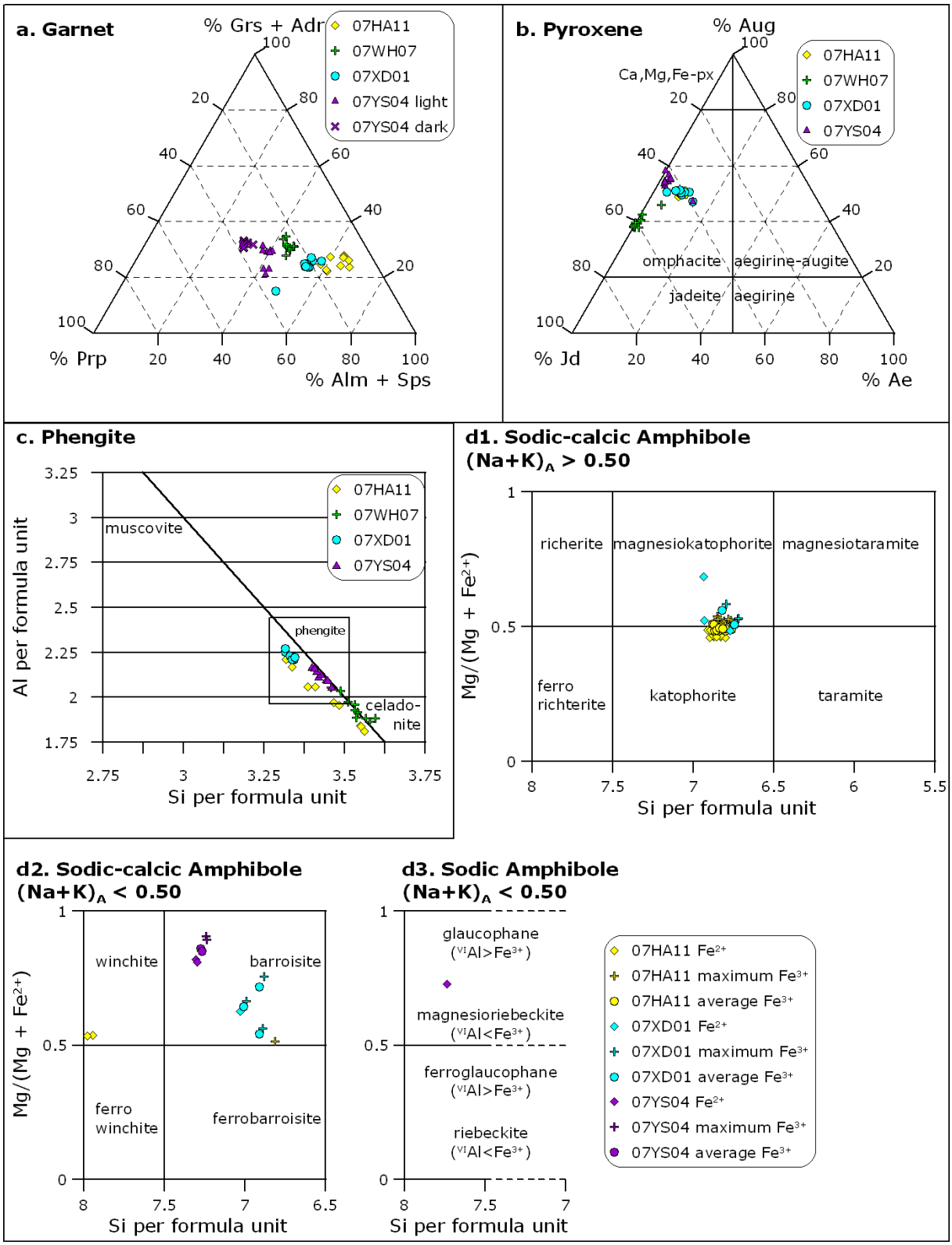

Figure 5.6 Mineral chemistry a) Ternary plot of garnet compositions. b) Ternary plot of pyroxene compositions. c) Phengite chemistry – compositional variation of white micas. d) Amphibole compositions – d1 sodic-calcic amphiboles (Na + K > 0.5 p.f.u.); d2 sodic-calcic amphiboles (Na + K < 0.50 p.f.u.); d3 sodic amphiboles (Na + K < 0.50 p.f.u.).

5.2.1 Garnet

Figure 5.6a shows a ternary diagram for all garnet EMP analyses. Per sample, the general composition of garnet is $Alm_{57-64}Adr_{0-1}Grs_{22-28}Prp_{8-17}Sps_{0-3}$ (07HA11), $Alm_{47-58}Adr_{3-7}Grs_{10-24}Prp_{16-36}Sps_{0-3}$ (07XD01), $Alm_{36-42}Adr_{0-1}Grs_{21-31}Prp_{30-36}Sps_{0-1}$ (07YS04, light), $Alm_{29-33}Adr_{0-}$

$_1Grs_{30-33}Prp_{35-38}Sps_{0-1}$ (07YS04, dark) and $Alm_{41-45}Adr_{0-7}Grs_{25-32}Prp_{22-26}Sps_{0-1}$ (07WH07). Each sample is clustered together, except for 07YS04 with light-coloured garnet. It is remarkable that the pyrope contribution is higher for the samples in East Dabie.

5.2.2 Omphacite
As expected, all pyroxene analyses plot within the omphacite field (Figure 5.6b). However, clusters of each sample are still visible. The composition of pyroxene consist mainly of a combination of jadeite and augite.

5.2.3 Phengite
White micas show a small variation in number of Si cations and Al cations per formula unit. Except for one sample, the composition of each sample is clustered. 07XD01 and 07YS04 plot within the phengite field (Figure 5.6c).

5.2.4 Amphibole
Amphibole is the most complicated mineral in this study to categorize. Following the procedure described by *Leake et al.* (1997) ferric iron numbers can be calculated by four different methods; no ferric iron, minimum, maximum and average number of ferric iron. The result of using the minimum number of ferric iron is equal to the results of no ferric iron. Amphibole compositions plot within three different diagrams. However, the majority plots in the field of sodic-calcic amphiboles (Figure 5.6d1), $(Na+K)_A > 0.5$, which is a type of actinolite. The rest of the compositions plot within the sodic-calcic amphibole field (Figure 5.6d2), $(Na+K)_A < 0.5$.

5.2.5 Results obtained by thermodynamic modelling
The results obtained by thermodynamic modelling are listed in Table 5.2 & Table 5.3, and are divided in two different sections. The first table shows the results obtained with Thermocalc version 3.25. The second table contains the results produced by the most recent version (3.31) of Thermocalc.

Parameters are calculated for all samples using version 3.25, based on a mineral assemblage of Grt-Omp-Phg-Ky-Coe-H_2O. The independent set of reactions consist for almost all calculations of three different reactions:

- Grs + Alm + 2Coe = 3Hed + 2Ky (5.1)
- 2Grs + Prp + 3Cel = 6Di + 3Ms (5.2)
- 2Grs + Alm + 3Cel = 3Di + 3 Hed +3Ms (5.3)

- 3Grs + 2Alm + 3Cel = Prp + 6Hed + 3Ms (5.4)

The latter is calculated for 07WH07 instead of reaction 5.3.
Kyanite is only present in sample 07YS04. However, it is used in the mineral assemblage of all samples due to problems with Thermocalc when kyanite is omitted. The results are also shown in a PT-diagram (Figure 5.7).

Sample	ID	T (°C)	P (kbar)	sdT	sdP	Sigfit	T(a-x)	Comments
07XD01 core	1c	613	22.4	42	2.0	0.25	700	2% SD for input,
	3c	626	20.0	50	2.4	1.30	700	Stoichiometric calculated
07XD01 rim	1r	618	21.4	40	1.8	0.28	700	ferric iron
	3r	607	22.4	39	1.9	0.02	700	
07WH07 core	1c	566	34.5	76	4.3	0.80	800	Thermocalc calculated
	2c	622	38.6	84	5.3	0.92	900	SD for input,
	3c	673	41.3	97	6.2	1.09	900	Stoichiometric calculated
	4c	731	43.2	107	6.7	0.73	800	ferric iron
	5c	591	42.1	130	9.3	1.76	900	
07WH07 rim	1r	684	37.7	95	5.4	0.82	900	
	2r	613	36.3	81	4.8	0.91	900	
	3r	731	36.0	108	5.7	0.53	900	
	4r	620	37.4	83	5.1	0.57	900	
	5r	630	40.7	122	7.7	1.46	900	
07HA11 core	1c	384	18.1	38	1.5	0.71	700	2% SD for input,
	2c	318	20.8	38	1.9	1.31	700	Stoichiometric calculated
	3c	361	15.3	37	1.3	0.97	700	ferric iron
	4c	441	25.3	59	3.5	2.00	700	
	5c	476	17.4	62	2.5	1.73	700	
07HA11 rim	1r	408	22.8	71	4.2	2.79	700	
	3r	475	22.5	55	3.0	1.82	700	
	4r	403	18.2	33	1.4	1.05	700	
	5r	464	21.7	31	1.6	0.88	700	
07YS04 core/dark	1cd1	821	35.4	166	9.2	2.36	800	Thermocalc calculated
	2cd1	850	35.4	160	8.6	2.10	800	SD for input,
	3cd1	879	31.1	202	9.4	2.44	800	Stoichiometric calculated
07YS04 rim/dark	1rd1	873	33.6	140	7.0	1.76	800	ferric iron
	2rd1	887	34.9	205	10.5	2.48	800	
	3rd1	822	34.1	174	9.3	2.38	800	
07YS04 core/light	1cl1	685	28.5	125	7.1	1.92	800	
	2cl1	752	31.8	117	6.3	1.65	800	
	3cl1	737	27.7	137	6.4	1.86	800	
07YS04 rim/light	1rl1	719	26.5	95	4.9	1.33	800	
	2rl1	782	31.3	155	8.0	2.03	800	
	3rl1	696	30.4	120	6.3	1.79	800	

Table 5.2 PT-results for Thermocalc modelling, using version 3.25.

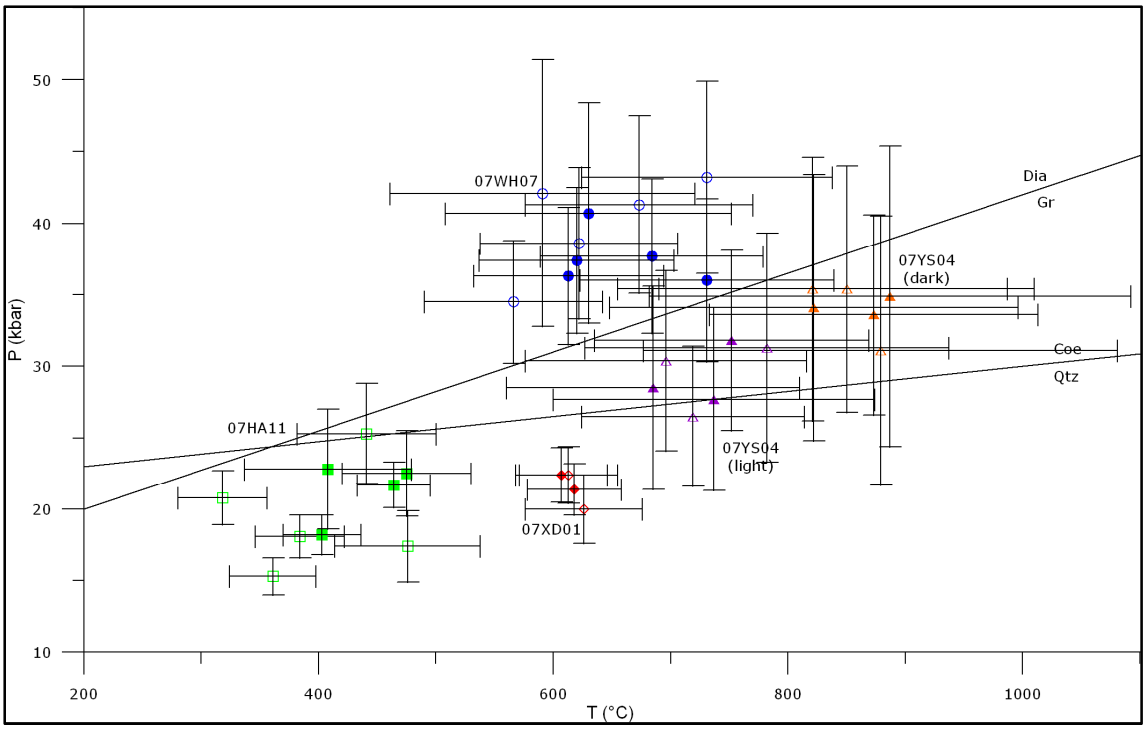

Figure 5.7 PT-diagram showing all Thermocalc (v. 3.25) modelling results. The filled symbols represent the conditions of the rim of the crystals, the open symbols represent the core of the crystals. For sample 07YS04 (purple and orange triangles) two different generations of garnet are used. Dia-Gr and Coe-Qtz reaction lines taken from *Sajeev and Santosh* (2006).

Although the error on PT-estimates of two samples (07WH07 and 07YS04) is very high, all samples plot within a distinctive PT-range. Samples 07XD01 and 07HA11 were subjected to lower pressure conditions (20 and 15-25 kbar, respectively) compared to the other two samples. These are also the two samples with the lowest temperature conditions. Samples 07YS04 and 07WH07 were subjected to ultrahigh-pressure metamorphism, which is in agreement with the models that West Dabie is overprinted by stronger lower pressure. In general there is no systematic difference between the core and rim of crystals. However, there is more a remarkable difference in the PT-estimates of the dark- and light-coloured garnet crystals of sample 07YS04. This implies the existence of more than one generation of garnet.

However, since an update version of the Thermocalc website is online, compatible input files for Thermocalc version 3.31 are available. Therefore it is possible to calculate PT-conditions for a mineral assemblage without kyanite. Input files are composed of three separate mineral sections of garnet, omphacite and phengite. The input for garnet and phengite is not changed, whereas the omphacite input is recalculated for a NCAFF^{3}MAS system; ferric iron is represented by acmite. In Section 3.3.2 input parameters and equations are described. The number of possible reactions is much higher when Alm, Prp, Grs, Jd, Di, Hed, Acm, Omp, Ms, Pg, Cel, Coe, Qtz and H_2O are included as endmembers. Therefore the set of independent reactions calculated by Thermocalc is extended by 5 reactions for each run. The results are listed in Table 5.3 and plotted in two PT-diagrams (Figure 5.8 & Figure 5.9).

Sample	ID	T (°C)	P (kbar)	sdT	sdP	Sigfit	T(a-x)	Comments
07XD01 core	1c	448	27	91	0,9	3,52	700	Thermocalc calculated
	3c	519	27,3	96	0,8	3,07	700	SD for input,
07XD01 rim	1r	478	27,2	91	0,8	3,3	700	Stoichiometric calculated
	3r	456	27,1	91	0,8	3,48	700	ferric iron
07WH07 core	1c	562	27,8	43	0,3	0,75	700	Thermocalc calculated
	2c	-	-	-	-	-	-	SD for input,
	3c	-	-	-	-	-	-	Stoichiometric calculated
	4c	-	-	-	-	-	-	ferric iron
	5c	-	-	-	-	-	-	
07WH07 rim	1r	-	-	-	-	-	-	
	2r	535	27,6	49	0,4	1,37	700	
	3r	593	27,8	77	0,5	1,95	700	
	4r	597	27,9	48	0,3	0,5	700	
	5r	569	27,8	56	0,4	1,28	700	
07HA11 core	1c	535	27,5	105	0,7	2,56	700	Thermocalc calculated
	2c	509	27,5	67	0,5	1,69	700	SD for input,
	3c	511	27,4	107	0,7	2,81	700	Stoichiometric calculated
	4c	520	27,5	65	0,4	1,6	700	ferric iron
	5c	479	27,2	99	0,8	3,22	700	
07HA11 rim	1r	656	28,1	59	0,4	1,05	700	
	3r	593	27,7	95	0,6	2,2	700	
	4r	521	27,4	101	0,7	2,7	700	
	5r	569	27,6	88	0,6	2,16	700	
07YS04 core/dark	1cd1	619	27,9	86	0,7	2,45	700	Thermocalc calculated
	2cd1	625	27,9	90	0,7	2,54	700	SD for input,
	3cd1	-	-	-	-	-	-	Stoichiometric calculated
07YS04 rim/dark	1rd1	677	28,1	97	0,7	2,4	700	ferric iron
	2rd1	646	27,9	102	0,8	2,79	700	
	3rd1	640	28	88	0,7	2,38	700	
07YS04 core/light	1cl1	610	27,8	65	0,6	2,01	700	
	2cl1	603	27,8	74	0,6	2,17	700	
	3cl1	-	-	-	-	-	-	
07YS04 rim/light	1rl1	637	27,9	75	0,6	1,99	700	
	2rl1	610	27,8	85	0,7	2,43	700	
	3rl1	601	27,8	66	0,5	1,89	700	

Table 5.3 PT-results for Thermocalc modelling, using the most recent version 3.31

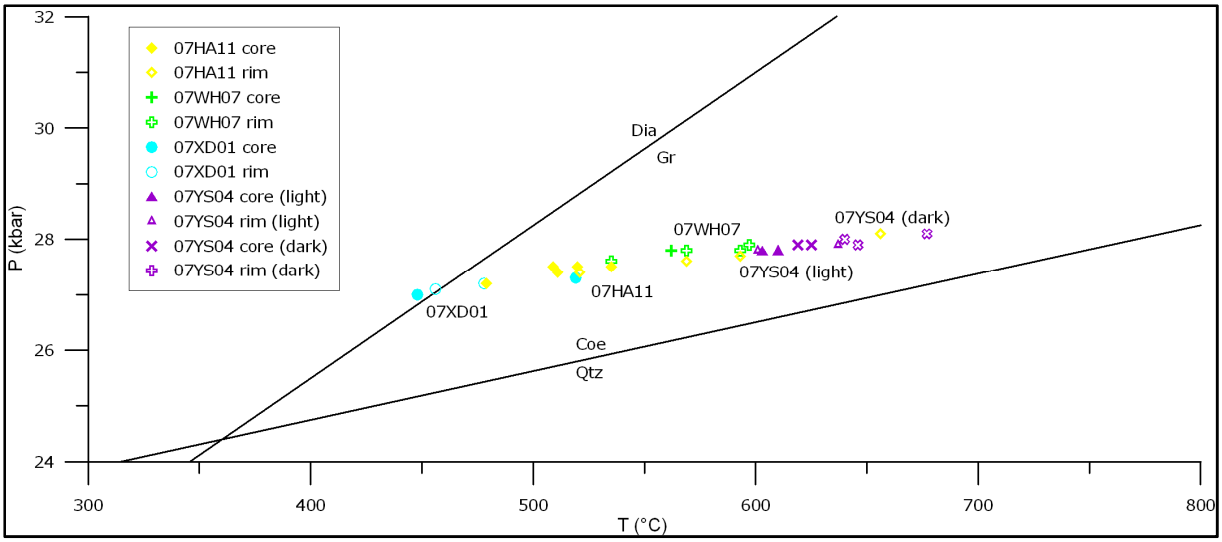

Figure 5.8 PT-diagram showing all Thermocalc (v. 3.31) modelling results. The filled symbols represent the conditions of the core of the crystals, the open symbols represent the rim of the crystals. For sample 07YS04 (purple and orange triangles) two different generations of garnet are used. Dia-Gr and Coe-Qtz reaction lines taken from *Sajeev and Santosh* (2006).

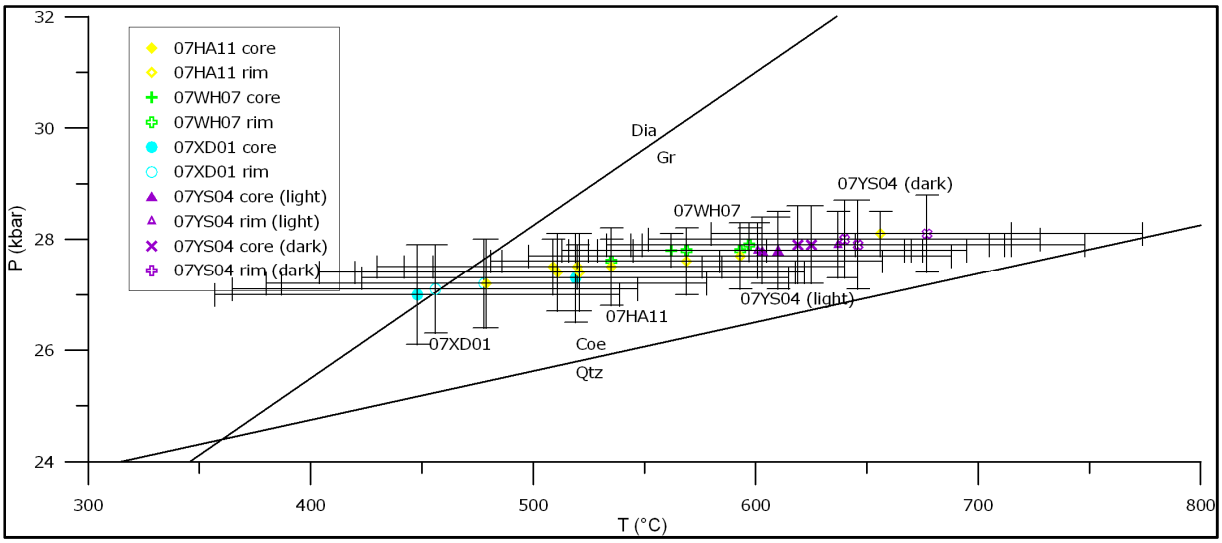

Figure 5.9 PT-diagram showing all Thermocalc (v. 3.31) modelling results, including error bars. The filled symbols represent the conditions of the core of the crystals, the open symbols represent the rim of the crystals. For sample 07YS04 (purple and orange triangles) two different generations of garnet are used. Dia-Gr and Coe-Qtz reaction lines taken from *Sajeev and Santosh* (2006).

The variation in pressure is reduced with a factor ten compared to the results of the older version. The pressure of all samples lies around 27.5 kbar. The strong consistency argues for better reliable data compared to the first results obtained with version 3.25. The error bars are reduced as well; the average error is approximately ±0.7 kbar. The variation in temperature is still high, but the absolute values are higher for the coldest sample, and lower for the hottest sample. The temperature varies between 450 and 700°C instead of 300 and 900°C, which is an expected temperature range for these rocks.

The most remarkable observation is that the results of each sample are still clustered. Samples from West Dabie still plot on the colder side, whereas East Dabie shows the highest temperatures.

In contrast with version 3.25 the most recent version of Thermocalc calculates the standard deviation for its given input. There is no possibility to give up own sd value based on the 2% error obtained by EMP analysis, which resulted in lower error bars for version 3.25. However, the error bars for pressure are already very low, even below the lower limit.

5.3 Lu-Hf isotopic data

Four samples seem suitable for Lu-Hf dating, because they contain fresh garnet and omphacite. These are the same four samples used for Microprobe analysis, to be able to link ages with PT-information. The rest of the samples are used for Argon dating of actinolite, hornblende, phengite, biotite and K-feldspar.

In Table 5.4 results for Lu-Hf isotopic measurements are given. For each sample three different garnet batches plus one clinopyroxene batch are measured. The second and fourth columns show the errors on the isotopic ratios (2 s.e.).
Because of an unexpected extremely low Hf content of the Grt samples, all the garnet separates are overspiked. Although a correction can be applied, the results get higher errors. Because these samples have undergone a very complicated metamorphic history, the results obtained are still very valuable.
The isotopic ratios are used to calculate an age. This is done with the program Isoplot (Microsoft Excel® add-on), based on the isochron method (Section 3.6.1).

Sample	Min.	$^{176}Lu/^{177}Hf$	± 2 s.e.	$^{176}Hf/^{177}Hf$	± 2 s.e.	Lu (ppm)	Hf (ppm)
07WH07	Grt	10.27682341	0.05138412	0.32990020	5.80624E-05	0.735	0.010
	Grt	8.89414395	0.04447072	0.32011722	5.18590E-05	0.724	0.011
	Grt	1.25400716	0.00627004	0.28765928	2.38757E-05	0.729	0.080
	Cpx	0.07001868	0.00035009	0.28219541	1.52386E-05	0.042	0.081
07XD01	Grt	2.04970195	0.01024851	0.29304751	2.13925E-05	0.654	0.044
	Grt	1.98980013	0.00994900	0.29285789	5.00787E-05	0.648	0.045
	Grt	1.83655872	0.00918279	0.29147253	2.04031E-05	0.620	0.046
	Cpx	0.00416565	0.00002083	0.28303459	1.40000E-05	0.015	0.482
07YS04	Grt	1.93889314	0.00969447	0.29091136	3.98549E-05	0.303	0.021
	Grt	2.95085479	0.01475427	0.29784102	3.39539E-05	0.303	0.014
	Grt	2.44205806	0.01221029	0.29374494	5.61053E-05	0.302	0.017
	Cpx	0.01896255	0.00009481	0.28281262	1.72516E-05	0.013	0.095
07HA11	Grt	31.79582988	0.15897915	0.42705798	7.25999E-05	2.286	0.010
	Grt	29.41350046	0.14706750	0.41369710	7.77751E-05	3.256	0.016
	Grt	45.47323123	0.22736616	0.48142691	6.83626E-05	2.310	0.007
	Cpx	0.08691218	0.00043456	0.28304837	1.61338E-05	0.075	0.119

Table 5.4 $^{176}Lu/^{177}Hf$ and $^{176}Hf/^{177}Hf$ isotopic data with error, measured on the Neptune (MC-ICPMS)

All Lu-Hf results from the Neptune are used for isochron calculation with Isoplot. The isochrons are based on four points; 1 Cpx- and 3 Grt-points. Appendix II.d shows the location of the samples (indicated by red triangles); two samples (07XD01 and 07HA11) are taken from West Dabie, the other two (07YS04 and 07WH07) were collected in East Dabie.

Figure 5.10 shows four diagrams representing the ages of the eclogites. *Scherer et al.* (2000) tried to define the closure temperature (T_C) for garnet crystals. This is done by using the already defined T_C of the Sm-Nd system, the cooling rate and the difference in age obtained by the Sm-Nd and Lu-Hf systems. An estimated closure temperature range of 540-700°C is found, mainly dependent on the size of garnet crystals; the radius of the garnets analysed is 0.24 mm – 4 cm. The garnets used in this study are 2 mm or smaller, which argues for a T_C close to 540°C. When this temperature is exceeded during metamorphism the system is expected to be open when peak conditions are reached.

All the ages plot within the Triassic Period, but two samples (HA and WH) show Middle Triassic ages, whereas the other two (XD and YS) show Early Triassic ages. Note that the rather high error largely due to overspiking caused by the surprisingly low [Hf] in garnet (average 33 Ma, 2σ) makes it difficult to compare the data. However, beside the Isoplot method all the results were age corrected using an estimated age of 220 Ma. The results for every garnet crystal agree with the Isoplot age, which enforces the value of the models. The reason for very extreme high εNd values can be explained by the fact that the samples are overspiked, but this does not affect the age result.

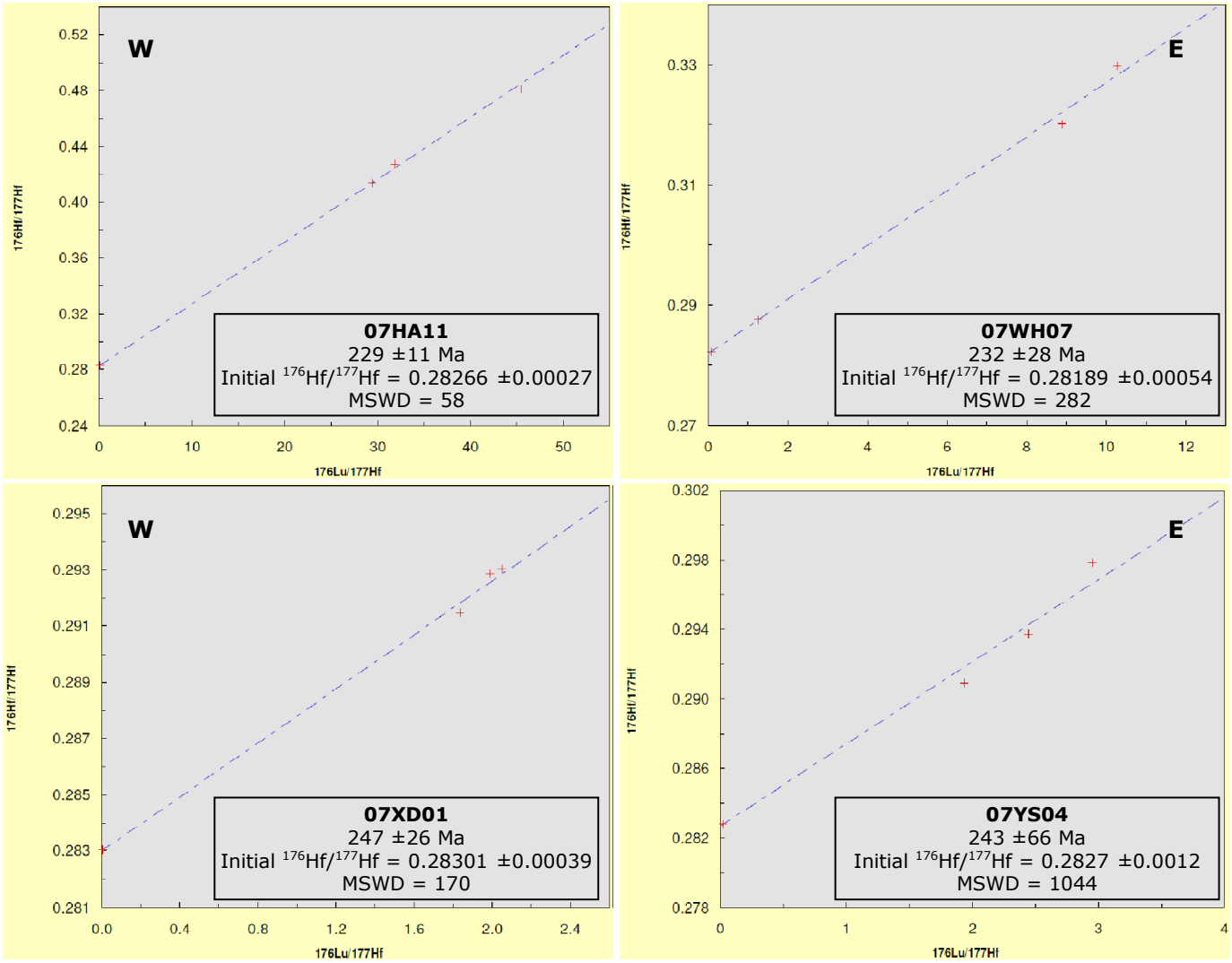

Figure 5.10 4-point isochron showing the age based on the Lu-Hf dating method. Samples in the left are collected in West Dabie, on the right in East Dabie.

5.4 Argon age calculations

Table 5.5 shows all results obtained by $^{40}Ar/^{39}Ar$ geochronology. For the micas duplicates were run and afterwards the two data points are combined, therefore these samples show 3 results. Results marked in bold are the most reliable ages for each calculation, based on the plateau and isochron plots (Appendix VI). Some of the age plateaus show a nice correlation and are therefore sometimes interpreted as a weighted plateau, even when these are indicated as an error plateau by the program. Errors are not always very large. The same is true for normal isochrons. EA denotes the samples that are probably affected by excess argon. A complete overview per sample showing the plateaus and tables is given in Appendix VI.

Sample	Material	Comment	ID #1	ID #2	Plateau age (Ma)	Error (2σ)	Type	Normal isochron age (Ma)	Error (2σ)	Type	
07HA01	Phengite	1st run	D15	M267	141.02	±47.16	EP	200.96	±152.39	EC	
07HA01	Phengite	2nd run	D15	M362	**211.96**	**±6.73**	WP	259.05	±92.29	EC	
07HA01	Phengite	combi	D15	-	**159.03**	**±3.94**	WP	295.01	±153.21	EC	
07HA02	Phengite	1st run	D16	M268	**189.43**	**±3.31**	EP	192.75	±5.37	NC	
07HA02	Phengite	2nd run	D16	M363	**188.31**	**±1.98**	EP	188.14	±3.97	NC	
07HA02	Phengite	combi	D16	-	**188.07**	**±2.26**	EP	187.36	±2.52	NC	
07HA11	Actinolite		D5	M312	395.32	±8.73	EP	**393.82**	**±13.48**	NC	EA
07LT01	Biotite	1st run[1]	D18	M261	144.50	±25.46	EP	115.80	±18.61	NC	
07LT01	Biotite	1st run[2]	D18	M261	**119.90**	**±1.21**	WP	120.66	±1.74	NC	
07LT01	Biotite	2nd run	D18	M356	**118.02**	**±1.09**	WP	117.42	±1.68	I	
07LT01	Biotite	combi	D18	-	**119.21**	**±1.15**	EP	117.52	±1.45	NC	
07LT01	Hornblende		D8	M314	**122.16**	**±1.16**	EP	122.72	±1.27	NC	
07LT01	K-feldspar		D10	M251	127.07	±3.23	EP	**118.13**	**±5.35**	NC	EA
07LT04	Actinolite		D9	M315	**128.45**	**±1.72**	EP	124.26	±4.62	NC	EA
07TH03	Biotite	1st run	D20	M262	**212.34**	**±3.48**	EP	215.69	±3.59	NC	
07TH03	Biotite	2nd run	D20	M357	**215.54**	**±2.61**	EP	215.03	±3.29	NC	
07TH03	Biotite	combi	D20	-	**214.37**	**±2.18**	EP	214.53	±2.67	NC	EA
07XD01	Actinolite		D6	M313	802.94	±70.09	EP	**545.73**	**±32.89**	EC	EA
07XD04	Phengite	1st run	D17	M269	**322.83**	**±4.86**	EP	319.67	±10.70	NC	
07XD04	Phengite	2nd run	D17	M364	**329.31**	**±19.27**	EP	364.26	±14.76	NC	
07XD04	Phengite	combi	D17	-	315.05	±20.84	EP	273.00	±8.12	NC	
07XX06	Actinolite		D3	M310	524.80	±51.00	EP	**453.99**	**±39.90**	NC	EA
07XX20	Actinolite		D2	M308	719.18	±78.07	EP	**495.33**	**±74.33**	EC	EA
07XX20	Phengite	1st run	D11	M264	**203.95**	**±5.48**	EP	203.93	±8.90	NC	
07XX20	Phengite	2nd run	D11	M358	281.05	±23.52	EP	153.16	±276.54	NC	EA
07XX20	Phengite	combi	D11	-	**197.30**	**±14.84**	EP	209.50	±19.34	NC	EA
07XX23	Hornblende		D4	M311	194.33	±33.71	EP	**136.23**	**±10.74**	EC	EA
07XX24	Phengite	1st run	D12	M265	212.67	±15.75	EP	175.77	±27.13	EC	EA
07XX24	Phengite	2nd run	D12	M359	137.19	±7.56	EP	**119.50**	**±12.89**	NC	EA
07XX24	Phengite	combi	D12	-	169.84	±27.00	EP	**117.61**	**±32.92**	NC	EA
07XX29	Phengite	1st run	D14	M266	**214.20**	**±11.15**	EP	218.50	±38.72	NC	
07XX29	Phengite	2nd run	D14	M361	**211.44**	**±2.89**	EP	210.34	±7.85	NC	
07XX29	Phengite	combi	D14	-	**214.23**	**±7.76**	EP	205.50	±14.85	NC	

Table 5.5 Results of Argon measurements. For each measurement two different ages are given, a plateau age and an isochron age; the most reliable age is marked (in bold) and taken as the age of the sample. Only for the minerals analysed twice, sometimes the plateau age neither the isochron age is marked; these measurements are less reliable and not taken in account. The type of plateau or isochron is given in the columns after the ages, where EP stands for Error Plateau, WP for Weighted Plateau, EC for Errorchron, NC for No Convergence and I for Isochron. Samples influenced by excess Argon are indicated with EA.
[1]this is the result when excess argon is the dominant factor, [2]this is the 'normal' radiogenic argon result.

Chapter 6 Interpretation

6.1 PT-conditions during subduction

Thermodynamic modelling is still a very complicated process, due to a high number of possible variables. Nevertheless, it is possible to get some valuable results. The mineral assemblage used for an eclogite in equilibrium was based on mineralogical observations. Calculations with this assemblage consisting of Grt-Omp-Phg-Ky-Coe/Qtz-H_2O result in quite good results. Each sample plotted in clusters together, and East Dabie shows higher pressure and temperature results than West Dabie. However, kyanite is not present in three of the four analysed samples, which makes the results unreliable. Further analyses without kyanite in the assemblage is not possible with Thermocalc version 3.25 due to technical problems. However, calculations with version 3.31 are possible. It is assumed that mineral chemistry for omphacite is completely in disorder to be possible to calculate input parameters. This is not representative for reality, but the new results show a very high consistency for the pressure values. According to *Hacker* (2006), reasonable accurate pressures can still be obtained from phengite eclogites.
An average pressure of 27.5 kbar is obtained from all measurements. In normal subduction circumstances this pressure represents a depth of approximately 100 km. This also suggests that both West and East Dabie experienced ultrahigh-pressure metamorphism. The only difference between the samples from East and West Dabie is the experienced temperature during metamorphism. West Dabie is exposed to temperatures 200°C lower than East Dabie. However, according to large error bars (~80°C), the results still overlap. Although each sample is clustered, the difference in temperature between the samples is less clear. Sample 07HA11 is well dispersed over the total temperature range and even plot on the 'hot side' at 650°C.

6.2 Age of eclogites

All samples show Triassic metamorphism. Two samples from East Dabie, 07WH07 and 07YS04 show 232 ±28 Ma and 243 ±66 Ma, respectively. Two samples from West Dabie, 07HA11 and 07XD01 show a comparable signal of 229 ±11 Ma and 247 ±26 Ma, respectively. The difference of 20 m.y. is smaller than the average error, suggesting that these samples recorded the same metamorphic event.
The western samples are collected in the vicinity of the suture between the Yangtze craton and the Qinling unit, whereas the eastern samples are collected more than 50 km southward from this suture. From the consistent ages it can be concluded that all samples belong to the same unit, the Yangtze craton, and therefore the most southern located suture should be drawn more to the north.
That this Triassic signal overprinted an older signal cannot obtained from these data. It is possible for both regions, East and West Dabie to have experienced more than one subduction event. Older (Lu-Hf) isotopic systems, produced by suggested Paleozoic metamorphism (e.g. *Ratschbacher et al.*, 2006) might be reset during the last event.

6.3 Age of retrogression

All the results acquired with the $^{40}Ar/^{39}Ar$ dating method are presented in two histograms (Figure 6.1), where the left histogram represents all the ages obtained by the age plateaus divided per mineral. In the right histogram the ages are divided in plateau and isochron ages.

The results on the left side of Figure 6.1 show several peaks in ages. The first peak lies around 125 Ma. Large bodies of granite intruded the basement around this time (*Ratschbacher et al.*, 2006; *Zhao et al.*, 2007). Not only the granites themselves, but due to large-scale magmatism, which caused regional heating, surrounding rocks also show these ages. A small peak is visible at 180 Ma for phengite and hornblende. For phengite and biotite a peak at 210 is visible. The same is shown in the right histogram. Note that the bars of the different methods in the right diagram are not drawn cumulatively, which would have made the peaks even higher. Whether the two peaks should be seen as two

different events is not clear. It is possible that (within error) it is the result of one subduction event of the Yangtze craton, during Triassic ages. Another explanation is that smaller units were subducted sequentially.

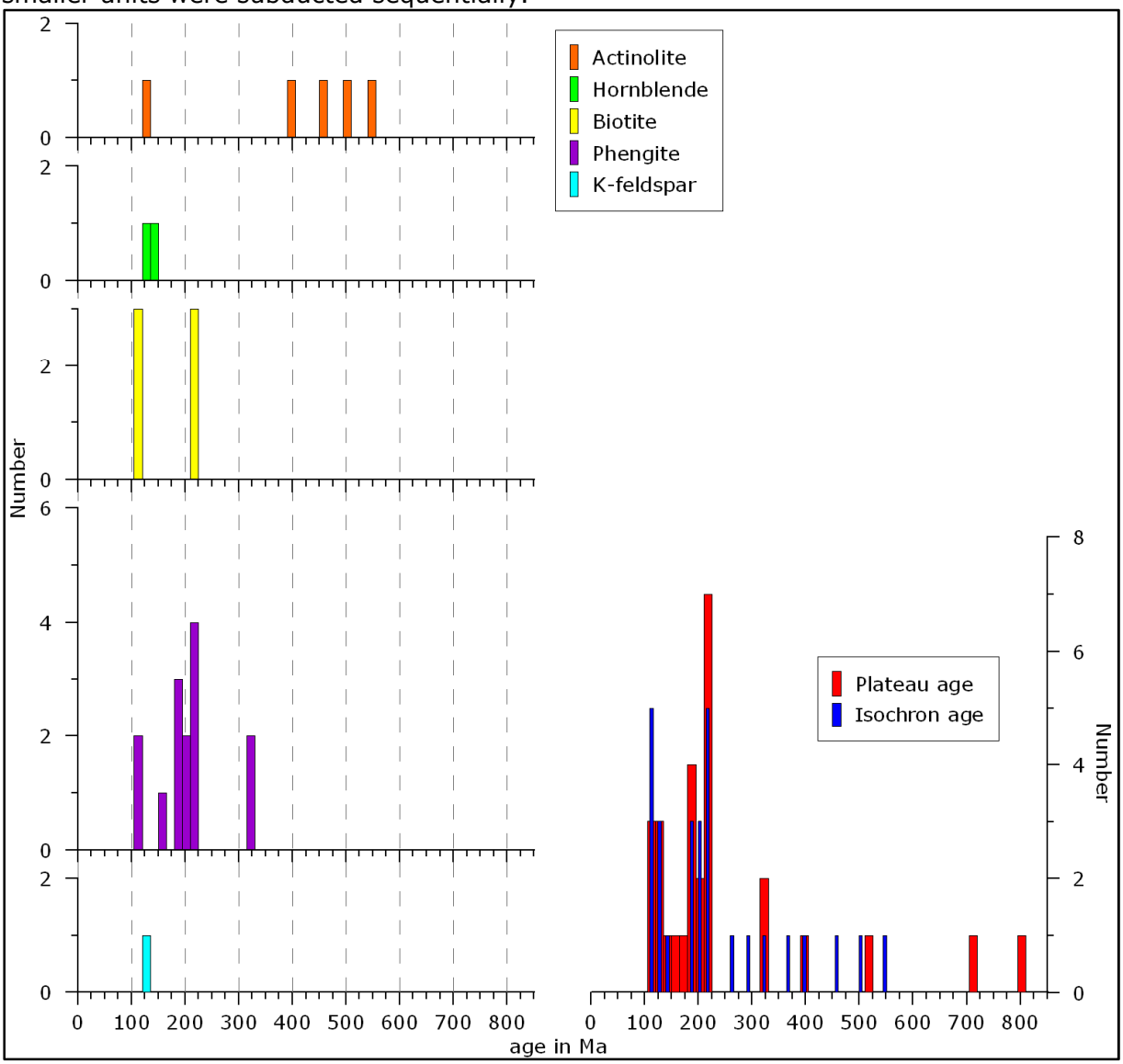

Figure 6.1 Histogram of argon results. Left: ages of samples which are marked in bold in Table 5.5, divided per mineral. Right: ages of all samples, taken from plateau or isochron. Bin size = 15 my.

The small peak around 325 Ma for phengite supports the theory of the existence of more than two events. If this age represents retrograde metamorphism of a subducted unit, the peak conditions must be reached before 325 Ma.
Actinolite shows a very dispersed age spectrum. Although corrections are already made for the effect of excess argon, the four ages at approximately 400, 450, 500 and 550 in the left diagram are difficult to interpret. The two plateau ages at 700 and 800 Ma in the right diagram are most probably reflecting an apparent age due to excess argon. According to *Qiu and Wijbrans* (2006) older ages may be the consequence of inherited argon rather than of excess argon. If the metamorphic event is short enough the argon system is not completely reset (*Qiu and Wijbrans*, 2008). However, the mobility of argon during UHP-metamorphism is still poorly understood.

Chapter 7 Discussion and conclusions

7.1 Discussion

All eclogite samples dated with the Lu-Hf method show ages indicating Triassic metamorphism. According to their pressure conditions obtained with Thermocalc's version 3.31, all samples were subducted to a minimum depth of about 100 km. We may conclude that during metamorphism the UHP eclogite facies was reached.
According to *Scherer et al.* (2000) the closure temperature of Lu and Hf in garnets varies from 540 to 700°C. This depends mainly on the size of the crystals, where the highest closure temperature is obtained for garnets of 4 cm in diameter. Garnets analysed in this study are not larger than 1 mm, which argues for a closure temperature at the lower boundary. The maximum temperature during subduction is modelled at 680°C. Very fast initial cooling rates of 40°C $m.y.^{-1}$ are obtained for the Bixiling eclogite complex (*Chavagnac and Jahn*, 1996). Therefore, according to the highest reached temperature the maximum cooling time until the isotopic decay system is trapped is about 4 m.y., which is smaller than the lowest error of 11 m.y. Thus, the age obtained by Lu-Hf isotopic dating shows the age of the peak metamorphic conditions.
According to the map taken from *Ratschbacher et al.* (2006) (Figure 2.3) 07XD01 and 07HA11 belong to the units of the Huwan mélange. Both samples are collected in the area near the suture between the Yangtze craton and the Huwan mélange. Samples 07YS04 and 07WH07 were collected in the southern unit, the Yangtze craton. *Ratschbacher et al.* (2006) found high-pressure and ultrahigh-pressure eclogites with ages of 240 Ma collected in the Xin-xian, Hong'an block. According to them this block belongs to the Huwan mélange, arguing for a Triassic detachment deformation of the mélange. *Wu et al.* (2008a) found also evidence for Triassic metamorphism of the Hong'an area in West Dabie. Measurements on zircons resulted in average values of 239 Ma (Th/U) and 227 Ma (Lu/Hf) for eclogites. *Schmidt et al.* (2008) suggested Triassic metamorphism for Dabie and Sulu. Lutetium-Hf measurements on Grt-Cpx pairs show a mean age of 222.4 Ma. Putting this all together confirms a (ultra)high-pressure event for the Yangtze craton. It is possible that these analysed samples belong all to the craton. Therefore the suture between the craton and the Huwan mélange should be drawn further north. According to the same theory the other units located to the north were probably subducted earlier (*Ratschbacher et al.*, 2003).

Both optically and by EMP, two generations of garnet are observable in sample 07YS04; lighter and darker crystals. It is hypothesized that one generation is crystallized at the prograde path, whereas the second generation is formed at peak metamorphic conditions. This weakens the age result obtained for this sample by Lu-Hf, because the resultant age is based on analysis of a mixture of two generations of garnet. Separation of these two generations of garnet fractions has proven impossible. However, also for East Dabie the T_C is exceeded, suggesting that the isotopic system is reset during peak metamorphic conditions. No significant difference is visible for the obtained temperature conditions for the darker and light garnets. Therefore, the calculated Lu-Hf age for 07YS04 in East Dabie represents a cooling age.

Because all the eclogites collected in this study were formed during Triassic metamorphism, there is no extra information available on Paleozoic UHP-metamorphism obtained from Lu-Hf isotopic analysis. The question whether the Triassic event overprinted an earlier metamorphic event remains unanswered. The argon dating method, however, shows evidence for several pre-Triassic peaks. For samples 07XD01 and 07HA11 the argon ages show very controversial results: 546 ±32.9 Ma and 394 ±13.5 Ma versus a Lu-Hf age of ~240 Ma. This implies that the amphibole crystals are either (1) strongly affected by excess argon, (2) the age shows an apparent age due to inherited argon (*Qiu and Wijbrans*, 2006), or (3) that these minerals were formed earlier and were preserved during the most recent metamorphic event. For the latter hypothesis, which is very unlikely, no evidence is found in the thin sections. All

amphibole crystals show a younger relative age compared to the garnet and omphacite minerals.
If it is assumed that either excess argon has a small effect, or corrections are already made for phengite argon results, and the samples belong to the same unit as the samples analysed for Lu-Hf, than the time of the metamorphic event would have been over 100 Ma. This number is based on the age peak of 325 Ma for phengite and ~240 Ma (Lu-Hf) for eclogites. If crustal rocks, which are involved, are exposed to an average temperature of 500°C for a period of 100 m.y. or longer, they would have molten. This suggests that the ages represents more than one event, which are responsible for the formation of Dabie Shan. Furthermore, with a closer temperature for Argon in phengite of about 300-350°C (*McDougall and Harrison*, 1999), which is lower than the metamorphic peak temperature, the argon system is suggested to be reset. Possible inherited argon would have lost during peak metamorphic conditions.

Uranium-Pb analyses were done on zircon crystals from samples belonging to the Huwan mélange that show distinct cores and rims *Wu et al.* (2009). It is believed that the core has a magmatic origin, whereas the rim is formed during later metamorphism. Because of lower HREE contents and $^{176}Lu/^{177}Hf$ ratios in the rim compared to the core, it is concluded that the rim formed during the prograde stage of metamorphism (*Wu et al.*, 2006). The zircon crystals have a significantly older age of 312 ±11 Ma compared to the Lu-Hf age of the garnet and omphacite pairs of 07HA11 and 07XD01. If the Lu-Hf age is representing the time after peak conditions, and the zircon age indicates the prograde path before the same peak in PT-conditions, then the minimum time of this metamorphic event is 60 m.y. However, according to *Zheng et al.* (2008) the subduction of continental crust and the exhumation of UHP slices from mantle depths may proceed in different episodes. Due to different mechanisms, like slab break-off, delaminating processes or a change in the stress field different pulses are generated at different time steps. This orogen is formed by a very complex long-lived tectonic system. It can be concluded that the Erlangping arc, the Qinling microcontinent, the Huwan mélange, but especially the Yangtze craton are subducted one after the other. The theory of two different metamorphic events forming an orogen should be slightly altered to a model where ongoing tectonic pressure subducted several slabs in a more continuous way. *Wu et al.* (2009) suggested a multistage evolution based on zircon Lu-Hf ages of 309 ±4 Ma for eclogite facies. The existence of a lot of different units before deformation resulted in a high variety of metamorphic units building up a complex orogen.

Large scale magmatism is confirmed by the results of argon measurements on all analysed minerals. Actinolite, Hornblende and K-feldspar show a peak around 125 Ma, whereas biotite and phengite show a peak around 110 Ma. This is in agreement with massive cooling clusters at 130-115 Ma as the result of granitoid injections, causing regional cretaceous heating, due to subduction of the Pacific plate *Wu et al.* (2005).

7.2 Conclusions

The main conclusions from this study are summarized as follows:

- UHP metamorphism occurred in West and East Dabie, obtained with thermodynamic modelling on eclogites. Average pressure conditions of 27.5 kbar are obtained. The temperature is limited from 450 to 680°C.
- This metamorphic event has occurred during Triassic subduction, obtained with the Lu-Hf isotopic dating method resulting in an average age of 238 ±27 Ma.
- Paleozoic events are not precluded. The Triassic event overprinted possible earlier events, but no evidence for that is found, using Lu-Hf isotopic analysis.
- Combined argon and Lu-Hf analyses on eclogites show an effect of inherited or excess argon. It is impossible that relative to garnet and omphacite younger actinolite crystals show metamorphic ages older than garnet and omphacite.
- Argon results from phengite analysis may confirm the existence of another metamorphic event at 325 Ma.

- Cretaceous magmatism is recorded by all minerals analysed for the argon dating method.

7.3 Future work

To get a better understanding about the actual P-T-t paths of the different units more information is needed. For the four eclogite samples used for PT-modelling and Lu-Hf dating Sm and Nd (and other LREE) are separated but not yet analysed. Using these for dating can give extra information about the cooling process and most likely about the timing, due to a lower T_C of Sm-Nd relative to Lu-Hf dating (*Scherer et al.*, 2000).
Some samples contain a significant amount of zoisite. This mineral might be suitable for Lu-Hf dating as well. It will produce an extra point on the isochron, and therefore hopefully improve precision of the results. The Lu-Hf dating method itself for such difficult samples should be tested for reliability with a second batch. Although it is a rather time-consuming method, it can be proved that the results make sense.

Another very interesting but challenging suggestion will be modelling for PT-information using water-bearing minerals like amphibole. The usage of another mineral-assemblage like Amp-Pl-Ep can add information to the PT-loop. It can give some insight on the stable conditions during retrograde metamorphism. PT-information from other lithologies is also interesting. This can solve the problem whether buoyant crustal rocks have experienced the same PT-loop as the eclogitic bodies.

Two versions of Thermocalc are used in this study. Due to some technical problems with version 3.25 it is decided to use the same data as input for the latest version 3.31. However, assumptions had to made which are probably not representing the real situation. For pyroxene analyses it is assumed that during equilibrium the system was in disorder. However, according to *Green et al.* (2007) Al and Fe^{3+} have preferences for either M1a or M1n sites, which means that the system is in order. This changes the input parameters and therefore the PT-results. However, very little is known about the exact process.

When more (suitable) samples are collected, more work can be done. This will hopefully enforce the findings in this study. When more data is available, the tectonic model for Dabie Shan can be supported. Even more interesting will be the results of the same techniques applied on samples collected further to the west. Dabie Shan and especially the area covered by this study is only a small part of a very large mountain belt. The combination of techniques applied on rock types from Dabie Shan and the area further to the west may give a good insight in the developing of the Central China mountain belt.

Acknowledgements

I would like to thank Jan Wijbrans and Fraukje Brouwer. They, as my supervisors helped me with the research, in the field, in the lab and during the writing up of this report. Also many thanks to Huaning Qui, Qijun Yang and YuanBao Wu, the Chinese colleagues, who were always with us in the field.
Furthermore, I would like to thank Roel van Elzas for helping me in the mineral separation lab and Richard Smeets for all the help in the clean lab.
I'm very grateful to Oliver Nebel, who gave me a lot of advice and help for all the Lu-Hf isotope work.
Also thanks to 'Stichting Molengraaff' who financially supported the trip to China.

References

Brouwer, F.M.; Burri, T.; Berger, A.; Eclogite relics in the Central Alps: PT-evolution, Lu-Hf ages and implications for formation of tectonic mélange zones; *Schweizerische Mineralogische und Petrographische Mitteilungen*; Vol. 85, p. 147-174, 2005

Brueckner, H.K.; Roermund, H.L.M.; Dunk tectonics: A multiple subduction/eduction model for the evolution of the Scandinavian Caledonides; *Tectonics*; Vol. 23, TC2004, 2004

Chavagnac, V.; Jahn, B.-M.; Coesite-bearing eclogites from the Bixiling Complex, Dabie Mountains, China: Sm-Nd ages, geochemical characteristics and tectonic implications; *Chemical Geology*; Vol. 133, p. 29-51, 1996

Chen, F.; Guo, J.-H.; Jiang, L.-L.; Siebel, W.; Cong, B.; Satir, M.; Provenance of the Beihuaiyang lower-grade metamorphic zone of the Dabie ultrahigh-pressure collision orogen, China: Evidence from zircon ages; *Journal of Asian Earth Sciences*; Vol. 22, p. 343-352, 2003

Cheng, H.; King, R.L.; Nakamura, E.; Vervoort, J.D.; Zhou, Z.; Coupled Lu-Hf and Sm-Nd geochronology constraints garnet growth in ultra-high-pressure eclogites from the Dabie orogen; *Journal of Metamorphic Geology*; Vol. 26, p. 741-758, 2008

Droop, G.; A general equation for estimating Fe3+ concentrations in ferromagnesian silicates and oxides from microprobe analyses, using stoichiometric criteria; *Mineralogical Magazine*; Vol. 51, p. 431-435, 1987

Green, E.; Holland, T.; Powell, R.; An order-disorder model for omphacite pyroxenes in the system jadeite-diopside-hedenbergite-acmite, with applications to eclogitic rocks; *American Mineralogist*; Vol. 92, p. 1181-1189, 2007

Groen, M.; de Groot, K.; de Zwaan, C.; Magma source evolution of Mount Etna (Sicily, Italy), using geochemistry and dating methods; *unpublished, VU University Amsterdam*; pp. 141, 2006

Hacker, B.R.; Pressures and temperatures of ultrahigh-pressure metamorphism: implications for UHP tectonics and H2O in subducting slabs; *International Geology Review*; Vol. 48, p. 1053-1066, 2006

Hacker, B.R.; Wang, Q.C.; Ar/Ar geochronology of ultrahigh-pressure metamorphism in central China; *Tectonics*; Vol. 14, p. 994-1006, 1995

Hacker, B.R.; Ratschbacher, L.; Webb, L.; McWilliams, M.; Calvert, A.; Dong, S.; Wenk, H.R.; Chateigner, D.; Exhumation of ultrahigh-pressure continental crust in east-central China: Late Triassic-Early Jurrassic tectonic unroofing; *Journal of Geophysical Research*; Vol. 105, p. 13339-13364, 2000

Koppers, A.A.P.; ArArCALC-software for 40Ar/39Ar age calculations; Computers & Geosciences; Vol. 28, p. 605-619, 2002

Kretz, R.; Symbols for rock-forming minerals; *American Mineralogist*; Vol. 68, p. 277-279, 1983

Kröner, A.; Compston, W.; Zhang, G.W.; Guo, A.L.; Todt, W.; Age and tectonic setting of late Archean greenstone-gneiss terrane in Henan province, China, as revealed by single-grain zircon dating; *Geology*; Vol. 16, p. 211-215, 1988

Kröner, A.; Zhang, G.; Sun, Y.; Granulites in the Tongbai area, Qinling belt, China: Geochemistry, petrology, single zircon geochronology and implications for the tectonic evolution of eastern Asia; *Tectonics*; Vol. 12, p. 245-255, 1993

Leake, B.E.; Woolley, A.R.; Arps, C.E.S.; Birch, W.D.; Gilbert, M.C.; Grice, J.D.; Hawthorne, F.C.; Kato, A.; Kisch, H.J.; Krivovichev, V.G.; Linthout, K.; Laird, J.; Mandarino, J.A.; Maresch, W.V.; Nickel, E.H.; Rock, N.M.S.; Schumacher, J.C.; Smith, D.C.; Stephenson, N.C.N.; Ungaretti, L.; Whittaker, E.J.W.; Youzhi, G.; Nomenclature of amphiboles: report of the subcommittee on amphiboles of the international mineralogical association, commission on new minerals and mineral names; *The Canadian Mineralogist*; Vol. 35, p. 219-246, 1997

Li, S.; Wang, S.; Chen, Y.; Liu, D.; Qiu, J.; Zhou, H.; Zhang, Z.; Excess argon in phengite from eclogite: evidence from the dating of eclogite minerals by the Sm-Nd, Rb-Sr and $^{40}Ar/^{39}Ar$ methods; *Chemical Geology*; Vol. 112, p. 343-350, 1994

Li, S.G.; Jagoutz, E.; Chen, Y.Z.; Li, Q.; Sm-Nd and Rb-Sr isotopic chronology and cooling history of ultrahigh pressure metamorphic rocks and their country rocks at Shuanghe in the Dabie Mountains, central China; *Geochimica et Cosmochimica Acta*; Vol. 64, p. 1077-1093, 2000

Li, S.G.; Huang, F.; Nie, Y.H.; Han, W.L.; Long, G.; Li, H.M.; Zhang, S.Q.; Zhang, Z.-H.; Geochemical and geochronological constraints on the suture location between the North and South China blocks in the Dabie orogen, central China; *Physics and Chemistry of the Earth, Part A: Solid Earth and Geodesy*; Vol. 26, p. 655-672; 2001

Li, X.-P.; Zheng, Y.-F.; Wu, Y.-B. et al.; Low-T eclogite in the Dabie terrane of China: Petrological and isotopic constraints on fluid activity and radiometric dating; *Contributions to Mineralogy and Petrology*; Vol. 148, p. 443-470, 2004

Liou, J.G.; Zhang, R.Y.; Petrogenesis of ultrahigh-P garnet-bearing ultramafic body from Maowu, the Dabie Mountains, central China; *The Island Arc*; Vol.7, p. 115-134, 1998

Liu, F.; Liou, J.G.; Xu, Z.; U-Pb SHRIMP ages recorded in the coesite-bearing zircon domains of paragneisses in the south-western Sulu terrane, eastern China: New interpretation; *American Mineralogist*; Vol. 90, p. 790-800, 2005

Liu, F.; Xu, Z.; Liou, J.G.; Song, B.; SHRIMP U-Pb ages of ultrahigh-pressure and retrograde metamorphism of gneissic rocks, southwestern Sulu terrane, eastern China; *Journal of Metamorphic Geology*; Vol. 22, p. 315-326, 2004

Liu, F.; Zhang, Z.; Katayama, I.; Xu, Z.; Maruyama, S.; Ultrahigh-pressure metamorphic records hidden in zircon from amphibolites in Sulu terrane, eastern China; *The Island Arc*; Vol. 12, p. 256-267, 2003

Liu, J.B.; Ye, K.; Maruyama, S.; Cong, B.L.; Fa, H.R.; Mineral inclusions in zircon from gneisses in the ultrahigh-pressure zone of the Dabie Mountains, China; *Journal of Geology*; Vol. 109, p. 523-535, 2001

Liu, L.; Sun, Y.; Xiao, P.; Che, Z.; Luo, J.; Chen, D.; Wang, Y.; Zhang, A.; Chen, L.; Wang, Y.; Discovery of ultrahigh-pressure magnesite-bearing garnet lherzolite (>3.8 GPa) in the Altyn Tagh, northwest China; *Chinese Science Bulletin*; Vol. 47, p. 881-886, 2002

Liu, Y.-C.; Li, S.-G.; Xu, S.-T.; Zircon SHRIMP U-Pb dating for gneisses in northern Dabie high T/P metamorphic zone, central China: Implications for decoupling within subducted continental crust; *Lithos*; Vol. 96, p. 170-185, 2007

Liu, X.; Jahn, B.M.; Liu, D.; Dong, S.; Li, S.; SHRIMP U-Pb zircon dating of a metagabbro and eclogites from western Dabieshan (Hong'an block), China, and its tectonic implications; *Tectonophysics*; Vol. 394, p. 171-192, 2004a

Liu, X.; Wei, C.; Liu, S.; Dong, S.; Liu, J.; Thermobaric structure of a traverse across western Dabieshan: Implications for collision tectonics between the Sino-Korean and Yangtze cratons; *Journal of Metamorphic Geology*; Vol. 22, p. 361-379, 2004b

McDougall, I.; Harrison, T.M.; Geochronology and Thermochronology by the $^{40}Ar/^{39}Ar$ Method, Second Edition; *Oxford University Press*, Oxford, New York, pp. 269, 1999

Morel, M.L.A.; Nebel, O.; Nebel-Jacobsen, Y.J.; Miller, J.S.; Vroon, P.Z.; Hafnium isotope characterization of the GJ-1 zircon reference material by solution and laser-ablation MC-ICPMS; *Chemical Geology*; Vol. 255, p. 231-235, 2008

Münker, C.; Weyer, S.; Scherer, E.; Mezger, K.; Separation of high field strength elements (Nb, Ta, Zr, Hf) and Lu from rock samples for MC-ICPMS measurements; *Geochemistry, Geophysics, Geosystems*; Vol. 2, 2001

Niu, B.; Liu, Z.; Ren, J.; The tectonic relationship between the Qinling Mountains and Tongbai-Dabie Mountains with notes on the tectonic evolution of the Hehuai Basin; *Bulletin of the Chinese Academy of Geological Sciences*; Vol. 26, p. 1-12, 1993

Niu, B.; Fu, Y.; Liu, Z.; Ren, J.; Chen, W.; Main tectonothermal events and $^{40}Ar/^{39}Ar$ dating of the Tongbai-Dabie Mts; *Acta Geoscientia Sinica*; Vol. 1994, p. 20-34, 1994

Proyer, A.; Dachs, E.; McCammon, C.; Pitfalls in geothermobarometry of eclogites: Fe^{3+} and changes in the mineral chemistry of omphacite at ultrahigh pressures; *Contribution to Mineralogy and Petrology*; Vol. 147, p. 305-318, 2004

Qiu, H.-N.; Wijbrans, J.R.; Paleozoic ages and excess ^{40}Ar in garnets from the Bixiling eclogite in Dabieshan, China: New insights from $^{40}Ar/^{39}Ar$ dating by stepwise crushing; *Geochimica et Cosmochimica Acta*; Vol. 70, p. 2354-2370, 2006

Qiu, H.-N.; Wijbrans, J.R.; The Paleozoic metamorphic history of the Central Orogenic Belt of China from $^{40}Ar/^{39}Ar$ geochronology of eclogite garnet fluid inclusions; *Earth and Planetary Science Letters*; Vol. 268, p. 501-514, 2008

Ratschbacher, L.; Hacker, B.; Webb, L.; McWilliams, M.; Ireland, T.; Dong, S.; Calvert, A.; Chateigner, D.; Wenk, H.R.; Exhumation of the ultrahigh-pressure continental crust in east-central China: Cretaceous and Cenozoic unroofing and the Tanlu fault; *Journal of Geophysical research*; Vol. 105 p. 13.303-13.338, 2000

Ratschbacher, L.; Hacker, B.R.; Calvert, A.; Webb, L.E.; Grimmer, J.C.; McWilliams, M.O.; Ireland, T.; Dong, S.; Hu, J.; Tectonics of the Qinling (Central China): tectonostratigraphy, geochronology, and deformation history; *Tectonophysics*; Vol. 366, p. 1-53, 2003

Ratschbacher, L.; Franz, L.; Enkelmann, E.; Jonckheere, R.; Pörschke, A.; Hacker, B.; Dong, S.; Zhang, Y.; The Sino-Korean-Yangtze suture, the Huwan detachment, and the Paleozoic-Tertiary exhumation of (ultra)high-pressure rocks along the Tongbai-Xinxian-Dabie Mountains; *Geological Society of America*; Spec. Vol. 403, p. 45-75, 2006

Rubatto, D.; Hermann, J.; Exhumation as fast as subduction?; *Geology*; Vol. 29, p. 3-6, 2001

Sajeev, K.; Santosh, M.; Extreme crustal metamorphism and crust-mantle processes: An introduction; *Lithos*; Vol. 92, p. 5-9, 2006

Scherer, E.E.; Cameron, K.L.; Blichert-Toft, J.; Lu-Hf garnet geochronology: Closure temperature relative to the Sm-Nd system and the effects of trace mineral inclusions; *Geochimica et Cosmochimica Acta*; Vol. 64, p. 3413-3432, 2000

Schmidt, A.; Weyer, S.; Mezger, K.; Scherer, E.E.; Xiao, Y.; Hoefs, J.; Brey, G.P.; Rapid eclogitisation of the Dabie-Sulu UHP terrane: Constraints from Lu-Hf garnet geochronology; *Earth and Planetary Science Letters*; Vol. 273, p. 203-213, 2008

Sun, W.; Williams, I.S.; Li, S.; Carboniferous and Triassic eclogites in the western Dabie Mountains, east-central China: evidence for protracted convergence of the North and South China blocks; *Journal of Metamorphic Geology*; Vol. 20, p. 873-886, 2002

Suo, S.; Zhong, Z.; Zhendong, Y.; Hanwen, Z.; Relic UHP structures in Dabie-Sulu region, China: structural expression and geodynamic significance; *Journal of China University of Geosciences*; Vol. 11, p. 234-241, 2000

Wang, X.; Liou, J.G.; Regional ultrahigh-pressure coesite-bearing eclogite terrane in central China: Evidence from country rocks, gneiss, marble and metapelite; *Geology*; Vol. 19, p. 933-936, 1991

Wu, F.-Y.; Lin, J.-Q.; Wilde, S.A.; Zhang, X.-O.; Yang, J.-H.; Nature and significance of the Early Cretaceous giant igneous event in eastern China; *Earth and Planetary Science Letters*; Vol. 233, p. 103-119, 2005

Wu, Y.-B.; Zheng, Y.-F.; Zhao, Z.-F.; Gong, B.; Liu, X.-M.; Wu, F.-Y.; U-Pb, Hf and O isotope evidence for two episodes of fluid-assisted zircon growth in marble-hosted eclogites from Dabie orogen; *Geochimica et Cosmochimica Acta*; Vol. 70, p. 3743-3761, 2006

Wu, Y.-B.; Zheng, Y.-F.; Zhang, S.-B.; Zhao, Z.-F.; Wu, F.-Y.; Liu, X.-M.; Zircon U-Pb ages and Hf isotope compositions of migmatite from the North Dabie terrane in China: constraints on partial melting; *Journal of Metamorphic Geology*; Vol. 25, p. 991-1009, 2007

Wu, Y.-B.; Gao, S.; Zhang, H.-F.; Yang, S.-H.; Jiao, W.-F.; Liu, Y.-S.; Yuan, H.-L.; Timing of UHP metamorphism in the Hong'an area, western Dabie Mountains, China: evidence from zircon U-Pb age, trace element and Hf isotope composition; *Contribution to Mineralogy and Petrology*; Vol. 155, p. 123-133, 2008a

Wu, Y.-B.; Zheng, Y.-F.; Gao, S.; Jiao, W.-F.; Liu, Y.-S.; Zircon U-Pb age and trace element evidence for Paleoproterozoic granulite-facies metamorphism and Archean crustal rocks in the Dabie Orogen; *Lithos*; Vol. 101, p. 308-322, 2008b

Wu, Y.-B.; Hanchar, J.M.; Gao, S.; Sylvester, P.J.; Tubrett, M.; Qiu, H.-N.; Wijbrans, J.R.; Brouwer, F.M.; Yang, S.-H.; Yang, Q.-J.; Liu, Y.-S.; Yuan, H.-L.; Age and nature of eclogites in the Huwan shear zone, and the multi-stage evolution of the Qinling-Dabie-Sulu orogen, central China; *Earth and Planetary Science Letters*; Vol. 277, p. 345-354, 2009

Xu, B.; Grove, M.; Wang, Ch.; Zhang, L.; Liu, S.; 40Ar/39Ar thermochronology from the northwestern Dabie Shan: Constraints on the evolution of Qinling-Dabie orogenic belt, east-central China; *Tectonophysics*; Vol. 322, p. 137-158, 2000

Xue, F.; Lerch, F.; Kröner, A.; Reischmann, T.; Tectonic evolution of the East Qinling Mountains, China, in the Paleozoic: A review and a new tectonic model; *Tectonophysics*; Vol. 253, p. 271-284, 1996

Ye, B.D.; Jiang, P.; Xu, J.; Cui, F.; Li, Z.; Zhang, Z.; The Sujiahe terrane collage belt and its constitution and evolution along the northern hillslope of the Tongbai-Dabie orogenic belt; *Wuhan, Press of China University of Geoscience*; p. 66-67, 1993

Ye, B.D.; Jiang, P.; Xu, J.; Cui, F.; Li, Z.; Zhang, Z.; Timing of the Sujiahe group in the Tongbai-Dabie orogenic belt; in Chen, H., ed., Research of isotope geochemistry; *Hangzhou Zhejiang University Press*; p. 175-186, 1994

Ye, K.; Yao, Y.; Katayama, I.; Cong, B.L.; Wang, Q.C.; Maruyama, S.; Large area extent of ultrahigh-pressure metamorphism in the Sulu ultrahigh-pressure terrane of East China: New implications from coesite and omphacite inclusions in zircon of granitic gneiss; *Lithos*; Vol. 52, p. 157-164, 2000

You, Z.; Han, Y.; Suo, S.; Chen, N.; Zhong, Z.; Metamorphic history and tectonic evolution of the Qinling complex, eastern Qinling Mountain, China; *Journal of Metamorphic Geology*; Vol. 11, p. 549-560, 1993

Zhang, G.W.; Yu, Z.P.; Sun, Y.; Cheng, S.Y.; Li, T.H.; Xue, F.; Zhang, C.L.; The major suture zone of the Qinling orogenic belt; *Journal of Southeast Asian Earth Sciences*; Vol. 3, p. 63-76, 1989

Zhang, R.Y.; Hirajima, T.; Banno, S.; Cong, B,; Liou, J.G.; Petrology of ultrahigh-pressure rocks from the southern Sulu region, eastern China; *Journal of Metamorphic Geology*; Vol. 13, p. 659-675, 1995a

Zhang, R.Y.; Liou, J.G.; Cong, B.L.; Talc-magnesite- and Ti-clinohumite-bearing ultrahigh-pressure mafic and ultramafic complex in the Dabie Mountains, China; *Journal of Petrology*; Vol. 36, p.1011-1037, 1995b

Zhang, R.Y.; Liou, J.G.; Shu, J.F.; Hydroxyl-rich topaz in high-pressure and ultrahigh-pressure kyanite quarzites, with retrograde woodhouseite, from the Sulu terrane, eastern China; *American Mineralogist*; Vol. 87, p. 445-453, 2002

Zhang, R.Y.; Liou, J.G.; Ernst, W.G.; Ultrahigh-pressure metamorphic belts in China: Major progress in the past several years; *International Geology Review*; Vol. 49, p. 504-519, 2007

Zhang, X.; Wang, R.; Song, M.; Zhang, H.; Discussion on the formation and exhumation of the Sulu eclogites on the basis of the relationship between the eclogites and the country gneisses; *Acta Geologica Sinica*; Vol. 76, p. 14-26, 2002

Zhao, Z.-F., Zheng, Y.-F.; Wei, C.-S.; Wu, Y.-B.; Post-collisional granitoids from the Dabie orogen in China: Zircon U-Pb age, element and O isotope evidence for recycling of subducted continental crust; *Lithos*; Vol. 2007, p. 248-272, 2007

Zheng, Y.; A perspective view on ultrahigh-pressure metamorphism and continental collision in the Dabie-Sulu orogenic belt; *Chinese Science Bulletin*; Vol. 53, p. 3081-3104, 2008

Zhong, Z.; Yang, Q.; Suo, S.; Zhou, H.; You, Z.; Structural evidence for the in-situ origin of the HP and UHP eclogites in the Dabie-Sulu orogenic belt; *Acta Geologica Sinica*; Vol. 77, p. 304-310, 2003

Websites:

http://earthref.org/tools/ararcalc/index.html; Argon software, ArArCalc

http://www.rsc.org; Figure 3.4

http://www.bgc.org/isoplot_etc/software.html; Isochron method software, Isoplot

http://www.metamorph.geo.uni-mainz.de/thermocalc/; Thermodynamic software, Thermocalc

Appendix I Geological map of the Dabie Mountains orogen, Central East China. *Xu, Chen, Liu, Wu, Suo, Zhong*, 2005.

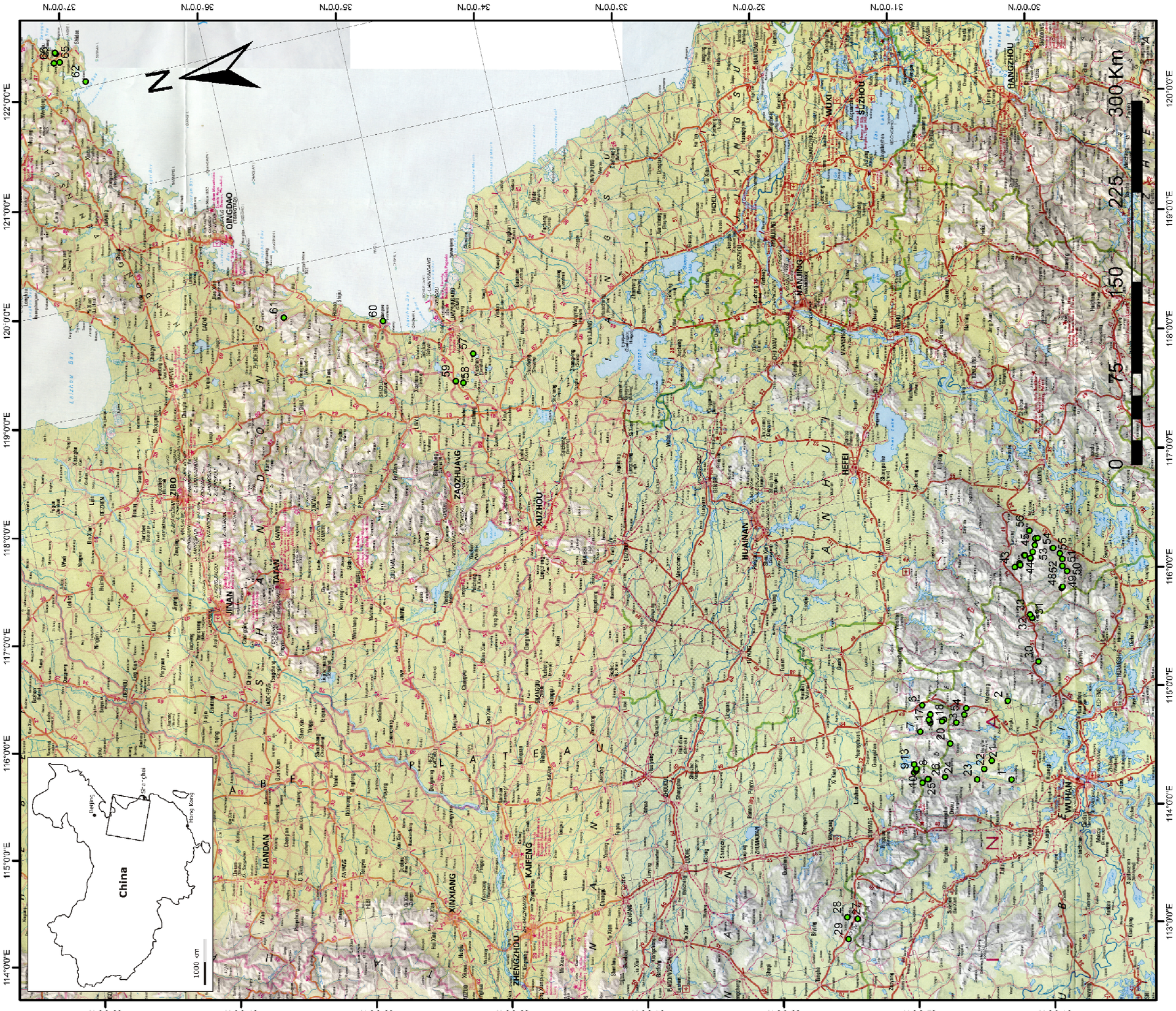

Appendix II.a
Map of Dabie Shan and Sulu (Central East China) showing all the stops. Original topographic map: Nelles Maps, Northern and Central China, original Scale: 1:1,500,000

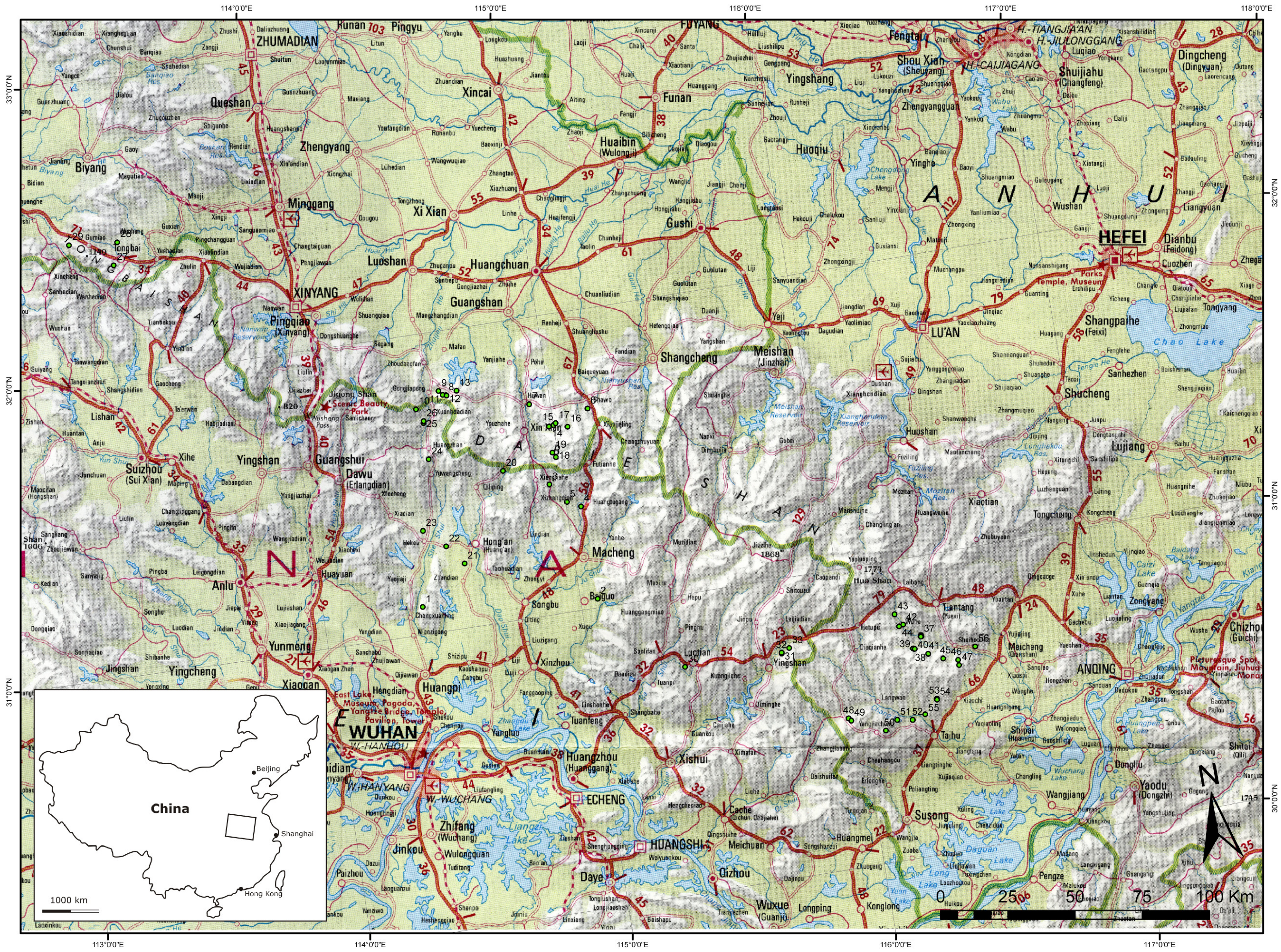

Appendix II.b Detailed map of Dabie Shan (Central East China), showing all stops of the western, central and eastern part of Dabie Shan. Zoom in of appendix II.a.

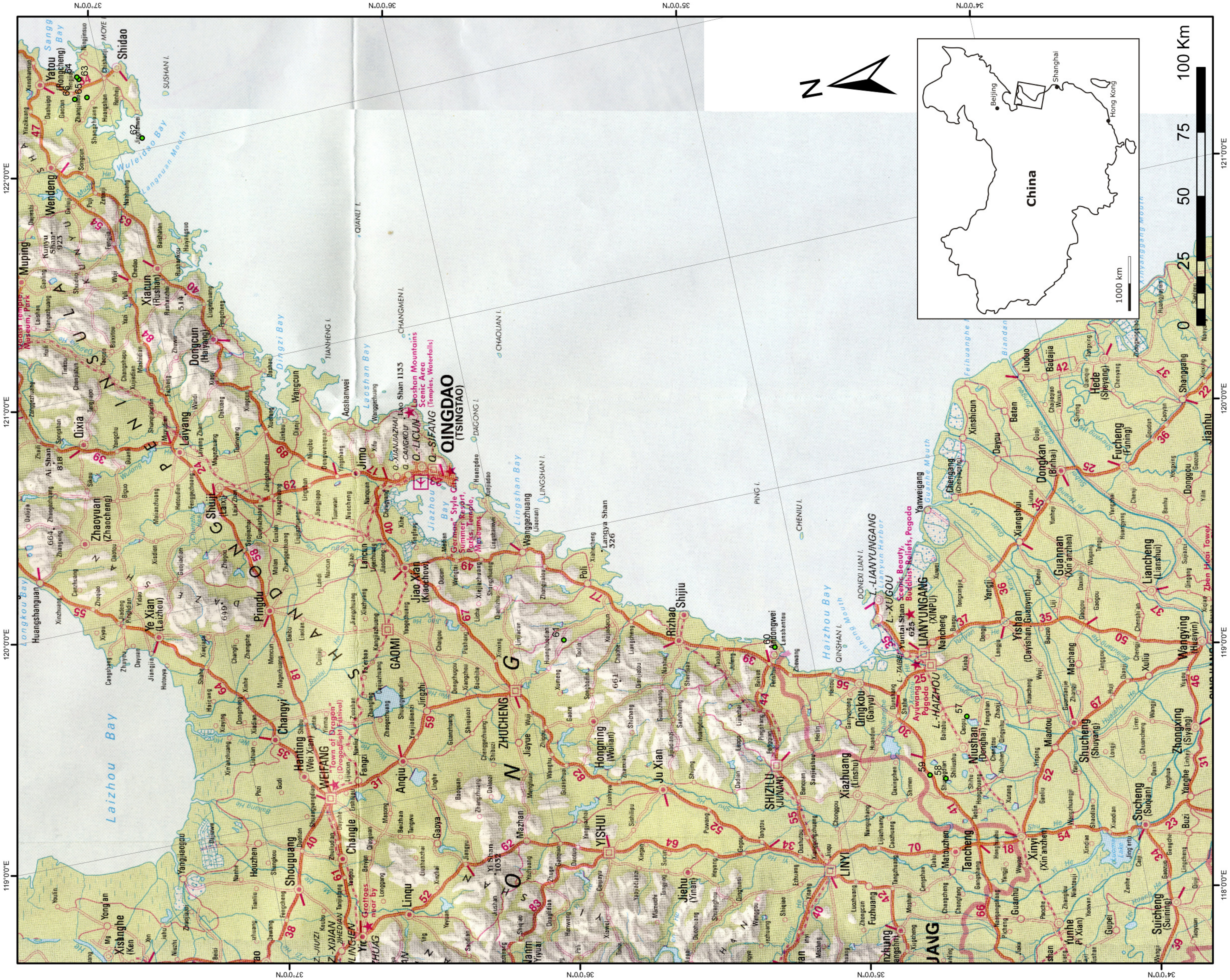

Appendix II.c
Detailed map of Sulu (Northern China), showing all stops near Donghai and Shandong. Zoom in of appendix II.a.

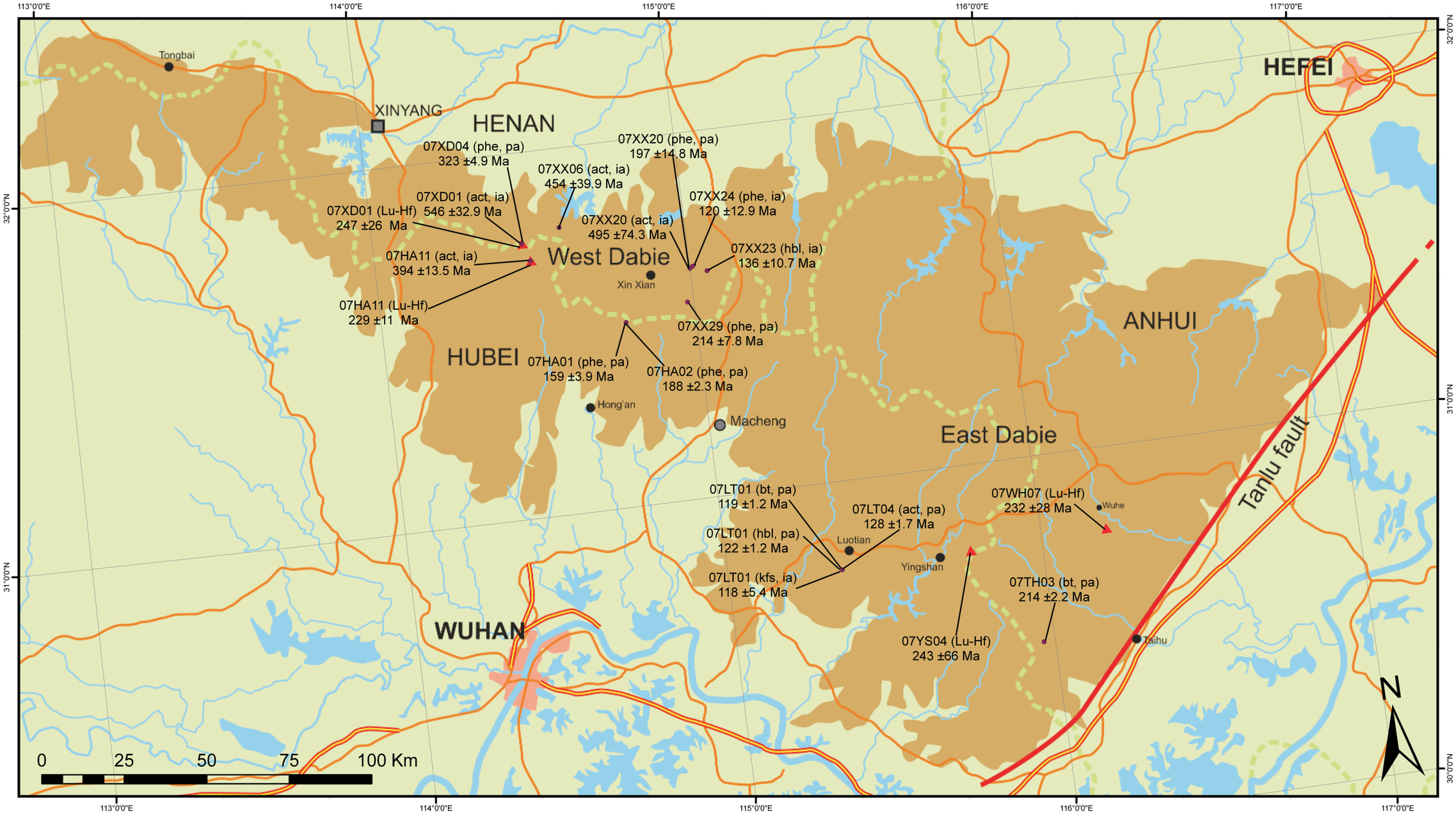

Appendix II.d
Schematic map of Dabie Shan (Central Eastern China), showing all the results of Argon- (purple circles) and Lu-Hf dating (red triangle). The analysed mineral and the used method (plateau- or isochron age, pa or ia, respectively) are indicated per sample. The brown coloured area represents the Dabie Shan mountain belt.

Appendix III Thin sections

This appendix gives the descriptions of the selected samples for further analyses. The samples are sorted by sample number.

07HA01
Amphibolite (retrogressed eclogite)
Large euhedral Phg (15%, 2-3 mm) and fractured Grt (10%) in a matrix of retrograde Act (55%) and Qtz (10%). The Grt contains many inclusions of Rt and opaque minerals. The original euhedral shape is still visible. Phengite is sometimes surrounded by Qtz crystals, but still rather fresh and therefore used for argon dating. Zoisite (10%) has probably formed cogenetically with, or shortly after Grt and Phg. It is partially replaced by Act and Qtz.

07HA02
Felsic Orthogneiss
This is a layered sample, where all minerals show a preferred shape orientation. Within a matrix of Qtz (75%) anhedral Phg crystals (15%) form bands. The rest of the rock is composed of Pl and opaque minerals (10%).
Phg is used for argon dating.

07HA11
Eclogite with fresher (1) and more retrogressed zones (2)
1) Very fresh, small (<0.5 mm) Omp (35%) together with Grt (40%). Some of the Grt crystals contain inclusions of small indefinable minerals (probably zircon), but the rest can be used for Lu-Hf isotopic analysis. Two generations of amphibole (20%) are present; a core of cogenetically with Grt and Omp (or slightly later) formed Gln, with a younger rim of Act. Because Grt is found as inclusion of Act, Act cannot be older than Grt. Therefore the youngest phase Act is used for argon dating methods. Phengite is present as very small crystals in minor abundances (<5%). Very small Qtz (<0.5 mm) present in the entire thin section.
2) This zone is comparable to the first one, except for the Omp being replaced by symplectite.
Rt, Ttn and opaques are present as accessory minerals.

07LT01
Othogneiss with bands of Bt and Hbl (1) and Pl (2).
1) small anhedral Bt crystals (5%) lineated together with anhedral Hbl (10%). Both are large enough to be separated and dated by the argon dating method.
2) large to very large anhedral Pl crystals (55%); Kfs is present as an accessory mineral which is dated (Argon) as well.
Quartz is present through the entire rock. Early stage small veins of an indefinable composition are formed during a younger deformation phase; the veins overgrow all other minerals.

07LT04
Amphibolite
Composed of subhedral Act (50%) and anhedral Pl (25%). Both minerals contain mini-inclusions. The Act crystals are surrounded by veins (20%) composed of very small Act crystals with symplectite rims. Only the bigger crystals of Act can be used for argon dating. Quartz (5%) is present as a minor mineral.

07TH03
Amphibolite, with garnet-bearing (1) and normal (2) composition
1) Matrix of Qtz (10%) with small euhedral Grt crystals (80%). They are homogeneously distributed, contain many inclusions and are partly replaced by Act (10%). Act is used for argon dating.
2) Lineated structure, with Qtz (60%) and epidote group minerals (40%) in bands.
Between the two compositions a sharp boundary is present.

07WH07
Eclogite
Very fresh eclogite consisting of Grt (45%), Omp (45%) and Phg (10%), together with Rt and opaques as accessories. Phengite is probably not cogenetic with the Grt and Omp, but slightly later, because it contains inclusions of Grt. Because of the inclusion free minerals this sample is suitable for Lu-Hf isotopic analysis. Inclusions of Coe are found in a (cracked) Omp crystal.
Veins are present existing of symplectite, Act and Qtz.

07XD01
Banded eclogite
Within this thin section three different bands can be distinguished; a Grt dominated (1), an Omp dominated (2) and a combined band (3).
1) Band of subhedral Grt (85%), Qtz (10%) and Phg (5%). The Grt contains a lot of inclusions of Zrn, Rt and Qtz. Some Ep and Rt are also present.
2) Narrow band of very fresh Omp (80%), with some Act (15%) and Zo (5%).
3) Band of Grt (50%), Omp (30%) and Act (20%). The Grt is significantly smaller than in band 1, and their rims are slightly alternated to Act.
Overall some Rt is present as an accessory mineral.

07XD04
Layered eclogite
Eclogite with a lot of Phg (30%), small crystals which are lineated, and clustered in layers itself. This mineral is used for argon dating. Crystals of Omp (30%) are two small for selection and analysis. Most of the Grt (20%) contain a lot of inclusions. Large Zo (10%, 2 mm) can be found through the entire rock, whereas Amp (10%) is only found in clusters or layers as a product of retrogression.

07XX06
Garnet-amphibolite with heavily deformed (1) and less deformed (2) zones.
1) mostly amphibole, with some remnants of Grt. Very fine reaction structures, not usable for mineral separation.
2) eclogitic composition, with Grt (25%), Omp (30%) and Ep (15%), but retrogressed to amphibolite and contain Act (30%). In between the minerals small 'dirty' veins of Act and symplectite are present. Grt and Omp are too small for separation, therefore only the Act is used for argon dating.

07XX20
Amphibolite (retrogressed eclogite)
Grt crystals (45%, 2-4 mm) are full with inclusions of Qtz and Rt, and the edges are reacted to Act. Also single grains of Act (10%) are present, probably as product from former Omp. Because they contain inclusions of Grt, large Phg grains (5%, 3 mm) are a product of a younger crystallization stage. Both Act and Phg are used for argon dating. Around clusters of Grt, fields of Qtz with small Ep (15%) are present. The rest of the thin section is occupied by symplectite of Act and Pl, probably also as product of Omp.

07XX23
Mafic body
Doloritic dyke mainly consisting of Hbl (65%) with some Act at the edges. Hbl crystals are very large (2-5 mm) and therefore useful for argon dating, but many opaque inclusions can influence the real age. Qtz and Pl (together 15%) are present as older phase minerals, where they are overgrown by the Hbl. The matrix is composed of symplectite, probably of Amp and Pl (20%).

07XX24
Eclogite
Heavily fractured Grt (35%), small Omp (35%) and Phg (10%) are the major minerals of this eclogite. During the early stage of retrogression Omp has reacted to Act; fifteen percent of the rock consists of symplectite. The Grt crystals contain many inclusions (mainly quartz). Zo needles (5%, 2-3 mm) seems to be the youngest phase.

07XX29
Eclogite
Large Grt (20%, 5 mm) fractured, with many inclusions and Act at the edges and in the cracks. A matrix of symplectite with Phg, Omp, Ky, Gln and Qtz (in order of abundances). Phg is small (~1 mm), but fresh and therefore usable for argon dating.

07YS04
Eclogite
Cogenetic Grt, Omp and Qtz form a fresh eclogite. Grt (35%) is fractured, but free of inclusions. Possibly two different generations of Grt are present; lighter and darker grains. The Omp crystals (40%, 1-3 mm) are sometimes euhedral and also inclusion free, but do show initiating break down on the edges. Rutile and Phg are present as accessory minerals. Some isolated fields of Qtz (15%) and Zo (10%) are present. The latter one is younger than the rest, because of inclusions of Grt. Because of the fresh Grt and Omp, this sample can be used of Lu-Hf isotopic analysis. Ky is present as accessory mineral, which makes the sample suitable for PT-modelling with an assemblage of Grt-Omp-Phe-Ky-Coe/Qtz-H_2O.

Mineral abbreviations (after *Kretz*, 1983*)*

Act	actinolite	Ky	kyanite
Amp	amphibole	Omp	omphacite
Bt	biotite	Phg	phengite
Coe	coesite	Pl	plagioclase
Ep	epidote	Qtz	quartz
Grt	garnet	Rt	rutile
Gln	glaucophane	Ttn	titanite
Hbl	hornblende	Zrn	zircon
Kfs	K-feldspar	Zo	zoisite

Appendix IV EMP results

07HA11, pdd9908

Mineral	gt1c	gt1r	gt2c	gt2r	gt3c	gt3r	gt4c	gt4r	gt5c	gt5r
SiO_2	38,41	38,50	38,14	38,23	38,07	39,09	38,22	38,23	38,50	38,37
TiO_2	0,09	0,06	0,18	0,14	0,15	0,02	0,11	0,02	0,03	0,03
Al_2O_3	21,44	21,69	21,57	21,22	21,44	21,86	21,52	21,29	21,70	21,70
Cr_2O_3	0,00	0,00	0,00	0,00	0,00	0,00	0,00	0,66	0,01	0,01
FeO	28,40	27,59	29,23	27,93	29,62	26,46	28,46	27,45	26,89	26,92
MnO	0,74	0,47	1,55	1,19	0,83	0,30	0,76	1,13	0,34	0,66
MgO	2,14	4,22	2,25	2,22	2,00	4,42	2,31	2,77	3,27	4,19
CaO	9,99	7,96	8,46	9,78	9,32	8,86	9,66	9,11	9,70	8,05
Na_2O	0,01	0,02	0,03	0,04	0,02	0,03	0,03	0,01	0,04	0,02
Total	101,23	100,52	101,41	100,75	101,45	101,04	101,07	100,00	100,47	99,93
Si	3,009	3,005	2,993	3,010	2,991	3,019	2,999	3,004	3,010	3,007
Ti	0,006	0,004	0,010	0,008	0,009	0,001	0,006	0,001	0,002	0,002
Al	1,978	1,994	1,993	1,968	1,984	1,988	1,989	1,970	1,998	2,003
Cr	0,000	0,000	0,000	0,000	0,000	0,000	0,000	0,041	0,000	0,001
Fe^{2+*}	1,861	1,801	1,919	1,839	1,923	1,709	1,868	1,803	1,758	1,764
Fe^{3+}	0,000	0,000	0,000	0,000	0,024	0,000	0,000	0,000	0,000	0,000
Mn	0,049	0,031	0,103	0,079	0,055	0,020	0,051	0,075	0,022	0,044
Mg	0,250	0,491	0,263	0,261	0,234	0,509	0,270	0,325	0,382	0,489
Ca	0,839	0,666	0,712	0,825	0,785	0,733	0,812	0,767	0,812	0,676
Na	0,002	0,003	0,005	0,006	0,003	0,004	0,004	0,002	0,006	0,003
Cations	7,994	7,995	7,998	7,996	8,008	7,983	7,999	7,988	7,990	7,989
Charge	23,994	23,999	23,99	23,99	23,997	23,99	23,993	23,995	23,996	23,997

Mineral	cpx1c	cpx1r	cpx2	cpx3c	cpx3r	cpx4c	cpx4r	cpx5c	cpx5r
SiO_2	56,64	56,45	56,31	56,22	55,93	56,34	56,01	56,45	56,01
TiO_2	0,04	0,04	0,04	0,04	0,07	0,03	0,04	0,02	0,06
Al_2O_3	9,90	9,28	9,27	9,33	9,42	9,62	9,29	9,38	9,67
Cr_2O_3	0,00	0,05	0,05	0,03	0,00	0,04	0,00	0,01	0,00
FeO	6,26	6,33	6,52	6,29	5,94	6,11	5,93	5,76	6,06
MnO	0,00	0,02	0,02	0,00	0,00	0,02	0,01	0,04	0,02
MgO	7,67	8,04	7,86	7,83	7,82	7,85	8,18	8,17	7,80
CaO	12,63	13,21	12,88	13,11	12,89	12,75	13,27	13,32	12,78
Na_2O	7,45	7,12	7,30	7,18	7,14	7,33	7,06	7,12	7,27
Total	100,58	100,54	100,24	100,02	99,20	100,07	99,79	100,26	99,68
Si	2,020	2,019	2,021	2,020	2,022	2,020	2,016	2,019	2,016
Ti	0,001	0,001	0,001	0,001	0,002	0,001	0,001	0,001	0,002
Al	0,416	0,391	0,392	0,395	0,401	0,406	0,394	0,395	0,410
Cr	0,000	0,001	0,001	0,001	0,000	0,001	0,000	0,000	0,000
Fe^{2+*}	0,098	0,100	0,089	0,100	0,104	0,094	0,080	0,086	0,091
Fe^{3+}	0,089	0,089	0,107	0,089	0,075	0,089	0,098	0,086	0,092
Mn	0,000	0,001	0,001	0,000	0,000	0,000	0,000	0,001	0,000
Mg	0,408	0,428	0,421	0,419	0,422	0,419	0,439	0,436	0,419
Ca	0,483	0,506	0,495	0,505	0,499	0,490	0,512	0,511	0,493
Na	0,515	0,494	0,508	0,500	0,500	0,510	0,493	0,494	0,508
Cations	4,030	4,030	4,036	4,030	4,025	4,030	4,033	4,029	4,031
Charge	12,003	11,998	12,001	11,998	11,999	11,999	12,001	11,999	12,000

* Fe^{3+} was calculated using the stoichiometric method of *Droop* (1987).

Mineral	phg1c	phg1r	phg2	phg3c	phg3r	phg4c	phg4r	phg5c	phg5r
SiO_2	49,06	52,47	52,37	48,63	51,05	52,01	50,37	48,54	51,24
TiO_2	0,82	0,57	0,51	0,59	0,50	0,50	0,58	0,62	0,57
Al_2O_3	25,31	22,63	23,05	26,82	24,30	22,82	25,81	27,41	24,71
Cr_2O_3	0,00	0,00	0,02	0,02	0,00	0,02	0,01	0,00	0,00
FeO*	3,90	3,51	3,46	3,80	3,65	3,41	3,83	3,50	3,49
MnO	0,00	0,00	0,00	0,00	0,02	0,00	0,00	0,00	0,00
MgO	3,08	3,96	3,92	2,87	3,50	3,94	3,15	2,73	3,52
CaO	0,04	0,04	0,00	0,01	0,02	0,00	0,02	0,01	0,00
Na_2O	0,31	0,11	0,19	0,37	0,31	0,19	0,36	0,71	0,32
K_2O	10,91	11,09	10,87	10,48	10,47	10,85	10,80	10,29	10,89
BaO	0,36	0,39	0,45	0,46	0,37	0,45	0,42	0,40	0,40
F	0,00	0,01	0,05	0,02	0,00	0,02	0,03	0,03	0,04
CL	0,00	0,00	0,00	0,00	0,02	0,00	0,00	0,00	0,00
Total	93,79	94,78	94,88	94,07	94,20	94,21	95,37	94,25	95,17
Si	6,771	7,124	7,098	6,675	6,965	7,100	6,816	6,636	6,932
Ti	0,085	0,059	0,051	0,061	0,052	0,051	0,059	0,064	0,058
Al	4,114	3,618	3,679	4,334	3,905	3,669	4,113	4,414	3,938
Cr	0,000	0,000	0,002	0,002	0,000	0,002	0,001	0,000	0,000
Fe	0,450	0,398	0,392	0,436	0,416	0,389	0,433	0,400	0,394
Mn	0,000	0,000	0,000	0,000	0,002	0,000	0,000	0,000	0,000
Mg	0,634	0,802	0,792	0,588	0,711	0,801	0,636	0,556	0,709
Ca	0,005	0,006	0,000	0,002	0,003	0,000	0,003	0,001	0,000
Na	0,083	0,029	0,051	0,100	0,081	0,051	0,096	0,189	0,083
K	1,922	1,921	1,880	1,835	1,822	1,890	1,865	1,794	1,879
Ba	0,020	0,021	0,024	0,025	0,020	0,024	0,022	0,021	0,021
Cations	14,084	13,978	13,969	14,058	13,977	13,977	14,044	14,075	14,014
Charge	-	-	-	-	-	-	-	-	-

Mineral	amp1cc	amp1cr	amp1rc	amp1rr	amp2c	amp2r	amp3c	amp3r	amp4c	amp4r	amp5c	amp5r
SiO_2	55,13	56,05	45,81	45,92	45,97	46,43	46,20	45,87	45,56	46,03	45,49	45,97
TiO_2	0,08	0,07	0,60	0,44	0,56	0,49	0,54	0,58	0,57	0,53	0,57	0,53
Al_2O_3	9,47	9,69	12,41	12,17	13,05	12,01	11,98	11,43	13,15	12,28	12,62	12,59
Cr_2O_3	0,05	0,00	0,01	0,00	0,04	0,01	0,00	0,00	0,00	0,04	0,00	0,01
FeO*	13,91	14,07	17,04	17,24	17,01	16,62	16,54	17,54	17,11	16,98	16,89	17,24
MnO	0,03	0,04	0,13	0,10	0,09	0,10	0,07	0,09	0,10	0,09	0,08	0,08
MgO	9,09	9,02	8,15	8,21	8,13	8,81	8,79	8,60	8,17	8,50	8,30	8,32
CaO	1,94	1,60	7,51	7,13	7,02	7,42	7,52	8,07	7,03	7,48	7,16	7,01
Na_2O	5,22	5,41	4,00	4,45	4,76	4,43	4,45	4,05	4,58	4,45	4,55	4,60
K_2O	0,12	0,09	0,59	0,57	0,51	0,54	0,57	0,66	0,56	0,55	0,59	0,54
F	0,00	0,00	0,00	0,01	0,00	0,06	0,00	0,00	0,00	0,00	0,00	0,07
CL	0,00	0,00	0,03	0,02	0,02	0,03	0,03	0,04	0,02	0,03	0,01	0,02
Total	95,02	96,05	96,29	96,25	97,16	96,94	96,68	96,91	96,86	96,94	96,27	96,96
Si	7,824	7,857	6,815	6,838	6,774	6,853	6,846	6,830	6,726	6,809	6,770	6,784
Ti	0,008	0,007	0,067	0,049	0,062	0,055	0,061	0,065	0,063	0,059	0,063	0,059
Al	1,582	1,599	2,174	2,134	2,265	2,087	2,091	2,004	2,286	2,138	2,213	2,189
Cr	0,006	0,000	0,002	0,000	0,005	0,001	0,000	0,000	0,000	0,004	0,000	0,001
Fe	1,651	1,649	2,120	2,147	2,096	2,052	2,050	2,184	2,113	2,100	2,102	2,128
Mn	0,004	0,005	0,017	0,012	0,012	0,013	0,008	0,011	0,013	0,012	0,010	0,010
Mg	1,922	1,885	1,808	1,822	1,787	1,938	1,942	1,908	1,798	1,875	1,842	1,830
Ca	0,294	0,241	1,198	1,138	1,108	1,173	1,194	1,287	1,112	1,185	1,141	1,108
Na	1,438	1,471	1,153	1,285	1,359	1,269	1,278	1,168	1,312	1,276	1,314	1,316
K	0,021	0,017	0,112	0,109	0,095	0,101	0,107	0,125	0,105	0,103	0,112	0,101
Cations	14,750	14,731	15,466	15,534	15,563	15,542	15,577	15,582	15,528	15,561	15,567	15,526
Charge	45,272	45,284	45,495	45,473	45,519	45,517	45,567	45,540	45,398	45,518	45,475	45,410

* All Fe is considered Fe^{2+}.

07WH07, pdd9912

Mineral	gt1c	gt1r	gt2c	gt2r	gt3c	gt3r	gt4c	gt4r	gt5c	gt5r
SiO_2	39,61	39,42	39,62	39,91	39,32	39,38	37,94	39,36	38,52	38,54
TiO_2	0,03	0,03	0,05	0,03	0,03	0,02	0,03	0,04	0,02	0,03
Al_2O_3	21,36	21,25	21,34	21,69	21,73	21,84	22,64	22,27	22,00	21,53
Cr_2O_3	0,01	0,02	0,06	0,00	0,03	0,00	0,04	0,00	0,08	0,05
FeO	21,99	21,10	22,49	21,20	20,45	21,68	21,59	21,90	21,68	20,65
MnO	0,43	0,42	0,41	0,44	0,37	0,44	0,38	0,42	0,40	0,40
MgO	6,37	6,39	5,91	6,45	6,03	6,96	6,21	5,91	6,24	6,27
CaO	11,01	11,33	11,50	11,26	12,72	10,24	11,12	11,49	11,50	12,13
Na_2O	0,03	0,04	0,02	0,01	0,02	0,01	0,02	0,01	0,01	0,02
Total	100,82	99,97	101,34	100,99	100,67	100,56	99,92	101,41	100,36	99,56
Si	3,025	3,029	3,020	3,031	3,001	3,005	2,926	2,990	2,960	2,979
Ti	0,002	0,002	0,003	0,002	0,001	0,001	0,002	0,002	0,001	0,002
Al	1,921	1,923	1,916	1,940	1,954	1,963	2,057	1,992	1,991	1,960
Cr	0,001	0,001	0,003	0,000	0,002	0,000	0,003	0,000	0,005	0,003
Fe^{2+*}	1,369	1,332	1,386	1,347	1,252	1,350	1,268	1,367	1,274	1,227
Fe^{3+}	0,036	0,024	0,048	0,000	0,054	0,033	0,125	0,024	0,119	0,108
Mn	0,028	0,027	0,026	0,028	0,024	0,028	0,025	0,027	0,026	0,026
Mg	0,725	0,732	0,672	0,730	0,686	0,792	0,714	0,669	0,715	0,723
Ca	0,901	0,933	0,939	0,916	1,040	0,837	0,919	0,935	0,947	1,005
Na	0,004	0,005	0,003	0,002	0,004	0,002	0,003	0,002	0,002	0,003
Cations	8,012	8,008	8,016	7,996	8,018	8,011	8,042	8,008	8,040	8,036
Charge	23,996	23,997	23,994	23,996	23,992	23,995	23,997	23,99	23,996	23,994

Mineral	cpx1c	cpx1r	cpx2c	cpx2r	cpx3c	cpx3r	cpx4c	cpx4r	cpx5c	cpx5r
SiO_2	56,78	57,78	57,63	56,86	57,61	57,16	56,98	56,79	57,35	55,94
TiO_2	0,04	0,02	0,04	0,04	0,06	0,05	0,06	0,04	0,04	0,04
Al_2O_3	11,80	14,26	15,07	13,57	15,68	14,49	14,60	14,92	15,28	13,83
Cr_2O_3	0,03	0,07	0,05	0,00	0,06	0,06	0,03	0,03	0,00	0,05
FeO	3,72	2,64	2,54	2,73	2,58	2,71	2,62	2,62	2,59	2,66
MnO	0,03	0,02	0,02	0,01	0,01	0,02	0,03	0,03	0,02	0,01
MgO	7,60	6,07	6,09	6,63	5,77	6,16	6,11	6,12	6,12	6,72
CaO	12,11	9,84	9,53	10,61	9,17	9,79	9,96	9,90	9,56	10,84
Na_2O	7,93	9,08	9,16	8,68	9,01	9,13	9,04	9,12	8,91	8,31
Total	100,04	99,78	100,14	99,13	99,95	99,57	99,42	99,58	99,88	98,40
Si	2,008	2,021	2,006	2,010	2,005	2,007	2,003	1,994	2,001	1,993
Ti	0,001	0,001	0,001	0,001	0,001	0,001	0,002	0,001	0,001	0,001
Al	0,491	0,587	0,618	0,565	0,642	0,599	0,605	0,617	0,628	0,580
Cr	0,001	0,002	0,001	0,000	0,002	0,002	0,001	0,001	0,000	0,001
Fe^{2+*}	0,065	0,077	0,074	0,072	0,075	0,077	0,077	0,065	0,076	0,079
Fe^{3+}	0,045	0,000	0,000	0,009	0,000	0,003	0,000	0,012	0,000	0,000
Mn	0,001	0,001	0,001	0,000	0,000	0,001	0,001	0,001	0,000	0,000
Mg	0,401	0,317	0,316	0,349	0,299	0,322	0,320	0,320	0,318	0,357
Ca	0,459	0,369	0,356	0,402	0,342	0,368	0,375	0,372	0,357	0,414
Na	0,543	0,616	0,619	0,595	0,608	0,621	0,616	0,621	0,603	0,574
Cations	4,015	3,991	3,992	4,003	3,974	4,001	4,000	4,004	3,984	3,999
Charge	11,997	11,999	11,998	11,998	11,996	11,998	12,000	11,995	11,997	11,993

* Fe^{3+} was calculated using the stoichiometric method of *Droop* (1987).

Mineral	phg1c	phg1r	phg2c	phg2r	phg3c	phg3r	phg4c	phg4r	phg5c	phg5r
SiO_2	53,18	52,00	52,55	52,46	52,40	51,37	52,42	52,73	52,71	53,19
TiO_2	0,28	0,27	0,29	0,25	0,30	0,27	0,31	0,27	0,31	0,24
Al_2O_3	23,82	25,73	24,12	24,68	23,71	25,91	25,01	24,42	23,43	23,51
Cr_2O_3	0,06	0,04	0,03	0,05	0,02	0,02	0,03	0,05	0,04	0,03
FeO*	1,39	1,48	1,37	1,30	1,93	2,17	1,64	1,67	0,00	1,42
MnO	0,01	0,00	0,00	0,00	0,00	0,00	0,01	0,01	0,00	0,00
MgO	4,48	3,89	4,45	4,13	4,79	3,83	4,13	4,46	4,41	4,59
CaO	0,00	0,01	0,00	0,00	0,01	0,00	0,00	0,00	0,00	0,00
Na_2O	0,18	0,40	0,10	0,32	0,11	0,40	0,26	0,18	0,15	0,18
K_2O	11,03	10,48	11,06	10,61	10,84	10,25	10,78	10,86	11,15	10,75
BaO	-	-	0,34	0,301	-	-	-	-	0,33	0,34
F	0,26	0,19	0,24	0,20	0,13	0,09	0,23	0,13	0,21	0,11
CL	0,02	0,02	0,02	0,02	0,01	0,02	0,01	0,02	0,02	0,01
Total	94,70	94,51	94,58	94,31	94,25	94,33	94,83	94,80	92,75	94,36
Si	7,132	6,973	7,080	7,062	7,073	6,915	7,022	7,062	7,188	7,156
Ti	0,029	0,027	0,030	0,025	0,030	0,028	0,031	0,027	0,032	0,025
Al	3,762	4,063	3,827	3,913	3,769	4,107	3,946	3,852	3,763	3,725
Cr	0,007	0,004	0,003	0,005	0,002	0,002	0,004	0,005	0,004	0,003
Fe	0,156	0,166	0,154	0,146	0,218	0,245	0,184	0,187	0,000	0,159
Mn	0,001	0,000	0,000	0,000	0,000	0,000	0,001	0,001	0,000	0,000
Mg	0,896	0,778	0,894	0,829	0,964	0,769	0,825	0,891	0,897	0,920
Ca	0,000	0,001	0,000	0,000	0,002	0,001	0,000	0,000	0,000	0,000
Na	0,048	0,105	0,027	0,083	0,029	0,105	0,067	0,046	0,039	0,047
K	1,886	1,792	1,901	1,822	1,867	1,760	1,842	1,856	1,940	1,845
Ba	0,000	0,000	0,018	0,016	0,000	0,000	0,000	0,000	0,018	0,018
Cations	13,917	13,909	13,934	13,901	13,954	13,932	13,922	13,927	13,881	13,898
Charge	-	-	-	-	-	-	-	-	-	-

* All Fe is considered Fe^{2+}.

07XD01, pdd9913

Mineral	gt1c	gt1r	gt2c	gt2r	gt3c	gt3r	gt4c	gt4r	gt5c	gt5r
SiO_2	38,42	38,50	37,81	37,76	38,12	37,79	39,57	38,72	38,30	38,66
TiO_2	0,07	0,08	0,09	0,05	0,02	0,01	0,05	0,02	0,03	0,06
Al_2O_3	21,31	21,62	21,64	21,89	22,36	21,47	21,57	21,36	21,22	21,58
Cr_2O_3	0,39	0,08	0,00	0,00	0,05	0,11	0,00	0,00	0,18	0,08
FeO	25,08	25,36	28,15	25,84	26,15	25,28	23,79	25,29	25,32	25,47
MnO	1,40	0,48	0,10	0,27	0,59	0,55	1,09	0,65	0,86	0,71
MgO	4,84	5,77	4,12	5,45	5,40	5,56	9,52	4,90	5,54	5,75
CaO	9,63	8,69	9,09	8,80	8,44	8,90	5,63	9,78	8,60	8,72
Na_2O	0,03	0,03	0,04	0,02	0,02	0,01	0,01	0,02	0,03	0,02
Total	100,78	100,53	101,03	100,07	101,11	99,58	101,23	100,74	99,90	100,96
Si	2,978	2,981	2,954	2,948	2,945	2,961	2,998	3,002	2,989	2,984
Ti	0,004	0,005	0,005	0,003	0,001	0,001	0,003	0,001	0,002	0,003
Al	1,945	1,971	1,992	2,013	2,034	1,981	1,924	1,951	1,950	1,961
Cr	0,024	0,005	0,000	0,000	0,003	0,007	0,000	0,000	0,011	0,005
Fe^{2+*}	1,527	1,564	1,709	1,562	1,584	1,535	1,402	1,583	1,565	1,560
Fe^{3+}	0,099	0,078	0,131	0,125	0,105	0,122	0,105	0,057	0,087	0,084
Mn	0,092	0,031	0,006	0,018	0,039	0,037	0,070	0,043	0,057	0,046
Mg	0,559	0,666	0,480	0,634	0,622	0,649	1,075	0,566	0,644	0,662
Ca	0,800	0,721	0,761	0,736	0,699	0,747	0,457	0,813	0,719	0,721
Na	0,005	0,004	0,006	0,003	0,003	0,001	0,001	0,003	0,005	0,002
Cations	8,033	8,026	8,044	8,042	8,035	8,041	8,035	8,019	8,029	8,028
Charge	23,994	23,996	23,992	23,996	23,996	23,993	23,995	23,992	23,996	23,994

Mineral	cpx1c	cpx1r	cpx3r	cpx5c	cpx5r	cpx3c	cpx4c	cpx4r
SiO_2	55,89	55,58	55,49	55,52	56,16	55,45	55,58	55,46
TiO_2	0,11	0,12	0,09	0,14	0,11	0,16	0,15	0,07
Al_2O_3	10,52	10,17	10,24	10,22	10,30	10,77	10,79	9,80
Cr_2O_3	0,09	0,01	0,17	0,25	0,32	0,10	0,05	0,12
FeO	6,25	6,57	5,99	6,42	5,72	6,70	6,73	7,20
MnO	0,03	0,00	0,02	0,03	0,04	0,02	0,01	0,03
MgO	7,49	7,74	7,76	7,49	7,56	7,47	7,28	7,33
CaO	12,80	13,05	12,98	12,76	12,68	12,73	12,68	12,04
Na_2O	7,34	7,15	7,16	7,17	7,15	7,05	7,09	7,61
Total	100,52	100,39	99,89	100,00	100,04	100,45	100,35	99,64
Si	1,997	1,993	1,995	1,997	2,010	1,986	1,991	2,008
Ti	0,003	0,003	0,002	0,004	0,003	0,004	0,004	0,002
Al	0,443	0,430	0,434	0,433	0,434	0,454	0,455	0,418
Cr	0,003	0,000	0,005	0,007	0,009	0,003	0,001	0,003
Fe^{2+*}	0,092	0,093	0,085	0,107	0,132	0,124	0,139	0,079
Fe^{3+}	0,095	0,104	0,095	0,086	0,039	0,077	0,063	0,139
Mn	0,001	0,000	0,001	0,001	0,001	0,001	0,000	0,001
Mg	0,399	0,414	0,416	0,402	0,403	0,399	0,389	0,396
Ca	0,490	0,501	0,500	0,492	0,486	0,489	0,487	0,467
Na	0,509	0,497	0,499	0,500	0,496	0,489	0,492	0,534
Cations	4,032	4,035	4,032	4,029	4,013	4,026	4,021	4,047
Charge	12,001	11,995	11,998	12,000	11,999	12,000	11,996	12,001

Mineral	ab2
SiO_2	68,07
Al_2O_3	19,32
$FeO^{\dagger}$	0,09
CaO	0,11
SrO	0,00
Na_2O	11,47
K_2O	0,05
BaO	0,00
Total	99,11
Si	2,998
Al	1,002
Fe	0,003
Ca	0,005
Sr	0,000
Na	0,980
K	0,003
Ba	0,000
Cations	4,991
Charge	-

* Fe^{3+} was calculated using the stoichiometric method of *Droop* (1987).
† All Fe is considered Fe^{2+}.

Mineral	phg1c	phg1r	phg2c	phg2r	phg3c	phg3r
SiO_2	49,05	49,23	49,57	49,14	49,24	49,79
TiO_2	0,54	0,48	0,50	0,45	0,47	0,43
Al_2O_3	28,27	27,95	27,81	27,60	28,63	28,04
Cr_2O_3	0,00	0,11	0,02	0,05	0,09	0,05
FeO*	2,59	2,57	2,87	3,63	2,53	2,50
MnO	0,01	0,01	0,00	0,01	0,01	0,02
MgO	2,83	2,92	2,79	2,61	2,66	2,93
CaO	0,00	0,00	0,00	0,00	0,00	0,01
Na_2O	1,08	0,93	1,14	0,81	0,72	0,97
K_2O	9,98	10,13	9,85	10,11	10,39	10,04
BaO	-	-	0,22	-	-	-
F	0,07	0,03	0,08	0,05	0,05	0,00
CL	0,00	0,00	0,00	0,01	0,01	0,00
Total	94,42	94,37	94,86	94,45	94,80	94,77
Si	6,632	6,660	6,685	6,674	6,632	6,692
Ti	0,055	0,049	0,051	0,046	0,048	0,043
Al	4,502	4,453	4,416	4,415	4,541	4,438
Cr	0,000	0,012	0,002	0,005	0,010	0,005
Fe	0,293	0,291	0,324	0,412	0,285	0,281
Mn	0,001	0,001	0,000	0,001	0,002	0,003
Mg	0,571	0,588	0,561	0,528	0,534	0,587
Ca	0,000	0,000	0,000	0,000	0,000	0,001
Na	0,282	0,244	0,299	0,214	0,188	0,253
K	1,721	1,749	1,695	1,751	1,785	1,722
Ba	0,000	0,000	0,012	0,000	0,000	0,000
Cations	14,057	14,047	14,045	14,046	14,025	14,025
Charge	-	-	-	-	-	-

Mineral	amp1c	amp1r	amp4r	amp4r2	amp5c	amp5r
SiO_2	46,87	46,04	47,68	45,94	48,33	48,67
TiO_2	0,31	0,27	0,33	0,27	0,31	0,27
Al_2O_3	12,10	11,33	11,98	13,24	13,10	11,79
Cr_2O_3	0,08	0,12	0,00	0,01	0,24	0,23
FeO*	15,45	15,44	15,93	16,68	10,20	12,29
MnO	0,09	0,10	0,08	0,08	0,04	0,12
MgO	10,20	10,62	9,77	8,80	12,44	11,52
CaO	9,33	10,17	8,93	8,53	7,68	8,62
Na_2O	3,41	3,01	3,45	3,90	4,16	3,54
K_2O	0,53	0,70	0,48	0,52	0,53	0,38
F	0,03	0,05	0,10	0,01	0,17	0,10
CL	0,07	0,09	0,08	0,10	0,01	0,04
Total	98,46	97,94	98,81	98,08	97,21	97,55
Si	6,799	6,763	6,886	6,722	6,883	6,991
Ti	0,034	0,030	0,036	0,030	0,033	0,029
Al	2,067	1,960	2,038	2,281	2,197	1,994
Cr	0,009	0,014	0,000	0,001	0,027	0,026
Fe	1,874	1,897	1,924	2,040	1,215	1,476
Mn	0,011	0,012	0,010	0,010	0,005	0,014
Mg	2,206	2,326	2,104	1,920	2,641	2,467
Ca	1,450	1,601	1,382	1,337	1,172	1,327
Na	0,960	0,858	0,966	1,106	1,149	0,985
K	0,097	0,131	0,089	0,098	0,096	0,069
Cations	15,507	15,592	15,435	15,545	15,418	15,378
Charge	45,602	45,624	45,608	45,574	45,551	45,693

* All Fe is considered Fe^{2+}.

07YS04, pdd9920

Mineral	gt1d1	gt1d2	gt1l1	gt1l2	gt2d1	gt2d2	gt2l1	gt2l2	gt3d1	gt3d2
SiO_2	40,45	40,50	39,97	39,74	40,43	40,65	40,26	40,24	40,52	40,52
TiO_2	0,05	0,04	0,04	0,03	0,04	0,02	0,02	0,04	0,04	0,03
Al_2O_3	22,55	22,73	22,66	22,48	22,58	22,90	22,69	22,48	22,59	22,50
Cr_2O_3	0,00	0,03	0,00	0,00	0,01	0,00	0,00	0,03	0,00	0,01
FeO	14,11	14,70	19,82	18,35	14,36	14,86	17,48	17,07	15,04	14,62
MnO	0,29	0,33	0,50	0,45	0,31	0,35	0,37	0,39	0,29	0,34
MgO	9,91	10,26	9,63	8,47	9,97	10,39	8,73	8,52	9,75	10,02
CaO	12,41	11,63	7,75	10,77	12,32	11,60	10,93	11,59	12,26	12,03
Na_2O	0,03	0,04	0,01	0,02	0,03	0,02	0,02	0,02	0,03	0,03
Total	99,79	100,22	100,37	100,30	100,04	100,79	100,48	100,35	100,51	100,09
Si	3,015	3,007	3,003	2,996	3,009	3,002	3,013	3,017	3,010	3,015
Ti	0,003	0,002	0,002	0,002	0,002	0,001	0,001	0,002	0,002	0,002
Al	1,979	1,987	2,005	1,996	1,980	1,992	2,000	1,985	1,976	1,971
Cr	0,000	0,002	0,000	0,000	0,000	0,000	0,000	0,001	0,000	0,001
Fe^{2+*}	0,879	0,913	1,245	1,145	0,894	0,918	1,094	1,070	0,934	0,910
Fe^{3+}	0,000	0,000	0,000	0,012	0,000	0,000	0,000	0,000	0,000	0,000
Mn	0,018	0,021	0,032	0,029	0,020	0,022	0,023	0,025	0,018	0,021
Mg	1,102	1,135	1,078	0,951	1,106	1,144	0,974	0,952	1,079	1,111
Ca	0,991	0,925	0,624	0,870	0,983	0,918	0,877	0,931	0,976	0,960
Na	0,004	0,005	0,001	0,003	0,004	0,003	0,003	0,003	0,004	0,004
Cations	7,991	7,997	7,990	8,004	7,998	8,000	7,985	7,986	7,999	7,995
Charge	23,993	23,996	23,994	23,997	23,994	23,995	23,995	23,993	23,994	23,992

Mineral	gt3l1	gt3l2	gt4d1	gt4l1	gt4d2	gt4l2	gt5d1	gt5d2	gt5l1	gt5l2
SiO_2	39,99	39,87	40,46	40,04	40,20	39,90	40,45	40,74	39,93	40,12
TiO_2	0,01	0,03	0,04	0,01	0,03	0,01	0,03	0,04	0,01	0,00
Al_2O_3	22,16	22,07	22,64	22,72	22,52	22,60	22,56	22,65	22,50	22,61
Cr_2O_3	0,00	0,01	0,00	0,00	0,01	0,00	0,02	0,00	0,00	0,00
FeO	18,50	18,72	14,39	19,01	15,71	18,80	14,64	14,72	18,58	19,99
MnO	0,45	0,43	0,29	0,44	0,33	0,47	0,33	0,34	0,47	0,50
MgO	7,62	8,14	10,12	9,50	9,26	7,94	10,25	10,36	8,24	9,10
CaO	11,72	11,02	12,13	8,52	11,89	10,88	11,95	11,70	10,69	8,55
Na_2O	0,02	0,00	0,02	0,03	0,01	0,00	0,02	0,03	0,02	0,01
Total	100,47	100,27	100,08	100,28	99,95	100,60	100,22	100,58	100,44	100,87
Si	3,019	3,013	3,008	3,006	3,010	3,004	3,006	3,014	3,007	3,007
Ti	0,001	0,001	0,002	0,000	0,002	0,001	0,002	0,002	0,001	0,000
Al	1,970	1,965	1,983	2,009	1,986	2,004	1,974	1,974	1,995	1,996
Cr	0,000	0,000	0,000	0,000	0,000	0,000	0,001	0,000	0,000	0,000
Fe^{2+*}	1,168	1,183	0,895	1,193	0,984	1,184	0,901	0,911	1,170	1,253
Fe^{3+}	0,000	0,000	0,000	0,000	0,000	0,000	0,009	0,000	0,000	0,000
Mn	0,028	0,028	0,018	0,028	0,021	0,030	0,021	0,022	0,030	0,032
Mg	0,857	0,917	1,122	1,064	1,034	0,891	1,135	1,143	0,925	1,016
Ca	0,948	0,892	0,966	0,685	0,954	0,877	0,951	0,927	0,863	0,686
Na	0,003	0,000	0,003	0,004	0,002	0,000	0,003	0,004	0,003	0,001
Cations	7,994	7,999	7,997	7,989	7,993	7,991	8,003	7,997	7,994	7,991
Charge	23,995	23,991	23,994	23,995	23,994	23,996	23,994	23,996	23,996	23,991

* Fe^{3+} was calculated using the stoichiometric method of *Droop* (1987).

Mineral	cpx1c	cpx1r	cpx2c	cpx2r	cpx3c	cpx3r	cpx5c	cpx5r	cpx6c	cpx6r
SiO_2	55,98	55,80	56,35	56,51	56,15	55,55	56,45	56,24	56,40	56,46
TiO_2	0,05	0,04	0,06	0,05	0,08	0,06	0,04	0,04	0,09	0,10
Al_2O_3	10,48	10,47	10,92	10,40	9,84	10,14	10,35	10,04	10,48	10,47
Cr_2O_3	0,02	0,02	0,03	0,02	0,01	0,03	0,00	0,02	0,05	0,03
FeO	3,80	3,93	3,97	4,28	4,09	4,42	3,97	4,03	4,06	4,11
MnO	0,03	0,00	0,00	0,01	0,02	0,01	0,01	0,00	0,02	0,00
MgO	8,65	8,65	8,42	8,49	9,12	8,53	8,63	8,92	8,86	9,17
CaO	13,88	13,82	13,60	13,63	14,52	13,89	13,85	14,22	14,21	14,33
Na_2O	6,57	6,61	6,87	6,75	6,06	6,48	6,70	6,51	6,54	6,33
Total	99,46	99,33	100,23	100,15	99,89	99,11	100,00	100,00	100,70	101,00
Si	2,000	1,998	1,998	2,007	2,002	1,999	2,007	2,002	1,994	1,990
Ti	0,001	0,001	0,002	0,001	0,002	0,002	0,001	0,001	0,002	0,003
Al	0,441	0,441	0,456	0,435	0,413	0,430	0,433	0,421	0,436	0,434
Cr	0,001	0,000	0,001	0,001	0,000	0,001	0,000	0,001	0,001	0,001
Fe^{2+*}	0,096	0,091	0,094	0,112	0,122	0,103	0,102	0,106	0,100	0,087
Fe^{3+}	0,018	0,027	0,024	0,015	0,000	0,030	0,018	0,015	0,018	0,033
Mn	0,001	0,000	0,000	0,000	0,000	0,000	0,000	0,000	0,000	0,000
Mg	0,461	0,462	0,445	0,450	0,485	0,458	0,457	0,474	0,467	0,482
Ca	0,532	0,530	0,516	0,519	0,555	0,535	0,528	0,543	0,538	0,541
Na	0,455	0,459	0,472	0,465	0,419	0,452	0,462	0,449	0,448	0,433
Cations	4,006	4,009	4,008	4,005	3,998	4,010	4,006	4,011	4,006	4,005
Charge	12,001	11,998	12,001	11,997	11,998	12,001	11,999	12,001	11,993	11,998

Mineral	phg1c	phg1r	phg2c	phg2r	phg3c	phg3r	phg4c	phg4r
SiO_2	51,24	50,53	51,07	51,22	49,87	51,14	50,42	50,54
TiO_2	0,29	0,33	0,29	0,38	0,33	0,28	0,31	0,33
Al_2O_3	25,85	26,52	26,45	27,01	26,98	26,40	26,89	27,22
Cr_2O_3	0,01	0,01	0,06	0,03	0,03	0,03	0,04	0,04
$FeO^{\dagger}$	1,49	1,78	1,43	1,49	1,56	1,37	1,22	1,12
MnO	0,00	0,00	0,00	0,00	0,00	0,00	0,00	0,00
MgO	3,93	3,62	3,64	3,45	3,49	3,71	3,70	3,65
CaO	0,00	0,01	0,01	0,00	0,00	0,00	0,01	0,02
Na_2O	0,39	0,39	0,44	0,48	0,39	0,37	0,47	0,37
K_2O	10,44	10,29	10,43	10,23	10,17	10,41	10,05	10,17
BaO	0,43	0,52	0,15	0,73	0,24	0,21	0,51	0,47
F	0,00	0,00	0,03	0,01	0,00	0,02	0,12	0,05
CL	0,01	0,01	0,00	0,00	0,00	0,00	0,00	0,01
Total	94,09	94,01	93,99	95,02	93,06	93,95	93,73	93,97
Si	6,918	6,841	6,885	6,851	6,796	6,895	6,826	6,814
Ti	0,030	0,034	0,030	0,038	0,033	0,028	0,032	0,033
Al	4,109	4,228	4,199	4,256	4,330	4,191	4,287	4,322
Cr	0,001	0,001	0,006	0,003	0,003	0,003	0,004	0,004
Fe	0,168	0,201	0,162	0,166	0,178	0,154	0,138	0,127
Mn	0,000	0,000	0,000	0,000	0,000	0,000	0,000	0,000
Mg	0,792	0,731	0,732	0,688	0,709	0,746	0,747	0,734
Ca	0,000	0,001	0,001	0,000	0,000	0,000	0,002	0,002
Na	0,103	0,103	0,115	0,123	0,103	0,097	0,124	0,095
K	1,798	1,777	1,794	1,746	1,767	1,790	1,735	1,749
Ba	0,023	0,027	0,008	0,038	0,013	0,011	0,027	0,025
Cations	13,942	13,944	13,932	13,909	13,932	13,915	13,922	13,905
Charge	-	-	-	-	-	-	-	-

[*] Fe^{3+} was calculated using the stoichiometric method of *Droop* (1987).
[†] All Fe is considered Fe^{2+}.

Mineral	amp4a	amp4b	amp5a
SiO_2	52,14	51,55	57,55
TiO_2	0,16	0,19	0,05
Al_2O_3	10,18	10,46	12,46
Cr_2O_3	0,00	0,03	0,02
FeO*	6,34	6,51	4,60
MnO	0,03	0,00	0,01
MgO	16,09	15,51	6,87
CaO	8,51	8,35	10,54
Na_2O	3,13	3,03	8,68
K_2O	0,27	0,26	0,01
F	0,05	0,01	0,00
CL	0,00	0,00	0,00
Total	96,91	95,91	100,78
Si	7,243	7,237	7,740
Ti	0,017	0,020	0,005
Al	1,666	1,728	1,973
Cr	0,000	0,003	0,002
Fe	0,736	0,764	0,517
Mn	0,004	0,000	0,001
Mg	3,333	3,246	1,377
Ca	1,266	1,256	1,518
Na	0,842	0,825	2,262
K	0,048	0,047	0,002
Cations	15,155	15,126	15,397
Charge	45,558	45,578	45,993

Mineral	kya1	kya2	kya3	kya4	kya4b	kya5	kya5b
SiO_2	37,43	37,55	37,59	37,61	37,50	37,70	37,49
TiO_2	0,03	0,02	0,01	0,01	0,00	0,00	0,00
Al_2O_3	62,22	61,11	61,56	61,35	61,82	62,49	62,09
Cr_2O_3	0,09	0,08	0,10	0,04	0,07	0,02	0,04
FeO*	0,54	0,78	0,82	0,82	0,85	0,70	0,66
MnO	0,00	0,00	0,00	0,00	0,00	0,02	0,01
MgO	0,00	0,00	0,00	0,00	0,00	0,01	0,00
CaO	0,00	0,00	0,00	0,01	0,00	0,00	0,01
Na_2O	0,00	0,01	0,00	0,01	0,00	0,00	0,00
K_2O	0,00	0,00	0,00	0,00	0,00	0,00	0,00
Total	100,31	99,54	100,08	99,84	100,24	100,93	100,30
Si	1,009	1,021	1,017	1,020	1,013	1,011	1,011
Ti	0,001	0,000	0,000	0,000	0,000	0,000	0,000
Al	1,975	1,956	1,961	1,958	1,966	1,973	1,972
Cr	0,002	0,002	0,002	0,001	0,002	0,000	0,001
Fe	0,012	0,018	0,018	0,019	0,019	0,016	0,015
Mn	0,000	0,000	0,000	0,000	0,000	0,000	0,000
Mg	0,000	0,000	0,000	0,000	0,000	0,000	0,000
Ca	0,000	0,000	0,000	0,000	0,000	0,000	0,000
Na	0,000	0,000	0,000	0,000	0,000	0,000	0,000
K	0,000	0,000	0,000	0,000	0,000	0,000	0,000
Cations	2,999	2,997	2,998	2,998	3,000	3,000	2,999
Charge	-	-	-	-	-	-	-

* All Fe is considered Fe^{2+}.

Appendix V Thermocalc (3.31) input file

An example of an input file for Thermocalc based on sample 07HA11, 1c

```
% ===================================================
% Garnet: CFMAS
% White, RW, Powell, R & Holland, TJB (2007) Progress relating to calculation
% of partial melting equilibria for metapelites. Journal of Metamorphic Geology,
% 25, 511-527.
%
% garnet here is LESS asymmetric than that of the above paper - 24-2-07)
%
% x(g) = Fe/(Fe + Mg),
% z(g) = Ca/(Fe + Mg + Ca)

g 3

   x(g)        0.882
   z(g)        0.284

% ------------------------------------------------

  p(alm)  1  2    1  1 -1  z    0  1  1  x

  p(py)   1  2    1  1 -1  z    1  1 -1  x

  p(gr)   1 1    0  1  1  z

% ------------------------------------------------
  asf

 W(alm,py)      2.5  0  0
 W(alm,gr)      10   0  0
 W(py,gr)       45  0  0


alm      1 0 0
py       1 0 0
gr       3 0 0

% ------------------------------------------------
  3     % no of site fractions

  xFeX   1  2    1  1 -1  z    0  1  1  x

  xMgX   1  2    1  1 -1  z    1  1 -1  x

  xCaX   1  1    0  1  1  z


% ------------------------------------------------
alm     1  1     xFeX  3

py      1  1     xMgX  3

gr      1  1     xCaX  3
```

```
% ================================================
% ------------------------------------------------
% cpx: NCFF3MAS
%
% Green, ECR, Holland, TJB & Powell, R (2007) An order-disorder model for
% omphacitic pyroxenes in the system jadeite-diopside-hedenbergite-acmite,
% with applications to eclogite rocks. American Mineralogist, 92, 1181-1189.
%
%      M1m             M1a             M2c       M2n
%      Mg  Fe  Fe3 Al   Mg  Fe  Fe3 Al   Na  Ca    Na  Ca
% jd    0   0   0   1/2   0   0   0   1/2   1/2 0     1/2 0
% di    1/2 0   0   0     1/2 0   0   0     0   1/2   0   1/2
% hed   0   1/2 0   0     0   1/2 0   0     0   1/2   0   1/2
% acm   0   0   1/2 0     0   0   1/2 0     1/2 0     1/2 0
% om    1/2 0   0   0     0   0   0   1/2   0   1/2   1/2 0
% cfm   0   1/2 0   0     1/2 0   0   0     0   1/2   0   1/2
% jac   0   0   0   1/2   0   0   1/2 0     1/2 0     1/2 0
%
%            xFe3M1a + xFe3M1m
% f -> ---------------------------------
%      xAlM1a + xAlM1m + xFe3M1a + xFe3M1m
%
%            xFeM1a + xFeM1m
% x -> -------------------------------
%      xFeM1a + xFeM1m + xMgM1a + xMgM1m
%
%      xNaM2c + xNaM2n
% j -> ---------------
%           2
%
%      -xNaM2c + xNaM2n
% Q -> ----------------
%           2
%
%       xFe3M1a - xFe3M1m
% Qaf -> -----------------
%             2
%
%              xFeM1a
% Qfm -> -x + ---------------
%           xFeM1a + xMgM1a
% ------------------------------------------------

o  7

  x(o)          0.200
  j(o)          0.256
  f(o)          0.171
  Q(o)          0.000
  Qaf(o)        0.000  range -0.5 0.5
  Qfm(o)        0.011  range -0.5 0.5

% ------------------------------------------------

p(jd)     2 1    0  3   1  j  -1  Q  -1  Qaf
          2    0  1  -1  f    0  1  1  j
```

```
p(di)     5 1    1  4  -1  j  -1  Q   1  Qfm  -1  x
          2    0  1  -1  j    0  1  1  Qfm
          2    0  1  -1  Q    0  1  1  Qfm
          2    0  1  1  j    0  1  1  x
          2    0  1  -1  Q    0  1  1  x

p(hed)    5 1    0  2   1  Qfm   1  x
          2    0  1  -1  j    0  1  1  Qfm
          2    0  1  -1  Q    0  1  1  Qfm
          2    0  1  -1  j    0  1  1  x
          2    0  1  -1  Q    0  1  1  x

p(acm)    2 1    0  1  -1  Qaf
          2    0  1  1  f    0  1  1  j

p(om)     1 1    0  1  2  Q

p(cfm)    4 1    0  1  -2  Qfm
          2    0  1  2  j    0  1  1  Qfm
          2    0  1  2  Q    0  1  1  Qfm
          2    0  1  2  Q    0  1  1  x

p(jac)    1 1    0  1  2  Qaf
% ------------------------------------------------
sf
W(jd,di)      26  0  0
W(jd,hed)     24  0  0
W(jd,acm)      5  0  0
W(jd,om)    15.5  0  0
W(jd,cfm)   25.2  0  0      % 14.8 + Wjdfom - y
W(jd,jac)      3  0  0
W(di,hed)      4  0  0
W(di,acm)     15  0  0
W(di,om)   15.75  0  0
W(di,cfm)      2  0  0
W(di,jac)  21.05  0  0
W(hed,acm)    14  0  0
W(hed,om)   17.2  0  0      % 6.3 + Whedfom - y
W(hed,cfm)     2  0  0
W(hed,jac)  20.1  0  0
W(acm,om)   12.8  0  0
W(acm,cfm)  15.5  0  0
W(acm,jac)     3  0  0
W(om,cfm)  18.45  0  0
W(om,jac)   19.3  0  0
W(cfm,jac) 21.05  0  0
% ------------------------------------------------
12

xMgM1m    5 1    1  4  -1  j   1  Q   1  Qfm  -1  x
          2    0  1  -1  j    0  1  1  Qfm
          2    0  1  -1  Q    0  1  1  Qfm
          2    0  1  1  j    0  1  1  x
          2    0  1  -1  Q    0  1  1  x

xFeM1m    5 1    0  2  -1  Qfm   1  x
          2    0  1  1  j    0  1  1  Qfm
```

```
        2   0  1  1  Q   0  1  1  Qfm
        2   0  1 -1  j   0  1  1  x
        2   0  1  1  Q   0  1  1  x

xFe3M1m   2 1   0  1 -1  Qaf
        2   0  1  1  f   0  1  1  j

xAlM1m    2 1   0  3  1  j -1  Q  1  Qaf
        2   0  1 -1  f   0  1  1  j

xMgM1a    5 1   1  4 -1  j -1  Q -1  Qfm -1  x
        2   0  1  1  j   0  1  1  Qfm
        2   0  1  1  Q   0  1  1  Qfm
        2   0  1  1  j   0  1  1  x
        2   0  1  1  Q   0  1  1  x

xFeM1a    5 1   0  2  1  Qfm  1  x
        2   0  1 -1  j   0  1  1  Qfm
        2   0  1 -1  Q   0  1  1  Qfm
        2   0  1 -1  j   0  1  1  x
        2   0  1 -1  Q   0  1  1  x

xFe3M1a   2 1   0  1  1  Qaf
        2   0  1  1  f   0  1  1  j

xAlM1a    2 1   0  3  1  j  1  Q -1  Qaf
        2   0  1 -1  f   0  1  1  j

xNaM2c    1 1   0  2  1  j -1  Q

xCaM2c    1 1   1  2 -1  j  1  Q

xNaM2n    1 1   0  2  1  j  1  Q

xCaM2n    1 1   1  2 -1  j -1  Q
% ------------------------------------------------

jd     1   4  xAlM1m 1/2  xAlM1a 1/2  xNaM2c 1/2  xNaM2n 1/2

di     1   4  xMgM1m 1/2  xMgM1a 1/2  xCaM2c 1/2  xCaM2n 1/2

hed    1   4  xFeM1m 1/2  xFeM1a 1/2  xCaM2c 1/2  xCaM2n 1/2

acm    1   4  xFe3M1m 1/2  xFe3M1a 1/2  xNaM2c 1/2  xNaM2n 1/2

om     1   4  xMgM1m 1/2  xAlM1a 1/2  xCaM2c 1/2  xNaM2n 1/2
 make  2  jd 1/2  di 1/2
 DQF  -2.9  0  0

cfm    1   4  xFeM1m 1/2  xMgM1a 1/2  xCaM2c 1/2  xCaM2n 1/2
 make  2  di 1/2  hed 1/2
 DQF  -1.5  0  0

jac    1   4  xAlM1m 1/2  xFe3M1a 1/2  xNaM2c 1/2  xNaM2n 1/2
 make  2  jd 1/2  acm 1/2
 DQF  -1.0  0  0
```

```
% ================================================
% Muscovite: NKFMASH
% Coggon, R. & Holland, T.J.B., 2002. Mixing properties of phengitic micas and revised
% garnet-phengite thermobarometers. Journal of Metamorphic Geology, 20, 683-696.
%
% fe(mu) = Fe/(Fe+Mg)
% y(mu) = X(Al,M2A)
% na(mu) = X(Na,A)

mu  4

  fe(mu)       0.415
  y(mu)        0.615
  na(mu)       0.042
% ------------------------------------------------
       p(mu)      1 1   0  2  1 y -1  na
       p(pa)      1 1   0  1  1 na
       p(cel)     1 2   1  1 -1 fe      1  1 -1  y
       p(fcel)    1 2   0  1  1 fe      1  1 -1  y
       % ------------------------------------------------
 asf
    W(mu,pa)     10.12 0.0034  0.353
    W(mu,cel)     0.00 0.0000  0.200
    W(mu,fcel)    0.00 0.0000  0.200
    W(pa,cel)    52.00 0.0000  0.000
    W(pa,fcel)   52.00 0.0000  0.000
    W(cel,fcel)   0.00 0.0000  0.000

    mu           0.63 0.0 0.0
    pa           0.37 0.0 0.0
    cel          0.63 0.0 0.0
    fcel         0.63 0.0 0.0
       % ------------------------------------------------

  7
    x(K,A)     1  1   1  1 -1  na
    x(Na,A)    1  1   0  1  1  na
    x(Al,M2A)  1  1   0  1  1  y
    x(Fe,M2A)  1  2   0  1  1  fe   1  1 -1  y
    x(Mg,M2A)  1  2   1  1 -1  fe   1  1 -1  y
    x(Si,T1)   1  1   1  1 -1/2  y
    x(Al,T1)   1  1   0  1  1/2  y

       % ------------------------------------------------

    mu        4  4  x(K,A) 1    x(Al,M2A) 1 x(Al,T1) 1  x(Si,T1) 1
                 check 0  1  0
    pa        4  4  x(Na,A) 1   x(Al,M2A) 1 x(Al,T1) 1  x(Si,T1) 1
                 check 0  1  1
    cel       1  3     x(K,A) 1    x(Mg,M2A) 1 x(Si,T1) 2
                 check 0  0  0
    fcel      1  3     x(K,A) 1    x(Fe,M2A) 1 x(Si,T1) 2
                 check 1  0  0
%_____________________________________________________________________________

coe q H2O
```

Appendix VI Argon results

07HA01 (phengite, 1st run)

Incremental Heating	36Ar(a)	37Ar(ca)	38Ar(cl)	39Ar(k)	40Ar(r)	Age ± 2σ (Ma)	40Ar(r) (%)	39Ar(k) (%)	K/Ca ± 2σ
1.50 W	0.001161	0.003775	0.000249	0.021371	0.358832	78.16 ± 4.76	51.12	17.49	2.434 ± 0.172
2.50 W	0.001689	0.005242	0.000264	0.026910	0.925189	156.58 ± 4.24	64.95	22.02	2.208 ± 0.125
3.50 W	0.000785	0.007100	0.000187	0.037538	1.320681	160.07 ± 3.01	85.05	30.71	2.273 ± 0.110
4.50 W	0.000139	0.000920	0.000000	0.009165	0.104445	53.42 ± 8.79	71.77	7.50	4.281 ± 1.120
7.00 W	0.000229	0.000758	0.000103	0.024286	0.150269	29.20 ± 3.31	68.97	19.87	13.769 ± 3.866
9.00 W	0.000040	0.000141	0.000072	0.001443	0.027721	89.14 ± 65.27	69.94	1.18	4.412 ± 8.939
12.00 W	0.000036	0.000000	0.000000	0.001508	0.031008	95.30 ± 48.08	74.66	1.23	
Σ	0.004079	0.017936	0.000875	0.122220	2.918145				

Information on Analysis	Results	40(r)/39(k) ± 2σ	Age ± 2σ (Ma)	MSWD	39Ar(k) (%, n)	K/Ca ± 2σ
VU75-D15	Error Plateau	30.8304 ± 10.7175 ± 34.76%	141.02 ± 47.16 ± 33.44%	467.19	70.22	2.280 ± 0.113
Phengite			External Error ± 47.25	4.30	3	Statistical T Ratio
07HA01			Analytical Error ± 47.16	21.6146		Error Magnification
MG						
Project = VU75	Total Fusion Age	23.8761 ± 0.4553 ± 1.91%	110.16 ± 2.14 ± 1.94%		7	0.083 ± 0.003
Irradiation = VU75			External Error ± 3.07			
J = 0.0026371 ± 0.0000079			Analytical Error ± 2.04			
DRA-1 = 25.260 ± 0.144 Ma						

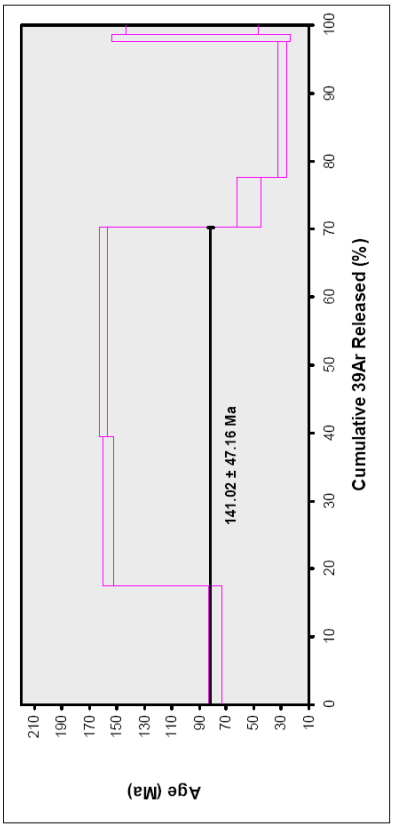

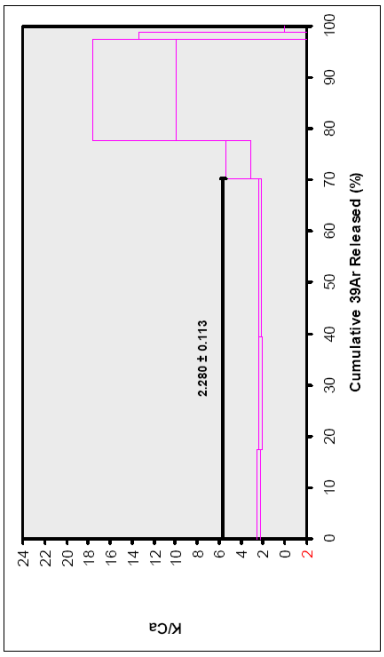

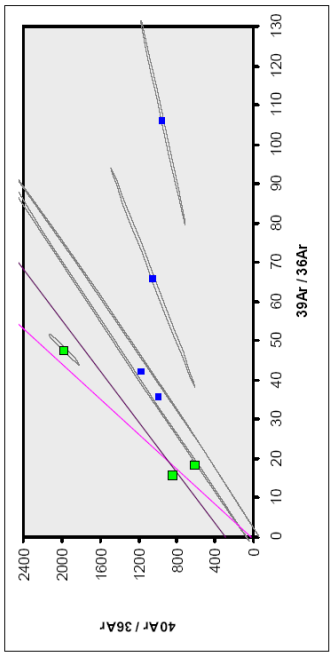

Results	40(a)/36(a) ± 2σ	40(r)/39(k) ± 2σ	Age ± 2σ (Ma)	MSWD
No Convergence	25.9885 ± 754.4591 ± 2903.05%	44.6831 ± 35.8048 ± 80.13%	200.96 ± 152.39 ± 75.83%	> 100
			External Error ± 152.44	
			Analytical Error ± 152.39	

07HA01 (phengite, 2nd run)

Incremental Heating	36Ar(a)	37Ar(ca)	38Ar(cl)	39Ar(k)	40Ar(r)	Age ± 2σ (Ma)	40Ar(r) (%)	39Ar(k) (%)	K/Ca ± 2σ
0.75 W	0.002142	0.000000	0.000000	0.051694	3.173192	270.68 ± 9.25	83.37	34.04	
1.00 W	0.002138	0.000556	0.000000	0.036314	2.226195	270.35 ± 7.34	77.89	23.91	28.061 ± 94.660
1.25 W	0.001877	0.008528	0.000000	0.026864	1.268031	211.65 ± 6.67	69.57	17.69	1.355 ± 0.335
1.50 W	0.000048	0.001661	0.000000	0.001762	0.079202	202.10 ± 86.85	84.73	1.16	0.456 ± 0.613
1.75 W	0.000005	0.002848	0.000000	0.000438	0.024360	246.83 ± 325.76	94.30	0.29	0.066 ± 0.048
3.00 W	0.000109	0.000945	0.000031	0.001584	0.090980	254.50 ± 71.74	73.85	1.04	0.721 ± 1.277
20.00 W	0.034913	0.009639	0.000000	0.033203	0.205208	29.17 ± 61.63	1.95	21.86	1.481 ± 0.354
Σ	0.041233	0.024176	0.000031	0.151858	7.067168				

Information on Analysis	Results	40(r)/39(k) ± 2σ	Age ± 2σ (Ma)	MSWD	39Ar(k) (%,n)	K/Ca ± 2σ
VU75-D15						
Phengite	Weighted Plateau	47.2745 ± 1.5658 ± 3.31%	211.96 ± 6.73 ± 3.18%	0.49	20.18 4	0.095 ± 0.211
07HA01			External Error ± 7.95	3.18	Statistical T Ratio	
MG			Analytical Error ± 6.62	1.0000	Error Magnification	
Project = VU75						
Irradiation = VU75	Total Fusion Age	46.5379 ± 3.0080 ± 6.46%	208.84 ± 12.80 ± 6.13%		7	0.076 ± 0.017
J = 0.0026371 ± 0.0000079			External Error ± 13.47			
DRA-1 = 25.260 ± 0.144 Ma			Analytical Error ± 12.75			

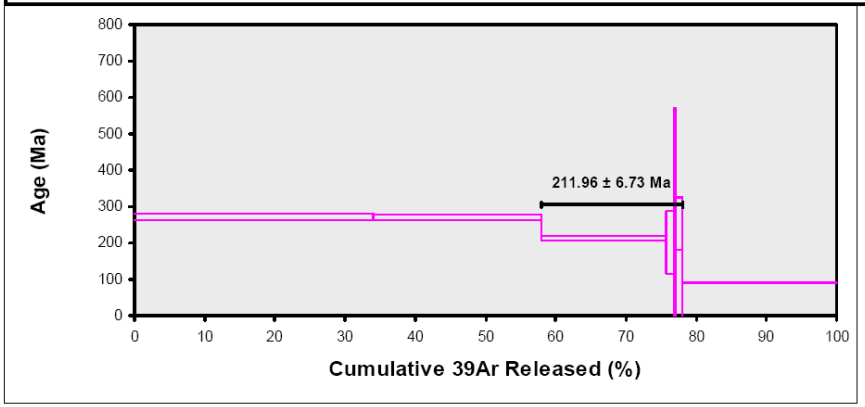

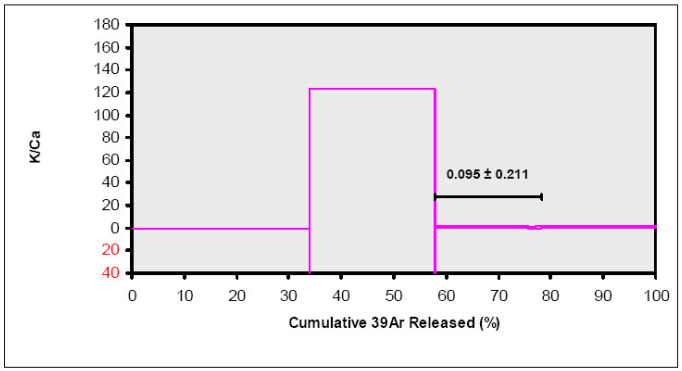

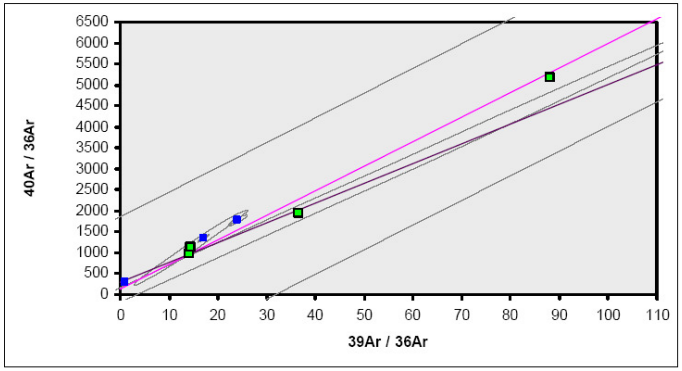

Results	40(a)/36(a) ± 2σ	40(r)/39(k) ± 2σ	Age ± 2σ (Ma)	MSWD
No Convergence	133.4670 ± 321.7564 ± 241.08%	58.5539 ± 22.3916 ± 38.24%	259.05 ± 92.29 ± 35.63%	1.52
			External Error ± 92.44	
			Analytical Error ± 92.28	

07HA01 (phengite, combination)

Incremental Heating	36Ar(a)	37Ar(ca)	38Ar(cl)	39Ar(k)	40Ar(r)	Age ± 2σ (Ma)	40Ar(r) (%)	39Ar(k) (%)	K/Ca ± 2σ
0.75 W	0.002142	0.000000	0.000000	0.051694	3.173192	270.68 ± 9.25	83.37	18.86	
1.00 W	0.002138	0.000556	0.000000	0.036314	2.226195	270.35 ± 7.34	77.89	13.25	28.061 ± 94.660
1.25 W	0.001877	0.008528	0.000000	0.026864	1.268031	211.65 ± 6.67	69.57	9.80	1.355 ± 0.335
1.50 W	0.001161	0.003775	0.000249	0.021371	0.358832	78.16 ± 4.76	51.12	7.80	2.434 ± 0.172
1.50 W	0.000048	0.001661	0.000000	0.001762	0.079202	202.10 ± 86.85	84.73	0.64	0.456 ± 0.613
1.75 W	0.000005	0.002848	0.000000	0.000438	0.024360	246.83 ± 325.76	94.30	0.16	0.066 ± 0.048
2.50 W	0.001689	0.005242	0.000264	0.026910	0.925189	156.58 ± 4.24	64.95	9.82	2.208 ± 0.125
3.00 W	0.000109	0.000945	0.000031	0.001584	0.090980	254.50 ± 71.74	73.85	0.58	0.721 ± 1.277
3.50 W	0.000785	0.007100	0.000187	0.037538	1.320681	160.07 ± 3.01	85.05	13.70	2.273 ± 0.110
4.50 W	0.000139	0.000920	0.000000	0.009165	0.104445	53.42 ± 8.79	71.77	3.34	4.281 ± 1.120
7.00 W	0.000229	0.000758	0.000103	0.024286	0.150269	29.20 ± 3.31	68.97	8.86	13.769 ± 3.866
9.00 W	0.000040	0.000141	0.000072	0.001443	0.027721	89.14 ± 65.27	69.94	0.53	4.412 ± 8.939
12.00 W	0.000036	0.000000	0.000000	0.001508	0.031008	95.30 ± 48.08	74.66	0.55	
20.00 W	0.034913	0.009639	0.000000	0.033203	0.205208	29.17 ± 61.63	1.95	12.11	1.481 ± 0.354
Σ	0.041233	0.024176	0.000031	0.151858	7.067168				

Information on Analysis	Results	40(r)/39(k) ± 2σ	Age ± 2σ (Ma)	MSWD	39Ar(k) (%,n)	K/Ca ± 2σ
VU75-D15	Weighted Plateau	34.9456 ± 0.8799 ± 2.52%	159.03 ± 3.94 ± 2.48%	2.44	24.89	0.608 ± 0.940
Phengite					5	
07HA01			External Error ± 5.06	2.78	Statistical T Ratio	
MG			Analytical Error ± 3.83	1.5634	Error Magnification	
Project = VU75	Total Fusion Age	36.4323 ± 1.6666 ± 4.57%	165.50 ± 7.30 ± 4.41%		14	0.079 ± 0.010
Irradiation = VU75						
J = 0.0026371 ± 0.0000079			External Error ± 8.01			
DRA-1 = 25.260 ± 0.144 Ma			Analytical Error ± 7.23			

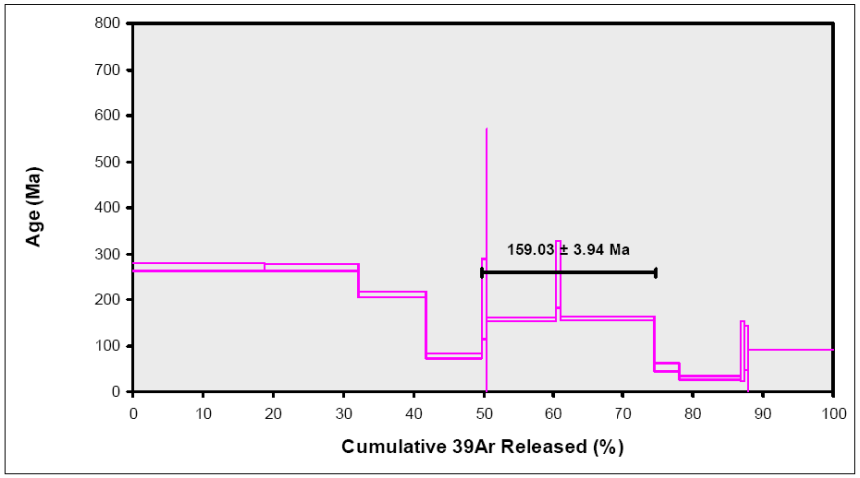

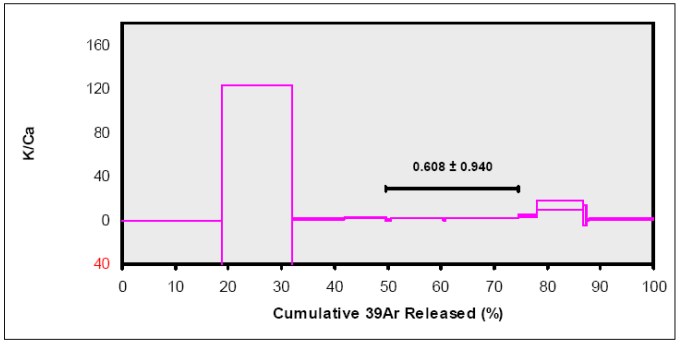

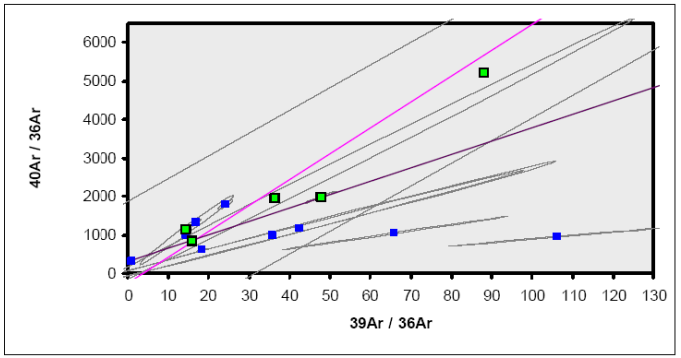

Results	40(a)/36(a) ± 2σ	40(r)/39(k) ± 2σ	Age ± 2σ (Ma)	MSWD
Error Chron	247.3142 ± 651.8106 ± 263.56%	67.3669 ± 37.9236 ± 56.29%	295.01 ± 153.21 ± 51.94%	> 100
			External Error ± 153.33	
			Analytical Error ± 153.21	

07HA02 (phengite, 1st run)

Incremental Heating	36Ar(a)	37Ar(ca)	38Ar(cl)	39Ar(k)	40Ar(r)	Age ± 2σ (Ma)	40Ar(r) (%)	39Ar(k) (%)	K/Ca ± 2σ
1.50 W	0.000876	0.000987	0.000000	0.206470	8.559762	187.25 ± 1.06	97.06	16.39	89.987 ± 18.372
2.50 W	0.000365	0.004299	0.000000	0.512221	21.359609	188.29 ± 0.97	99.49	40.66	51.238 ± 3.704
3.50 W	0.000164	0.046105	0.000475	0.395384	16.863388	192.36 ± 0.96	99.71	31.39	3.688 ± 0.119
4.50 W	0.000069	0.001918	0.000000	0.033728	1.372074	183.91 ± 2.57	98.53	2.68	7.561 ± 0.974
7.00 W	0.000050	0.001506	0.000000	0.026742	1.046870	177.31 ± 2.88	98.61	2.12	7.636 ± 1.194
9.00 W	0.001746	0.002792	0.000208	0.060669	1.264155	96.54 ± 1.89	71.01	4.82	9.343 ± 0.920
12.00 W	0.000000	0.000900	0.000000	0.020262	0.806275	180.09 ± 2.28	100.00	1.61	9.686 ± 2.958
16.00 W	0.000000	0.000187	0.000000	0.004226	0.177157	189.24 ± 7.98	100.00	0.34	9.725 ± 9.422
Σ	0.003270	0.058693	0.000683	1.259702	51.449292				

Information on Analysis	Results	40(r)/39(k) ± 2σ	Age ± 2σ (Ma)	MSWD	39Ar(k) (%,n)	K/Ca ± 2σ
VU75-D16	Error Plateau	41.9661 ± 0.7313 ± 1.74%	189.43 ± 3.31 ± 1.75%	29.72	88.44 3	3.740 ± 2.303
Phengite			External Error ± 5.03	4.30	Statistical T Ratio	
07HA02			Analytical Error ± 3.13	5.4519	Error Magnification	
MG						
Project = VU75	Total Fusion Age	40.8424 ± 0.1247 ± 0.31%	184.61 ± 1.18 ± 0.64%		8	0.260 ± 0.007
Irradiation = VU75			External Error ± 3.88			
J = 0.0026381 ± 0.0000079			Analytical Error ± 0.54			
DRA-1 = 25.260 ± 0.144 Ma						

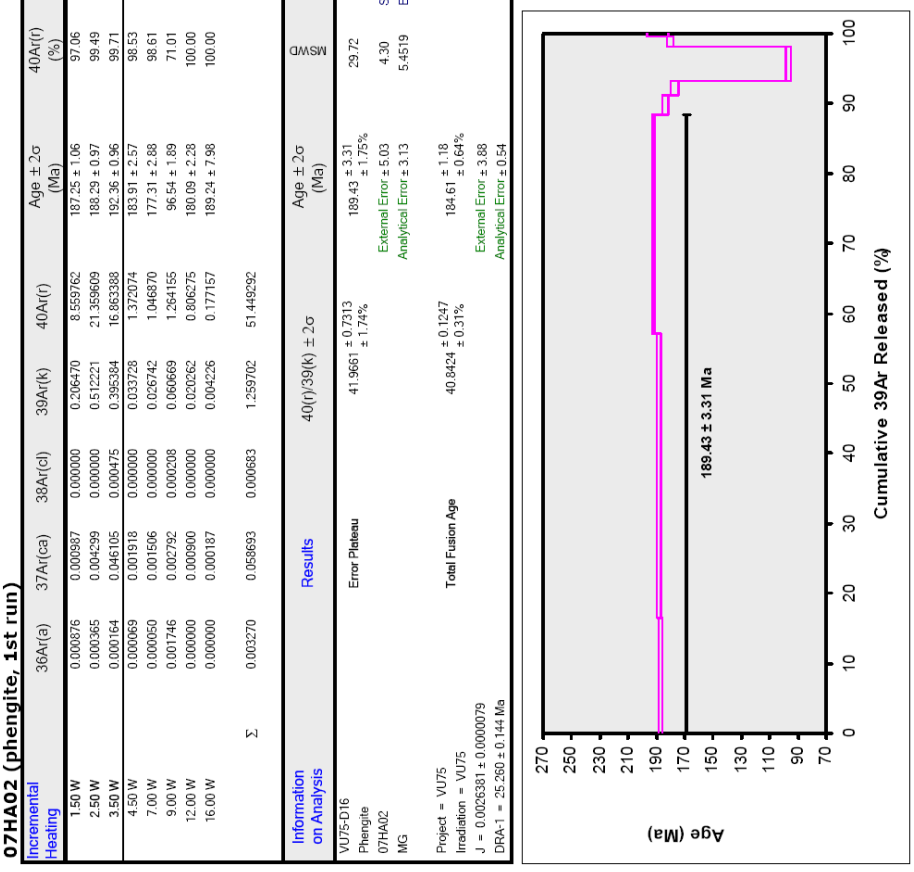

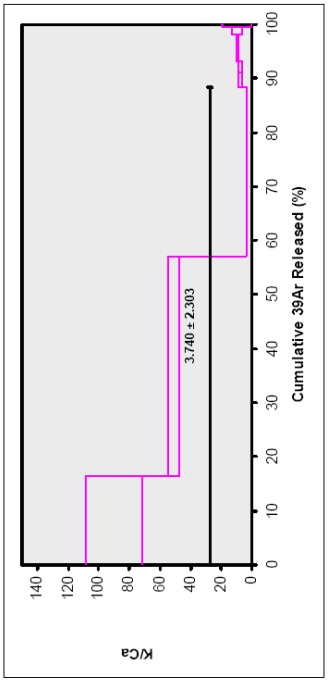

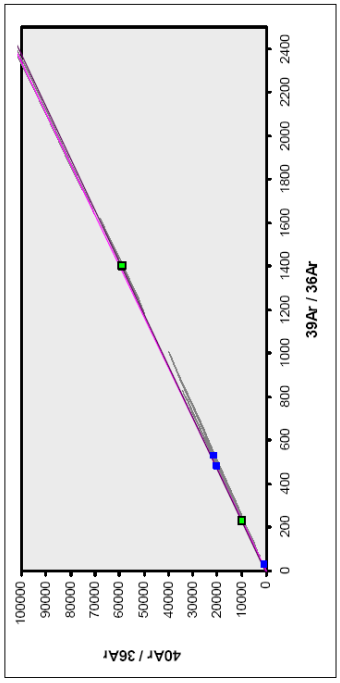

Results	40(a)/36(a) ± 2σ	40(r)/39(k) ± 2σ	Age ± 2σ (Ma)	MSWD
No Convergence	30.7660 ± 480.5491 ± 1561.95%	42.7421 ± 1.2295 ± 2.88%	192.75 ± 5.37 ± 2.79% External Error ± 6.61 Analytical Error ± 5.26	38.89

07HA02 (phengite, 2nd run)

Incremental Heating	36Ar(a)	37Ar(ca)	38Ar(cl)	39Ar(k)	40Ar(r)	Age ± 2σ (Ma)	40Ar(r) (%)	39Ar(k) (%)	K/Ca ± 2σ
0.75 W	0.000083	0.000000	0.000000	0.241866	12.442119	229.58 ± 5.12	99.80	2.82	280.709 ± 649.432
1.00 W	0.001498	0.002915	0.000000	0.623210	38.193197	270.36 ± 7.87	98.85	7.28	91.929 ± 52.866
1.25 W	0.001498	0.002953	0.000000	0.809946	34.372608	191.45 ± 2.25	98.72	9.46	117.928 ± 93.148
1.50 W	0.001815	0.003719	0.000000	0.858633	35.894672	188.74 ± 1.95	98.52	10.02	99.289 ± 63.468
1.75 W	0.001469	0.003480	0.000000	1.295457	53.859086	187.75 ± 1.90	99.20	15.12	160.048 ± 137.054
2.00 W	0.000489	0.001719	0.000000	1.540369	64.334654	188.57 ± 1.90	99.77	17.98	385.400 ± 662.808
3.00 W	0.001769	0.003886	0.000000	2.097772	86.363994	186.01 ± 1.88	99.39	24.49	232.152 ± 158.773
4.00 W	0.000190	0.004061	0.000000	0.609457	24.214535	179.83 ± 1.82	99.76	7.12	64.539 ± 44.083
6.00 W	0.000070	0.000000	0.000000	0.338766	14.138634	188.44 ± 1.96	99.85	3.96	89.990 ± 125.483
7.50 W	0.000042	0.000704	0.000000	0.026852	1.106434	186.17 ± 5.08	98.88	0.31	16.398 ± 46.518
25.00 W	0.000806	0.000863	0.000000	0.123133	5.106337	187.30 ± 2.16	95.54	1.44	61.344 ± 138.427
Σ	0.009731	0.024299	0.000000	8.565460	370.026272				

Information on Analysis	Results	40(r)/39(k) ± 2σ	Age ± 2σ (Ma)	MSWD	39Ar(k) (%,n)	K/Ca ± 2σ
VU75-D16	Error Plateau	41.7043 ± 0.3881 ± 0.93%	188.31 ± 1.98 ± 1.05%	3.59	77.08	123.935 ± 46.692
Phengite					5	
07HA02			External Error ± 4.25	2.78	Statistical T Ratio	
MG			Analytical Error ± 1.66	1.8945	Error Magnification	
Project = VU75	Total Fusion Age	43.1998 ± 0.2034 ± 0.47%	194.71 ± 1.41 ± 0.72%		11	4.269 ± 1.386
Irradiation = VU75						
J = 0.0026381 ± 0.0000079			External Error ± 4.14			
DRA-1 = 25.260 ± 0.144 Ma			Analytical Error ± 0.87			

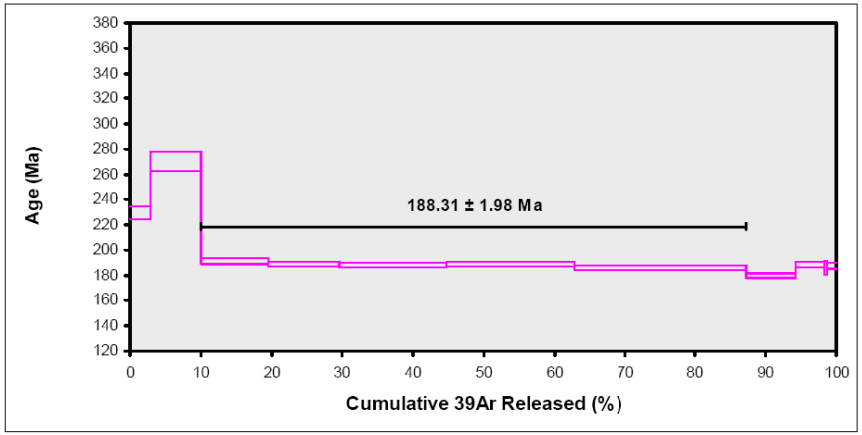

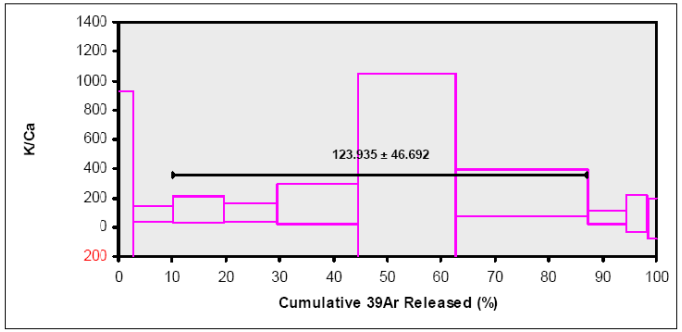

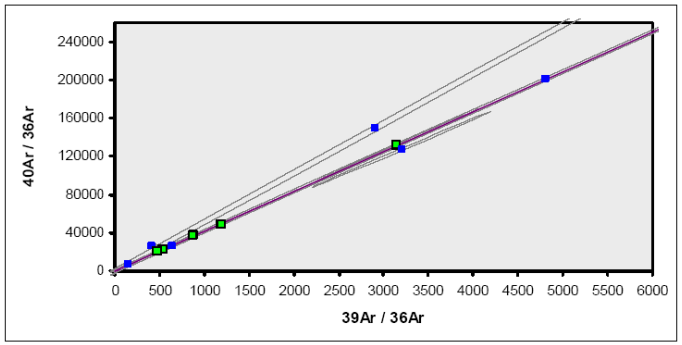

Results	40(a)/36(a) ± 2σ	40(r)/39(k) ± 2σ	Age ± 2σ (Ma)	MSWD
No Convergence	387.2166 ± 650.3268 ± 167.95%	41.6647 ± 0.8922 ± 2.14%	188.14 ± 3.97 ± 2.11%	4.29
			External Error ± 5.47	
			Analytical Error ± 3.83	

07HA02 (phengite, combination)

Incremental Heating	36Ar(a)	37Ar(ca)	38Ar(cl)	39Ar(k)	40Ar(r)	Age ± 2σ (Ma)	40Ar(r) (%)	39Ar(k) (%)	K/Ca ± 2σ
0.75 W	0.000083	0.000000	0.000000	0.241866	12.442119	229.58 ± 5.12	99.80	2.47	9.725 ± 9.422
1.00 W	0.001498	0.002915	0.000000	0.623210	38.193197	270.36 ± 7.87	98.85	6.36	91.929 ± 52.866
1.25 W	0.001498	0.002953	0.000000	0.809946	34.372608	191.45 ± 2.25	98.72	8.26	117.928 ± 93.148
1.50 W	0.000876	0.000987	0.000000	0.206470	8.559762	187.25 ± 1.06	97.06	2.11	89.987 ± 18.372
1.50 W	0.001815	0.003719	0.000000	0.858633	35.894672	188.74 ± 1.95	98.52	8.76	99.289 ± 63.468
1.75 W	0.001469	0.003480	0.000000	1.295457	53.859086	187.75 ± 1.90	99.20	13.22	160.048 ± 137.054
2.00 W	0.000489	0.001719	0.000000	1.540369	64.334654	188.57 ± 1.90	99.77	15.72	385.400 ± 662.808
2.50 W	0.000365	0.004299	0.000000	0.512221	21.359609	188.29 ± 0.97	99.49	5.23	51.238 ± 3.704
3.00 W	0.001769	0.003886	0.000000	2.097772	86.363994	186.01 ± 1.88	99.39	21.40	232.152 ± 158.773
3.50 W	0.000164	0.046105	0.000475	0.395384	16.863388	192.36 ± 0.96	99.71	4.03	3.688 ± 0.119
4.00 W	0.000190	0.004061	0.000000	0.609457	24.214535	179.83 ± 1.82	99.76	6.22	64.539 ± 44.083
4.50 W	0.000069	0.001918	0.000000	0.033728	1.372074	183.91 ± 2.57	98.53	0.34	7.561 ± 0.974
6.00 W	0.000070	0.000000	0.000000	0.338766	14.138634	188.44 ± 1.96	99.85	3.46	9.725 ± 9.422
7.00 W	0.000050	0.001506	0.000000	0.026742	1.046870	177.31 ± 2.88	98.61	0.27	7.636 ± 1.194
7.50 W	0.000042	0.000704	0.000000	0.026852	1.106434	186.17 ± 5.08	98.88	0.27	16.398 ± 46.518
9.00 W	0.001746	0.002792	0.000208	0.060669	1.264155	96.54 ± 1.89	71.01	0.62	9.343 ± 0.920
25.00 W	0.000806	0.000863	0.000000	0.123133	5.106337	187.30 ± 2.16	95.54	1.26	61.344 ± 138.427
Σ	0.013001	0.081906	0.000683	9.800673	420.492131				

Information on Analysis	Results	40(r)/39(k) ± 2σ	Age ± 2σ (Ma)	MSWD	39Ar(k) (%,n)	K/Ca ± 2σ
VU75-D16	Error Plateau	41.6483 ± 0.4637 ± 1.11%	188.07 ± 2.26 ± 1.20%	20.54	89.30	3.836 ± 1.012
Phengite					13	
07HA02			External Error ± 4.39	2.18	Statistical T Ratio	
MG			Analytical Error ± 1.99	4.5324	Error Magnification	
Project = VU75	Total Fusion Age	42.9044 ± 0.1773 ± 0.41%	193.44 ± 1.34 ± 0.69%		17	1.449 ± 0.142
Irradiation = VU75						
J = 0.0026381 ± 0.0000079			External Error ± 4.09			
DRA-1 = 25.260 ± 0.144 Ma			Analytical Error ± 0.76			

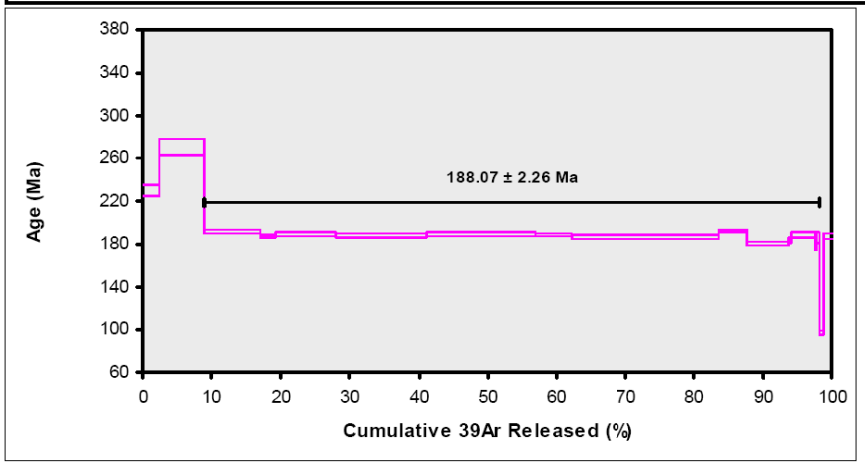

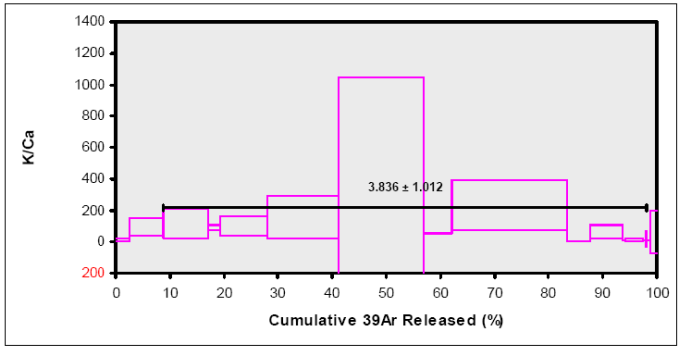

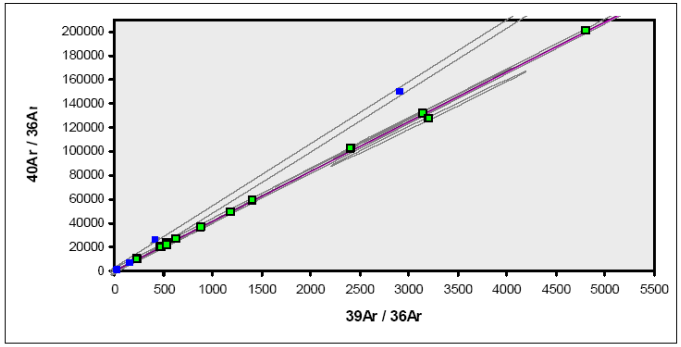

Results	40(a)/36(a) ± 2σ	40(r)/39(k) ± 2σ	Age ± 2σ (Ma)	MSWD
No Convergence	298.1131 ± 236.1799 ± 79.22%	41.4832 ± 0.5323 ± 1.28%	187.36 ± 2.52 ± 1.35%	8.75
			External Error ± 4.52	
			Analytical Error ± 2.28	

07HA11 (actinolite)

Incremental Heating	36Ar(a)	37Ar(ca)	38Ar(cl)	39Ar(k)	40Ar(r)	Age ± 2σ (Ma)	40Ar(r) (%)	39Ar(k) (%)	K/Ca ± 2σ
4.00 W	0.107111	0.438198	0.000000	0.124093	36.732390	1035.24 ± 22.79	53.72	0.62	0.122 ± 0.006
4.50 W	0.041330	0.486682	0.000084	0.124867	12.311106	414.30 ± 12.32	50.20	0.62	0.110 ± 0.006
5.00 W	0.026310	0.481956	0.000000	0.138658	11.659982	359.02 ± 7.65	60.00	0.69	0.124 ± 0.007
6.00 W	0.036949	1.509955	0.000086	0.444007	45.486049	428.70 ± 4.43	80.64	2.21	0.126 ± 0.007
7.00 W	0.047211	3.473945	0.000000	1.036379	100.446749	408.01 ± 3.39	87.80	5.17	0.128 ± 0.007
8.00 W	0.032456	6.038260	0.000767	1.395791	133.298012	402.65 ± 3.08	93.29	6.96	0.099 ± 0.005
7.00 W	0.035681	1.505348	0.000000	0.351842	30.198213	365.73 ± 4.75	74.12	1.75	0.101 ± 0.006
8.00 W	0.039756	7.160645	0.001405	1.380268	131.295267	401.23 ± 3.11	91.79	6.88	0.083 ± 0.005
9.00 W	0.036962	11.931946	0.002424	2.592781	238.857781	389.85 ± 2.94	95.63	12.92	0.093 ± 0.005
12.00 W	0.080381	22.562454	0.004603	5.004904	490.044821	411.75 ± 3.20	95.38	24.94	0.095 ± 0.005
14.00 W	0.037011	14.319672	0.004214	3.473399	323.379417	393.57 ± 2.90	96.73	17.31	0.104 ± 0.006
17.00 W	0.021592	8.528849	0.000000	1.733356	158.537027	387.33 ± 3.08	96.13	8.64	0.087 ± 0.005
22.00 W	0.020691	7.136729	0.002457	1.269663	116.482968	388.40 ± 2.92	95.01	6.33	0.076 ± 0.004
27.00 W	0.014866	5.181669	0.000827	0.843783	75.430929	379.44 ± 2.95	94.49	4.21	0.070 ± 0.004
25.00 W	0.012378	1.159295	0.000120	0.150267	11.474176	328.83 ± 4.47	75.83	0.75	0.056 ± 0.003
Σ	0.590684	91.915601	0.016985	20.064057	1915.634888				

Information on Analysis	Results	40(r)/39(k) ± 2σ	Age ± 2σ (Ma)	MSWD	39Ar(k) (%,n)	K/Ca ± 2σ
VU75-D5 Actinolite 07HA11 MG	Error Plateau	93.5630 ± 2.2308 ± 2.38%	395.32 ± 8.73 ± 2.21% External Error ± 11.78 Analytical Error ± 8.46	76.03 2.23 8.7197	97.32 11 Statistical T Ratio Error Magnification	0.091 ± 0.010
Project = VU75 Irradiation = VU75 J = 0.0026184 ± 0.0000079 DRA-1 = 25.260 ± 0.144 Ma	Total Fusion Age	95.4760 ± 0.3065 ± 0.32%	402.56 ± 2.46 ± 0.61% External Error ± 8.42 Analytical Error ± 1.16		15	0.003 ± 0.000

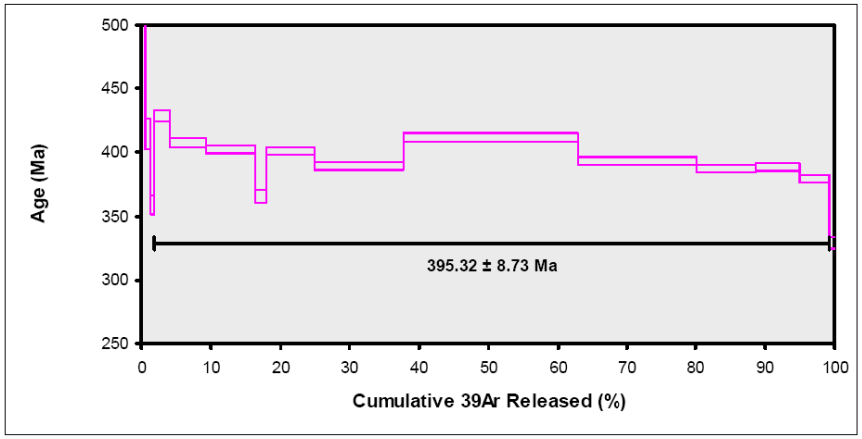

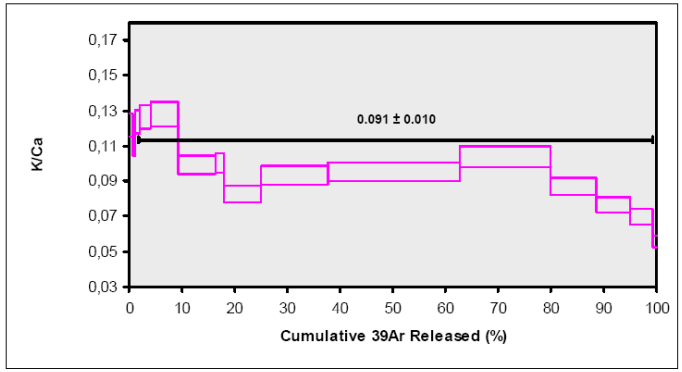

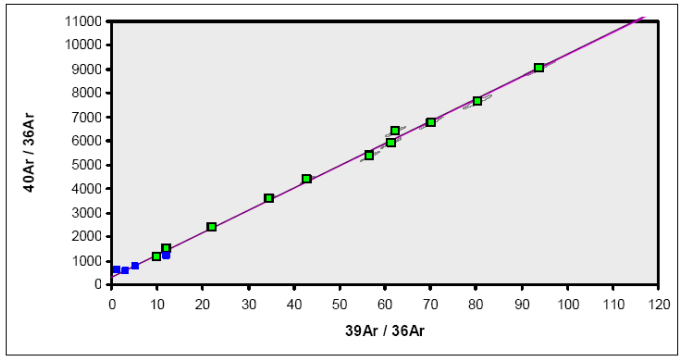

Results	40(a)/36(a) ± 2σ	40(r)/39(k) ± 2σ	Age ± 2σ (Ma)	MSWD
No Convergence	297.1828 ± 99.2650 ± 33.40%	93.1696 ± 3.5065 ± 3.76%	393.82 ± 13.48 ± 3.42% External Error ± 15.62 Analytical Error ± 13.32	81.54

07LT01 (biotite, 1st run, excess argon isochron)

Incremental Heating	36Ar(a)	37Ar(ca)	38Ar(cl)	39Ar(k)	40Ar(r)	Age ± 2σ (Ma)	40Ar(r) (%)	39Ar(k) (%)	K/Ca ± 2σ
1.00 W	0.000265	0.000141	0.000069	0.001597	0.048468	139.01 ± 39.35	38.19	0.14	4.862 ± 7.472
1.50 W	0.000339	0.000115	0.000000	0.020408	0.511877	115.66 ± 4.68	83.62	1.83	76.115 ± 128.138
2.50 W	0.000807	0.000467	0.000108	0.071300	1.854692	119.81 ± 1.88	88.60	6.38	65.668 ± 26.439
3.50 W	0.000418	0.000321	0.000114	0.111820	2.890156	119.07 ± 1.14	95.89	10.00	149.888 ± 76.950
4.50 W	0.000160	0.000899	0.000181	0.136006	3.562967	120.64 ± 0.94	98.68	12.17	65.066 ± 19.911
7.00 W	0.001444	0.000592	0.000260	0.251798	8.283261	150.23 ± 0.81	95.10	22.53	182.809 ± 62.355
9.00 W	0.000060	0.000230	0.000135	0.027025	0.692409	118.07 ± 2.54	97.51	2.42	50.570 ± 50.957
9.00 W	0.001890	0.008790	0.000618	0.479533	16.051891	152.76 ± 0.78	96.63	42.90	23.459 ± 1.425
12.00 W	0.000939	0.003439	0.000000	0.018193	1.557432	367.57 ± 5.85	84.87	1.63	2.275 ± 0.240
Σ	0.006322	0.014994	0.001484	1.117679	35.453152				

Information on Analysis	Results	40(r)/39(k) ± 2σ	Age ± 2σ (Ma)	MSWD	39Ar(k) (%,n)	K/Ca ± 2σ
VU75-D18	Error Plateau	31.5890 ± 5.7889 ± 18.33%	144.50 ± 25.46 ± 17.62%	2807.40	79.23	2.870 ± 4.170
Biotite					4	
07LT01			External Error ± 25.62	3.18	Statistical T Ratio	
MG			Analytical Error ± 25.45	52.9849	Error Magnification	
Project = VU75	Total Fusion Age	31.7203 ± 0.1035 ± 0.33%	145.07 ± 0.95 ± 0.66%		9	0.903 ± 0.052
Irradiation = VU75						
J = 0.0026398 ± 0.0000079			External Error ± 3.05			
DRA-1 = 25.260 ± 0.144 Ma			Analytical Error ± 0.45			

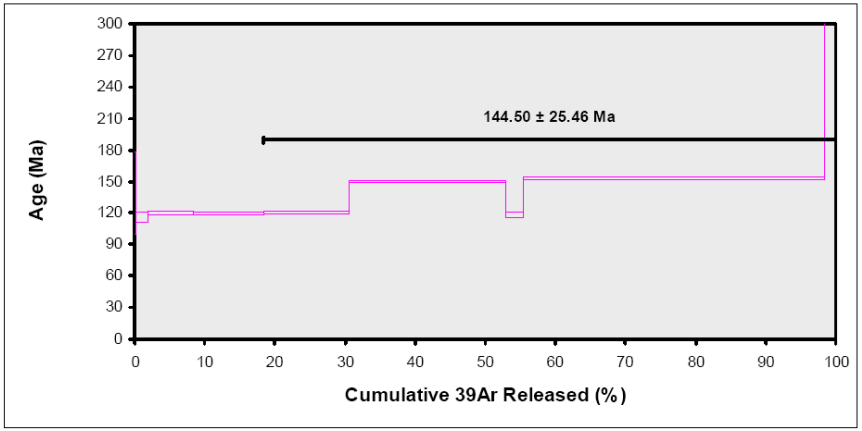

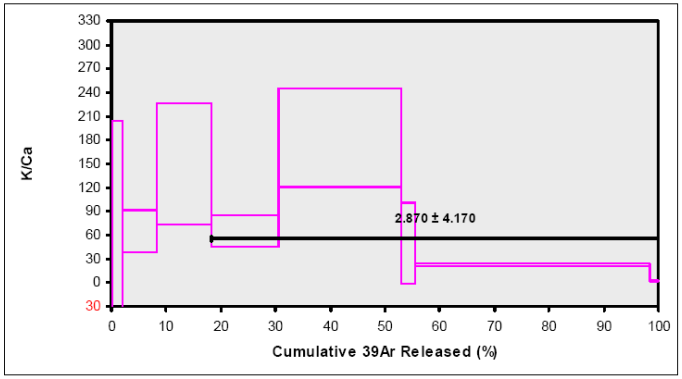

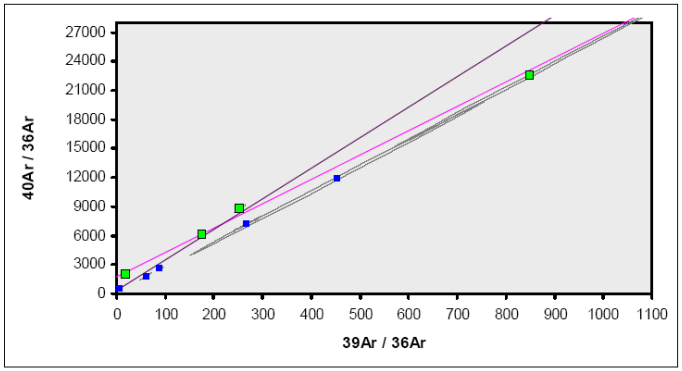

Results	40(a)/36(a) ± 2σ	40(r)/39(k) ± 2σ	Age ± 2σ (Ma)	MSWD
No Convergence	1765.7578 ± 853.5943 ± 48.34%	25.1126 ± 4.1651 ± 16.59%	115.80 ± 18.61 ± 16.08%	82.91
			External Error ± 18.76	
			Analytical Error ± 18.60	

07LT01 (biotite, 1st run, radiogenic argon isochron)

Incremental Heating	36Ar(a)	37Ar(ca)	38Ar(cl)	39Ar(k)	40Ar(r)	Age ± 2σ (Ma)	40Ar(r) (%)	39Ar(k) (%)	K/Ca ± 2σ
1.00 W	0.000265	0.000141	0.000069	0.001597	0.048468	139.01 ± 39.35	38.19	0.14	4.862 ± 7.472
1.50 W	0.000339	0.000115	0.000000	0.020408	0.511877	115.66 ± 4.68	83.62	1.83	76.115 ± 128.138
2.50 W	0.000807	0.000467	0.000108	0.071300	1.854692	119.81 ± 1.88	88.60	6.38	65.668 ± 26.439
3.50 W	0.000418	0.000321	0.000114	0.111820	2.890156	119.07 ± 1.14	95.89	10.00	149.888 ± 76.950
4.50 W	0.000160	0.000899	0.000181	0.136006	3.562967	120.64 ± 0.94	98.68	12.17	65.066 ± 19.911
7.00 W	0.001444	0.000592	0.000260	0.251798	8.283261	150.23 ± 0.81	95.10	22.53	182.809 ± 62.355
9.00 W	0.000060	0.000230	0.000135	0.027025	0.692409	118.07 ± 2.54	97.51	2.42	50.570 ± 50.957
9.00 W	0.001890	0.008790	0.000618	0.479533	16.051891	152.76 ± 0.78	96.63	42.90	23.459 ± 1.425
12.00 W	0.000939	0.003439	0.000000	0.018193	1.557432	367.57 ± 5.85	84.87	1.63	2.275 ± 0.240
Σ	0.006322	0.014994	0.001484	1.117679	35.453152				

Information on Analysis	Results	40(r)/39(k) ± 2σ	Age ± 2σ (Ma)	MSWD	39Ar(k) (%,n)	K/Ca ± 2σ
VU75-D18	Weighted Plateau	26.0308 ± 0.2224 ± 0.85%	119.90 ± 1.21 ± 1.01%	2.20	30.52	16.978 ± 26.100
Biotite					5	
07LT01			External Error ± 2.69	2.78	Statistical T Ratio	
MG			Analytical Error ± 0.99	1.4841	Error Magnification	
Project = VU75	Total Fusion Age	31.7203 ± 0.1035 ± 0.33%	145.07 ± 0.95 ± 0.66%		9	0.903 ± 0.052
Irradiation = VU75						
J = 0.0026398 ± 0.0000079			External Error ± 3.05			
DRA-1 = 25.260 ± 0.144 Ma			Analytical Error ± 0.45			

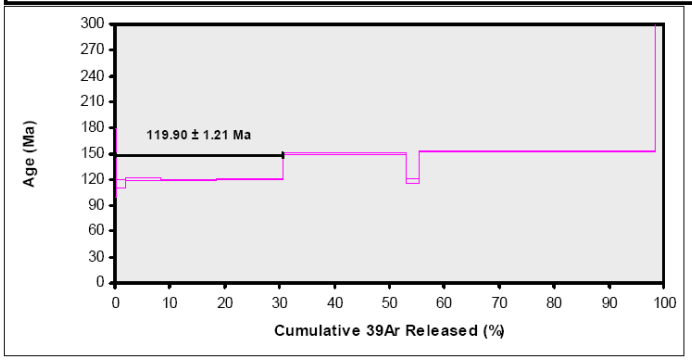

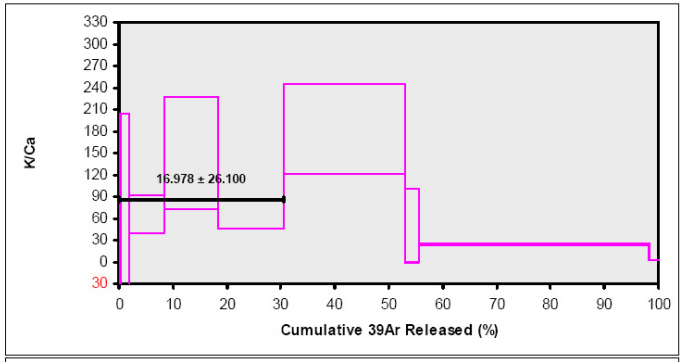

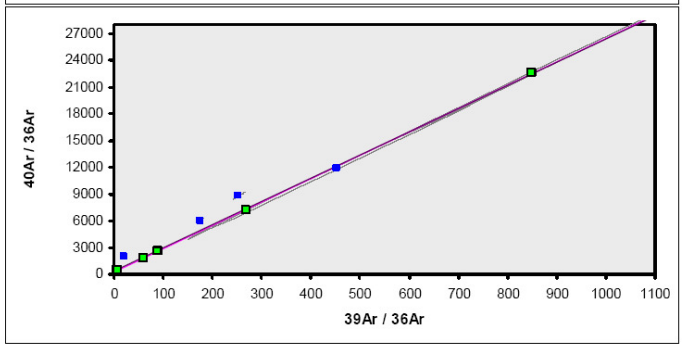

Results	40(a)/36(a) ± 2σ	40(r)/39(k) ± 2σ	Age ± 2σ (Ma)	MSWD
No Convergence	263.5121 ± 59.2928 ± 22.50%	26.2029 ± 0.3565 ± 1.36%	120.66 ± 1.74 ± 1.44%	3.56
			External Error ± 2.97	
			Analytical Error ± 1.59	

07LT01 (biotite, 2nd run)

Incremental Heating	36Ar(a)	37Ar(ca)	38Ar(cl)	39Ar(k)	40Ar(r)	Age ± 2σ (Ma)	40Ar(r) (%)	39Ar(k) (%)	K/Ca ± 2σ
1.50 W	0.000406	0.001217	0.000000	0.941276	26.138687	127.63 ± 4.36	99.54	35.39	332.552 ± 608.801
1.00 W	0.000013	0.001350	0.000000	0.068472	2.434910	161.87 ± 6.23	99.84	2.57	21.814 ± 47.074
1.25 W	0.000014	0.000000	0.000000	0.114200	3.896223	155.58 ± 2.27	99.89	4.29	166.655 ± 956.262
1.50 W	0.000255	0.002601	0.000000	0.540913	13.731420	117.02 ± 1.64	99.45	20.34	89.428 ± 84.027
1.75 W	0.000295	0.004997	0.000000	0.727461	18.595441	117.81 ± 1.40	99.53	27.35	62.596 ± 24.678
2.00 W	0.000151	0.002492	0.000438	0.230433	5.950786	118.98 ± 1.45	99.25	8.66	39.759 ± 34.877
2.50 W	0.000038	0.000000	0.000000	0.022682	0.586825	119.19 ± 6.40	98.09	0.85	5.077 ± 4.555
3.00 W	0.000070	0.001725	0.000000	0.014335	0.364157	117.10 ± 11.53	94.60	0.54	3.574 ± 4.111
Σ	0.001243	0.014382	0.000438	2.659771	71.698449				

Information on Analysis	Results	40(r)/39(k) ± 2σ	Age ± 2σ (Ma)	MSWD	39Ar(k) (%,n)	K/Ca ± 2σ
VU75-D18	Weighted Plateau	25.6093 ± 0.1898 ± 0.74%	118.02 ± 1.09 ± 0.92%	0.87	57.74	5.495 ± 8.283
Biotite					5	
07LT01			External Error ± 2.60	2.78	Statistical T Ratio	
MG			Analytical Error ± 0.85	1.0000	Error Magnification	
Project = VU75	Total Fusion Age	26.9566 ± 0.3649 ± 1.35%	124.02 ± 1.77 ± 1.43%		8	2.240 ± 0.942
Irradiation = VU75						
J = 0.0026398 ± 0.0000079			External Error ± 3.05			
DRA-1 = 25.260 ± 0.144 Ma			Analytical Error ± 1.62			

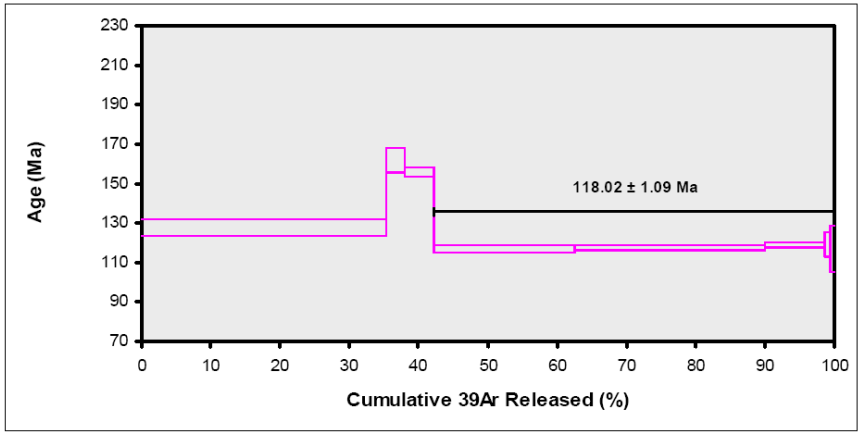

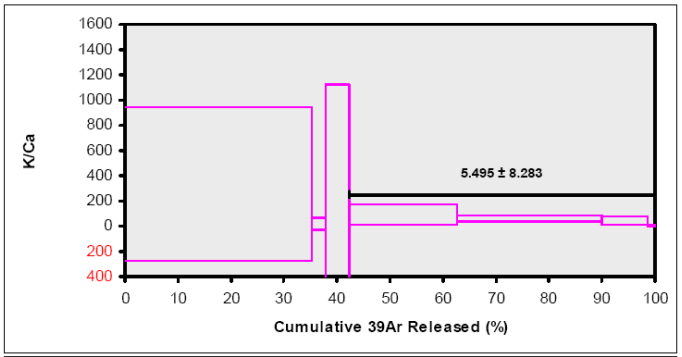

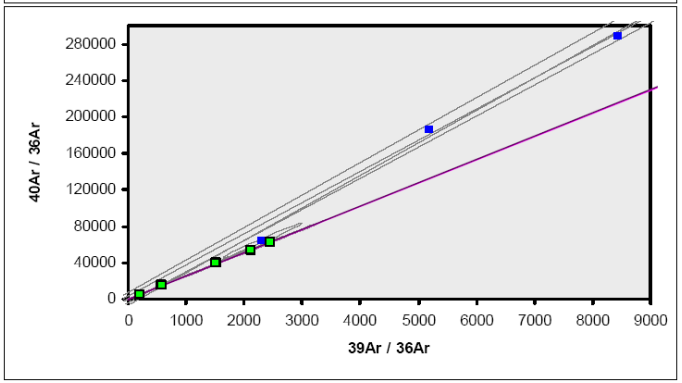

Results	40(a)/36(a) ± 2σ	40(r)/39(k) ± 2σ	Age ± 2σ (Ma)	MSWD
Isochron	402.2400 ± 523.7228 ± 130.20%	25.4751 ± 0.3450 ± 1.35%	117.42 ± 1.68 ± 1.43%	0.74
			External Error ± 2.89	
			Analytical Error ± 1.54	

07LT01 (biotite, combination)

Incremental Heating	36Ar(a)	37Ar(ca)	38Ar(cl)	39Ar(k)	40Ar(r)	Age ± 2σ (Ma)	40Ar(r) (%)	39Ar(k) (%)	K/Ca ± 2σ
1.00 W	0.000013	0.001350	0.000000	0.068472	2.434910	161.87 ± 6.23	99.84	1.81	21.814 ± 47.074
1.25 W	0.000014	0.000000	0.000000	0.114200	3.896223	155.58 ± 2.27	99.89	3.02	2.275 ± 0.240
1.50 W	0.000339	0.000115	0.000000	0.020408	0.511877	115.66 ± 4.68	83.62	0.54	76.115 ± 128.138
1.50 W	0.000406	0.001217	0.000000	0.941276	26.138687	127.63 ± 4.36	99.54	24.93	332.552 ± 608.801
1.50 W	0.000255	0.002601	0.000000	0.540913	13.731420	117.02 ± 1.64	99.45	14.33	89.428 ± 84.027
1.75 W	0.000295	0.004997	0.000000	0.727461	18.595441	117.81 ± 1.40	99.53	19.27	62.596 ± 24.678
2.00 W	0.000151	0.002492	0.000438	0.230433	5.950786	118.98 ± 1.45	99.25	6.10	39.759 ± 34.877
2.50 W	0.000807	0.000467	0.000108	0.071300	1.854692	119.81 ± 1.88	88.60	1.89	65.668 ± 26.439
2.50 W	0.000038	0.000000	0.000000	0.022682	0.586825	119.19 ± 6.40	98.09	0.60	2.275 ± 0.240
3.00 W	0.000070	0.001725	0.000000	0.014335	0.364157	117.10 ± 11.53	94.60	0.38	3.574 ± 4.111
3.50 W	0.000418	0.000321	0.000114	0.111820	2.890156	119.07 ± 1.14	95.89	2.96	149.888 ± 76.950
4.50 W	0.000160	0.000899	0.000181	0.136006	3.562967	120.64 ± 0.94	98.68	3.60	65.066 ± 19.911
7.00 W	0.001444	0.000592	0.000260	0.251798	8.283261	150.23 ± 0.81	95.10	6.67	182.809 ± 62.355
9.00 W	0.000060	0.000230	0.000135	0.027025	0.692409	118.07 ± 2.54	97.51	0.72	50.570 ± 50.957
9.00 W	0.001890	0.008790	0.000618	0.479533	16.051891	152.76 ± 0.78	96.63	12.70	23.459 ± 1.425
12.00 W	0.000939	0.003439	0.000000	0.018193	1.557432	367.57 ± 5.85	84.87	0.48	2.275 ± 0.240
Σ	0.007300	0.029234	0.001854	3.775853	107.103133				

Information on Analysis	Results	40(r)/39(k) ± 2σ	Age ± 2σ (Ma)	MSWD	39Ar(k) (%,n)	K/Ca ± 2σ
VU75-D18 Biotite 07LT01 MG	Error Plateau	25.8781 ± 0.2059 ± 0.80%	119.21 ± 1.15 ± 0.96% External Error ± 2.65 Analytical Error ± 0.92	3.02 2.36 1.7390	49.13 8 Statistical T Ratio Error Magnification	2.303 ± 0.952
Project = VU75 Irradiation = VU75 J = 0.0026398 ± 0.0000079 DRA-1 = 25.260 ± 0.144 Ma	Total Fusion Age	28.3653 ± 0.2672 ± 0.94%	130.27 ± 1.40 ± 1.08% External Error ± 2.96 Analytical Error ± 1.18		16	1.564 ± 0.327

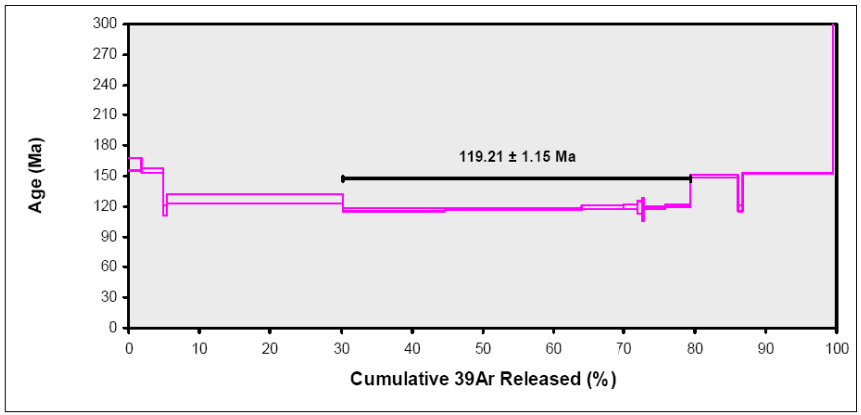

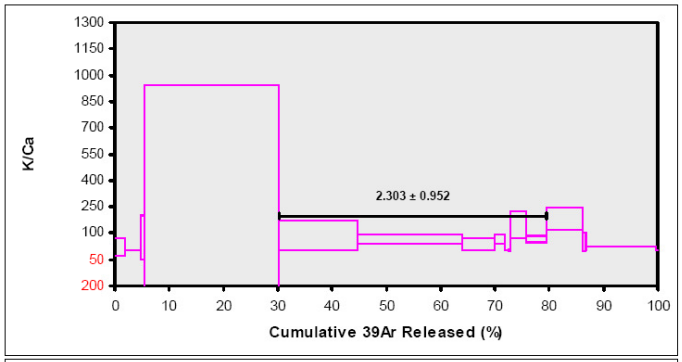

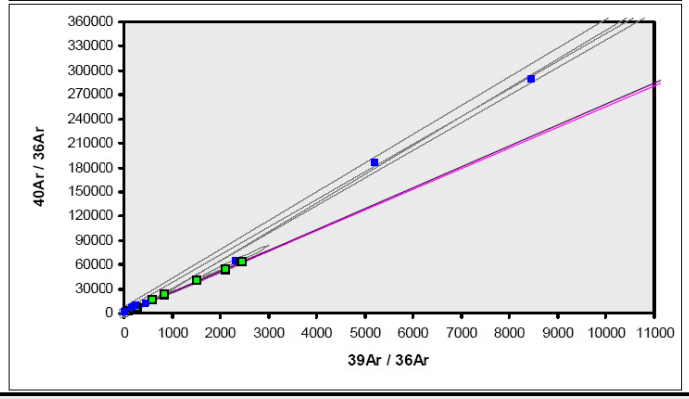

Results	40(a)/36(a) ± 2σ	40(r)/39(k) ± 2σ	Age ± 2σ (Ma)	MSWD
No Convergence	357.8587 ± 67.9585 ± 18.99%	25.4973 ± 0.2876 ± 1.13%	117.52 ± 1.45 ± 1.24% External Error ± 2.76 Analytical Error ± 1.28	2.38

07LT01 (hornblende)

Incremental Heating	36Ar(a)	37Ar(ca)	38Ar(cl)	39Ar(k)	40Ar(r)	Age ± 2σ (Ma)	40Ar(r) (%)	39Ar(k) (%)	K/Ca ± 2σ
3.00 W	0.023473	0.068562	0.000000	0.345894	9.869554	130.22 ± 3.11	58.72	0.65	2.169 ± 0.115
4.00 W	0.020301	0.833314	0.002018	1.064367	27.983990	120.33 ± 1.29	82.34	2.00	0.549 ± 0.029
4.50 W	0.013080	0.181144	0.000606	0.561393	14.256190	116.35 ± 1.41	78.67	1.06	1.333 ± 0.071
5.00 W	0.008817	0.244430	0.000741	0.695574	17.801480	117.23 ± 1.10	87.23	1.31	1.224 ± 0.068
6.00 W	0.016212	0.451098	0.001448	1.465323	38.506346	120.27 ± 1.08	88.93	2.75	1.397 ± 0.076
7.00 W	0.015757	1.569792	0.003752	2.421857	64.338574	121.54 ± 0.99	93.25	4.55	0.663 ± 0.036
8.00 W	0.014612	3.166737	0.007415	3.285548	87.459053	121.78 ± 0.98	95.29	6.18	0.446 ± 0.024
7.00 W	0.026259	8.076892	0.016331	6.537890	179.037920	125.16 ± 1.00	95.84	12.29	0.348 ± 0.019
8.00 W	0.018078	11.436547	0.022353	7.417912	201.642250	124.27 ± 0.98	97.41	13.94	0.279 ± 0.015
9.00 W	0.014927	11.724009	0.018909	6.562244	175.428131	122.28 ± 0.96	97.54	12.33	0.241 ± 0.013
12.00 W	0.031788	16.425726	0.032373	10.475029	282.115766	123.16 ± 0.97	96.77	19.69	0.274 ± 0.015
14.00 W	0.026123	9.850114	0.018419	5.763786	153.702573	121.99 ± 0.98	95.21	10.83	0.252 ± 0.014
17.00 W	0.016993	5.963109	0.007228	3.810205	100.975188	121.25 ± 0.97	95.26	7.16	0.275 ± 0.016
22.00 W	0.018253	4.040839	0.006787	1.983866	52.184317	120.38 ± 1.03	90.63	3.73	0.211 ± 0.012
27.00 W	0.022746	1.592279	0.002519	0.687247	18.028431	120.07 ± 1.74	72.84	1.29	0.186 ± 0.011
25.00 W	0.014698	0.260673	0.000273	0.126754	3.242332	117.17 ± 5.51	42.74	0.24	0.209 ± 0.012
Σ	0.302117	75.885267	0.141171	53.204889	1426.572096				

Information on Analysis	Results	40(r)/39(k) ± 2σ	Age ± 2σ (Ma)	MSWD	39Ar(k) (%,n)	K/Ca ± 2σ
VU75-D8	Error Plateau	26.7071 ± 0.2083 ± 0.78%	122.16 ± 1.16 ± 0.95%	8.91	94.99	0.256 ± 0.061
Hornblende					12	
07LT01			External Error ± 2.71	2.20	Statistical T Ratio	
MG			Analytical Error ± 0.92	2.9851	Error Magnification	
Project = VU75	Total Fusion Age	26.8128 ± 0.0751 ± 0.28%	122.63 ± 0.78 ± 0.64%		16	0.008 ± 0.000
Irradiation = VU75						
J = 0.0026233 ± 0.0000079			External Error ± 2.58			
DRA-1 = 25.260 ± 0.144 Ma			Analytical Error ± 0.33			

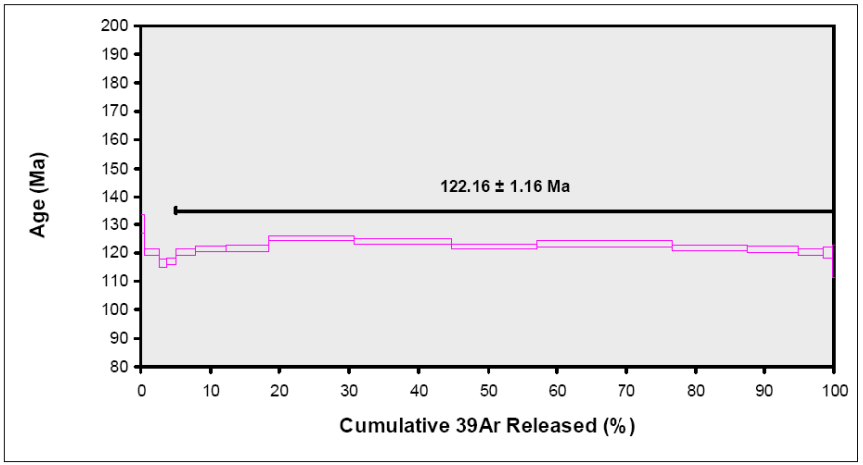

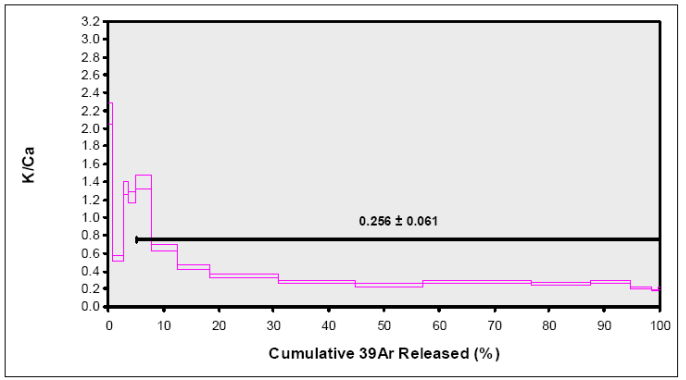

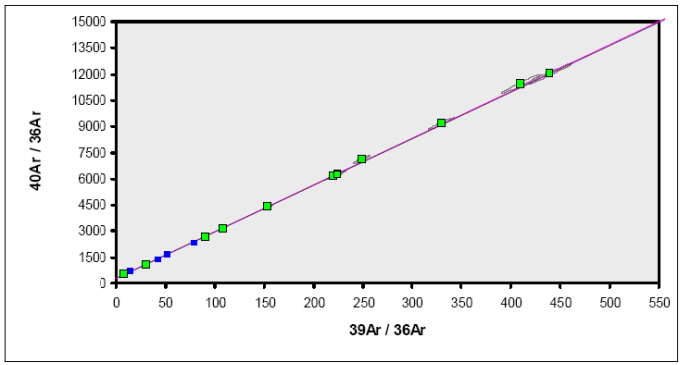

Results	40(a)/36(a) ± 2σ	40(r)/39(k) ± 2σ	Age ± 2σ (Ma)	MSWD
No Convergence	275.2463 ± 22.2593 ± 8.09%	26.8331 ± 0.2371 ± 0.88%	122.72 ± 1.27 ± 1.03%	7.45
			External Error ± 2.76	
			Analytical Error ± 1.05	

07LT01 (k-feldspar)

Incremental Heating	36Ar(a)	37Ar(ca)	38Ar(cl)	39Ar(k)	40Ar(r)	Age ± 2σ (Ma)	40Ar(r) (%)	39Ar(k) (%)	K/Ca ± 2σ
1.00 W	0.017358	0.002976	0.000000	0.010298	7.526966	1934.14 ± 30.34	59.47	0.07	1.488 ± 0.193
1.50 W	0.022545	0.074160	0.000133	0.240803	17.505133	315.50 ± 2.27	72.43	1.65	1.396 ± 0.060
2.50 W	0.025852	0.227353	0.000000	0.658299	30.729767	208.83 ± 1.28	80.09	4.51	1.245 ± 0.053
3.50 W	0.008262	0.160051	0.000000	1.164577	33.245376	130.55 ± 0.52	93.15	7.98	3.129 ± 0.136
4.50 W	0.011010	0.241709	0.000000	1.359117	41.782525	140.21 ± 0.57	92.77	9.31	2.418 ± 0.104
5.50 W	0.011309	0.259654	0.000000	1.759914	50.864170	132.11 ± 0.50	93.83	12.06	2.915 ± 0.125
6.50 W	0.002703	0.087761	0.000035	0.798048	21.740026	124.78 ± 0.47	96.45	5.47	3.910 ± 0.181
8.00 W	0.002175	0.095546	0.000070	0.487457	13.895561	130.37 ± 0.65	95.57	3.34	2.194 ± 0.098
8.00 W	0.013562	0.378754	0.000000	1.955772	57.420419	134.13 ± 0.58	93.47	13.40	2.220 ± 0.097
10.00 W	0.017955	0.332383	0.000000	2.034125	57.624992	129.59 ± 0.51	91.56	13.94	2.632 ± 0.116
12.00 W	0.008085	0.268843	0.000000	1.388623	38.142501	125.78 ± 0.49	94.10	9.51	2.221 ± 0.099
16.00 W	0.004114	0.156188	0.000000	1.333761	35.832695	123.12 ± 0.46	96.71	9.14	3.672 ± 0.166
20.00 W	0.003450	0.161608	0.000000	1.405135	37.258839	121.57 ± 0.49	97.33	9.63	3.739 ± 0.168
Σ	0.148381	2.446986	0.000238	14.595928	443.568969				

Information on Analysis	Results	40(r)/39(k) ± 2σ	Age ± 2σ (Ma)	MSWD	39Ar(k) (%,n)	K/Ca ± 2σ
VU75-D10*	Error Plateau	27.7592 ± 0.7110 ± 2.56%	127.07 ± 3.23 ± 2.54%	303.53	76.48	2.637 ± 0.446
K-feldspar					8	
07LT01			External Error ± 4.11	2.36	Statistical T Ratio	
MG			Analytical Error ± 3.14	17.4223	Error Magnification	
Project = VU75	Total Fusion Age	30.3899 ± 0.0420 ± 0.14%	138.66 ± 0.82 ± 0.59%		13	0.072 ± 0.001
Irradiation = VU75						
J = 0.0026289 ± 0.0000079			External Error ± 2.89			
DRA-1 = 25.260 ± 0.144 Ma			Analytical Error ± 0.18			

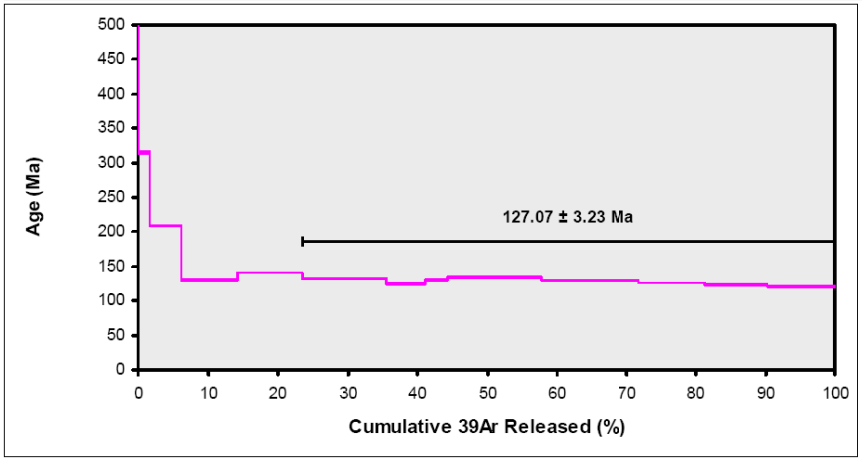

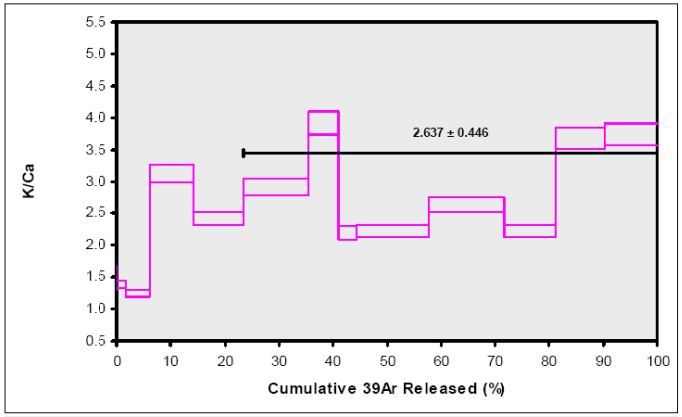

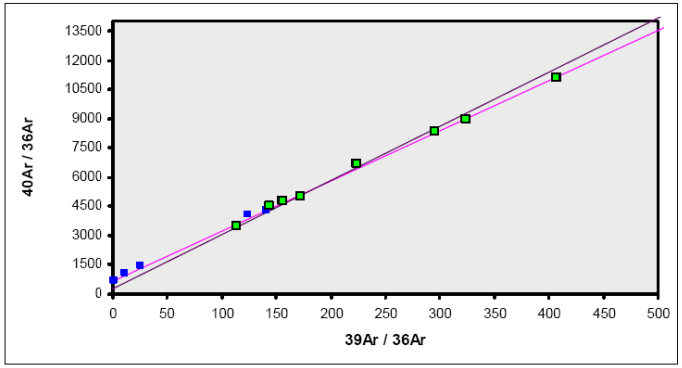

Results	40(a)/36(a) ± 2σ	40(r)/39(k) ± 2σ	Age ± 2σ (Ma)	MSWD
No Convergence	679.6451 ± 218.7616 ± 32.19%	25.7412 ± 1.1943 ± 4.64%	118.13 ± 5.35 ± 4.53%	> 100
			External Error ± 5.85	
			Analytical Error ± 5.31	

07LT04 (actinolite)

Incremental Heating	36Ar(a)	37Ar(ca)	38Ar(cl)	39Ar(k)	40Ar(r)	Age ± 2σ (Ma)	40Ar(r) (%)	39Ar(k) (%)	K/Ca ± 2σ
4.00 W	0.023619	0.653747	0.000000	0.062257	3.517410	249.54 ± 16.88	33.51	0.21	0.041 ± 0.002
4.50 W	0.015700	0.451672	0.000000	0.047625	1.679530	159.76 ± 14.89	26.58	0.16	0.045 ± 0.002
5.00 W	0.007906	0.598005	0.000000	0.071414	2.352963	149.68 ± 5.65	50.18	0.25	0.051 ± 0.003
6.00 W	0.018159	1.511602	0.000093	0.187308	6.047909	146.81 ± 4.68	52.99	0.64	0.053 ± 0.003
7.00 W	0.018416	2.617710	0.000663	0.331159	10.015123	137.85 ± 2.78	64.79	1.14	0.054 ± 0.003
8.00 W	0.017533	4.708122	0.001410	0.594040	17.538251	134.69 ± 1.80	77.19	2.04	0.054 ± 0.003
7.00 W	0.013223	1.031419	0.000000	0.122667	3.731974	138.64 ± 5.06	48.85	0.42	0.051 ± 0.003
8.00 W	0.029046	9.093568	0.002555	1.140509	32.934290	131.85 ± 1.63	79.32	3.91	0.054 ± 0.003
9.00 W	0.041023	16.070936	0.004613	2.091673	59.838364	130.66 ± 1.37	83.15	7.18	0.056 ± 0.003
12.00 W	0.083490	39.705107	0.012370	5.143915	145.634904	129.36 ± 1.31	85.51	17.65	0.056 ± 0.003
14.00 W	0.064568	30.641873	0.011503	4.079192	114.973007	128.80 ± 1.29	85.76	14.00	0.057 ± 0.003
17.00 W	0.052394	27.751039	0.005274	3.623471	101.180105	127.64 ± 1.26	86.72	12.44	0.056 ± 0.003
22.00 W	0.051464	50.382550	0.017877	6.516280	182.142797	127.77 ± 1.10	92.29	22.36	0.056 ± 0.003
27.00 W	0.068928	34.789313	0.011925	4.647617	127.224795	125.22 ± 1.24	86.19	15.95	0.057 ± 0.003
25.00 W	0.022998	3.391600	0.001205	0.480134	12.119986	115.77 ± 2.40	64.07	1.65	0.061 ± 0.004
Σ	0.528468	223.398264	0.069487	29.139260	820.931407				

Information on Analysis	Results	40(r)/39(k) ± 2σ	Age ± 2σ (Ma)	MSWD	39Ar(k) (%,n)	K/Ca ± 2σ
VU75-D9 Actinolite 07LT04 MG	Error Plateau	28.1067 ± 0.3507 ± 1.25%	128.45 ± 1.72 ± 1.34% External Error ± 3.09 Analytical Error ± 1.55	10.05 2.45 3.1702	93.49 7 Statistical T Ratio Error Magnification	0.056 ± 0.001
Project = VU75 Irradiation = VU75 J = 0.0026256 ± 0.0000079 DRA-1 = 25.260 ± 0.144 Ma	Total Fusion Age	28.1727 ± 0.1095 ± 0.39%	128.74 ± 0.89 ± 0.69% External Error ± 2.72 Analytical Error ± 0.48		15	0.002 ± 0.000

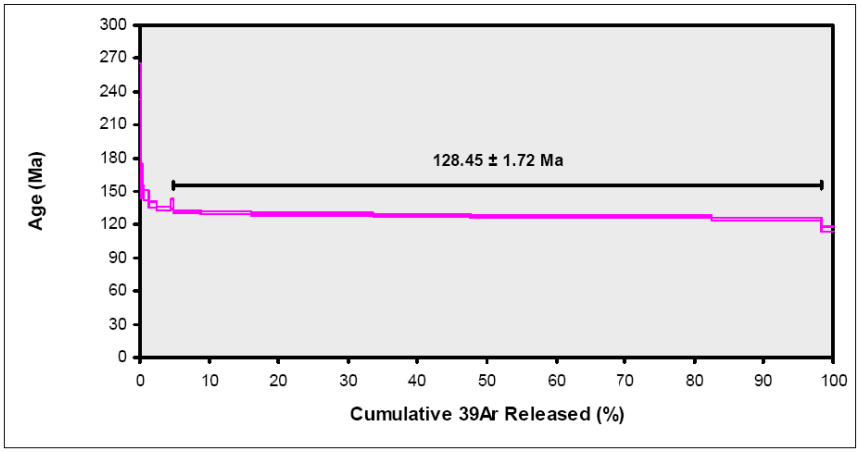

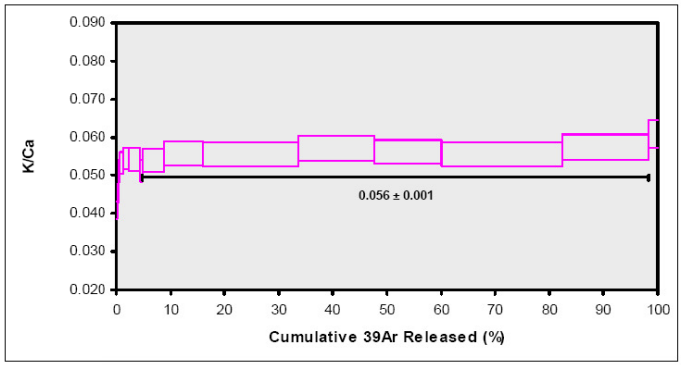

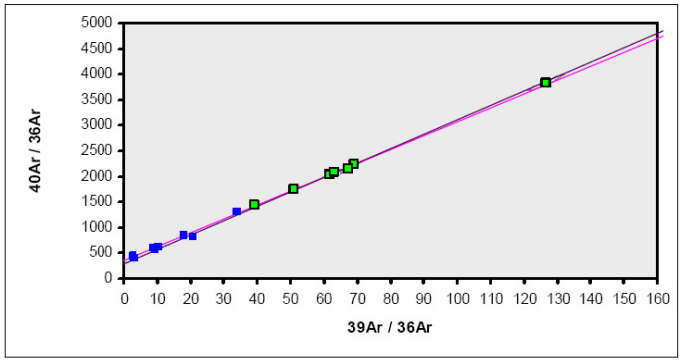

Results	40(a)/36(a) ± 2σ	40(r)/39(k) ± 2σ	Age ± 2σ (Ma)	MSWD
No Convergence	356.3067 ± 65.2238 ± 18.31%	27.1566 ± 1.0326 ± 3.80%	124.26 ± 4.62 ± 3.72% External Error ± 5.25 Analytical Error ± 4.57	6.79

07TH03 (biotite, 1st run)

Incremental Heating	36Ar(a)	37Ar(ca)	38Ar(cl)	39Ar(k)	40Ar(r)	Age ± 2σ (Ma)	40Ar(r) (%)	39Ar(k) (%)	K/Ca ± 2σ
2.50 W	0.000163	0.000108	0.000000	0.001685	0.053026	144.00 ± 46.36	52.41	0.23	6.701 ± 9.801
3.50 W	0.000286	0.000000	0.000009	0.011456	0.514364	202.08 ± 6.65	85.88	1.58	
4.50 W	0.000144	0.000000	0.000000	0.042053	1.880733	201.33 ± 2.57	97.78	5.80	
7.00 W	0.000403	0.000365	0.000000	0.126522	5.915045	209.95 ± 1.58	98.02	17.46	149.108 ± 88.708
9.00 W	0.000114	0.000325	0.000000	0.027436	1.282350	209.90 ± 3.38	97.43	3.79	36.315 ± 20.699
9.00 W	0.000392	0.000668	0.000000	0.288428	13.959621	216.92 ± 1.15	99.17	39.80	185.547 ± 79.932
12.00 W	0.000123	0.001209	0.000026	0.066673	3.160366	212.70 ± 2.34	98.86	9.20	23.722 ± 4.185
16.00 W	0.000203	0.001259	0.000048	0.144769	6.824171	211.59 ± 1.40	99.12	19.98	49.434 ± 12.838
20.00 W	0.000124	0.000337	0.000054	0.015627	0.733276	210.69 ± 5.92	95.24	2.16	19.930 ± 11.517
Σ	0.001953	0.004271	0.000137	0.724649	34.322951				

Information on Analysis	Results	40(r)/39(k) ± 2σ	Age ± 2σ (Ma)	MSWD	39Ar(k) (%,n)	K/Ca ± 2σ
VU75-D20						
Biotite	Error Plateau	47.3149 ± 0.7713 ± 1.63%	212.34 ± 3.48 ± 1.64%	22.84	99.77 8	3.380 ± 7.384
07TH03			External Error ± 5.49	2.36	Statistical T Ratio	
MG			Analytical Error ± 3.27	4.7788	Error Magnification	
Project = VU75						
Irradiation = VU75	Total Fusion Age	47.3649 ± 0.1642 ± 0.35%	212.55 ± 1.39 ± 0.65%		9	2.055 ± 0.322
J = 0.0026399 ± 0.0000079			External Error ± 4.47			
DRA-1 = 25.260 ± 0.144 Ma			Analytical Error ± 0.70			

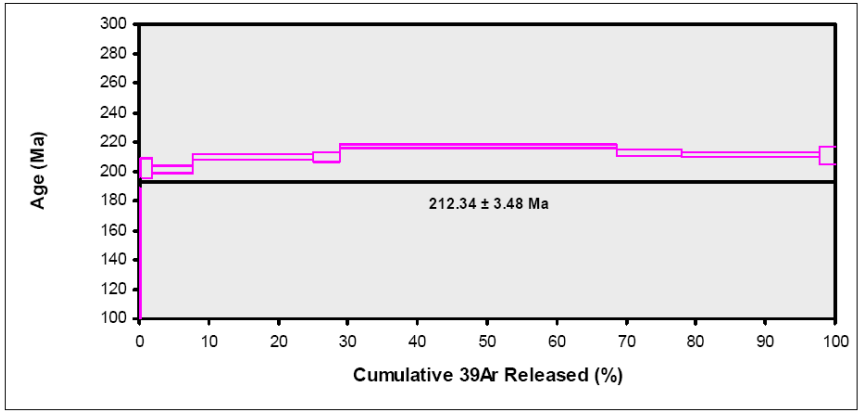

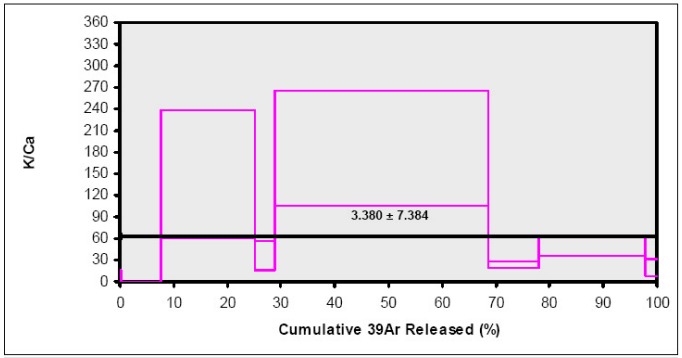

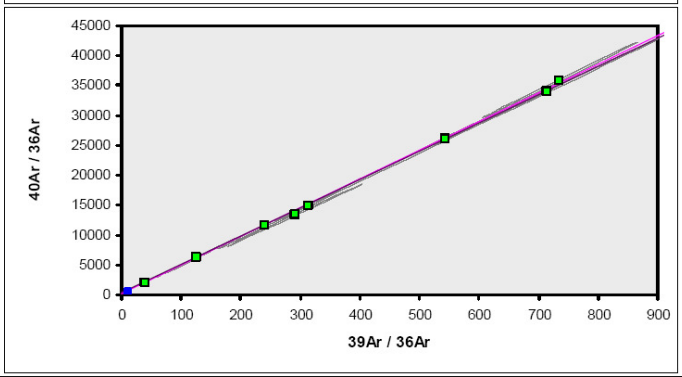

Results	40(a)/36(a) ± 2σ	40(r)/39(k) ± 2σ	Age ± 2σ (Ma)	MSWD
No Convergence	103.5852 ± 178.8456 ± 172.66%	48.1060 ± 0.7997 ± 1.66%	215.69 ± 3.59 ± 1.67%	14.82
			External Error ± 5.61	
			Analytical Error ± 3.38	

07TH03 (biotite, 2nd run)

Incremental Heating	36Ar(a)	37Ar(ca)	38Ar(cl)	39Ar(k)	40Ar(r)	Age ± 2σ (Ma)	40Ar(r) (%)	39Ar(k) (%)	K/Ca ± 2σ
1.00 W	0.000066	0.000000	0.000000	0.059139	4.283116	315.64 ± 8.82	99.54	1.76	
1.25 W	0.000066	0.000000	0.000000	0.137305	8.469246	272.16 ± 8.63	99.77	4.09	
1.50 W	0.000782	0.002835	0.000000	0.270547	12.282024	204.20 ± 2.92	98.15	8.05	41.029 ± 35.687
1.75 W	0.000684	0.004782	0.000000	0.222578	9.789897	198.18 ± 2.40	97.97	6.62	20.016 ± 13.027
2.00 W	0.000767	0.006844	0.000000	0.272119	12.931640	213.22 ± 2.59	98.27	8.10	17.097 ± 5.862
2.50 W	0.001827	0.002683	0.000000	0.407260	19.284728	212.50 ± 2.28	97.27	12.12	65.279 ± 56.879
3.00 W	0.000827	0.003271	0.000000	0.391941	18.369385	210.45 ± 2.31	98.68	11.66	51.518 ± 27.990
4.00 W	0.000383	0.003414	0.000000	0.191818	9.059688	211.98 ± 2.33	98.76	5.71	24.160 ± 16.589
5.50 W	0.000579	0.000000	0.000000	0.303906	14.766002	217.72 ± 2.29	98.85	9.04	
7.00 W	0.000708	0.001661	0.000000	0.249228	12.040219	216.55 ± 2.30	98.29	7.42	64.505 ± 79.751
9.00 W	0.000294	0.000000	0.000000	0.167876	8.162470	217.87 ± 2.34	98.94	5.00	
8.50 W	0.000559	0.004433	0.000064	0.140990	6.934330	220.23 ± 2.41	97.67	4.20	13.677 ± 6.290
11.00 W	0.002019	0.004072	0.000079	0.471922	23.167378	219.85 ± 2.19	97.49	14.04	49.838 ± 25.548
14.00 W	0.001059	0.002489	0.000230	0.032987	1.550229	210.99 ± 5.07	83.20	0.98	5.699 ± 5.034
17.00 W	0.000545	0.000668	0.000017	0.023108	0.958113	187.39 ± 7.72	85.60	0.69	14.875 ± 54.685
25.00 W	0.001289	0.005989	0.000151	0.017821	0.246960	64.82 ± 8.89	39.33	0.53	1.280 ± 0.455
Σ	0.012454	0.043141	0.000541	3.360544	162.295425				

Information on Analysis	Results	40(r)/39(k) ± 2σ	Age ± 2σ (Ma)	MSWD	39Ar(k) (%,n)	K/Ca ± 2σ
VU75-D20	Error Plateau	48.0711 ± 0.5461 ± 1.14%	215.54 ± 2.61 ± 1.21%	9.04	78.26	0.731 ± 1.493
Biotite					10	
07TH03			External Error ± 5.04	2.26	Statistical T Ratio	
MG			Analytical Error ± 2.31	3.0063	Error Magnification	
Project = VU75	Total Fusion Age	48.2944 ± 0.1837 ± 0.38%	216.48 ± 1.45 ± 0.67%		16	0.943 ± 0.197
Irradiation = VU75						
J = 0.0026399 ± 0.0000079			External Error ± 4.57			
DRA-1 = 25.260 ± 0.144 Ma			Analytical Error ± 0.78			

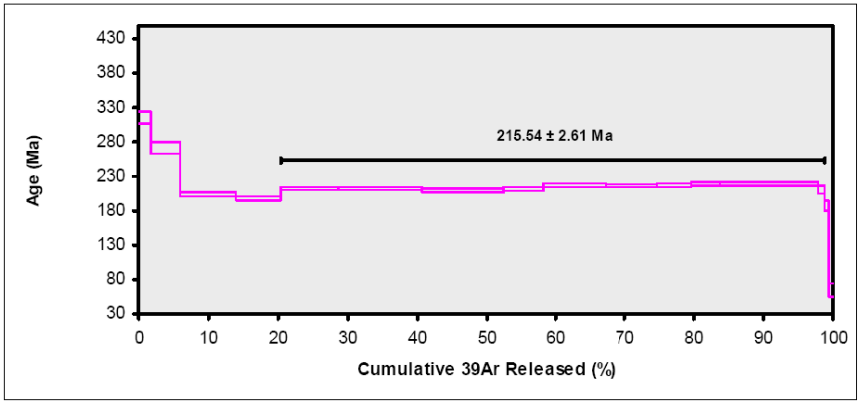

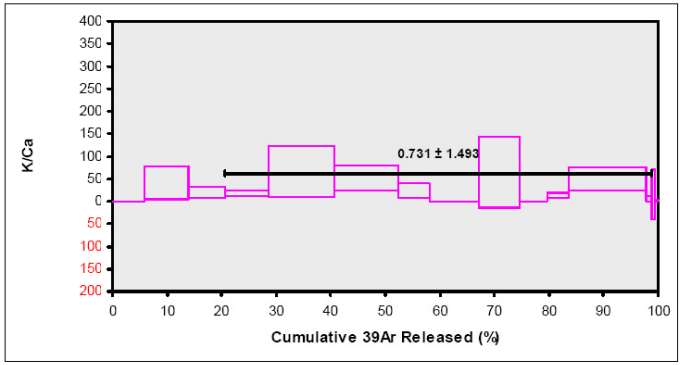

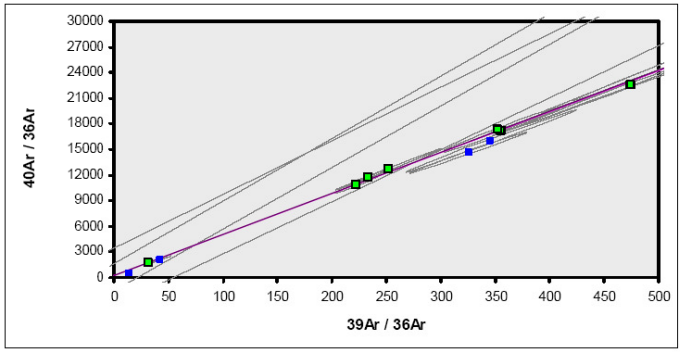

Results	40(a)/36(a) ± 2σ	40(r)/39(k) ± 2σ	Age ± 2σ (Ma)	MSWD
No Convergence	284.7799 ± 116.7642 ± 41.00%	47.9500 ± 0.7229 ± 1.51%	215.03 ± 3.29 ± 1.53%	9.39
			External Error ± 5.41	
			Analytical Error ± 3.06	

07TH03 (biotite, combination)

Incremental Heating	36Ar(a)	37Ar(ca)	38Ar(cl)	39Ar(k)	40Ar(r)	Age ± 2σ (Ma)	40Ar(r) (%)	39Ar(k) (%)	K/Ca ± 2σ
1.00 W	0.000066	0.000000	0.000000	0.059139	4.283116	315.64 ± 8.82	99.54	1.45	19.930 ± 11.517
1.25 W	0.000066	0.000000	0.000000	0.137305	8.469246	272.16 ± 8.63	99.77	3.36	19.930 ± 11.517
1.50 W	0.000782	0.002835	0.000000	0.270547	12.282024	204.20 ± 2.92	98.15	6.63	41.029 ± 35.687
1.75 W	0.000684	0.004782	0.000000	0.222578	9.789897	198.18 ± 2.40	97.97	5.45	20.016 ± 13.027
2.00 W	0.000767	0.006844	0.000000	0.272119	12.931640	213.22 ± 2.59	98.27	6.66	17.097 ± 5.862
2.50 W	0.001827	0.002683	0.000000	0.407260	19.284728	212.50 ± 2.28	97.27	9.97	65.279 ± 56.879
3.00 W	0.000827	0.003271	0.000000	0.391941	18.369385	210.45 ± 2.31	98.68	9.60	51.518 ± 27.990
3.50 W	0.000286	0.000000	0.000009	0.011456	0.514364	202.08 ± 6.65	85.88	0.28	
4.00 W	0.000383	0.003414	0.000000	0.191818	9.059688	211.98 ± 2.33	98.76	4.70	24.160 ± 16.589
4.50 W	0.000144	0.000000	0.000000	0.042053	1.880733	201.33 ± 2.57	97.78	1.03	
5.50 W	0.000579	0.000000	0.000000	0.303906	14.766002	217.72 ± 2.29	98.85	7.44	19.930 ± 11.517
7.00 W	0.000403	0.000365	0.000000	0.126522	5.915045	209.95 ± 1.58	98.02	3.10	149.108 ± 88.708
7.00 W	0.000708	0.001661	0.000000	0.249228	12.040219	216.55 ± 2.30	98.29	6.10	64.505 ± 79.751
8.50 W	0.000559	0.004433	0.000064	0.140990	6.934330	220.23 ± 2.41	97.67	3.45	13.677 ± 6.290
9.00 W	0.000114	0.000325	0.000000	0.027436	1.282350	209.90 ± 3.38	97.43	0.67	36.315 ± 20.699
9.00 W	0.000294	0.000000	0.000000	0.167876	8.162470	217.87 ± 2.34	98.94	4.11	19.930 ± 11.517
9.00 W	0.000392	0.000668	0.000000	0.288428	13.959621	216.92 ± 1.15	99.17	7.06	185.547 ± 79.932
11.00 W	0.002019	0.004072	0.000079	0.471922	23.167378	219.85 ± 2.19	97.49	11.56	49.838 ± 25.548
12.00 W	0.000123	0.001209	0.000026	0.066673	3.160366	212.70 ± 2.34	98.86	1.63	23.722 ± 4.185
14.00 W	0.001059	0.002489	0.000230	0.032987	1.550229	210.99 ± 5.07	83.20	0.81	5.699 ± 5.034
16.00 W	0.000203	0.001259	0.000048	0.144769	6.824171	211.59 ± 1.40	99.12	3.55	49.434 ± 12.838
17.00 W	0.000545	0.000668	0.000017	0.023108	0.958113	187.39 ± 7.72	85.60	0.57	14.875 ± 54.685
20.00 W	0.000124	0.000337	0.000054	0.015627	0.733276	210.69 ± 5.92	95.24	0.38	19.930 ± 11.517
25.00 W	0.001289	0.005989	0.000151	0.017821	0.246960	64.82 ± 8.89	39.33	0.44	1.280 ± 0.455
Σ	0.014244	0.047304	0.000678	4.083508	196.565350				

Information on Analysis	Results	40(r)/39(k) ± 2σ	Age ± 2σ (Ma)	MSWD	39Ar(k) (%,n)	K/Ca ± 2σ
VU75-D20 Biotite	Error Plateau	47.7956 ± 0.4276 ± 0.89%	214.37 ± 2.18 ± 1.02%	11.89	80.42 15	18.810 ± 6.369
07TH03			External Error ± 4.81	2.14	Statistical T Ratio	
MG			Analytical Error ± 1.81	3.4479	Error Magnification	
Project = VU75 Irradiation = VU75 J = 0.0026399 ± 0.0000079 DRA-1 = 25.260 ± 0.144 Ma	Total Fusion Age	48.1364 ± 0.1535 ± 0.32%	215.81 ± 1.38 ± 0.64% External Error ± 4.53 Analytical Error ± 0.65		24	1.045 ± 0.200

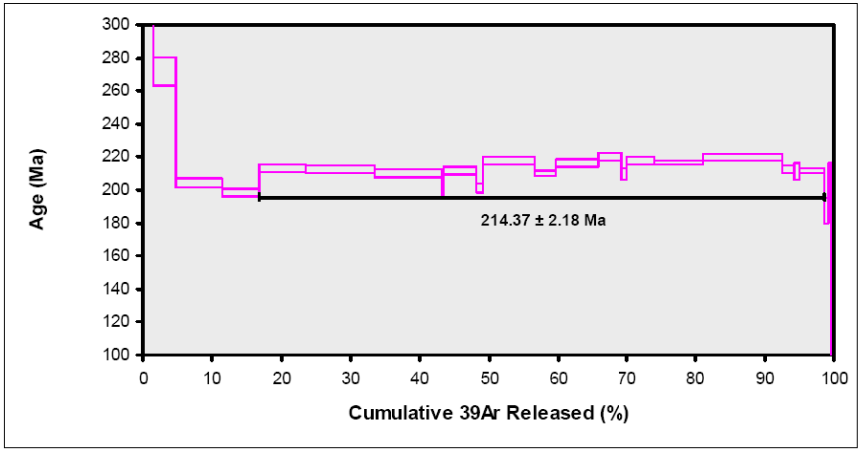

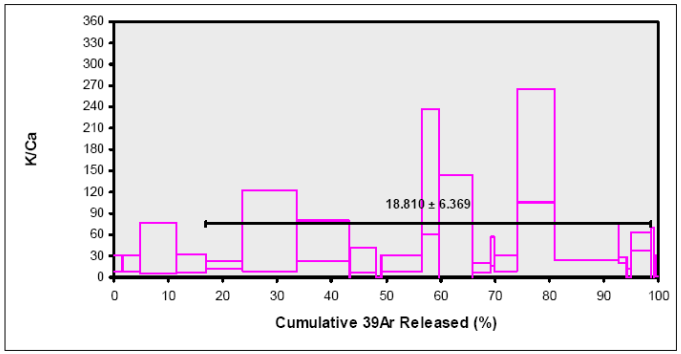

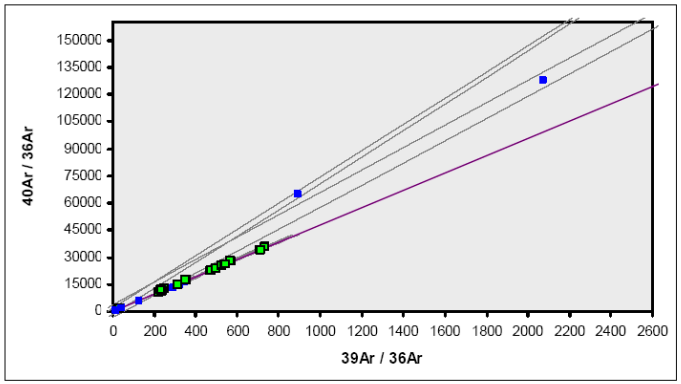

Results	40(a)/36(a) ± 2σ	40(r)/39(k) ± 2σ	Age ± 2σ (Ma)	MSWD
No Convergence	261.2136 ± 125.9932 ± 48.23%	47.8318 ± 0.5635 ± 1.18%	214.53 ± 2.67 ± 1.25% External Error ± 5.06 Analytical Error ± 2.38	11.93

07XD01 (actinolite)

Incremental Heating	36Ar(a)	37Ar(ca)	38Ar(cl)	39Ar(k)	40Ar(r)	Age ± 2σ (Ma)	40Ar(r) (%)	39Ar(k) (%)	K/Ca ± 2σ
3.00 W	0.016207	0.097127	0.000000	0.027255	59.835295	3445.99 ± 32.53	92.59	0.16	0.121 ± 0.007
4.00 W	0.014193	0.692807	0.002523	0.144526	62.943846	1373.77 ± 9.00	93.75	0.83	0.090 ± 0.005
4.50 W	0.008380	0.692405	0.003296	0.133629	41.955690	1083.21 ± 8.04	94.43	0.76	0.083 ± 0.004
5.00 W	0.005260	0.805526	0.004625	0.145090	34.422343	872.34 ± 6.01	95.68	0.83	0.077 ± 0.004
6.00 W	0.010722	1.766334	0.010461	0.325154	80.899087	905.72 ± 6.11	96.23	1.86	0.079 ± 0.004
7.00 W	0.012444	2.887203	0.017673	0.507889	110.975611	816.85 ± 5.49	96.79	2.90	0.076 ± 0.004
8.00 W	0.015838	3.752450	0.020888	0.649216	143.345050	823.73 ± 5.52	96.84	3.71	0.074 ± 0.004
7.00 W	0.020583	4.422985	0.024128	0.772658	183.862301	874.42 ± 5.72	96.80	4.41	0.075 ± 0.004
8.00 W	0.021292	5.602430	0.032965	0.958887	201.153063	790.42 ± 5.34	96.97	5.48	0.074 ± 0.004
9.00 W	0.033705	9.228234	0.047115	1.610573	346.683180	807.05 ± 5.36	97.21	9.20	0.075 ± 0.004
12.00 W	0.064590	16.573985	0.093560	2.877521	576.403373	761.31 ± 5.18	96.79	16.43	0.075 ± 0.004
14.00 W	0.038113	9.798884	0.050503	1.654063	338.983261	775.60 ± 5.29	96.78	9.45	0.073 ± 0.004
17.00 W	0.039993	13.726350	0.075668	2.379713	450.648785	727.06 ± 4.91	97.44	13.59	0.075 ± 0.004
22.00 W	0.039043	16.321395	0.090016	2.696679	502.842575	717.86 ± 4.93	97.76	15.40	0.071 ± 0.004
27.00 W	0.025596	10.694657	0.060809	1.754933	311.080869	688.38 ± 4.72	97.63	10.02	0.071 ± 0.004
25.00 W	0.024291	5.116577	0.027226	0.873742	134.170762	610.19 ± 4.36	94.92	4.99	0.073 ± 0.004
Σ	0.390250	102.179348	0.561455	17.511529	3580.205091				

Information on Analysis	Results	40(r)/39(k) ± 2σ	Age ± 2σ (Ma)	MSWD	39Ar(k) (%,n)	K/Ca ± 2σ
VU75-D6 Actinolite 07XD01 MG	Error Plateau	213.8941 ± 23.0969 ± 10.80%	802.94 ± 70.09 ± 8.73% External Error ± 71.90 Analytical Error ± 69.98	2192.63 2.14 46.8255	95.01 15 Statistical T Ratio Error Magnification	0.077 ± 0.004
Project = VU75 Irradiation = VU75 J = 0.0026209 ± 0.0000079 DRA-1 = 25.260 ± 0.144 Ma	Total Fusion Age	204.4485 ± 0.5543 ± 0.27%	774.09 ± 4.14 ± 0.54% External Error ± 16.03 Analytical Error ± 1.71		16	0.002 ± 0.000

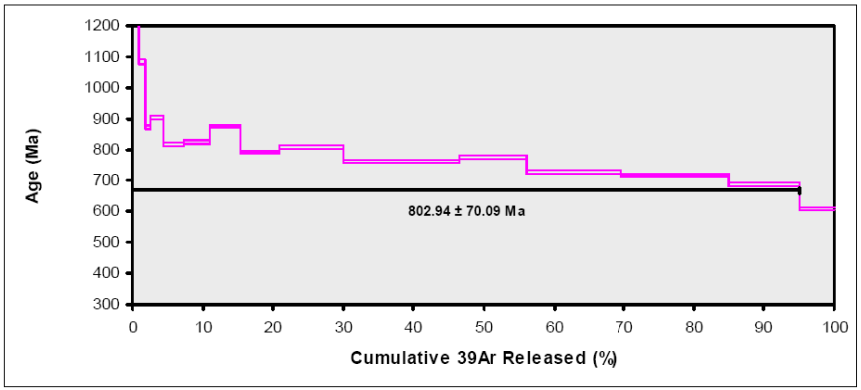

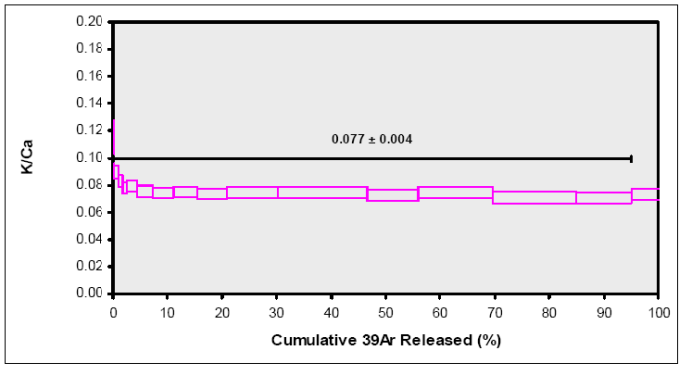

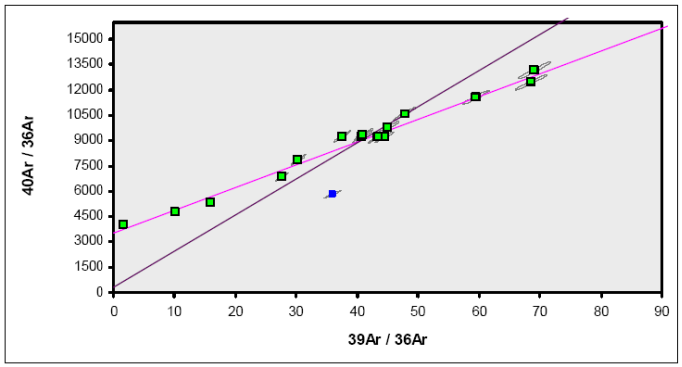

Results	40(a)/36(a) ± 2σ	40(r)/39(k) ± 2σ	Age ± 2σ (Ma)	MSWD
Error Chron	3528.7480 ± 380.9257 ± 10.79%	134.7755 ± 9.3788 ± 6.96%	545.73 ± 32.89 ± 6.03% External Error ± 34.66 Analytical Error ± 32.77	25.66

07XD04 (phengite, 1st run)

Incremental Heating	36Ar(a)	37Ar(ca)	38Ar(cl)	39Ar(k)	40Ar(r)	Age ± 2σ (Ma)	40Ar(r) (%)	39Ar(k) (%)	K/Ca ± 2σ
1.50 W	0.000903	0.000311	0.000000	0.020139	1.720135	366.77 ± 5.91	86.57	2.11	27.836 ± 14.539
2.50 W	0.001776	0.000592	0.000000	0.322882	26.025159	347.99 ± 1.96	98.02	33.88	234.439 ± 66.079
3.50 W	0.001400	0.000502	0.000000	0.504087	37.119189	320.43 ± 1.56	98.90	52.90	432.068 ± 223.388
4.50 W	0.000082	0.000068	0.000051	0.009443	0.673284	311.07 ± 8.06	96.53	0.99	59.875 ± 181.387
7.00 W	0.000156	0.000000	0.000000	0.016232	1.226433	328.07 ± 4.67	96.37	1.70	
9.00 W	0.000013	0.000016	0.000000	0.001287	0.099524	335.16 ± 48.34	96.38	0.14	35.011 ± 579.216
9.00 W	0.000297	0.000486	0.000001	0.064723	4.919797	329.88 ± 2.75	98.24	6.79	57.299 ± 30.634
12.00 W	0.000611	0.000023	0.000000	0.011631	0.554717	213.91 ± 8.46	75.45	1.22	216.415 ± 2494.330
16.00 W	0.000075	0.000000	0.000059	0.002519	0.224407	380.98 ± 29.62	91.03	0.26	
Σ	0.005312	0.001997	0.000110	0.952944	72.562645				

Information on Analysis	Results	40(r)/39(k) ± 2σ	Age ± 2σ (Ma)	MSWD	39Ar(k) (%,n)	K/Ca ± 2σ
VU75-D17 Phengite 07XD04 MG	Error Plateau	74.2384 ± 1.1355 ± 1.53%	322.83 ± 4.86 ± 1.50% External Error ± 8.08 Analytical Error ± 4.52	12.39 2.78 3.5203	62.52 5 Statistical T Ratio Error Magnification	0.095 ± 2.157
Project = VU75 Irradiation = VU75 J = 0.0026395 ± 0.0000079 DRA-1 = 25.260 ± 0.144 Ma	Total Fusion Age	76.1457 ± 0.2768 ± 0.36%	330.40 ± 2.12 ± 0.64% External Error ± 6.94 Analytical Error ± 1.10		9	5.777 ± 2.075

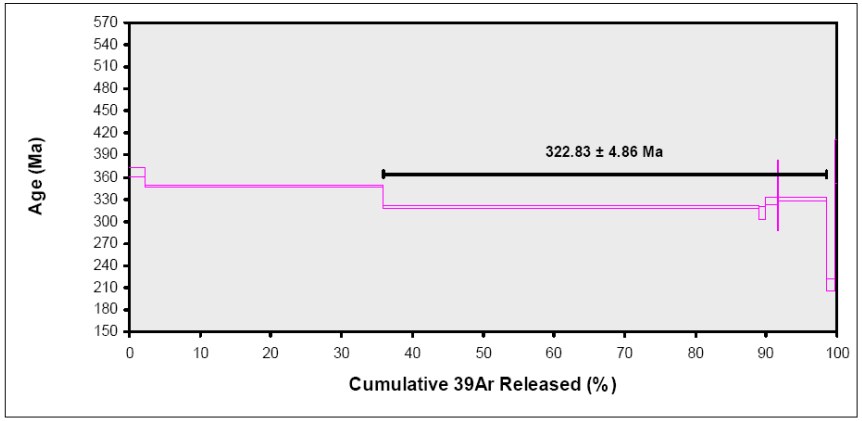

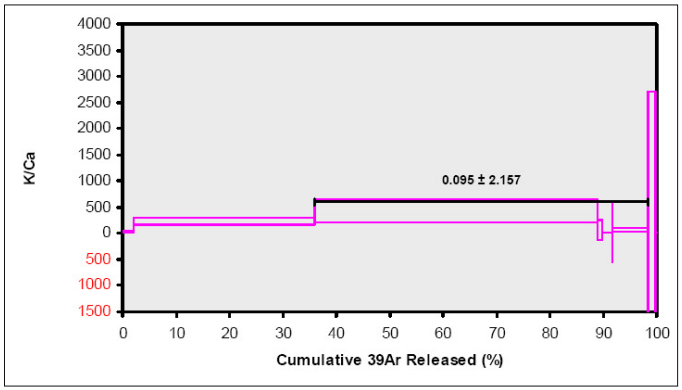

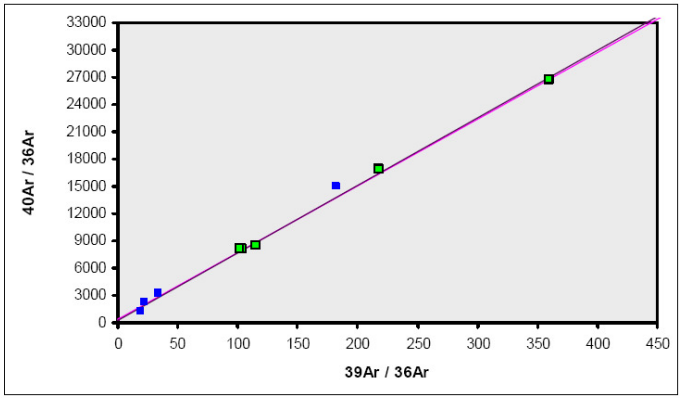

Results	40(a)/36(a) ± 2σ	40(r)/39(k) ± 2σ	Age ± 2σ (Ma)	MSWD
No Convergence	357.1132 ± 640.5707 ± 179.37%	73.4476 ± 2.6451 ± 3.60%	319.67 ± 10.70 ± 3.35% External Error ± 12.46 Analytical Error ± 10.55	12.90

07XD04 (phengite, 2nd run)

Incremental Heating	36Ar(a)	37Ar(ca)	38Ar(cl)	39Ar(k)	40Ar(r)	Age ± 2σ (Ma)	40Ar(r) (%)	39Ar(k) (%)	K/Ca ± 2σ
0.75 W	0.004951	0.053899	0.000000	0.243086	22.098826	388.01 ± 5.51	93.79	19.21	1.939 ± 0.144
1.00 W	0.004951	0.054336	0.000000	0.382822	39.405751	433.61 ± 6.89	96.42	30.25	3.030 ± 0.220
1.25 W	0.004951	0.055048	0.000000	0.335601	23.345780	304.12 ± 3.15	94.10	26.52	2.621 ± 0.187
1.50 W	0.000337	0.001081	0.000000	0.098371	8.327413	363.82 ± 4.49	98.82	7.77	39.128 ± 64.923
1.75 W	0.000172	0.002080	0.000156	0.012383	0.871530	307.41 ± 12.64	94.49	0.98	2.560 ± 2.326
2.00 W	0.000157	0.000000	0.000107	0.015165	1.025090	296.18 ± 9.51	95.66	1.20	2.342 ± 2.065
3.00 W	0.000378	0.001593	0.000000	0.117612	9.281930	341.37 ± 4.26	98.81	9.29	31.748 ± 43.783
4.00 W	0.000133	0.002907	0.000000	0.008439	0.613178	316.54 ± 11.74	93.99	0.67	1.248 ± 0.820
25.00 W	0.000191	0.000865	0.000067	0.052129	4.148789	344.00 ± 4.07	98.66	4.12	25.899 ± 62.763
Σ	0.016222	0.171809	0.000330	1.265610	109.118288				

Information on Analysis	Results	40(r)/39(k) ± 2σ	Age ± 2σ (Ma)	MSWD	39Ar(k) (%,n)	K/Ca ± 2σ
VU75-D17 Phengite 07XD04 MG	Error Plateau	75.8700 ± 4.8363 ± 6.37%	329.31 ± 19.27 ± 5.85% External Error ± 20.37 Analytical Error ± 19.19	106.88 2.45 10.3382	50.54 7 Statistical T Ratio Error Magnification	2.553 ± 0.279
Project = VU75 Irradiation = VU75 J = 0.0026395 ± 0.0000079 DRA-1 = 25.260 ± 0.144 Ma	Total Fusion Age	86.2180 ± 0.6151 ± 0.71%	369.91 ± 3.12 ± 0.84% External Error ± 8.03 Analytical Error ± 2.39		9	0.089 ± 0.004

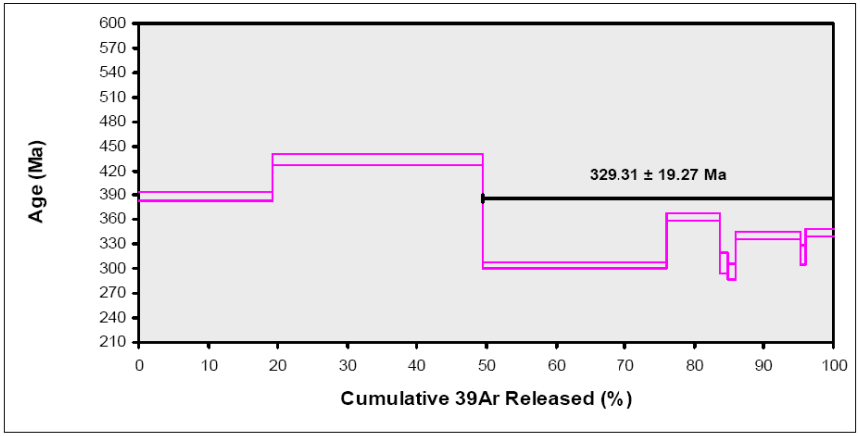

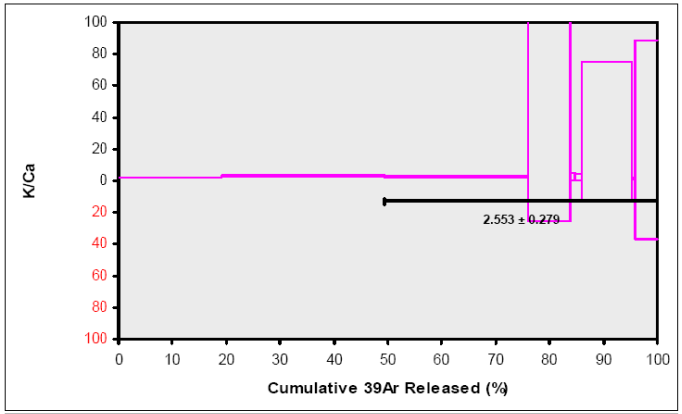

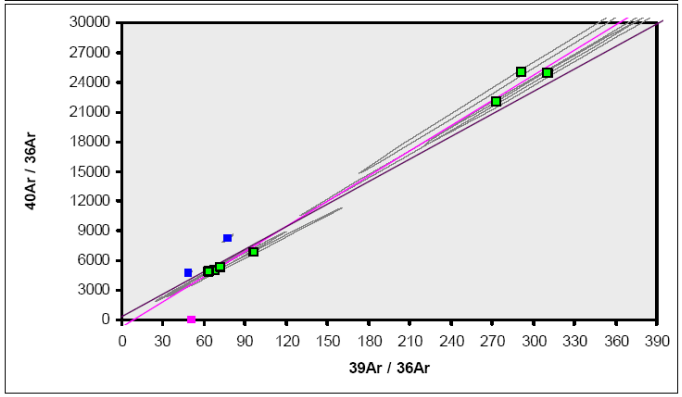

Results	40(a)/36(a) ± 2σ	40(r)/39(k) ± 2σ	Age ± 2σ (Ma)	MSWD
No Convergence	700.0351 ± 372.1798 ± 53.17%	84.7648 ± 3.7587 ± 4.43%	364.26 ± 14.76 ± 4.05% External Error ± 16.46 Analytical Error ± 14.63	9.88

07XD04 (phengite, combination)

Incremental Heating	36Ar(a)	37Ar(ca)	38Ar(cl)	39Ar(k)	40Ar(r)	Age ± 2σ (Ma)	40Ar(r) (%)	39Ar(k) (%)	K/Ca ± 2σ
0.75 W	0.004951	0.053899	0.000000	0.243086	22.098826	388.01 ± 5.51	93.79	10.98	1.939 ± 0.144
1.00 W	0.004951	0.054336	0.000000	0.382822	39.405751	433.61 ± 6.89	96.42	17.29	3.030 ± 0.220
1.25 W	0.004951	0.055048	0.000000	0.335601	23.345780	304.12 ± 3.15	94.10	15.15	2.621 ± 0.187
1.50 W	0.000337	0.001081	0.000000	0.098371	8.327413	363.82 ± 4.49	98.82	4.44	39.128 ± 64.923
1.50 W	0.000903	0.000311	0.000000	0.020139	1.720135	366.77 ± 5.91	86.57	0.91	27.836 ± 14.539
1.75 W	0.000172	0.002080	0.000156	0.012383	0.871530	307.41 ± 12.64	94.49	0.56	2.560 ± 2.326
2.00 W	0.000157	0.000000	0.000107	0.015165	1.025090	296.18 ± 9.51	95.66	0.68	
2.50 W	0.001776	0.000592	0.000000	0.322882	26.025159	347.99 ± 1.96	98.02	14.58	234.439 ± 66.079
3.00 W	0.000378	0.001593	0.000000	0.117612	9.281930	341.37 ± 4.26	98.81	5.31	31.748 ± 43.783
3.40 W	0.001400	0.000502	0.000000	0.504087	37.119189	320.43 ± 1.56	98.90	22.76	432.068 ± 223.388
4.00 W	0.000133	0.002907	0.000000	0.008439	0.613178	316.54 ± 11.74	93.99	0.38	1.248 ± 0.820
4.50 W	0.000082	0.000068	0.000051	0.009443	0.673284	311.07 ± 8.06	96.53	0.43	59.875 ± 181.387
7.00 W	0.000156	0.000000	0.000000	0.016232	1.226433	328.07 ± 4.67	96.37	0.73	
9.00 W	0.000297	0.000486	0.000001	0.064723	4.919797	329.88 ± 2.75	98.24	2.92	57.299 ± 30.634
12.00 W	0.000611	0.000023	0.000000	0.011631	0.554717	213.91 ± 8.46	75.45	0.53	216.415 ± 2494.330
25.00 W	0.000191	0.000865	0.000067	0.052129	4.148789	344.00 ± 4.07	98.66	2.35	25.899 ± 62.763
Σ	0.021446	0.173791	0.000381	2.214748	181.357002				

Information on Analysis	Results	40(r)/39(k) ± 2σ	Age ± 2σ (Ma)	MSWD	39Ar(k) (%,n)	K/Ca ± 2σ
VU75-D17 Phengite 07XD04 MG	Error Plateau	72.2889 ± 5.1937 ± 7.18%	315.05 ± 20.84 ± 6.62% External Error ± 21.77 Analytical Error ± 20.77	73.01 2.57 8.5447	18.11 6 Statistical T Ratio Error Magnification	31.244 ± 32.721
Project = VU75 Irradiation = VU75 J = 0.0026395 ± 0.0000079 DRA-1 = 25.260 ± 0.144 Ma	Total Fusion Age	81.8861 ± 0.3582 ± 0.44%	353.02 ± 2.38 ± 0.67% External Error ± 7.45 Analytical Error ± 1.40		16	0.154 ± 0.007

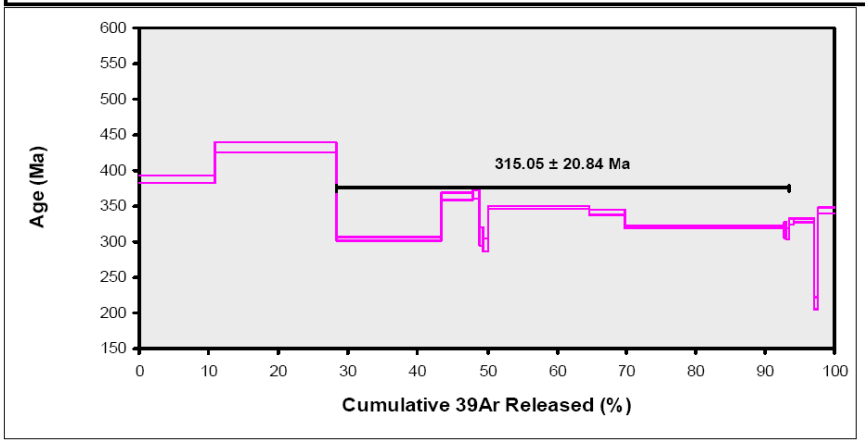

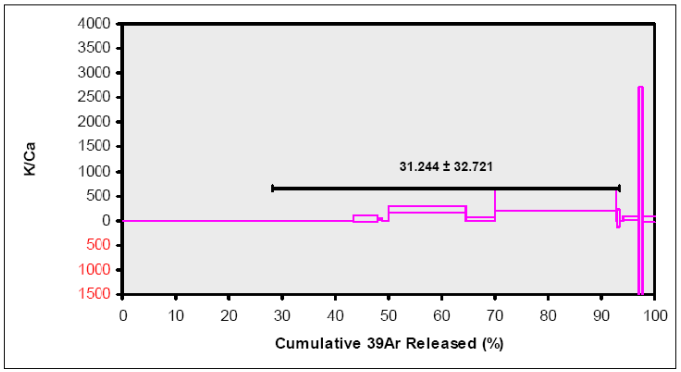

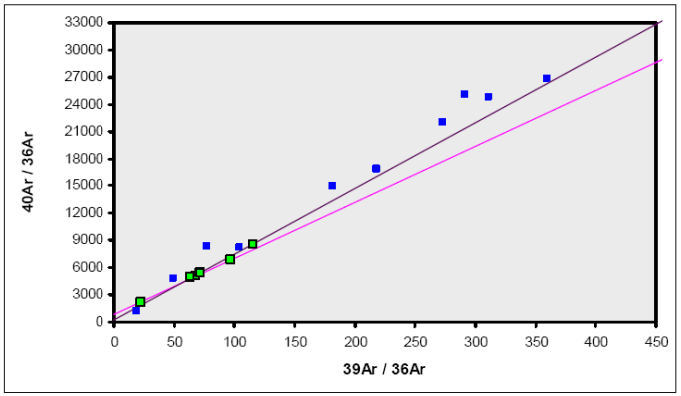

Results	40(a)/36(a) ± 2σ	40(r)/39(k) ± 2σ	Age ± 2σ (Ma)	MSWD
No Convergence	820.4682 ± 105.3271 ± 12.84%	61.8958 ± 1.9493 ± 3.15%	273.00 ± 8.12 ± 2.98% External Error ± 9.79 Analytical Error ± 7.98	0.52

07XX06 (actinolite)

Incremental Heating	36Ar(a)	37Ar(ca)	38Ar(cl)	39Ar(k)	40Ar(r)	Age ± 2σ (Ma)	40Ar(r) (%)	39Ar(k) (%)	K/Ca ± 2σ
2.00 W	0.051789	0.028496	0.000349	0.003387	22.989171	5284.53 ± 120.96	60.04	0.02	0.051 ± 0.005
3.00 W	0.086572	0.208776	0.001558	0.033072	53.837783	2991.11 ± 33.48	67.79	0.23	0.068 ± 0.004
4.00 W	0.117751	0.525236	0.001585	0.094243	63.272384	1826.47 ± 24.03	64.52	0.65	0.077 ± 0.004
4.50 W	0.021138	0.237030	0.000250	0.043267	8.717979	762.35 ± 16.42	58.26	0.30	0.078 ± 0.004
5.00 W	0.031687	0.321153	0.000898	0.063332	11.287132	689.07 ± 16.75	54.66	0.44	0.085 ± 0.005
6.00 W	0.061273	1.273487	0.005977	0.176741	33.090164	717.77 ± 12.10	64.63	1.22	0.060 ± 0.003
7.00 W	0.044182	2.010612	0.008348	0.285216	39.128566	552.14 ± 6.76	74.98	1.97	0.061 ± 0.003
8.00 W	0.066639	4.110254	0.020325	0.627361	79.121161	513.34 ± 5.12	80.07	4.34	0.066 ± 0.004
7.00 W	0.050751	3.390256	0.017168	0.440332	59.776986	547.16 ± 5.63	79.94	3.05	0.056 ± 0.003
8.00 W	0.106436	10.709335	0.057154	1.434523	164.462650	472.24 ± 4.27	83.95	9.93	0.058 ± 0.003
9.00 W	0.098761	15.364168	0.074595	1.761118	224.273136	517.69 ± 4.17	88.48	12.19	0.049 ± 0.003
12.00 W	0.164721	30.400223	0.149935	3.375772	493.059248	582.63 ± 4.49	91.01	23.37	0.048 ± 0.003
14.00 W	0.063391	19.201077	0.078307	1.975030	251.167026	517.07 ± 3.88	93.06	13.67	0.044 ± 0.003
17.00 W	0.049698	19.280923	0.061092	1.700673	217.721616	520.07 ± 3.96	93.68	11.77	0.038 ± 0.002
22.00 W	0.056914	19.655359	0.060885	1.651382	195.889821	486.59 ± 3.77	92.09	11.43	0.036 ± 0.002
27.00 W	0.028822	8.272529	0.016876	0.624499	55.814788	378.25 ± 3.41	86.76	4.32	0.032 ± 0.002
25.00 W	0.007368	2.413726	0.001926	0.154756	8.282490	235.88 ± 3.29	79.18	1.07	0.028 ± 0.002
Σ	1.107893	137.402640	0.557226	14.444703	1981.892100				

Information on Analysis	Results	40(r)/39(k) ± 2σ	Age ± 2σ (Ma)	MSWD	39Ar(k) (%,n)	K/Ca ± 2σ
VU75-D3 Actinolite 07XX06 MG	Error Plateau	129.3646 ± 14.4666 ± 11.18%	524.80 ± 51.00 ± 9.72% External Error ± 52.06 Analytical Error ± 50.92	1217.29 2.14 34.8896	94.61 15 Statistical T Ratio Error Magnification	0.052 ± 0.007
Project = VU75 Irradiation = VU75 J = 0.0026099 ± 0.0000078 DRA-1 = 25.260 ± 0.144 Ma	Total Fusion Age	137.2055 ± 0.4635 ± 0.34%	552.19 ± 3.28 ± 0.59% External Error ± 11.52 Analytical Error ± 1.61		17	0.001 ± 0.000

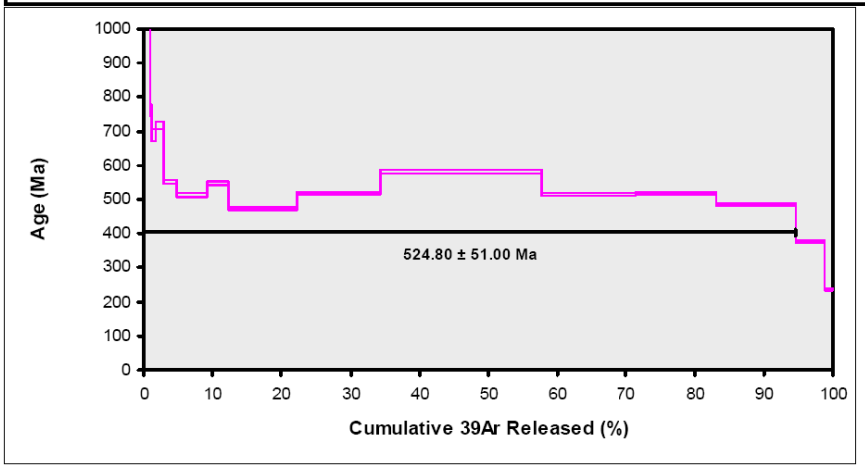

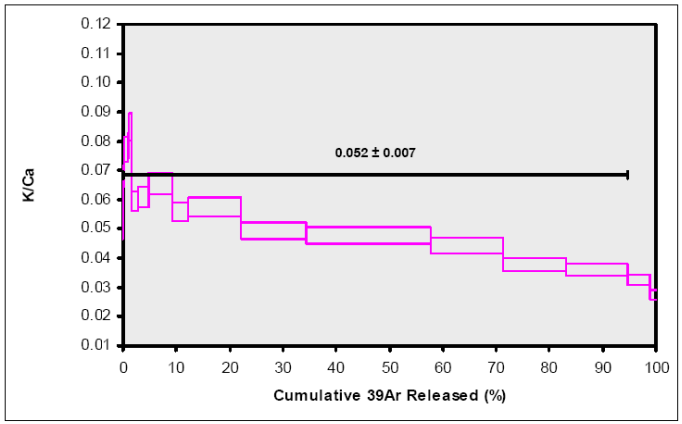

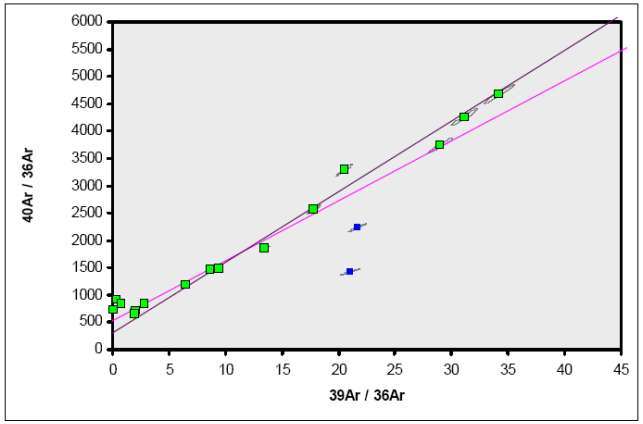

Results	40(a)/36(a) ± 2σ	40(r)/39(k) ± 2σ	Age ± 2σ (Ma)	MSWD
No Convergence	537.2563 ± 117.0857 ± 21.79%	109.6356 ± 10.8785 ± 9.92%	453.99 ± 39.90 ± 8.79% External Error ± 40.92 Analytical Error ± 39.83	> 100

07XX20 (actinolite)

Incremental Heating	36Ar(a)	37Ar(ca)	38Ar(cl)	39Ar(k)	40Ar(r)	Age ± 2σ (Ma)	40Ar(r) (%)	39Ar(k) (%)	K/Ca ± 2σ
2.00 W	0.047834	0.007225	0.000000	0.002520	21.345442	5663.10 ± 164.32	60.16	0.03	0.150 ± 0.019
3.00 W	0.047626	0.112373	0.000000	0.017535	27.207880	2919.63 ± 41.69	65.91	0.24	0.067 ± 0.004
4.00 W	0.040743	0.726349	0.000000	0.070460	30.085752	1349.71 ± 16.00	71.42	0.96	0.042 ± 0.002
4.50 W	0.026271	0.209569	0.000000	0.028097	12.771690	1410.05 ± 25.18	62.19	0.38	0.058 ± 0.003
5.00 W	0.025668	0.557073	0.000000	0.060335	14.412550	873.34 ± 13.41	65.52	0.82	0.047 ± 0.003
6.00 W	0.036314	1.241775	0.000000	0.123480	34.623752	989.84 ± 10.31	76.34	1.68	0.043 ± 0.002
7.00 W	0.038526	3.322824	0.000000	0.307816	64.230177	783.59 ± 6.48	84.94	4.18	0.040 ± 0.002
8.00 W	0.042794	4.575540	0.000000	0.398639	82.424041	777.79 ± 6.12	86.70	5.42	0.037 ± 0.002
7.00 W	0.050798	4.692253	0.000000	0.415054	84.590737	768.73 ± 6.43	84.93	5.64	0.038 ± 0.002
8.00 W	0.060955	5.966438	0.000000	0.504471	101.370793	759.92 ± 6.28	84.91	6.86	0.036 ± 0.002
9.00 W	0.049117	6.901117	0.000000	0.580628	113.767535	744.40 ± 5.75	88.68	7.89	0.036 ± 0.002
12.00 W	0.161262	18.180855	0.000000	1.507019	280.288628	713.16 ± 5.95	85.47	20.48	0.036 ± 0.002
14.00 W	0.093428	13.891388	0.000071	1.183300	188.063281	625.36 ± 5.13	87.20	16.08	0.037 ± 0.002
17.00 W	0.061549	9.385073	0.000000	0.798826	112.731783	565.14 ± 5.04	86.11	10.86	0.037 ± 0.002
22.00 W	0.050406	7.332958	0.000000	0.698885	87.792166	511.04 ± 4.43	85.49	9.50	0.041 ± 0.002
27.00 W	0.033478	5.657075	0.000000	0.566125	65.452985	475.25 ± 4.05	86.87	7.69	0.043 ± 0.002
25.00 W	0.027501	0.725921	0.000000	0.095618	6.740693	304.35 ± 11.25	45.34	1.30	0.057 ± 0.003
Σ	0.894273	83.485806	0.000071	7.358807	1327.899885				

Information on Analysis	Results	40(r)/39(k) ± 2σ	Age ± 2σ (Ma)	MSWD	39Ar(k) (%,n)	K/Ca ± 2σ
VU75-D2	Error Plateau	187.8939 ± 24.7058 ± 13.15%	719.18 ± 78.07 ± 10.86%	1554.62	81.51	0.040 ± 0.004
Actinolite					14	
07XX20			External Error ± 79.38	2.16	Statistical T Ratio	
MG			Analytical Error ± 77.99	39.4287	Error Magnification	
Project = VU75	Total Fusion Age	180.4504 ± 0.6118 ± 0.34%	695.53 ± 3.98 ± 0.57%		17	0.001 ± 0.000
Irradiation = VU75						
J = 0.0026068 ± 0.0000078			External Error ± 14.47			
DRA-1 = 25.260 ± 0.144 Ma			Analytical Error ± 1.96			

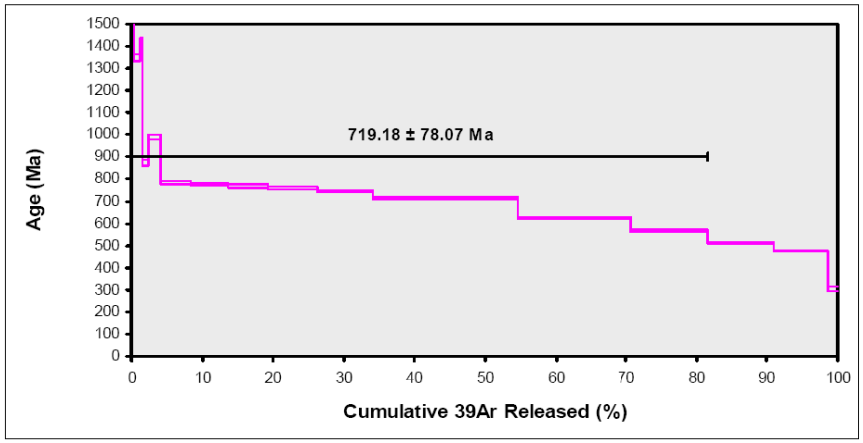

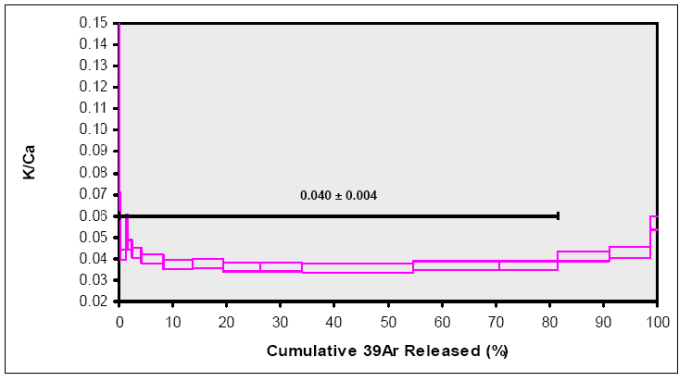

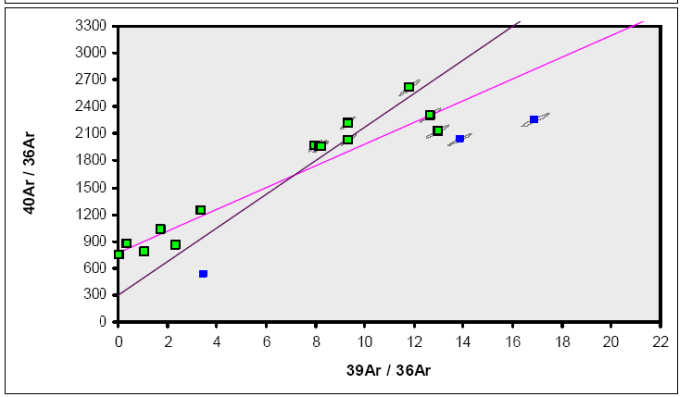

Results	40(a)/36(a) ± 2σ	40(r)/39(k) ± 2σ	Age ± 2σ (Ma)	MSWD
Error Chron	776.8466 ± 146.7564 ± 18.89%	121.2034 ± 20.7865 ± 17.15%	495.33 ± 74.33 ± 15.01%	> 100
			External Error ± 74.99	
			Analytical Error ± 74.29	

07XX20 (phengite, 1st run)

Incremental Heating	36Ar(a)	37Ar(ca)	38Ar(cl)	39Ar(k)	40Ar(r)	Age ± 2σ (Ma)	40Ar(r) (%)	39Ar(k) (%)	K/Ca ± 2σ
1.50 W	0.001451	0.002191	0.000045	0.012161	0.526103	194.61 ± 9.61	55.09	12.63	2.386 ± 0.296
2.50 W	0.000795	0.006360	0.000040	0.037811	1.748698	207.29 ± 3.44	88.16	39.26	2.556 ± 0.166
3.50 W	0.000295	0.016189	0.000162	0.035084	1.573404	201.35 ± 3.81	94.74	36.43	0.932 ± 0.050
4.50 W	0.000152	0.014291	0.000000	0.007117	0.260618	166.04 ± 11.69	85.28	7.39	0.214 ± 0.010
7.00 W	0.000061	0.000241	0.000000	0.001009	0.026117	118.90 ± 54.41	59.09	1.05	1.799 ± 1.634
9.00 W	0.000020	0.000356	0.000037	0.001531	0.061277	180.79 ± 53.98	91.20	1.59	1.847 ± 1.435
12.00 W	0.000066	0.000021	0.000000	0.001123	0.016011	66.48 ± 74.43	44.96	1.17	23.459 ± 259.603
16.00 W	0.000014	0.000182	0.000029	0.000481	0.003177	31.09 ± 117.47	42.95	0.50	1.137 ± 1.670
Σ	0.002855	0.039832	0.000313	0.096316	4.215404				

Information on Analysis	Results	40(r)/39(k) ± 2σ	Age ± 2σ (Ma)	MSWD	39Ar(k) (%,n)	K/Ca ± 2σ
VU75-D11	Error Plateau	45.4591 ± 1.2638 ± 2.78%	203.95 ± 5.48 ± 2.69%	4.71	88.31	1.098 ± 0.687
Phengite					3	
07XX20			External Error ± 6.83	4.30	Statistical T Ratio	
MG			Analytical Error ± 5.36	2.1711	Error Magnification	
Project = VU75	Total Fusion Age	43.7662 ± 0.6641 ± 1.52%	196.75 ± 3.04 ± 1.55%		8	0.029 ± 0.001
Irradiation = VU75						
J = 0.0026328 ± 0.0000079			External Error ± 4.97			
DRA-1 = 25.260 ± 0.144 Ma			Analytical Error ± 2.83			

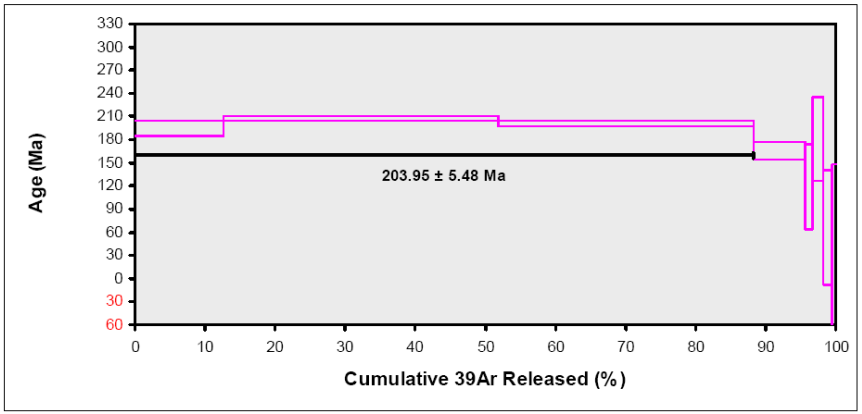

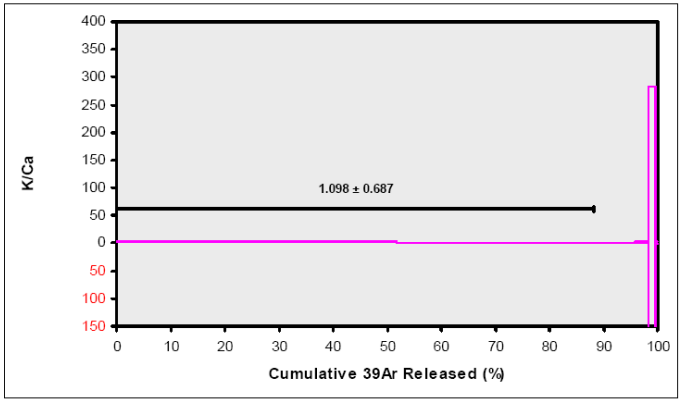

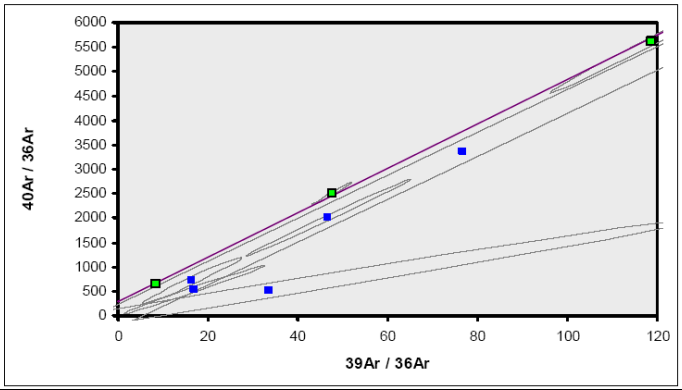

Results	40(a)/36(a) ± 2σ	40(r)/39(k) ± 2σ	Age ± 2σ (Ma)	MSWD
No Convergence	284.5853 ± 58.1039 ± 20.42%	45.4558 ± 2.0791 ± 4.57%	203.93 ± 8.90 ± 4.36%	7.78
			External Error ± 9.79	
			Analytical Error ± 8.82	

07XX20 (phengite, 2nd run)

Incremental Heating	36Ar(a)	37Ar(ca)	38Ar(cl)	39Ar(k)	40Ar(r)	Age ± 2σ (Ma)	40Ar(r) (%)	39Ar(k) (%)	K/Ca ± 2σ
0.75 W	0.000599	0.000000	0.000000	0.042673	2.876651	294.75 ± 6.70	94.20	21.73	
1.00 W	0.000617	0.000000	0.000000	0.027938	1.859995	291.37 ± 13.26	91.07	14.23	
1.25 W	0.000493	0.000000	0.000000	0.034263	2.016713	259.92 ± 7.74	93.26	17.45	15.236 ± 33.977
1.50 W	0.000441	0.022819	0.001508	0.023669	0.751125	144.77 ± 8.20	85.21	12.05	0.446 ± 0.069
20.00 W	0.003494	0.065131	0.000120	0.067852	2.563802	171.10 ± 4.09	71.29	34.55	0.448 ± 0.035
Σ	0.005644	0.087950	0.001627	0.196394	10.068286				

Information on Analysis	Results	40(r)/39(k) ± 2σ	Age ± 2σ (Ma)	MSWD	39Ar(k) (%,n)	K/Ca ± 2σ
VU75-D11	Error Plateau	64.0301 ± 5.7748 ± 9.02%	281.05 ± 23.52 ± 8.37%	24.59	53.40 3	0.026 ± 1.413
Phengite			External Error ± 24.19	4.30	Statistical T Ratio	
07XX20			Analytical Error ± 23.47	4.9591	Error Magnification	
MG						
Project = VU75	Total Fusion Age	51.2658 ± 0.7296 ± 1.42%	228.41 ± 3.31 ± 1.45%		5	0.027 ± 0.002
Irradiation = VU75			External Error ± 5.64			
J = 0.0026328 ± 0.0000079			Analytical Error ± 3.05			
DRA-1 = 25.260 ± 0.144 Ma						

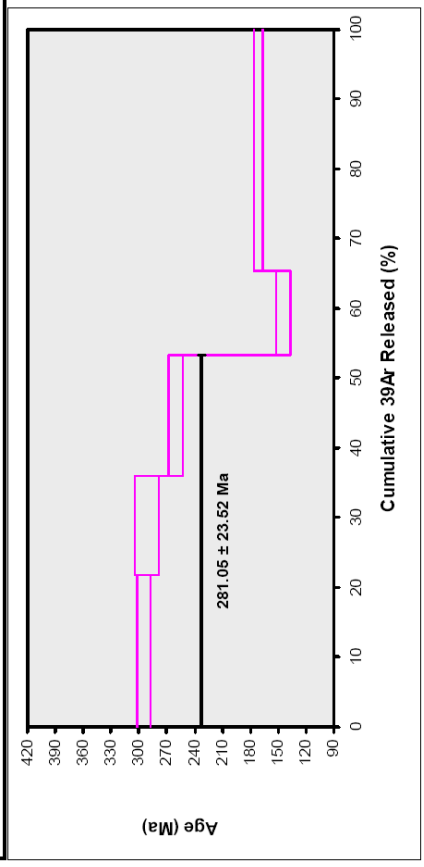

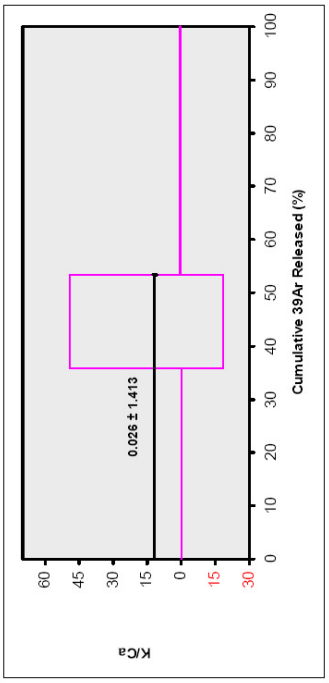

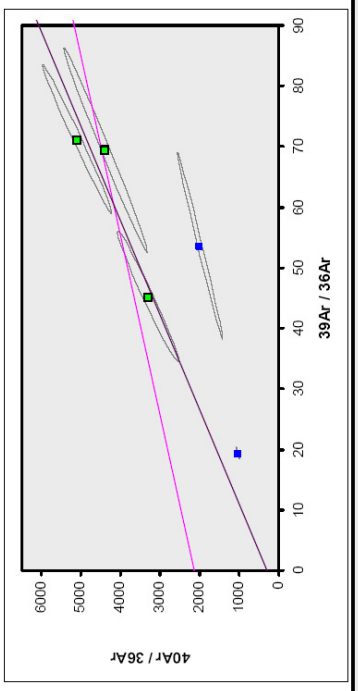

Results	40(a)/36(a) ± 2σ	40(r)/39(k) ± 2σ	Age ± 2σ (Ma)	MSWD
No Convergence	2152.8304 ± 3911.8623 ± 181.71%	33.6533 ± 63.3790 ± 188.33%	153.16 ± 276.54 ± 180.56%	8.52
			External Error ± 276.55	
			Analytical Error ± 276.53	

07XX20 (phengite, combination)

Incremental Heating	36Ar(a)	37Ar(ca)	38Ar(cl)	39Ar(k)	40Ar(r)	Age ± 2σ (Ma)	40Ar(r) (%)	39Ar(k) (%)	K/Ca ± 2σ
0.75 W	0.000599	0.000000	0.000000	0.042673	2.876651	294.75 ± 6.70	94.20	14.58	1.137 ± 1.670
1.00 W	0.000617	0.000000	0.000000	0.027938	1.859995	291.37 ± 13.26	91.07	9.54	1.137 ± 1.670
1.25 W	0.000493	0.000000	0.000000	0.034263	2.016713	259.92 ± 7.74	93.26	11.71	1.137 ± 1.670
1.50 W	0.001451	0.002191	0.000045	0.012161	0.526103	194.61 ± 9.61	55.09	4.15	2.386 ± 0.296
1.50 W	0.000441	0.022819	0.001508	0.023669	0.751125	144.77 ± 8.20	85.21	8.09	0.446 ± 0.059
2.50 W	0.000795	0.006360	0.000040	0.037811	1.748698	207.29 ± 3.44	88.16	12.92	2.556 ± 0.166
3.50 W	0.000295	0.016189	0.000162	0.035084	1.573404	201.35 ± 3.81	94.74	11.99	0.932 ± 0.050
4.50 W	0.000152	0.014291	0.000000	0.007117	0.260618	166.04 ± 11.69	85.28	2.43	0.214 ± 0.010
7.00 W	0.000061	0.000241	0.000000	0.001009	0.026117	118.90 ± 54.41	59.09	0.34	1.799 ± 1.634
9.00 W	0.000020	0.000356	0.000037	0.001531	0.061277	180.79 ± 53.98	91.20	0.52	1.847 ± 1.435
12.00 W	0.000066	0.000021	0.000000	0.001123	0.016011	66.48 ± 74.43	44.96	0.38	23.459 ± 259.603
16.00 W	0.000014	0.000182	0.000029	0.000481	0.003177	31.09 ± 117.47	42.95	0.16	1.137 ± 1.670
20.00 W	0.003494	0.065131	0.000120	0.067852	2.563802	171.10 ± 4.09	71.29	23.18	0.448 ± 0.035
Σ	0.008499	0.127782	0.001940	0.292710	14.283690				

Information on Analysis	Results	40(r)/39(k) ± 2σ	Age ± 2σ (Ma)	MSWD	39Ar(k) (%,n)	K/Ca ± 2σ
VU75-D11 Phengite 07XX20 MG	Error Plateau	43.8943 ± 3.4752 ± 7.92%	197.30 ± 14.84 ± 7.52% External Error ± 15.35 Analytical Error ± 14.80	40.91 2.45 6.3960	40.44 7 Statistical T Ratio Error Magnification	0.259 ± 0.172
Project = VU75 Irradiation = VU75 J = 0.0026328 ± 0.0000079 DRA-1 = 25.260 ± 0.144 Ma	Total Fusion Age	48.7981 ± 0.5288 ± 1.08%	218.05 ± 2.54 ± 1.17% External Error ± 5.05 Analytical Error ± 2.23		13	0.028 ± 0.001

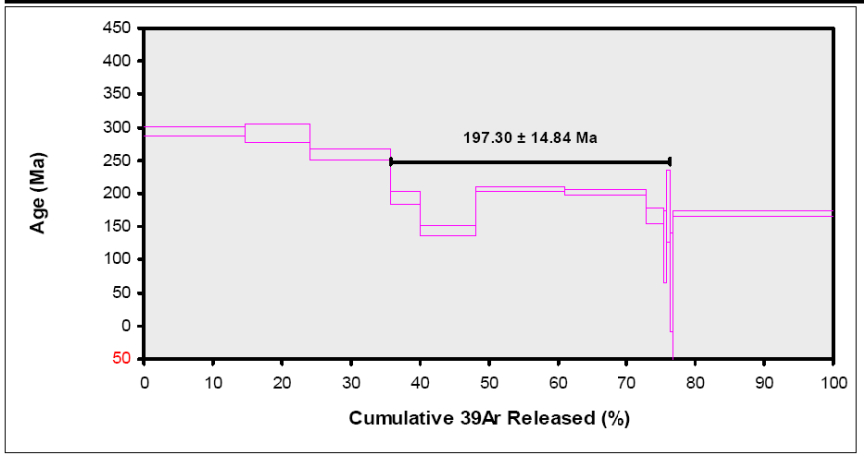

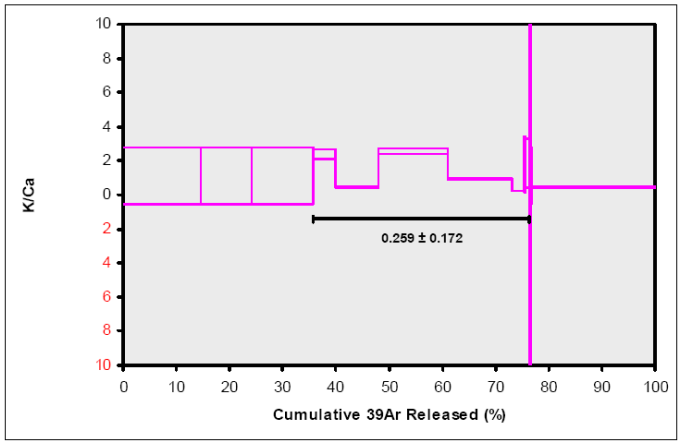

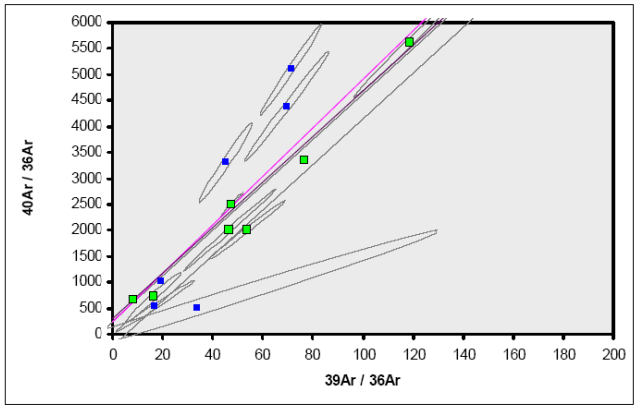

Results	40(a)/36(a) ± 2σ	40(r)/39(k) ± 2σ	Age ± 2σ (Ma)	MSWD
No Convergence	235.0623 ± 135.4797 ± 57.64%	46.7694 ± 4.5635 ± 9.76%	209.50 ± 19.34 ± 9.23% External Error ± 19.78 Analytical Error ± 19.30	46.04

07XX23 (hornblende)

Incremental Heating	36Ar(a)	37Ar(ca)	38Ar(cl)	39Ar(k)	40Ar(r)	Age ± 2σ (Ma)	40Ar(r) (%)	39Ar(k) (%)	K/Ca ± 2σ
2.00 W	0.052100	0.098399	0.000000	0.019576	16.949104	2133.19 ± 42.72	52.40	0.05	0.086 ± 0.005
3.00 W	0.081012	0.238183	0.000147	0.048367	32.232643	1819.27 ± 30.39	57.38	0.13	0.087 ± 0.005
4.00 W	0.077141	0.255097	0.000000	0.092924	32.189439	1162.81 ± 21.08	58.54	0.25	0.157 ± 0.008
4.50 W	0.032951	0.129086	0.000000	0.040604	8.071289	754.67 ± 25.16	45.32	0.11	0.135 ± 0.007
5.00 W	0.027954	0.189288	0.000000	0.053283	8.403692	622.55 ± 17.90	50.43	0.14	0.121 ± 0.007
6.00 W	0.046150	0.468889	0.000000	0.110940	25.055472	836.74 ± 13.24	64.75	0.30	0.102 ± 0.006
7.00 W	0.035517	0.612676	0.000000	0.139583	19.663025	565.41 ± 9.52	65.20	0.38	0.098 ± 0.005
8.00 W	0.044147	1.079399	0.000388	0.244726	32.391337	535.84 ± 7.16	71.29	0.66	0.097 ± 0.005
7.00 W	0.076272	4.599817	0.004264	1.003612	93.114957	391.60 ± 4.05	80.51	2.72	0.094 ± 0.005
8.00 W	0.064428	7.469003	0.008434	1.631560	112.024310	297.69 ± 2.71	85.47	4.42	0.094 ± 0.005
9.00 W	0.071672	11.652396	0.012341	2.606414	153.491780	258.21 ± 2.27	87.87	7.05	0.096 ± 0.005
12.00 W	0.097201	26.862774	0.033523	6.100928	288.877511	210.44 ± 1.75	90.95	16.51	0.098 ± 0.006
14.00 W	0.063236	20.509553	0.025841	4.755823	197.905238	186.21 ± 1.55	91.37	12.87	0.100 ± 0.006
17.00 W	0.056377	26.174111	0.025182	6.050061	238.835858	177.10 ± 1.46	93.48	16.38	0.099 ± 0.006
22.00 W	0.064928	35.889624	0.045725	8.333626	329.279950	177.26 ± 1.42	94.49	22.56	0.100 ± 0.006
27.00 W	0.033316	18.918550	0.024257	4.447804	158.887664	160.99 ± 1.31	94.16	12.04	0.101 ± 0.006
25.00 W	0.013916	5.092278	0.006815	1.264823	41.315011	147.76 ± 1.30	90.94	3.42	0.107 ± 0.006
Σ	0.938319	160.239121	0.186916	36.944653	1788.688281				

Information on Analysis	Results	40(r)/39(k) ± 2σ	Age ± 2σ (Ma)	MSWD	39Ar(k) (%,n)	K/Ca ± 2σ
VU75-D4 Hornblende 07XX23 MG	Error Plateau	43.5265 ± 7.9612 ± 18.29%	194.33 ± 33.71 ± 17.35% External Error ± 33.94 Analytical Error ± 33.70	3041.35 2.36 55.1485	94.55 8 Statistical T Ratio Error Magnification	0.097 ± 0.002
Project = VU75 Irradiation = VU75 J = 0.0026129 ± 0.0000078 DRA-1 = 25.260 ± 0.144 Ma	Total Fusion Age	48.4153 ± 0.1640 ± 0.34%	214.90 ± 1.40 ± 0.65% External Error ± 4.52 Analytical Error ± 0.69		17	0.003 ± 0.000

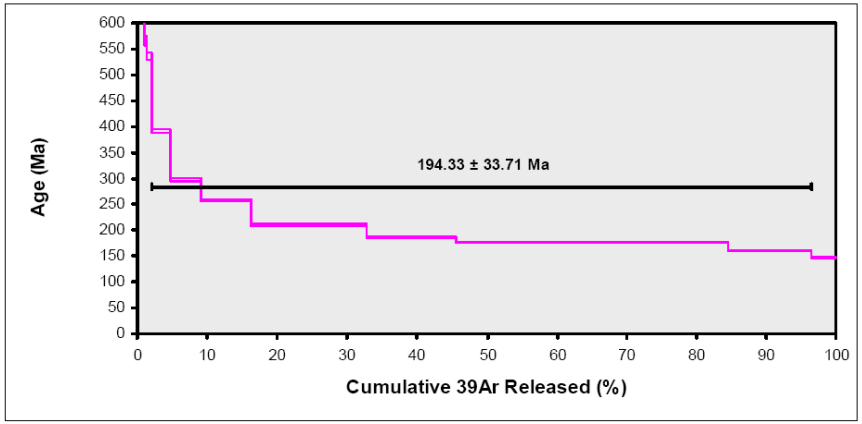

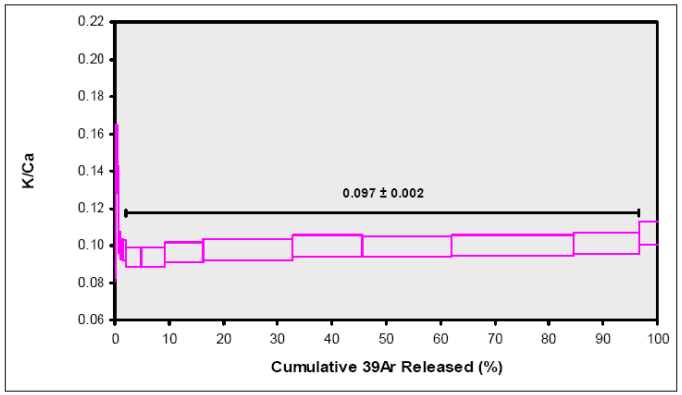

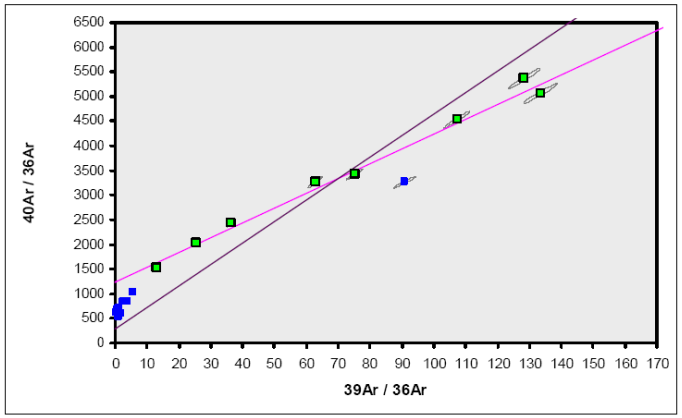

Results	40(a)/36(a) ± 2σ	40(r)/39(k) ± 2σ	Age ± 2σ (Ma)	MSWD
Error Chron	1244.6759 ± 180.6807 ± 14.52%	30.0197 ± 2.4496 ± 8.16%	136.23 ± 10.74 ± 7.88% External Error ± 11.08 Analytical Error ± 10.71	38.59

07XX24 (phengite, 1st run)

Incremental Heating	36Ar(a)	37Ar(ca)	38Ar(cl)	39Ar(k)	40Ar(r)	Age ± 2σ (Ma)	40Ar(r) (%)	39Ar(k) (%)	K/Ca ± 2σ
1.50 W	0.000908	0.002375	0.000034	0.013340	0.700761	233.83 ± 9.83	72.30	10.82	2.415 ± 0.264
2.50 W	0.001039	0.004910	0.000081	0.024433	1.225247	223.85 ± 4.75	79.97	19.81	2.140 ± 0.132
3.50 W	0.000416	0.003916	0.000196	0.020621	0.978958	212.59 ± 4.77	88.85	16.72	2.264 ± 0.221
4.50 W	0.000172	0.006589	0.000014	0.011038	0.447018	182.89 ± 6.72	89.77	8.95	0.720 ± 0.034
7.00 W	0.000096	0.001428	0.000137	0.002762	0.123682	201.17 ± 20.67	81.30	2.24	0.832 ± 0.116
9.00 W	0.000555	0.001096	0.000104	0.015981	0.166187	48.76 ± 5.41	50.33	12.96	6.271 ± 2.106
12.00 W	0.000205	0.000642	0.000111	0.018848	0.113274	28.34 ± 3.48	65.12	15.28	12.632 ± 5.819
16.00 W	0.000064	0.000226	0.000067	0.016305	0.050826	14.75 ± 4.96	72.83	13.22	31.066 ± 44.785
Σ	0.003455	0.021181	0.000744	0.123327	3.805953				

Information on Analysis	Results	40(r)/39(k) ± 2σ	Age ± 2σ (Ma)	MSWD	39Ar(k) (%,n)	K/Ca ± 2σ
VU75-D12	Error Plateau	47.4915 ± 3.7188 ± 7.83%	212.67 ± 15.75 ± 7.41%	30.40	58.54	0.858 ± 0.420
Phengite					5	
07XX24			External Error ± 16.32	2.78	Statistical T Ratio	
MG			Analytical Error ± 15.71	5.5136	Error Magnification	
Project = VU75	Total Fusion Age	30.8606 ± 0.4541 ± 1.47%	141.01 ± 2.16 ± 1.53%		8	0.071 ± 0.003
Irradiation = VU75						
J = 0.0026344 ± 0.0000079			External Error ± 3.55			
DRA-1 = 25.260 ± 0.144 Ma			Analytical Error ± 2.00			

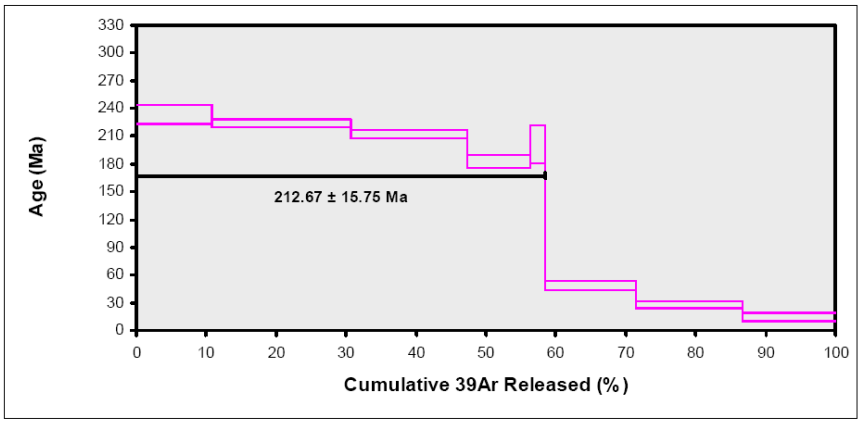

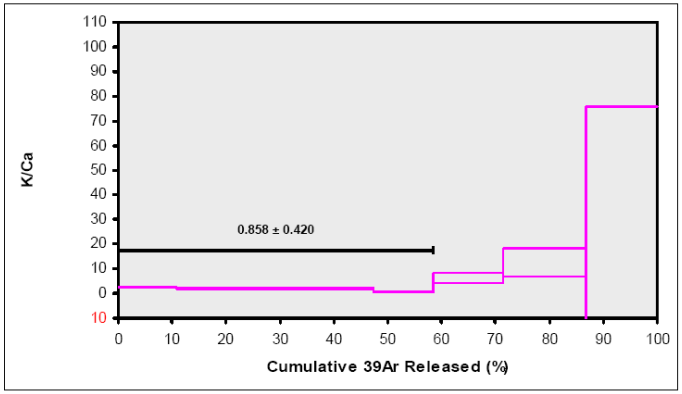

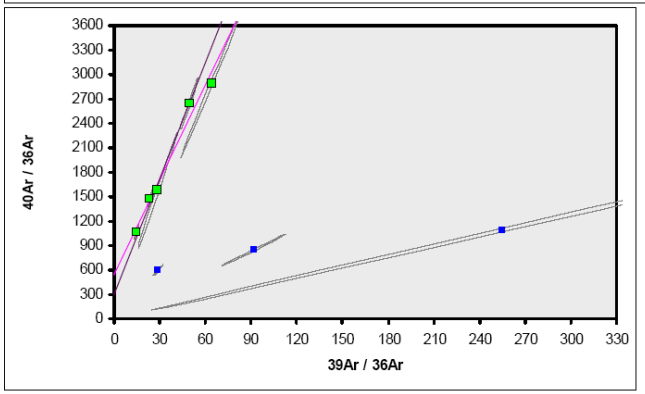

Results	40(a)/36(a) ± 2σ	40(r)/39(k) ± 2σ	Age ± 2σ (Ma)	MSWD
Error Chron	541.1238 ± 172.2499 ± 31.83%	38.8442 ± 6.2878 ± 16.19%	175.77 ± 27.13 ± 15.43%	8.40
			External Error ± 27.36	
			Analytical Error ± 27.11	

07XX24 (phengite, 2nd run)

Incremental Heating	36Ar(a)	37Ar(ca)	38Ar(cl)	39Ar(k)	40Ar(r)	Age ± 2σ (Ma)	40Ar(r) (%)	39Ar(k) (%)	K/Ca ± 2σ
0.75 W	0.001272	0.000000	0.000000	0.033130	2.616127	340.95 ± 13.65	87.44	8.61	
1.00 W	0.001290	0.000000	0.000000	0.067175	4.926315	318.66 ± 11.98	92.81	17.45	
1.25 W	0.001166	0.000000	0.000000	0.104762	5.217053	222.39 ± 7.80	93.80	27.22	
1.50 W	0.001111	0.035799	0.004372	0.151214	4.624946	139.80 ± 2.87	93.37	39.29	1.816 ± 0.216
1.75 W	0.000076	0.001987	0.000001	0.016779	0.421747	115.67 ± 8.85	94.95	4.36	3.630 ± 3.348
2.00 W	0.000054	0.000224	0.000155	0.001741	0.058189	152.24 ± 73.55	78.63	0.45	3.343 ± 26.284
3.00 W	0.000652	0.002121	0.000000	0.003513	0.136370	175.65 ± 44.82	41.44	0.91	0.712 ± 0.704
4.00 W	0.000547	0.000694	0.000000	0.001366	0.033487	112.88 ± 102.24	17.15	0.35	0.847 ± 2.185
20.00 W	0.001089	0.000000	0.000121	0.005225	0.113854	100.70 ± 25.96	26.13	1.36	0.808 ± 0.709
Σ	0.007257	0.040825	0.004649	0.384905	18.148087				

Information on Analysis	Results	40(r)/39(k) ± 2σ	Age ± 2σ (Ma)	MSWD	39Ar(k) (%,n)	K/Ca ± 2σ
VU75-D12 Phengite 07XX24 MG	Error Plateau	29.9916 ± 1.7077 ± 5.69%	137.19 ± 7.56 ± 5.51% External Error ± 8.05 Analytical Error ± 7.52	7.71 2.57 2.7771	46.72 6 Statistical T Ratio Error Magnification	1.650 ± 0.365
Project = VU75 Irradiation = VU75 J = 0.0026344 ± 0.0000079 DRA-1 = 25.260 ± 0.144 Ma	Total Fusion Age	47.1495 ± 0.7672 ± 1.63%	211.22 ± 3.46 ± 1.64% External Error ± 5.46 Analytical Error ± 3.24		9	0.114 ± 0.019

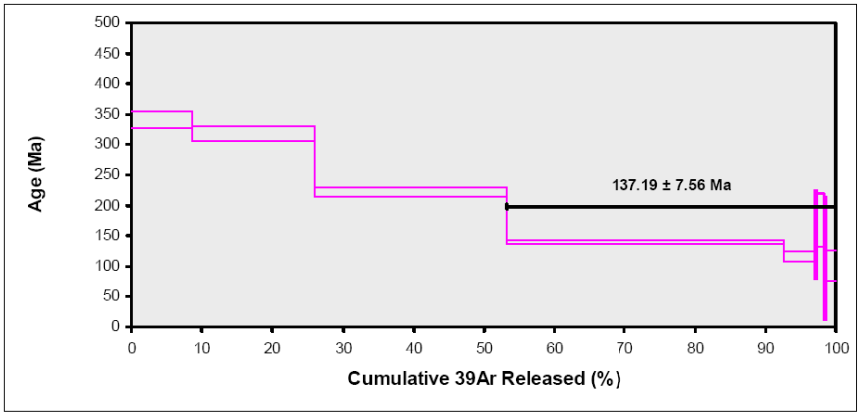

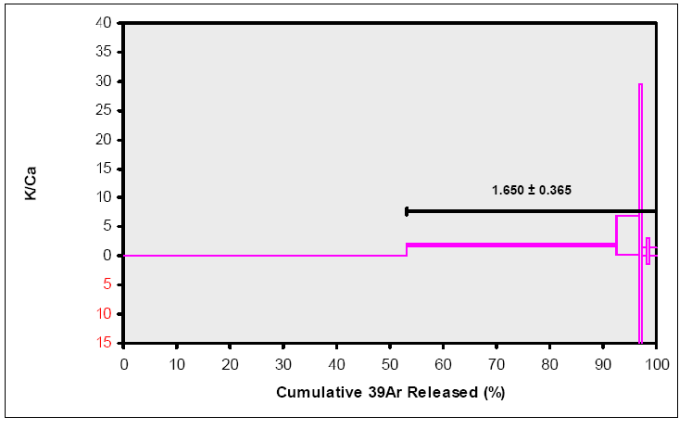

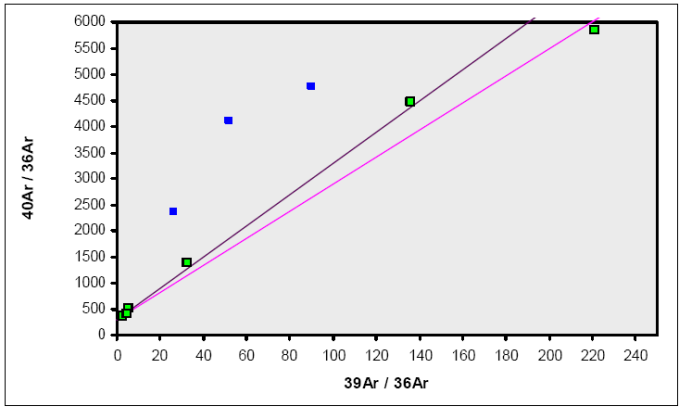

Results	40(a)/36(a) ± 2σ	40(r)/39(k) ± 2σ	Age ± 2σ (Ma)	MSWD
No Convergence	293.9248 ± 84.9813 ± 28.91%	25.9946 ± 2.8939 ± 11.13%	119.50 ± 12.89 ± 10.79% External Error ± 13.11 Analytical Error ± 12.87	13.59

07XX24 (phengite, combination)

Incremental Heating	36Ar(a)	37Ar(ca)	38Ar(cl)	39Ar(k)	40Ar(r)	Age ± 2σ (Ma)	40Ar(r) (%)	39Ar(k) (%)	K/Ca ± 2σ
0.75 W	0.001272	0.000000	0.000000	0.033130	2.616127	340.95 ± 13.65	87.44	6.52	31.066 ± 44.785
1.00 W	0.001290	0.000000	0.000000	0.067175	4.926315	318.66 ± 11.98	92.81	13.22	31.066 ± 44.785
1.25 W	0.001166	0.000000	0.000000	0.104762	5.217053	222.39 ± 7.80	93.80	20.61	31.066 ± 44.785
1.50 W	0.000908	0.002375	0.000034	0.013340	0.700761	233.83 ± 9.83	72.30	2.62	2.415 ± 0.264
1.50 W	0.001111	0.035799	0.004372	0.151214	4.624946	139.80 ± 2.87	93.37	29.75	1.816 ± 0.216
1.75 W	0.000076	0.001987	0.000001	0.016779	0.421747	115.67 ± 8.85	94.95	3.30	3.630 ± 3.348
2.00 W	0.000054	0.000224	0.000155	0.001741	0.058189	152.24 ± 73.55	78.63	0.34	3.343 ± 26.284
2.50 W	0.001039	0.004910	0.000081	0.024433	1.225247	223.85 ± 4.75	79.97	4.81	2.140 ± 0.132
3.00 W	0.000652	0.002121	0.000000	0.003513	0.136370	175.65 ± 44.82	41.44	0.69	0.712 ± 0.704
3.50 W	0.000416	0.003916	0.000196	0.020621	0.978958	212.59 ± 4.77	88.85	4.06	2.264 ± 0.221
4.00 W	0.000547	0.000694	0.000000	0.001366	0.033487	112.88 ± 102.24	17.15	0.27	0.847 ± 2.185
4.50 W	0.000172	0.006589	0.000014	0.011038	0.447018	182.89 ± 6.72	89.77	2.17	0.720 ± 0.034
7.00 W	0.000096	0.001428	0.000137	0.002762	0.123682	201.17 ± 20.67	81.30	0.54	0.832 ± 0.116
9.00 W	0.000555	0.001096	0.000104	0.015981	0.166187	48.76 ± 5.41	50.33	3.14	6.271 ± 2.106
12.00 W	0.000205	0.000642	0.000111	0.018848	0.113274	28.34 ± 3.48	65.12	3.71	12.632 ± 5.819
16.00 W	0.000064	0.000226	0.000067	0.016305	0.050826	14.75 ± 4.96	72.83	3.21	31.066 ± 44.785
20.00 W	0.001089	0.000000	0.000121	0.005225	0.113854	100.70 ± 25.96	26.13	1.03	31.066 ± 44.785
Σ	0.010712	0.062006	0.005393	0.508232	21.954039				

Information on Analysis	Results	40(r)/39(k) ± 2σ	Age ± 2σ (Ma)	MSWD	39Ar(k) (%,n)	K/Ca ± 2σ
VU75-D12 Phengite 07XX24 MG	Error Plateau	37.4717 ± 6.2373 ± 16.65%	169.84 ± 27.00 ± 15.90% External Error ± 27.21 Analytical Error ± 26.98	180.22 2.31 13.4247	45.94 9 Statistical T Ratio Error Magnification	0.856 ± 0.284
Project = VU75 Irradiation = VU75 J = 0.0026344 ± 0.0000079 DRA-1 = 25.260 ± 0.144 Ma	Total Fusion Age	43.1969 ± 0.5681 ± 1.32%	194.44 ± 2.66 ± 1.37% External Error ± 4.71 Analytical Error ± 2.42		17	0.099 ± 0.011

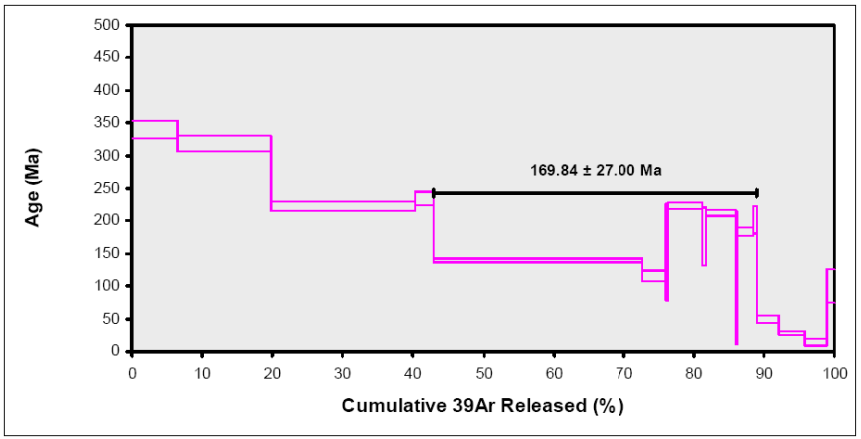

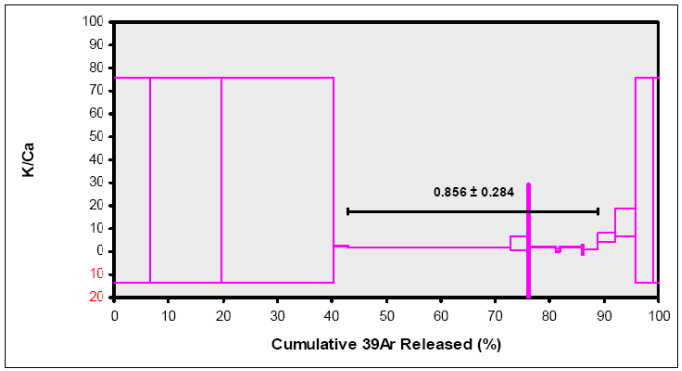

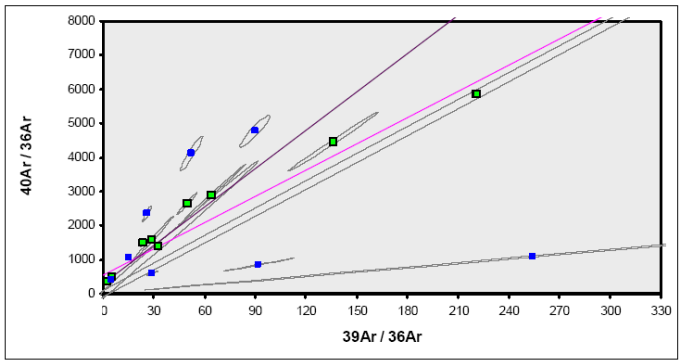

Results	40(a)/36(a) ± 2σ	40(r)/39(k) ± 2σ	Age ± 2σ (Ma)	MSWD
No Convergence	562.3719 ± 278.9148 ± 49.60%	25.5700 ± 7.3911 ± 28.91%	117.61 ± 32.92 ± 27.99% External Error ± 33.00 Analytical Error ± 32.91	51.50

07XX29 (phengite, 1st run)

Incremental Heating	36Ar(a)	37Ar(ca)	38Ar(cl)	39Ar(k)	40Ar(r)	Age ± 2σ (Ma)	40Ar(r) (%)	39Ar(k) (%)	K/Ca ± 2σ
1.50 W	0.000463	0.000026	0.000000	0.010182	0.453252	200.16 ± 9.02	76.82	0.69	168.043 ± 1128.646
2.50 W	0.001454	0.000388	0.000000	0.095044	4.588008	216.08 ± 1.60	91.43	6.40	105.389 ± 68.737
3.50 W	0.004004	0.000207	0.000000	0.381443	19.385566	226.80 ± 1.28	94.24	25.67	793.241 ± 1049.910
4.50 W	0.002533	0.002997	0.000019	0.369141	16.389936	199.67 ± 1.01	95.63	24.84	52.957 ± 4.991
7.00 W	0.002887	0.001796	0.000088	0.336331	15.776556	210.31 ± 1.08	94.87	22.63	80.529 ± 14.524
9.00 W	0.000569	0.000969	0.000000	0.145679	7.860292	239.90 ± 1.37	97.90	9.80	64.613 ± 22.917
9.00 W	0.000609	0.002981	0.000007	0.087521	3.889756	199.86 ± 2.24	95.57	5.89	12.626 ± 1.411
12.00 W	0.000584	0.000464	0.000000	0.040650	1.881274	207.65 ± 3.18	91.60	2.74	37.666 ± 22.641
16.00 W	0.000019	0.000264	0.000000	0.008019	0.384298	214.60 ± 7.90	98.55	0.54	13.057 ± 9.942
20.00 W	0.000044	0.000288	0.000097	0.012008	0.605423	225.12 ± 6.33	97.91	0.81	17.934 ± 16.236
Σ	0.013165	0.010380	0.000211	1.486019	71.214362				

Information on Analysis	Results	40(r)/39(k) ± 2σ	Age ± 2σ (Ma)	MSWD	39Ar(k) (%,n)	K/Ca ± 2σ
VU75-D14						
Phengite	Error Plateau	47.8267 ± 2.6246 ± 5.49%	214.20 ± 11.15 ± 5.21%	409.02	92.92 8	16.366 ± 9.340
07XX29			External Error ± 11.94	2.36	Statistical T Ratio	
MG			Analytical Error ± 11.08	20.2243	Error Magnification	
Project = VU75						
Irradiation = VU75	Total Fusion Age	47.9229 ± 0.1279 ± 0.27%	214.61 ± 1.33 ± 0.62%		10	1.734 ± 0.146
J = 0.0026359 ± 0.0000079			External Error ± 4.49			
DRA-1 = 25.260 ± 0.144 Ma			Analytical Error ± 0.54			

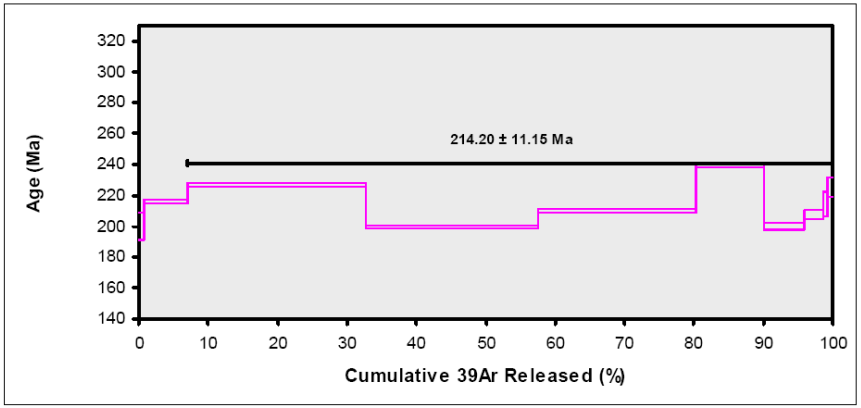

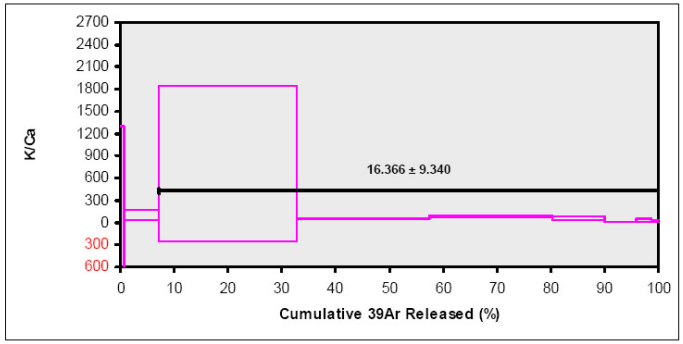

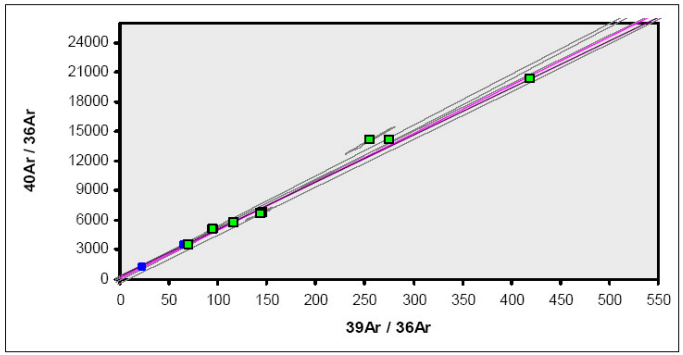

Results	40(a)/36(a) ± 2σ	40(r)/39(k) ± 2σ	Age ± 2σ (Ma)	MSWD
No Convergence	114.2494 ± 1072.1753 ± 938.45%	48.8472 ± 9.1851 ± 18.80%	218.50 ± 38.72 ± 17.72%	> 100
			External Error ± 38.96	
			Analytical Error ± 38.70	

07XX29 (phengite, 2nd run)

Incremental Heating	36Ar(a)	37Ar(ca)	38Ar(cl)	39Ar(k)	40Ar(r)	Age ± 2σ (Ma)	40Ar(r) (%)	39Ar(k) (%)	K/Ca ± 2σ
0.75 W	0.000233	0.002840	0.000000	0.349557	21.793883	274.50 ± 3.39	99.68	58.14	52.919 ± 15.172
1.00 W	0.000004	0.000534	0.000000	0.165187	11.044662	292.84 ± 3.13	99.99	27.47	133.114 ± 260.597
1.25 W	0.000108	0.000000	0.000000	0.032048	1.478050	206.97 ± 2.82	97.88	5.33	6.259 ± 4.712
1.50 W	0.000001	0.000000	0.000000	0.013700	0.643507	210.58 ± 4.93	99.95	2.28	2.591 ± 2.247
1.75 W	0.000013	0.000778	0.000000	0.005475	0.285365	232.26 ± 12.68	98.67	0.91	3.026 ± 3.210
2.00 W	0.000030	0.000000	0.000000	0.018440	0.893385	216.82 ± 3.58	99.00	3.07	2.176 ± 1.210
3.00 W	0.000046	0.000576	0.000023	0.003436	0.172354	224.05 ± 15.22	92.76	0.57	2.567 ± 3.335
20.00 W	0.028193	0.001583	0.000091	0.013424	0.124978	43.74 ± 59.66	1.48	2.23	3.645 ± 2.331
Σ	0.028628	0.006311	0.000114	0.601266	36.436185				

Information on Analysis	Results	40(r)/39(k) ± 2σ	Age ± 2σ (Ma)	MSWD	39Ar(k) (%,n)	K/Ca ± 2σ
VU75-D14 Phengite 07XX29 MG	Error Plateau	47.1747 ± 0.6675 ± 1.41%	211.44 ± 2.89 ± 1.36% External Error ± 3.58 Analytical Error ± 2.82	2.04 1.06 1.4268	12.16 5 Statistical T Ratio Error Magnification	2.521 ± 0.948
Project = VU75 Irradiation = VU75 J = 0.0026359 ± 0.0000079 DRA-1 = 25.260 ± 0.144 Ma	Total Fusion Age	60.5991 ± 0.5909 ± 0.98%	267.35 ± 2.54 ± 0.95% External Error ± 3.68 Analytical Error ± 2.42		8	1.154 ± 0.472

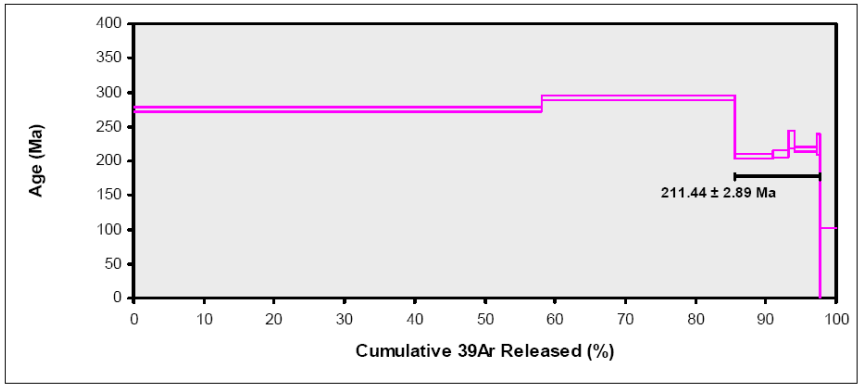

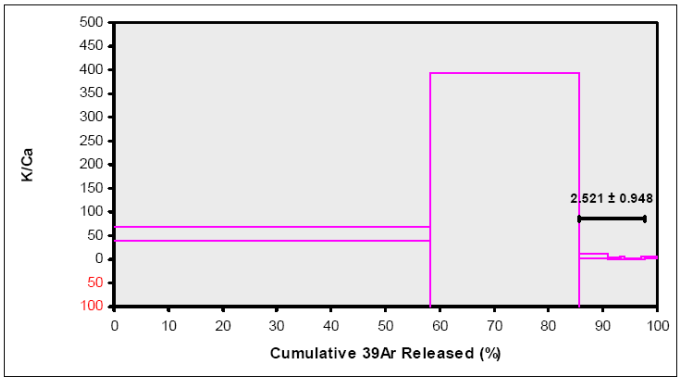

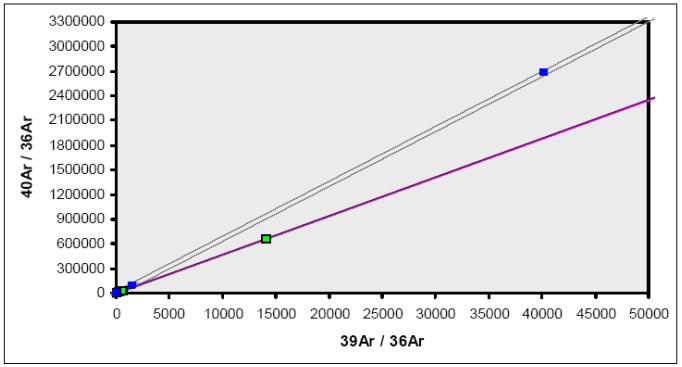

Results	40(a)/36(a) ± 2σ	40(r)/39(k) ± 2σ	Age ± 2σ (Ma)	MSWD
No Convergence	97.7865 ± 537.0064 ± 549.16%	46.9139 ± 1.8500 ± 3.94%	210.34 ± 7.85 ± 3.73% External Error ± 8.13 Analytical Error ± 7.83	0.45

07XX29 (phengite, 2nd run)

Incremental Heating	36Ar(a)	37Ar(ca)	38Ar(cl)	39Ar(k)	40Ar(r)	Age ± 2σ (Ma)	40Ar(r) (%)	39Ar(k) (%)	K/Ca ± 2σ
0.75 W	0.000233	0.002840	0.000000	0.349557	21.793883	274.50 ± 6.78	99.68	16.75	52.919 ± 30.345
1.00 W	0.000004	0.000534	0.000000	0.165187	11.044662	292.84 ± 6.25	99.99	7.91	133.114 ± 521.195
1.25 W	0.000108	0.000000	0.000000	0.032048	1.478050	206.97 ± 5.64	97.88	1.54	17.934 ± 16.236
1.50 W	0.000001	0.000000	0.000000	0.013700	0.643507	210.58 ± 9.85	99.95	0.66	17.934 ± 16.236
1.50 W	0.000463	0.000026	0.000000	0.010182	0.453252	200.16 ± 9.02	76.82	0.49	168.043 ± 1128.646
1.75 W	0.000013	0.000778	0.000000	0.005475	0.285365	232.26 ± 25.37	98.67	0.26	3.026 ± 6.419
2.00 W	0.000030	0.000000	0.000000	0.018440	0.893385	216.82 ± 7.16	99.00	0.88	17.934 ± 16.236
2.50 W	0.001454	0.000388	0.000000	0.095044	4.588008	216.08 ± 1.60	91.43	4.55	105.389 ± 68.737
3.00 W	0.000046	0.000576	0.000023	0.003436	0.172354	224.05 ± 30.44	92.76	0.16	2.567 ± 6.671
3.50 W	0.004004	0.000207	0.000000	0.381443	19.385566	226.80 ± 1.28	94.24	18.27	793.241 ± 1049.910
4.50 W	0.002533	0.002997	0.000019	0.369141	16.389936	199.67 ± 1.01	95.63	17.69	52.957 ± 4.991
7.00 W	0.002887	0.001796	0.000088	0.336331	15.776556	210.31 ± 1.08	94.87	16.11	80.529 ± 14.524
9.00 W	0.000569	0.000969	0.000000	0.145679	7.860292	239.90 ± 1.37	97.90	6.98	64.613 ± 22.917
9.00 W	0.000609	0.002981	0.000007	0.087521	3.889756	199.86 ± 2.24	95.57	4.19	12.626 ± 1.411
12.00 W	0.000584	0.000464	0.000000	0.040650	1.881274	207.65 ± 3.18	91.60	1.95	37.666 ± 22.641
16.00 W	0.000019	0.000264	0.000000	0.008019	0.384298	214.60 ± 7.90	98.55	0.38	13.057 ± 9.942
20.00 W	0.000044	0.000288	0.000097	0.012008	0.605423	225.12 ± 6.33	97.91	0.58	17.934 ± 16.236
20.00 W	0.028193	0.001583	0.000091	0.013424	0.124978	43.74 ± 119.31	1.48	0.64	3.645 ± 4.663
Σ	0.041793	0.016691	0.000325	2.087285	107.650547				

Information on Analysis	Results	40(r)/39(k) ± 2σ	Age ± 2σ (Ma)	MSWD	39Ar(k) (%,n)	K/Ca ± 2σ
VU75-D14 Phengite 07XX29 MG	Error Plateau	47.8335 ± 1.8145 ± 3.79%	214.23 ± 7.76 ± 3.62% External Error ± 8.86 Analytical Error ± 7.66	221.28 2.16 14.8755	74.12 14 Statistical T Ratio Error Magnification	15.393 ± 6.904
Project = VU75 Irradiation = VU75 J = 0.0026359 ± 0.0000079 DRA-1 = 25.260 ± 0.144 Ma	Total Fusion Age	51.5744 ± 0.3254 ± 0.63%	229.96 ± 1.88 ± 0.82% External Error ± 4.97 Analytical Error ± 1.36		18	1.514 ± 0.475

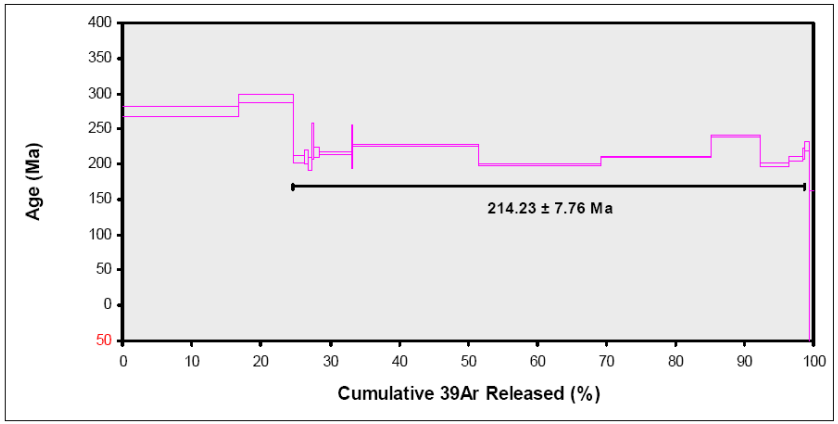

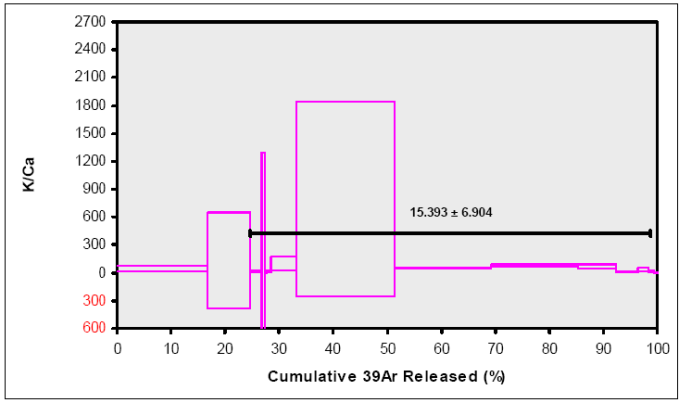

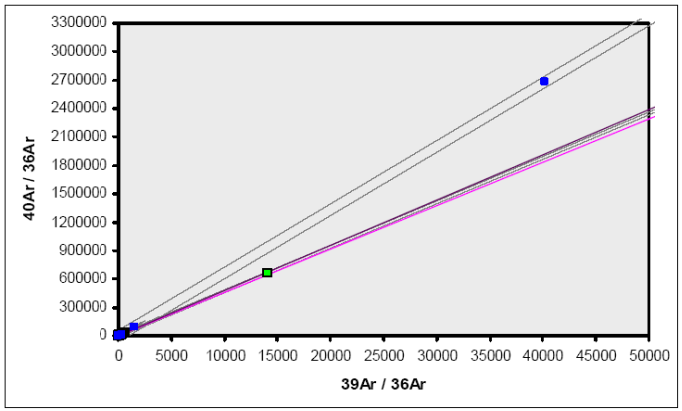

Results	40(a)/36(a) ± 2σ	40(r)/39(k) ± 2σ	Age ± 2σ (Ma)	MSWD
No Convergence	394.6414 ± 359.5994 ± 91.12%	45.7722 ± 3.4882 ± 7.62%	205.50 ± 14.85 ± 7.22% External Error ± 15.41 Analytical Error ± 14.80	97.07

Appendix VII Supplementary chapter, Argon methods

VII.1 Principles of $^{40}Ar/^{39}Ar$ isotopic dating

In the 1930's ^{40}K was recognized as a radioactive isotope. *Nier* (1935) suggested subsequently that isotopic anomalies in ^{40}Ar and ^{40}K could be used as a geochronometer. ^{40}K can decay to both ^{40}Ar and ^{40}Ca. This has to be taken into account when calculating the age using both the $^{40}K/^{40}Ar$ dating technique and the $^{40}Ar/^{39}Ar$ dating technique. With the following formulas, in which λ is the decay constant of ^{40}K, the amount of radiogenic Ar and Ca from ^{40}K can be calculated. In these equations 't' is the time since decay of ^{40}K started in this material; usually the time of crystallization of the rock.

$$^{40}Ar^* + {}^{40}Ca^* = {}^{40}K\left(e^{\lambda t} - 1\right) \quad \text{(VII.1)}$$

$$^{40}Ar^* = \frac{\lambda_{(^{40}K \rightarrow {}^{40}Ar)}}{\lambda^{40}K\left(e^{\lambda t}-1\right)} \quad \text{(VII.2)}$$

$$^{40}Ca^* = \frac{\lambda_{(^{40}K \rightarrow {}^{40}Ca)}}{\lambda^{40}K\left(e^{\lambda t}-1\right)} \quad \text{(VII.3)}$$

As argon is a noble gas, it is only retained in solidified rock. The time passed after solidification is calculated with equation VII.4:

$$t = \frac{1}{\lambda} ln(1 + D/N) = \frac{1}{\lambda} ln\left(1 + \left(\lambda / \lambda_{^{40}K \rightarrow {}^{40}Ar}\right) \times \left({}^{40}Ar^*/{}^{40}K\right)\right) \quad \text{(VII.4)}$$

In this equation D and N represent the amount of daughter and parent isotopes, respectively. The disadvantage of this technique, besides the decay of ^{40}K to both ^{40}Ar and ^{40}Ca, is that K and Ar cannot be measured on the same mass spectrometer, so the sample has to be split into two parts that have to be measured separately: potassium with wet chemical methods or XRF, and argon with isotope dilution. To overcome this problem, the sample is irradiated with fast neutrons at the high flux reactor in Petten (The Netherlands), to produce ^{39}Ar from ^{39}K, the main isotope of K. Because $^{40}K/^{39}K$ is constant in our systems, ^{39}Ar is ultimately a measure for ^{40}K. This method was first introduced by *Merrihue and Turner* in 1966, though it took some years before it was more widely used.
It has as advantages that no sample splitting is needed, therefore it has a greater accuracy. The age information is directly derived from the $^{40}Ar/^{39}Ar$ ratio, which increases the analytical precision. Smaller amounts can be measured, so single crystal dating and spot fusion dating are possible. Incremental heating of the sample by a laser allows for a test for assumption of a closed system. If the released argon gas has removed from the sample, the measured isotopic ratio for each temperature step represents the age of this step. The basis for the equations used to calculate the age is introduced next:

$$^{40}Ar^* = \lambda_{(^{40}K \rightarrow {}^{40}Ar)} / \lambda^{40}K\left(e^{\lambda t} - 1\right) \quad \text{(VII.5)}$$

$$^{39}Ar_K = {}^{39}K \times \Delta T \times \int\left(\rho(\varepsilon)\sigma(\varepsilon)\delta(\varepsilon)\right) \quad \text{(VII.6)}$$

$^{40}Ar^*$ is produced by the decay of ^{40}K over geological time (eq. 5). $^{39}Ar_K$ is the ^{39}Ar produced from ^{39}K at the high flux reactor (equation VII.6). ΔT is the length of irradiation at the reactor, ρ(ε) is the neutron flux density at energy ε, σ(ε) is the capture cross section of 39K for neutrons having energy ε, integrated over the entire energy spectrum ε of the neutrons. If these parameters are known, one can obtain an apparent age. By measuring the $^{40}Ar^*/^{39}Ar_K$ of a standard with a known age (t(m)) (DRA1 sanidine with an age of 25.26 ±0.05 Ma) the irradiation parameters for the entire package of standards and unknowns can be calculated, summarized in the J-factor:

$$^{40}Ar^{*}/^{39}Ar_{K} = \left(e^{\lambda t} - 1\right)/J \qquad \text{(VII.7)}$$

in which J is known as the irradiation factor, described in equation 8. It varies for each package irradiated at the high flux reactor, depending on the flux and the duration of irradiation. The assumption is made that the J-value for the standard is the same as for the sample.

$$J = \frac{\left(e^{\lambda t(m)} - 1\right)}{\left(^{40}Ar^{*}/^{39}Ar\right)} \qquad \text{(VII.8)}$$

$$J_{sample} = J_{standard} \qquad \text{(VII.9)}$$

Now the apparent age of the sample can be calculated:

$$t = \frac{1}{\lambda} ln\left(^{40}Ar^{*}/^{39}Ar_{K} \times J + 1\right) \qquad \text{(VII.10)}$$

The uncertainty of the method is limited by the precision with which we can determine the $^{40}Ar/^{39}Ar$ ratios in both the standard and the unknown. In practice there is an additional limiting factor in the precision with which ^{36}Ar can be measured (cf. equation VII.11). In addition, there is currently a lot of discussion about the uncertainty of the absolute ages of the standards. This uncertainty and the uncertainty of the decay constant of ^{40}K to ^{40}Ar decreases the accuracy of the J-factor. These systematic errors stir up the discussion about the accuracy of the obtained age.

There are also some disadvantages to this technique, like the interference of Ar-isotopes derived from the radiation of other nuclides (^{40}K, ^{40}Ca, ^{42}Ca, ^{35}Cl and ^{37}Cl). For this, corrections can be made by irradiating synthetic glass samples of pure K_2SiO_4 and $CaSiO_4$. Chloride interference is less common, therefore corrections are not always applied. All interfering reactions are given in Table VII.1.

Argon produced	Calcium	Potassium	Argon	Chlorine
^{36}Ar	^{40}Ca(n, nα)			
^{37}Ar	^{40}Ca(n, α)	^{39}K(n, nd)	^{36}Ar(n, γ)	^{37}Cl(n, γ, β^-)
^{38}Ar	^{42}Ca(n, nα)	^{39}K(n, d) ^{41}K(n, α, β^-)	^{40}Ar(n, nd, β^-)	
^{39}Ar	^{42}Ca(n, α) ^{43}Ca(n, nα)	^{39}K(n, p)[a] ^{40}K(n, d)	^{38}Ar(n, γ) ^{40}Ar(n, d, β^-)	
^{40}Ar	^{43}Ca(n, α) ^{44}Ca(n, nα)	^{40}K(n, p) ^{41}K(n, d)		

Table VII.1 Interfering nuclear reactions caused by neutron irradiation of mineral samples (*Brereton*, 1970). [a]Principal reaction for the $^{40}Ar/^{3}9Ar$ dating method

Other corrections have to be made for the contribution of atmospheric argon to the ^{40}Ar signal. It is assumed that the $^{40}Ar/^{36}Ar$ ratio of atmospheric argon has a constant value of 295.5. This has to be taken into account when measuring the ratio of the sample, using the following equation:

$$^{40}Ar^{*}/^{39}Ar = \left(^{40}Ar/^{39}Ar\right)_{m} - 295.5\left(^{36}Ar/^{39}Ar\right)_{m} \qquad \text{(VII.11)}$$

An important correction has to be made on the K/Ca-ratio. This ratio contains information on the chemical composition of the mineral phases. It can reveal if groundmass separation was adequate. Incomplete removal of a Ca-rich mineral phase, like plagioclase can induce an anomalously high age. ^{36}Ar is produced from ^{40}Ca during irradiation. This has to be taken into account when corrections for atmospheric argon are made. If not, the atmospheric ^{40}Ar will be overcorrected (*McDougall et al.*, 1988). ^{37}Ar is no natural component of air. It is present in small amounts due to the irradiation of (K) Ca. ^{37}Ar is used for the correction of ^{36}Ar and ^{39}Ar produced by irradiation of Ca. In order to

minimize the effect of the correction factors, the irradiation time has to be chosen such that there is sufficient production of $^{39}Ar_K$ and a minimum of $^{36}Ar_{Ca}$ and $^{39}Ar_{Ca}$. A convenient way to estimate the correct duration is given by equation VII.12:

$$J \leq 4.9 \times 10^{20} C(K/Ca)\left(e^{\lambda t} - 1\right) \qquad \text{(VII.12)}$$

where C is a constant for a given reactor facility. In order to obtain the K/Ca-ratio, standard values are taken for the correction factors for K- and Ca-derived Ar. The cumulative ^{39}Ar released by the sample can be plotted against the calculated K/Ca-ratio. This ratio is indicative for the degree of purity of the groundmass and for the correction on the age of the sample. Phenocrysts, crystallized prior to the groundmass, may give an inherited and therefore older age. The higher the ratio is, the lower the correction.

Different heat sources are used to release argon gas from samples. A CO_2 laser is used for single crystal fusion experiments, but it is also used to date small amounts of groundmass or mineral separations. The laser beam has a diameter of 2 mm and can be focused to 200 micrometer. Another technique is incremental heating in an oven. The advantage of this technique is that younger samples can be analysed (young samples contain small amounts of radiogenic Ar; by loading more sample still sufficient argon for a precise measurement can be extracted). Incremental heating techniques allow for testing for homogeneous distribution of radiogenic ^{40}Ar, identification of inherited ^{40}Ar and the presence of excess ^{40}Ar components (*Dalrymple and Lanphere*, 1969). Further results from incremental heating can be plotted as isochrons. With the isochron it can be tested whether the gas is a mixture of radiogenic argon and atmospheric argon (i.e. that no excess or inherited argon contributes to the gas mixture). A disadvantage is that the amount of sample has to be large, depending on the expected age of the sample, because of the small amount of radiogenic Ar in young samples.

VII.2 References

Brereton, N.R.; Corrections for isotopes in the $^{40}Ar/^{39}Ar$ dating method; *Earth and Planetary Science Letters*; Vol. 8, p. 427-433, 1970

Dalrymple, G.B.; Lanphere, M.A.; Potassium-Argon Dating. Principle Techniques and Applications to Geochronology; *Freeman Co.*, San Francisco, CA; pp. 258, 1969

McDougall, I.; Harrison, T.M.; Geochronology and thermochronology by the $^{40}Ar/^{39}Ar$ method; *Oxford University Press*; p. 40-63, 1988

Merrihue, C.; Turner, G.; Potassium-Argon dating by activation of fast neutrons; *Journal of Geophysical Research*; Vol. 71, p. 2852-2857, 1966

Nier, A.O.; Evidence for the existence of an isotope of potassium of mass 40; *Physical Review*; Vol. 48, p. 283-284, 1935